

**VIDEO UNDERSTANDING: THROUGH A TEMPORAL LENS**

by

**NGUYEN THANH THONG**

**A THESIS SUBMITTED FOR THE DEGREE OF**

**DOCTOR OF PHILOSOPHY**

in

**INSTITUTE OF DATA SCIENCE**

in the

**GRADUATE DIVISION**

of the

**NATIONAL UNIVERSITY OF SINGAPORE**

**2025**

Supervisor:

Professor See-Kiong Ng

Thesis Examiners:

Associate Professor Yao Yingjie Angela  
Assistant Professor Bryan Hooi Kuen-Yew

## Declaration

I hereby declare that this thesis is my original work and it has been written by me in its entirety. I have duly acknowledged all the sources of information which have been used in the thesis.

This thesis has also not been submitted for any degree in any university previously.

阮通

---

NGUYEN THANH THONG

02 June 2025

## Acknowledgments

First and foremost, I am deeply indebted to my supervisor, Prof. See-Kiong Ng, for his guidance, advice and encouragement, as well as giving me extraordinary experiences throughout my doctoral program. Above all and the most needed, he has provided me with unflinching encouragement and support in a wide variety of ways. Without his guidance, this thesis would not have been completed or written.

I am deeply grateful to Prof. Luu Anh Tuan, who is my external supervisor and collaborator ever since my undergraduate years. He has inspired me to take on this PhD journey, and I have continued to benefit from his advice during my PhD years. Thanks to his detailed comments and advice, my research journey has become extremely fruitful and enjoyable.

I also wish to express my gratitude to Prof. Angela Yao, Prof. Min-Yen Kan, and Prof. Bryan Hooi for their priceless advice. I thank them for their thorough comments and suggestions towards my research works and research direction. Their critical comments contribute to the backbone of this research. I also want to thank Prof. Bryan Low for his valuable advice towards my research career.

I would like to thank AI Singapore and Google Inc. for providing me with the scholarship to pursue this research, as well as supporting the finance for me to present papers in several overseas conferences.

Besides, I am thankful to my friends, colleagues, and collaborators. I am grateful for their friendship throughout my study, and I really enjoy my time with these brilliant people.

Finally, I would like to sincerely and deeply thank my parents, who have taken care of me with great love in these years, and my sister for all of her jokes. Most importantly, my heartfelt thanks go to my spouse. It is her constant support and encouragement that gives me strength to persevere throughout my research journey.

# Contents

<b>Acknowledgments</b>	<b>3</b>
<b>Abstract</b>	<b>9</b>
<b>1 Introduction</b>	<b>16</b>
1.1 Challenges of Video Understanding . . . . .	17
1.2 Research Objectives . . . . .	19
1.3 Contributions and Outline of This Thesis . . . . .	20
<b>2 Literature Review</b>	<b>23</b>
2.1 Video Understanding Tasks . . . . .	23
2.2 Challenges of Video Understanding . . . . .	25
2.3 Model Architecture for Video- Language Understanding . . . . .	28
2.3.1 Pre-Transformer Architecture . . . . .	28
2.3.2 Transformer-based Architecture . . . . .	29
2.3.3 LLM-Augmented Architecture . . . . .	31
2.3.4 Architecture Analysis . . . . .	32
2.4 Model Training for Video Understanding . . . . .	32
2.4.1 Pre-training for Video Understanding . . . . .	33
2.4.2 Fine-tuning for Video Understanding . . . . .	35
2.5 Data Perspective for Video Understanding . . . . .	36
2.5.1 Data curation . . . . .	36
2.5.2 Label annotation . . . . .	37
2.6 Future Directions . . . . .	38
<b>3 MAMA: Meta-optimized Angular Margin Contrastive Framework for Video-Language Representation Learning</b>	<b>40</b>

3.1	Introduction . . . . .	40
3.2	MAMA Framework . . . . .	42
3.2.1	Video-Language Representation Learning . . . . .	42
3.2.2	Meta-optimized Angular Margin Contrastive Framework . .	44
3.2.3	Large Vision-Language Model for Augmentation . . . . .	47
3.3	Experiments . . . . .	48
3.3.1	Experimental Settings . . . . .	48
3.3.2	Main Results . . . . .	50
3.3.3	Ablation Study . . . . .	52
3.3.4	Analysis . . . . .	55
3.4	Summary . . . . .	56
<b>4</b>	<b>READ: Recurrent Adapter with Partial Video-Language Alignment for Parameter-Efficient Transfer Learning in Low-Resource Video-Language Modeling</b>	<b>57</b>
4.1	Introduction . . . . .	57
4.2	Methodology . . . . .	60
4.2.1	Preliminary – Transformer Architecture for Video-Language Modeling . . . . .	60
4.2.2	Recurrent Adapter (READ) . . . . .	62
4.2.3	Partial Video-Language Alignment (PVLA) . . . . .	63
4.3	Experiments . . . . .	64
4.3.1	Experimental Settings . . . . .	65
4.3.2	Main Results . . . . .	69
4.3.3	Ablation Studies . . . . .	70
4.3.4	Qualitative Assessment . . . . .	71
4.4	Conclusion . . . . .	71
<b>5</b>	<b>Encoding and Controlling Global Semantics for Long-form Video Question Answering</b>	<b>73</b>
5.1	Introduction . . . . .	73
5.2	Methodology . . . . .	75
5.2.1	Gated State Space Multi-Modal Transformer (GSMT) . . .	76

5.2.2	Cross-modal Compositional Congruence (C <sup>3</sup> ) Objective . . . . .	79
5.2.3	Overall Objective . . . . .	80
5.3	Ego-QA and MAD-QA Benchmarks . . . . .	80
5.3.1	Ego-QA . . . . .	80
5.3.2	MAD-QA . . . . .	81
5.4	Experiments . . . . .	81
5.4.1	Standard Benchmarks . . . . .	81
5.4.2	Implementation Details . . . . .	83
5.4.3	Baselines . . . . .	84
5.4.4	Quantitative Results . . . . .	86
5.4.5	Ablation Study . . . . .	87
5.4.6	Qualitative Results . . . . .	89
5.5	Summary . . . . .	89
<b>6</b>	<b>Motion-aware Contrastive Learning for Temporal Panoptic Scene Graph Generation</b>	<b>90</b>
6.1	Introduction . . . . .	90
6.2	Problem Formulation . . . . .	93
6.3	Methodology . . . . .	94
6.3.1	Temporal Panoptic Segmentation . . . . .	94
6.3.2	Relation Classification . . . . .	96
6.3.3	Contrastive Learning for Temporal Panoptic Scene Graph Generation . . . . .	96
6.3.4	Shuffle-based contrastive learning . . . . .	97
6.3.5	Triplet-based contrastive learning . . . . .	98
6.3.6	Optimal Transport for Mask Tube Relation Quantification .	98
6.4	Experiments . . . . .	99
6.4.1	Experiment Settings . . . . .	100
6.4.2	Main Results . . . . .	103
6.4.3	Ablation Study . . . . .	104
6.4.4	Qualitative Analysis . . . . .	105
6.5	Summary . . . . .	105

<b>7 Multi-Scale Contrastive Learning for Video Temporal Grounding</b>	<b>106</b>
7.1 Introduction . . . . .	106
7.2 Methodology . . . . .	110
7.2.1 Preliminary - Video Temporal Grounding . . . . .	110
7.2.2 Cross-scale Contrastive Learning . . . . .	113
7.2.3 Training Objective . . . . .	114
7.3 Experiments . . . . .	114
7.3.1 Datasets . . . . .	115
7.3.2 Evaluation Metrics . . . . .	115
7.3.3 Implementation Details . . . . .	115
7.3.4 Baselines . . . . .	116
7.4 Experimental Results . . . . .	117
7.4.1 Main Results . . . . .	117
7.4.2 Ablation Study . . . . .	119
7.4.3 Qualitative Analysis . . . . .	121
7.5 Summary . . . . .	121
<b>8 Temporal-Oriented Recipe for Transferring Large Vision-Language Model to Video Understanding</b>	<b>122</b>
8.1 Introduction . . . . .	122
8.2 Temporal-Oriented Recipe for Large Vision-Language Model . . . . .	126
8.3 Experimental Results . . . . .	135
8.4 Summary . . . . .	136
<b>9 Conclusion</b>	<b>137</b>
9.1 Overall Summary . . . . .	137
9.2 Future Directions and Challenges . . . . .	139
9.2.1 Streaming Video Understanding (RO1, RO2) . . . . .	139
9.2.2 Multi-Video Reasoning and Understanding (RO2, RO3) . . . . .	139
9.2.3 Probing Models for Temporal Understanding (RO3) . . . . .	140
9.2.4 Cost-Accuracy Tradeoff for Video Understanding (RO1) . . . . .	140
9.3 Reflections . . . . .	140
9.3.1 Choosing a Steady Research Direction is Important . . . . .	140

9.3.2 Scalability is important but we still need principled research	141
9.3.3 Academia versus Industry: Does Industry have more resources than Academia in all cases? . . . . .	142
<b>Bibliography</b>	<b>144</b>

## Abstract

The fundamental difference between an image and a video is that a video introduces a temporal dimension. Such dimension triggers our awareness of temporal relations present among video elements, such as object positions, frames, and events. For example, when an object changes position, we perceive its positional changes as a movement. When we watch a video, we experience motion in the flow of frames. Additionally, one can recall the way we connect the events in a movie, seeking to construct a coherent narrative. These examples demonstrate that a video is indicative of temporal relations among its elements, requiring any video-understanding model to possess an awareness of temporality. Thus, in this thesis we aim to address the following question:

*“How to utilize the existence of temporal relations among video elements to advance video understanding?”*

First, video understanding performance has been constrained by training data of limited scale and quality, a bottleneck caused by the labor-intensiveness and expensive cost of obtaining high-quality annotated video data. To overcome this, we introduce an automatic annotation approach that harnesses the large vision-language model’s capacity to form a temporal progression among video frames to generate language annotations for videos. Because such automatically generated annotations may introduce noise to training, we propose a contrastive learning objective with a subtractive angular margin to regularize a model against perfect similarity between representations of a video and its language description. Our approach is theoretically guaranteed based on the intuition that a video and its caption often convey overlapping but not identical information.

Second, in resource-constrained scenarios, both manual and automatic approaches are unable to generate sufficient supervised training data for video understanding models. In these cases, fully updating model parameters can lead to overfitting and degraded performance. To address this issue, we employ a parameter-efficient

training approach to finetune only a finite subset of modules, which we call adapters. We equip our adapters with recurrent computation layers to construct recurrent adapters that specifically adapt to modeling temporal relations among video frames. Furthermore, we integrate a partial video-language alignment objective into training, ensuring that our model effectively captures temporal semantics relevant to the task. Our approach demonstrates improved performance in multi-task scenarios with limited training data.

Third, existing works focus on short videos with independent or simple events. Most of them seek to infer temporal relations among coarsely sampled video elements, such as visual patches and video frames. However, for long videos, coarsely sampled elements hardly fully capture video content, while densely sampled elements will result in excessive computational cost. To cope with this issue, we introduce a state space layer (SSL) to our video understanding model to efficiently model temporal relations among densely sampled video elements for long-term video understanding. Moreover, recognizing that there is a lack of benchmarks that authentically evaluate long-term video understanding, we introduce two new long-term video understanding benchmarks: one based on egocentric videos averaging 18 minutes and another based on movies spanning up to 2 hours. We carefully construct detailed prompts to instruct GPT-4 to generate highly difficult questions that require a model to simultaneously summarize, compare, and compress information across a long video. Experiments show that our method demonstrates superiority over self-attention and recurrent layers for long-term video understanding.

Fourth, despite the existence of temporal relations among video elements, the attention to such relations still remains scarce compared to the attention to cross-modal relations between a video and its language description. To address this gap, we first propose a novel contrastive learning framework to drive a model to focus on relations between two motions in videos. Then, we extend our framework to capture relations between video moments. Extensive experiments indicate that our explicit temporal modeling approach significantly improves video understanding by making representations more aware of fine-grained temporal relations.

Finally, with the advent of large language models (LLMs) featuring outstanding reasoning capabilities, several works have sought to employ LLMs by constructing large vision-language models (LVLM) for video understanding. Unfortunately, rather

than explicitly modeling temporal relationships in a video, they often rely on spatial inductive biases, assuming that spatial knowledge can smoothly extend to temporal comprehension. Such reliance has prevented modern video understanding models from fully utilizing their understanding capability. To overcome this limitation, we conduct a thorough empirical study to demystify crucial components that influence temporal understanding in LVLMs. Our empirical study reveals that the crucial component lies in the intermediate interface between the visual encoder and the LLM. Building on such insight, we propose a temporal-oriented recipe that encompasses temporal-oriented training scheme and an upscaled interface. Our final model developed using our recipe significantly enhances previous LVLMs across standard video understanding benchmarks.

# Authorship Attribution Statement

This thesis contains material from the following paper(s) published in the respective peer-reviewed conferences in which I am listed as an author.

**Chapter 2** is published with material from the following paper(s):

1. Thong Nguyen, Yi Bin, Junbin Xiao, Leigang Qu, Yicong Li, Jay Zhangjie Wu, Cong-Duy T Nguyen, See-Kiong Ng, Luu Anh Tuan. *Video-Language Understanding: A Survey from Model Architecture, Model Training, and Data Perspectives*. Annual Meeting of the Association for Computational Linguistics (ACL), 2024 (Findings)

**Chapter 3** is published with material from:

1. Thong Nguyen, Yi Bin, Xiaobao Wu, Xinshuai Dong, Zhiyuan Hu, Khoi Le, Cong-Duy Nguyen, See-Kiong Ng, Luu Anh Tuan. *MAMA: A Meta-optimized Angular Margin Contrastive Framework for Video-Language Representation Learning*. The European Conference on Computer Vision (ECCV), 2024

**Chapter 4** is published with material from:

1. Thong Nguyen, Xiaobao Wu, Xinshuai Dong, Khoi Le, Zhiyuan Hu, Cong-Duy Nguyen, See-Kiong Ng, Luu Anh Tuan. *READ: Recurrent Adapter with Partial Video-Language Alignment for Parameter-Efficient Transfer Learning in Low-Resource Video-Language Modeling*. Proceedings of AAAI Conference on Artificial Intelligence (AAAI), 2024

**Chapter 5** is published with material from:

1. Thong Nguyen, Zhiyuan Hu, Xiaobao Wu, Cong-Duy Nguyen, See-Kiong Ng, Luu Anh Tuan. *Encoding and Controlling Global Semantics for Long-form Video Question Answering*. Proceedings of Empirical Methods in Natural Language Processing (EMNLP), 2024

**Chapter 6** is published with material from:

1. Thong Nguyen, Xiaobao Wu, Yi Bin, Cong-Duy Nguyen, See-Kiong Ng, Luu Anh Tuan. *Motion-aware Contrastive Learning for Temporal Panoptic Scene Graph Generation*. Proceedings of AAAI Conference on Artificial Intelligence (AAAI), 2025

**Chapter 7** is published with material from:

1. Thong Nguyen, Yi Bin, Xiaobao Wu, Zhiyuan Hu, Cong-Duy Nguyen, See-Kiong Ng, Luu Anh Tuan. *Multi-Scale Contrastive Learning for Video Temporal Grounding*. Proceedings of AAAI Conference on Artificial Intelligence (AAAI), 2025

**Chapter 8** is published with material from:

1. Thong Nguyen, Zhiyuan Hu, Xu Lin, Cong-Duy Nguyen, See-Kiong Ng, Luu Anh Tuan. *Temporal-Oriented Recipe for Transferring Large Vision-Language Model to Video Understanding*. In submission to Conference on Neural Information Processing (NeurIPS), 2025

Other publications during my PhD study:

1. Cong-Duy Nguyen, Xiaobao Wu, Thong Nguyen, Shuai Zhao, Khoi Le, Viet-Anh Nguyen, Feng Yichao, Luu Anh Tuan. *Enhancing Multimodal Entity Linking with Jaccard Distance-based Conditional Contrastive Learning and Contextual Visual Augmentation*. Proceedings of Annual Conference of the North American Chapter of the Association for Computational Linguistics (NAACL), 2025
2. Thong Nguyen, Xiaobao Wu, Xinshuai Dong, Cong-Duy T Nguyen, See-Kiong Ng, Luu Anh Tuan. *Topic Modeling as Multi-Objective Contrastive Optimization*. Proceedings of International Conference on Learning Representations (ICLR), 2024
3. Xiaobao Wu, Fengjun Pan, Thong Nguyen, Yichao Feng, Chaoqun Liu, Cong-Duy Nguyen, Luu Anh Tuan. *On the affinity, rationality, and diversity of*

*hierarchical topic modeling.* Proceedings of AAAI Conference on Artificial Intelligence (**AAAI**), 2024

4. Xiaobao Wu, Thong Nguyen, Luu Anh Tuan. *A survey on neural topic models: methods, applications, and challenges.* Artificial Intelligence Review, 2024
5. Xiaobao Wu, Thong Nguyen, Delvin Ce Zhang, William Yang Wang, Luu Anh Tuan. *FASTopic: A Fast, Adaptive, Stable, and Transferable Topic Modeling Paradigm.* Proceedings of Advances in Neural Information Processing Systems (**NeurIPS**), 2024
6. Cong-Duy Nguyen, Thong Nguyen, Duc Anh Vu, Luu Anh Tuan. *KDMCSE: Knowledge distillation multimodal sentence embeddings with adaptive angular margin contrastive learning.* Proceedings of Annual Conference of the North American Chapter of the Association for Computational Linguistics (**NAACL**), 2024
7. Thong Nguyen, Xiaobao Wu, Xinshuai Dong, Cong-Duy Nguyen, See-Kiong Ng, Luu Anh Tuan. *DemaFormer: Damped Exponential Moving Average Transformer with Energy-Based Modeling for Temporal Language Grounding.* Proceedings of Empirical Methods in Natural Language Processing (**EMNLP**), 2023 (Findings)
8. Cong-Duy Nguyen, Thong Nguyen, Anh Vu, Luu Anh Tuan. *Improving multimodal sentiment analysis: Supervised angular margin-based contrastive learning for enhanced fusion representation.* Proceedings of Empirical Methods in Natural Language Processing (**EMNLP**), 2023 (Findings)
9. Xiaobao Wu, Xinshuai Dong, Thong Nguyen, Luu Anh Tuan. *Effective Neural Topic Modeling with Embedding Clustering Regularization.* Proceedings of International Conference on Machine Learning (**ICML**), 2023
10. Thong Nguyen, Xiaobao Wu, Xinshuai Dong, Luu Anh Tuan, Cong-Duy Nguyen, Zhen Hai, Lidong Bing. *Gradient-Boosted Decision Tree for Listwise Context Model in Multimodal Review Helpfulness Prediction.* Annual Meeting of the Association for Computational Linguistics (**ACL**), 2023 (Findings)

11. Xiaobao Wu, Xinshuai Dong, Thong Nguyen, Chaoqun Liu, Liangming Pan, Luu Anh Tuan. *InfoCTM: A Mutual Information Maximization Perspective of Cross-lingual Topic Modeling*. Proceedings of AAAI Conference on Artificial Intelligence (**AAAI**), 2023
12. Thong Nguyen, Xiaobao Wu, Tuan Luu, Cong-Duy Nguyen, Zhen Hai, Li-dong Bing. *Adaptive Contrastive Learning on Multimodal Transformer for Review Helpfulness Predictions*. Proceedings of Empirical Methods in Natural Language Processing (**EMNLP**), 2022

# Chapter 1

## Introduction

Video data is among the richest and most rapidly growing forms of digital information in the world. Every day, millions of videos, spanning hundreds of thousands of hours, are uploaded to online platforms. This steadily increasing data treasure is highly diverse, reflecting real-world complexity not only through static visual cues but also through temporal dynamics. There are two fundamental video types, *i.e.* natural footage and edited videos. Natural footage captures events as they unfold, whereas edited videos are shaped by human interventions such as cuts, splits, and transitions.

In this work, we aim to develop artificial intelligence capable of understanding video content by constructing video understanding models. Different from image understanding, which primarily captures static visual information, video understanding must model both spatial and temporal aspects to determine what happens, when it happens, and how events evolve over time.

Both natural and edited video understanding have extensive applications. For instance, analyzing natural footage enables tasks such as temporal grounding to localize video moments of anomalous activities, such as arson, shoplifting, and fighting. Similarly, video summarization can distill long meeting recordings into concise highlights to support business decision-making. Edited video understanding also offers practical applications. For example, text-video retrieval models can help users locate relevant movies based on queries, enhancing entertainment experiences.

Unlike images, videos inherently encompass a temporal dimension, marking events as they unfold. Nevertheless, this temporal aspect is difficult to represent explicitly. To robustly capture this temporal aspect of videos, we develop strong temporal understanding capabilities for video understanding models. Humans

naturally perceive temporal context, such as when we see a friend waving, we infer their movement; when a ball is suspended mid-air, we understand that it is moving. This awareness of change, sequence, and continuity stems from our lifelong exposure to dynamic events, and arguably from evolutionary experiences encoded in our genes. In contrast, instilling such temporal awareness in neural models is computationally demanding. Videos consist of numerous high-resolution frames, and processing hundreds of them often already exceeds the memory capacity of modern GPUs. Moreover, beyond frame-level analysis, effectively extracting and leveraging meaningful temporal cues remains a major challenge. As a result, video understanding has not reached the same level of success as achieved in image or language understanding, primarily due to the complexity of modeling temporal dynamics.

Therefore, this thesis argues that explicitly modeling temporal signals for video understanding can substantially enhance video understanding. In particular, we concentrate on relations that only emerge when time is considered, *e.g.* relations between object motions or relations between video moments, and investigate techniques to capture these temporal cues across three dimensions, *i.e.* data, model, and training. While the datasets used in this dissertation are predominantly edited videos, our methods are designed to generalize to both natural footage and edited videos. We believe that tailoring approaches to either natural or edited videos offers a promising future research avenue.

The following chapters of this thesis delve into the specifics of our temporal-oriented approach, demonstrate its advantages, and discuss its implications for advancing the field of video understanding.

## 1.1 Challenges of Video Understanding

**Performance Limits In Video Understanding.** Prior research has established scaling laws in deep learning, showing that performance tends to improve as both model size and training data increase (Hestness et al., 2017; Kaplan et al., 2020). This implies that, regardless of advancements in architecture or training techniques, meaningful performance gains will eventually stall without a corresponding increase in scale. Video understanding faces unique challenges in this regard: a single video

can comprise hundreds or thousands of high-resolution frames, making processing computationally expensive. Moreover, videos demand significantly more storage than images due to their multi-frame nature. As a result, video models and datasets have lagged behind those in image and language domains in terms of scale. Building on established scaling laws, this thesis aims to push the boundaries of video understanding by proposing strategies to scale models and training datasets to enable the effective capture of implicit temporal relations among video elements for video understanding.

**Inefficient capture of temporal relations in video understanding models.** Most video understanding architectures leverage self-attention-based modules originally designed for language understanding tasks. These modules require large volumes of training samples to capture useful inductive biases required for accurate semantic interpretation of text or video. Prior work has shown inferior performance under data scarcity (Dosovitskiy et al., 2020). Unfortunately, as mentioned, video datasets are generally far smaller than their image or language counterparts—a gap that widens in privacy-sensitive or long-tail scenarios. As a consequence, we must develop efficient techniques that enable models to quickly extract useful cues from limited training data.

**Ineffective capture of temporal relations in video understanding models.** A key challenge addressed in this thesis is the under-utilization of temporal cues in video understanding. Since many prior works focus on static frame-level features, they overlook deeper semantics that arise from temporal phenomena such as motion continuity, event formation, and long-range temporal dependencies. These elements derive their semantics only when we consider core temporal properties: change (*e.g.* detecting motion through variation across object masks), duration (*e.g.* identifying the span of an event), and succession (*e.g.* understanding how moments build into narratives). For instance, when an object shifts position across time—such as hand waving—we instinctively infer the motion, not just a sequence of static poses. Similarly, we interpret a stream of frames not as isolated images, but as a cohesive event, often organizing them into structured stories that unfold over time. In this thesis, we focus on emphasizing these semantics in representations generated by video understanding models by forming internal relations for motions, events, and long-term context.

## 1.2 Research Objectives

Given the challenges, we seek to advance video understanding by addressing them. As such, we tackle the following objectives which respectively correspond to the aforementioned challenges.

- **Research Objective 1 (RO1): Pushing the Frontier of Video Understanding.** Video understanding remains constrained by both architecture and dataset scale. We will expand these dimensions by (a) scaling up the model components most critical for temporal understanding, and (b) introducing an automatic annotation approach that automatically annotates a video by temporally linking sampled frames into a coherent video caption.
- **Research Objective 2 (RO2): Efficient Capture of Temporal Relations in Video Understanding Models.** In certain scenarios—such as privacy-sensitive environments or settings with limited computational and storage resources—acquiring large-scale video training data, whether supervised or non-supervised, is often infeasible. In such cases, models may lack access to rich temporal cues, particularly if their architectures do not inherently target video data. Furthermore, these low-resource contexts might also demand high adaptability, requiring support for multiple downstream tasks such as video summarization or temporal grounding. Therefore, beyond simply improving effectiveness, we also design modular components or training strategies that facilitate efficient temporal modeling under resource constraints. Our proposed solution offers a lightweight, task-adaptable framework that maintains strong performance across diverse video understanding tasks while minimizing training and storage costs.
- **Research Objective 3 (RO3): Effective Capture of Temporal Relations in Video Understanding Models.** We seek to integrate our inductive biases that emphasize temporal semantics in videos. These biases reflect common temporal relations among video elements: *(i) Relation between Motions:* When an object changes positions over time, it exhibits motion. Actions belonging to the same semantic category often share similar motion patterns. We encourage the model to learn representations that are close in feature space

for actions of the same type, thereby reinforcing motion-level consistency. *(ii)* *Relation between Events*: As frames progress sequentially, temporal properties such as duration, succession, and order emerge, forming a coherent event. To encode the content of an event, models generate compact representations for temporally ordered frame sequences that capture event-level temporal dynamics. In our work, we encourage the model to map events of similar semantics into similar embeddings, while separating dissimilar events. *(iii)* *Long-Term Context*: Videos typically consist of temporally linked that form a coherent narrative or context. In longer videos, such as movies, modeling this long-term temporal context poses both computational and representational challenges. We enhance the capacity of video models to capture and utilize long-range temporal dependencies, and we validate our approach on datasets featuring extended video content.

### 1.3 Contributions and Outline of This Thesis

In this section, we describe our contributions of this thesis with the according research objectives. For each contribution, we provide reference to the respective chapter in this thesis. The outline of the thesis is illustrated in Figure 1.1.

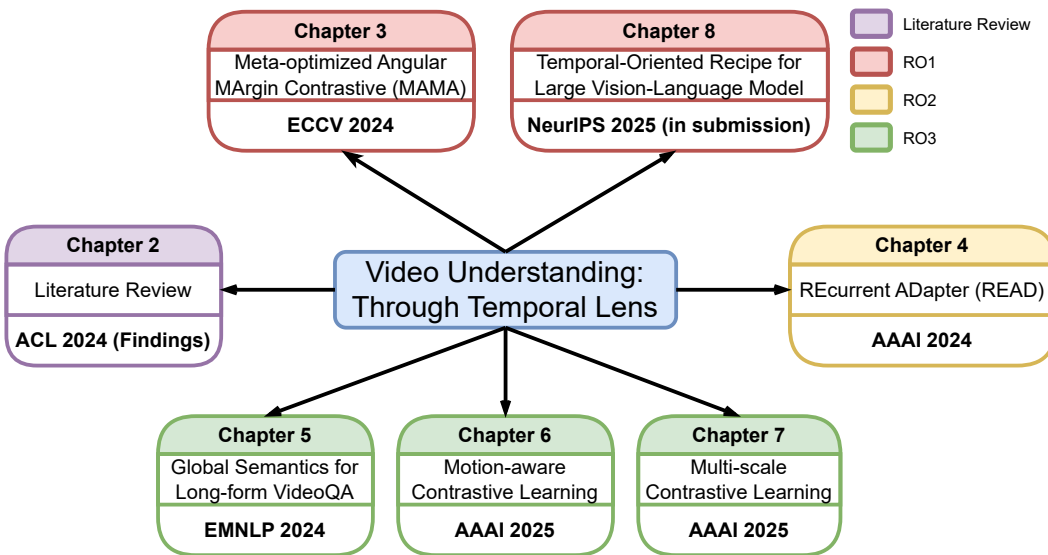


Figure 1.1: Outline of the thesis.

- **Contribution 1 - RO1 - Chapter 3: Meta-optimized Angular MArgin (MAMA) contrastive framework** for pushing the limit of video understanding through escalating training data. Particularly, MAMA utilizes a pretrained large vision-language model to annotate a vast set of video data. Because automatically annotated data can contain noise, MAMA uses regularization training which consist of a subtractive angular margin integrated in the contrastive objective along with a multi-layer perceptron (MLP) to dynamically adjust model’s attention to training samples. This can alleviate the noisy effect of synthetic data upon video understanding model training.
- **Contribution 2 - RO2 - Chapter 4: REcurrent ADapter (READ)** for efficient capture of temporal relations in low-resource video understanding. In low-resource scenarios, there exists limited video data to provide sufficient temporal cues for video understanding models to learn from. To remedy this problem, we incorporate recurrent computation into low-dimensional adapters to encourage temporal modeling capability. We further implement a video-text alignment training objective to motivate the model to focus upon task-related information during video encoding.
- **Contribution 3 - RO3 - Chapter 5: Encoding Global Video Semantics** for effective capture of temporal long-term context in long videos. Prior works cope with excessive computational cost of long-form video understanding by selecting a small number of frames for video understanding model, which leads to significant information loss. We mitigate this problem by incorporating SSLs into model architectures to encode all densely sampled frames which can absorb video’s global semantics with reduced complexity. We target our SSL-augmented architecture for long-form VideoQA, and validate its superiority on our two collected benchmarks involving movies and egocentric videos.
- **Contribution 3 - RO3 - Chapter 6: Motion-aware Contrastive Learning (MCL)** for effective capture of relations between object motions. MCL employs a novel contrastive training objective to pull closer representations for pairs of object masks possess similar actions. We explicitly target dynamic actions such as “*run*”, “*walk*”, and “*throw*” with strong motion cues. Experi-

ments demonstrate the effectiveness of our method for video panoptic scene graph generation, a comprehensive video understanding task whose aim is to segment a video into object masks and predict their relations.

- **Contribution 4 - RO3 - Chapter 7: Multi-Scale Contrastive Learning (MSCL)** for effective capture of relations between video moments. Our MSCL iteratively learns close representations for short-range and long-range video moments that are commonly described by an event description. By modeling the relations between short-range and long-range moments, we are able to deconfound the effect of surface properties of video elements, *e.g.* video moment length. Moreover, we can adopt a query-based sampling strategy for our framework to significantly reduce computational and memory cost, which are significant burdens of previous contrastive learning frameworks.
- **Contribution 5 - RO1 - Chapter 8: Temporal-Oriented Recipe for Transferring Large Vision-Language Model to Video Understanding** for pushing the limit of video understanding through advancing model architecture. With the advent of large language models (LLMs), a popular research avenue is to design LLM-oriented systems to inherit LLM’s impressive reasoning capability for video understanding. In our work, to further push the frontier of these systems, we first conduct extensive experiments to demystify essential components that significantly affect video understanding performance. As we discover that the vision-language interface is the most influential part, we devise a recipe centered on the interface. In our recipe, we progressively choose Q-Former as the vision-language interface, add temporal-oriented training schemes, incorporate temporal memory bank to store video representations, and augment mixture-of-experts (MoE) into the interface. These steps result in notable improvement for large vision-language models, as demonstrated by their strong performance on standard video understanding benchmarks.

# Chapter 2

## Literature Review

### 2.1 Video Understanding Tasks

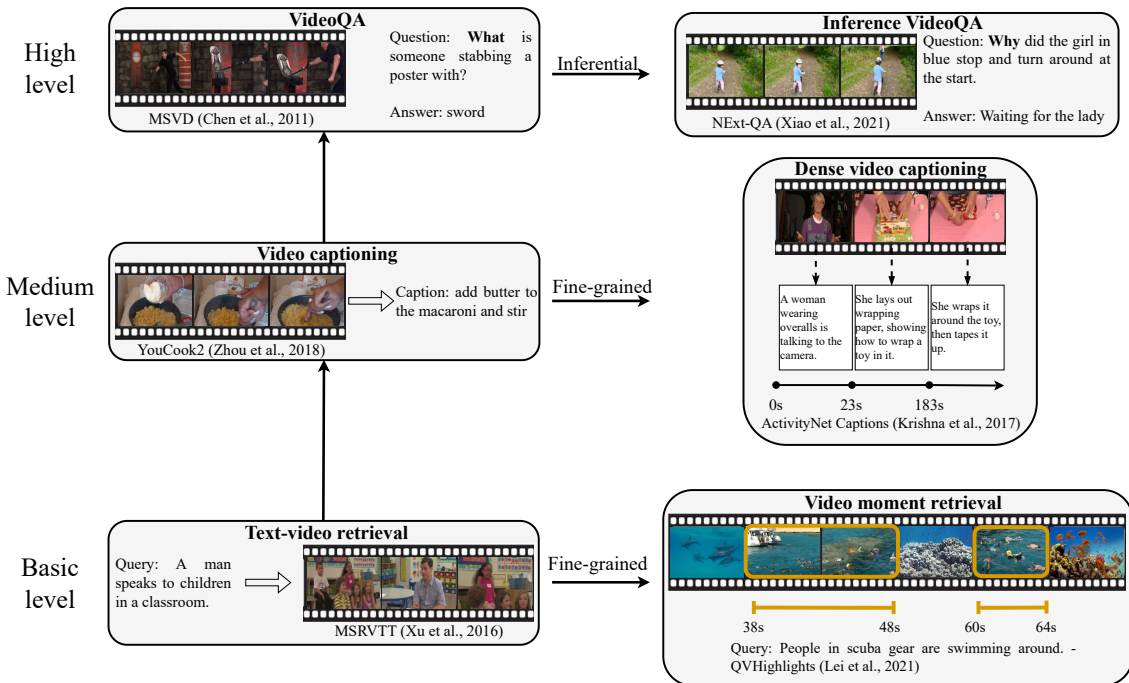


Figure 2.1: Level hierarchy of video understanding tasks.

**Text-video retrieval.** Text-video retrieval is the task to search for the corresponding video given a language query (text-to-video), or oppositely search for the language description given a video (video-to-text).

In practical applications, returning an entire video may not be desirable. Hence, video moment retrieval (VMR) has emerged with an aim to accurately locating relevant moments within a video based on user queries. VMR examines more nuanced and fine-grained understanding to capture different concepts and events

in a video in order to pinpoint specific moments rather than capturing the overall theme in standard text-video retrieval.

**Video captioning.** Video captioning is the task to generate a concise language description for a video. A video captioning model receives as input a video and optionally a language transcript transcribed from the audio in the video. Typically, a model produces a sentence-level caption for the whole video, or might also generate a paragraph as a more detailed summary.

**Video question answering (VideoQA).** Video question answering is the task to predict the correct answer based on a question  $q$  and a video  $v$ . There are two fundamental types of VideoQA, *i.e.* **multi-choice** VideoQA and **open-ended** VideoQA. In multi-choice VideoQA, a model is presented with a certain number of candidate answers and it will choose the correct answer among them. Open-ended VideoQA can be formulated as a classification problem, a generation problem, or a regression problem. Classification-based VideoQA associates a video-question pair with an answer from a pre-defined vocabulary set. Generation-based VideoQA is not restricted to a vocabulary set, in which a model can generate a sequence of tokens that represent the answer to a question. Regression-based VideoQA is often used for counting questions, *e.g.* counting the repetitions of an action or counting the number of an object in a video.

**Connections among video understanding tasks.** These tasks constitute the three fundamental testbeds for evaluating video understanding (see Figures 2.3 and 2.4 for their examples). Despite their operational differences, they can be unified under a common framework. Formally, let  $V = \{f_1, f_2, \dots, f_N\}$  denote a video with  $N$  frames, and let  $T$  denote a textual input, such as a query, question, or prompt. A video-language model  $M$  learns a mapping from the video  $V$  and text input  $T$  into an output  $Y$ , *i.e.*  $f : (V, T) \rightarrow Y$ . In text-video retrieval,  $Y$  is a relevance score between  $V$  and  $T$ . In video captioning,  $Y$  is a sequence of words describing  $V$ . In VideoQA,  $Y$  is the predicted answer conditioned on  $V$  and  $T$ . This unified formulation highlights that video understanding tasks share a foundation of joint video-language representation learning.

These video understanding tasks can also be organized into a hierarchy of understanding levels, as illustrated in Figure 2.1. At the basic level, text-video retrieval globally aligns a video with its textual counterpart. At the intermediate

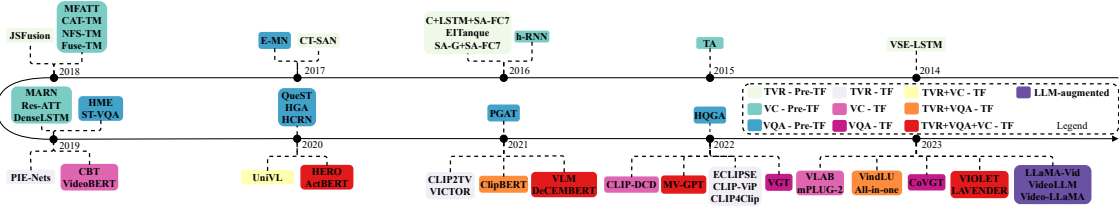


Figure 2.2: Timeline of the established video understanding methods (TVR: Text-video retrieval, VC: video captioning, VQA: video question answering, TF: Transformer, LLM: large language model). From left to right, our legend table follows the order: pre-Transformer (Pre-TF), task-specific Transformer, multi-task Transformer, and LLM-augmented architectures.

level, video captioning requires mapping salient entities and events in a video to a coherent language description, make it a more difficult task than text-video retrieval. At the highest level, VideoQA demands reasoning over both modalities to generate accurate answers. Each level further extends to more fine-grained or inferential variants. In particular, video moment retrieval, or temporal grounding, extends text-video retrieval; dense video captioning (Zhou et al., 2018b) and video chapter generation (Yang et al., 2023b) extend captioning; and inference-focused VideoQA (Xiao et al., 2021b; Li et al., 2022b) extends VideoQA. These advanced tasks pose greater challenges and are increasingly central to advancing video research towards human-level intelligence (Fei-Fei and Krishna, 2022).

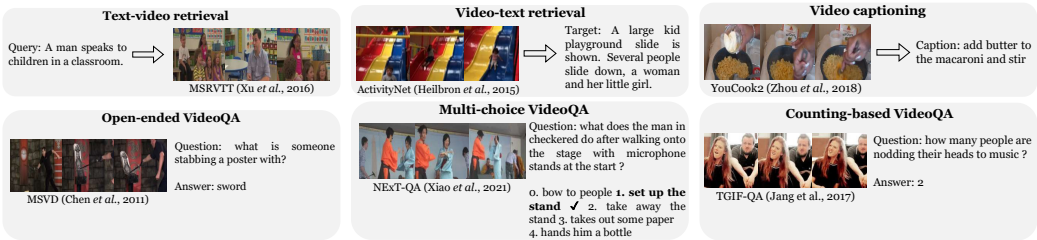


Figure 2.3: Illustration of text-video retrieval, video captioning, and video question answer (videoQA) tasks.

## 2.2 Challenges of Video Understanding

The discussed video understanding tasks present unique challenges compared with image-language understanding, since a video incorporates an additional temporal channel. We summarize their important challenges as follows:

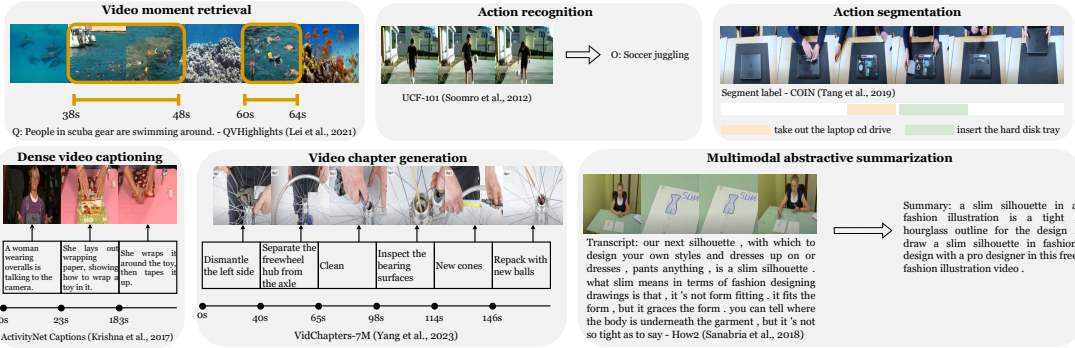


Figure 2.4: More illustration of video moment retrieval, action recognition, action segmentation, dense video captioning, video chapter generation, and multimodal abstractive summarization tasks.

**Intra-modal and cross-modal interaction.** While intra-modal interaction modeling within language can be directly taken from image-language understanding, intra-modal interaction modeling within video is different since it jointly consists of spatial interaction and temporal interaction. Spatial interaction delves into the relationships among pixels, patches, regions, or objects within an individual frame, whereas temporal interaction captures sequential dependencies among video frames or video segments. Longer video durations amplify the complexity of temporal modeling by necessitating the recognition of more objects and events in a higher number of video frames (Yu et al., 2020; Lin et al., 2022b), and reasoning their long-term dependencies Zhao et al. (2018). Particular video domains, such as egocentric videos, also complicate temporal interaction modeling, as objects undergo drastic appearance and disappearance dynamics over time, posing challenges in capturing their relationships (Bansal et al., 2022; Tang et al., 2023).

Given the larger semantic gap for video-language compared to image-language, cross-modal interaction plays a crucial role in video understanding. The interaction between visual and language features is pivotal for aligning the semantics of video and text query to associate them for text-video retrieval, or identifying relevant parts to answer the question and writing the caption in videoQA and video captioning, respectively. In addition, incorporating the interaction of motion and language features can mitigate the extraction of noisy information from videos (Ding et al., 2022). Lin et al. (2022b) also discover that the interaction between audio and language features can compactly capture information related to objects, actions,

and complex events, compensating for sparsely extracted video frames.

**Cross-domain adaptation.** Given the infinitude of online videos, that our video understanding model will encounter testing scenarios which are identically distributed to our training data is an impractical assumption. Moreover, with the advent of LLM-augmented models that can tackle a variety video understanding tasks (Li et al., 2023c,g), it is currently more advisable to train a model that can effectively adapt to multiple tasks and domains than to obtain a model which specializes in a specific understanding task. Furthermore, since a video can be considered as a sequence of images, training a model on video-text data is more computationally expensive than image-text data. Combined with the large-scale of recent video understanding models (Jiang et al., 2022a; Yang et al., 2022a), there is also a need to devise an efficient fine-tuning strategy to save the computational cost of fine-tuning these models.

**Data preparation.** Although Lei et al. (2021c) only use image-text data to train models for video understanding tasks, in essence, video-text data are crucial for the effectiveness of these models. In particular, compared with a static image, a video offers richer information with diverse spatial semantics with consistent temporal dynamics (Zhuang et al., 2023). As such, Cheng et al. (2023) find that training on videos outperforms training on images, but jointly training on both data achieves the best performance. As additional evidence, Yuan et al. (2023) shows that video-pretrained models outperform image-pretrained models in classifying motion-rich videos. However, video-text data takes up more storage cost than image-text data since a video comprises multiple images as video frames. Moreover, annotating a video is also more time-consuming and labor-intensive than annotating an image (Xing et al., 2023). Therefore, video understanding models have been limited by the small size of clean paired video-text corpora in contrast to billion-scale image-text datasets (Zhao et al., 2023b). Various efforts (Zhao et al., 2023b; Xing et al., 2023) have been put into devising efficient and economical methods to curate and label video-text data.

**Addressing challenges.** These identified challenges encompass three critical perspectives: model architecture, model training, and data preparation in the field of video understanding. In general, there should be a synergistic relationship among these components. Specifically, model architecture should be designed to effectively

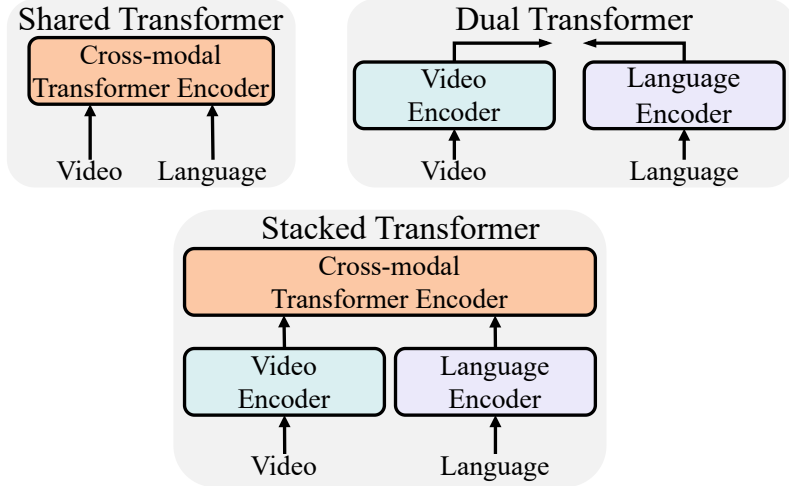


Figure 2.5: Illustration of Transformer-based architectures.

capture video-language interactions. Concurrently, model training should be tailored to enable the architecture to adapt to target domains with their captured video-language interactions. Lastly, data preparation plays a pivotal role in shaping model training, which in turn significantly impacts the development of an efficacious model architecture.

## 2.3 Model Architecture for Video- Language Understanding

Addressing the challenge of intra-modal and cross-modal interaction is the key aim in designing video understanding model architectures, which can be divided into **Pre-transformer** and **Transformer-based architectures**. The advent of LLMs with remarkable zero-shot capability in addressing multiple tasks led to the design of **LLM-augmented architectures** that exhibit cross-domain adaptation ability to various video understanding tasks.

### 2.3.1 Pre-Transformer Architecture

Pre-transformer architectures typically comprise unimodal video and language encoders for implementing intra-modal interactions and cross-modal encoders for cross-modal interactions.

**Unimodal encoders.** A video encoder often encodes raw videos by extracting

frame appearance and clip motion features as spatial and temporal representations, respectively. As each video frame can be considered as a single image, various works have utilized CNNs to extract spatial representations (Simonyan and Zisserman, 2014; Feichtenhofer et al., 2016; Zhao et al., 2017b). For temporal representations, the sequential nature of RNN makes it a popular choice in pre-transformer architectures (Yang et al., 2017; Zhao et al., 2017a; Venugopalan et al., 2015; Wang et al., 2019a). Furthermore, 3D CNNs with an additional temporal channel inserted to 2D CNN have also demonstrated effectiveness in extracting spatio-temporal representations (Tran et al., 2017; Carreira and Zisserman, 2017). In addition to CNN and RNN, Chen et al. (2018), Gay et al. (2019), and Wei et al. (2017) also build graphs to incorporate intra-modal relationships among video entities such as video segments or visual objects. These graph-structured works emphasize the reasoning ability of the model architecture.

A common framework of language encoder is to extract pre-trained word embeddings such as word2vec (Kaufman et al., 2016; Yu et al., 2017) or GloVe (Torabi et al., 2016; Kiros et al., 2014), then proceed with RNN-based modules such as LSTM or GRU. Such framework is taken from language model architectures before the era of Transformer.

**Cross-modal encoders.** Gao et al. (2017) and Zeng et al. (2017) apply element-wise multiplication to fuse the global video and question representations for video question answering. It demonstrates the advantage of a simple operation for video-language fusion. Attention has also been used to model video-language relations, in order to identify salient parts in video and language sentence (Yuan et al., 2019), or to refine the representation of the video based on the language question (Xu et al., 2017). Pre-transformer video-language works have also combined attention with a wide variety of techniques, including hierarchical learning (Baraldi et al., 2017), memory networks (Fan et al., 2019), and graph networks (Xiao et al., 2022a; Wei et al., 2023).

### 2.3.2 Transformer-based Architecture

Developed based on the self-attention mechanism, which exhaustively correlates every pair of input tokens with each other, Transformer-based architecture has the

capacity to capture long-term dependencies and learn from web-scale data. It has demonstrated remarkable performance in many video-language tasks. Similar to the pre-transformer architecture, the Transformer-based framework also comprises unimodal encoders and cross-modal encoders to model intra-modal and cross-modal interactions, respectively. For unimodal encoders, several works find vision transformer for video encoding and BERT encoder for language encoding outperform RNN- and CNN-based encoding (Fu et al., 2021; Bain et al., 2021; Seo et al., 2022). We then summarize fundamental types of Transformer-based architectures and illustrate them in Figure 2.5.

**Shared Transformer.** Motivated by the success of Transformer in language modeling (Devlin et al., 2018), Akbari et al. (2021) and Wang et al. (2023a) construct a shared Transformer encoder for video understanding. Their encoder architectures receive the concatenation of visual patches and language tokens, then jointly calculate their interactions in a BERT-based manner. Akbari et al. (2021) additionally incorporate modality embeddings which comprise three values to denote three kinds of input modalities, *i.e.* (video, audio, text).

**Stacked Transformer.** Li et al. (2020) reveals that a shared Transformer encoder is weak in modeling temporal relations between videos and texts. To address this problem, they introduce a stacked Transformer architecture, with a hierarchical stack consisting of unimodal encoders to encode video and language inputs separately, and then a cross-modal Transformer to compute video-language interactions. A multitude of video understanding works follow such design to stack a cross-modal Transformer-based encoder above unimodal encoders (Fu et al., 2023; Li et al., 2023d; Lei et al., 2021c; Wei et al., 2022; Luo et al., 2022; Nie et al., 2022; Wei et al., 2024). To perform video captioning, Seo et al. (2022) and Luo et al. (2020) further insert a causal Transformer-based decoder that generates language tokens based on the encoded cross-modal representations.

**Dual Transformer.** Dual Transformer architectures have been favored for text-video retrieval (Luo et al., 2022; Bain et al., 2021, 2022; Lin et al., 2022b; Xue et al., 2022b). These architectures use two Transformer encoders to encode video and language separately, yielding global representations for each input modality, then applying simple operations such as cosine similarity to compute cross-modal interaction. Such a separate encoding scheme enables them to mitigate the com-

putational cost of computing pairwise interactions between every pair of video and language inputs. They have accomplished not only efficiency but also effectiveness in text-video retrieval problems.

### 2.3.3 LLM-Augmented Architecture

Large language models (LLMs) have achieved impressive results in simultaneously tackling multiple NLP tasks. Recent efforts have sought to apply LLMs for video understanding to extend its cross-domain adaptation ability to video-language settings (Chen et al., 2023; Li et al., 2023c). These efforts can be categorized into two approaches. The first approach employs LLM as a controller and video understanding models as helping tools. The controller will call the specific tool according to the language input instruction. The second approach utilizes LLM as the output generator and seeks to align video pre-trained models to the LLM. For video understanding, since the second approach dominates the first one with a long list of recent works (Chen et al., 2023; Li et al., 2023c; Chen et al., 2023; Li et al., 2023g; Zhang et al., 2023b; Maaz et al., 2023), we review them as follows:

**LLM as Output Generator.** The framework comprises a visual encoder, a semantic translator, and an LLM as the output generator. Regarding visual encoder, LLM-augmented architectures often use vision transformer and CNN models of the pre-Transformer and Transformer-based architectures (Chen et al., 2023). Since an LLM has never seen a video during its training, a semantic translator is needed to translate the visual semantics of a video to the LLM’s semantics. For the translator, Video-LLaMA (Zhang et al., 2023b) and VideoChat (Li et al., 2023c) implement a Q-Former as a Transformer-based module that uses a sequence of query embeddings that interact with visual features of the video to extract informative video information. Instead of Q-Former, VideoLLM (Chen et al., 2023), Video-ChatGPT (Maaz et al., 2023), and LLaMA-Vid (Li et al., 2023g) find that a simple linear projection that projects visual features into the LLM’s input dimension can achieve effective performance. Subsequently, these visual-based query embeddings or projected visual features are combined with the language instruction to become the input fed to the LLM to produce the final output.

### 2.3.4 Architecture Analysis

In Figure 2.2, we show the timeline of video understanding methodologies, categorized according to our defined architecture taxonomy and their affiliated downstream tasks. The evolution of pre-transformer models aligns with our hierarchy of video understanding levels, *i.e.* models for video captioning generally appear subsequent to those for text-video retrieval, followed by the development of videoQA models. Owing to their impressive capacity, Transformer-based models capable of addressing multiple tasks have been introduced concurrently with task-specific Transformer frameworks. Recently, large language models (LLMs) have gained prominence for their superior in-context learning ability, enabling them to handle diverse tasks without fine-tuning. Consequently, new LLM-augmented architectures have emerged to utilize this capability to address multiple understanding tasks.

Among Transformer-based architectures, the dual Transformer stands out as the most effective for text-video retrieval, adeptly associating global semantics of video and language modality. On the other hand, the stacked Transformer architecture excels at facilitating intra-modal and cross-modal interactions through its specialized unimodal and cross-modal encoders. These encoders are particularly efficient at correlating video content with the question in videoQA. Additionally, for video captioning, cross-modal encoder plays a crucial role in translating video content into textual descriptions. Recent LLM-augmented models have begun to outperform Transformer-based architectures in videoQA, signalling their potential as the next frontier in video understanding research. We provide full details of performance in text-video retrieval, video captioning, and videoQA tasks in Table 2.1, 2.2, and 2.3, respectively.

## 2.4 Model Training for Video Understanding

Model training seeks to address the cross-domain adaptation ability of video understanding models. To achieve this goal, pre-training strategies have been devised to gain world knowledge that generalizes across multiple scenarios, then task-specific fine-tuning is conducted to specifically improve downstream task performance.

Methods	Model architecture	Video	Text	R@1	R@5	R@10
VSE-LSTM (Kiros et al., 2014) C+LSTM+SA-FC7 (Torabi et al., 2016) EITanque (Kaufman et al., 2016) SA-G+SA-FC7 (Torabi et al., 2016) CT-SAN (Yu et al., 2017) JSFusion (Yu et al., 2018)	Pre-TF	ConvNet/OxfordNet	GloVe-LSTM	3.8	12.7	17.1
		VGG	GloVe-LSTM	4.2	12.9	19.9
		VGG	word2vec-LSTM	4.7	16.6	24.1
		VGG	GloVe	3.1	9.0	13.4
		RN	word2vec-LSTM	4.4	16.6	22.3
		RN	GloVe-LSTM	10.2	31.2	43.2
		Shared TF	Linear	37.9	68.1	77.1
		Shared TF	S3D	28.1	55.5	67.4
All-in-one (Wang et al., 2023a) VLM (Xu et al., 2021) DeCEMBERT (Tang et al., 2021) ActBERT (Zhu and Yang, 2020) VIOLET (Fu et al., 2023) VindLU (Cheng et al., 2023) HERO (Li et al., 2020) MV-GPT (Seo et al., 2022) CLIP2TV (Gao et al., 2021b) CLIP-ViP (Xue et al., 2022a) CLIP4Clip (Luo et al., 2022)	Faster-RCNN	RN	BT	17.5	44.3	58.6
		Stacked TF	BT	16.3	42.8	56.9
		Stacked TF	VS-TF	37.2	64.8	75.8
		Stacked TF	ViT	BT	<u>48.8</u>	<u>72.4</u>
		Stacked TF	RN+SlowFast	BT	16.8	43.4
		Stacked TF	ViViT	BT	37.3	65.5
		Dual TF	ViT	CLIP-text	32.4	58.2
		Dual TF	ViT	CLIP-text	<b>49.6</b>	<b>74.5</b>
		Dual TF	ViT	CLIP-text	44.5	71.4
		Dual TF	ViT	CLIP-text	44.5	71.4
		Dual TF	ViT	CLIP-text	44.5	71.4
		Dual TF	ViT	CLIP-text	44.5	71.4
		Dual TF	ViT	CLIP-text	44.5	71.4
		Dual TF	ViT	CLIP-text	44.5	71.4

Table 2.1: Performance on text-video retrieval. (Pre-TF: Pre-transformer, Shared TF: Shared Transformer, Stack TF: Stack Transformer, Dual TF: Dual Transformer, RN: ResNet/ResNeXt (He et al., 2016; Xie et al., 2017), ViT: Vision Transformer (Dosovitskiy et al., 2020), BT: BERT (Devlin et al., 2018), ViViT: Video Vision Transformer (Arnab et al., 2021)). We report recall at rank 1 (R@1), 5 (R@5), and 10 (R@10). We choose MSRVTT as one of the most popular datasets for text-video retrieval.

### 2.4.1 Pre-training for Video Understanding

In this section, we mainly summarize pre-training strategies for video understanding models into three groups:

**Language-based pre-training.** The most popular language-based pre-training task is masked language modeling (MLM) (Lei et al., 2021c; Sun et al., 2019; Cheng et al., 2023), which randomly masks a portion of words in the language input and trains the model to predict the masked words based on unmasked language words and video entities. Instead of masking a portion of words, UniVL (Luo et al., 2020) and VICTOR (Lei et al., 2021a) discover that masking the whole language modality benefits video captioning task. MLM can be combined with other language-based pre-training task, *e.g.* masked sentence order modeling which is to classify the original order of the shuffled language sentences (Lei et al., 2021a).

**Video-based pre-training.** Video-based pre-training tasks help video-language models capture contextual information in the video modality. As a counterpart of MLM, masked video modeling (MVM) trains the model to predict the portion of masked video entities based upon the unmasked entities and language words. The continuous nature of videos leads to different choices of video entities, such as frame patches (Li et al., 2020) or video frames (Fu et al., 2021). In terms of

Methods	Model architecture	Video	BLEU-4	METEOR	CIDEr
TA (Yao et al., 2015)	Pre-TF	Video: 3D-CNN	36.5	25.7	-
h-RNN (Yu et al., 2016)		Video: VGG	36.8	25.9	-
MFATT (Long et al., 2018)		Video: RN+C3D	39.1	26.7	-
CAT-TM (Long et al., 2018)		Video: RN+C3D	36.6	25.6	-
NFS-TM (Long et al., 2018)		Video: RN+C3D	37.0	25.9	-
Fuse-TM (Long et al., 2018)		Video: RN+C3D	37.5	25.9	-
MARN (Pei et al., 2019)		Video: RN	-	-	46.8
Res-ATT (Li et al., 2019)		Video: RN	37.0	26.9	40.7
DenseLSTM (Zhu and Jiang, 2019)		Video: VGG	38.1	27.2	42.8
VIOLET (Fu et al., 2023)		VS-TF	-	-	58.0
LAVENDER (Li et al., 2023d)	Stacked TF	VS-TF	-	-	57.4
VLAB (He et al., 2023)		EVA-G	54.6	33.4	74.9
UniVL (Luo et al., 2020)		S3D	41.8	28.9	50.0
MV-GPT (Seo et al., 2022)		ViViT	48.9	38.7	60.0
CLIP-DCD (Yang et al., 2022b)		ViT	48.2	30.9	64.8
DeCEMBERT (Tang et al., 2021)		RN	45.2	29.7	52.3
mPLUG-2 (Xu et al., 2023a)		ViT	57.8	34.9	80.3

Table 2.2: Performance on video captioning. (Pre-TF: Pre-transformer, Stacked TF: Stacked Transformer, RN: ResNet/ResNeXt (He et al., 2016; Xie et al., 2017), ViViT: Video Vision Transformer (Arnab et al., 2021), EVA-G: Fang et al. (2023)). We report BLEU-4 and METEOR, which are two popular metrics for language generation. We choose MSRVTT as one of the most popular datasets for video captioning.

the training objective, Li et al. (2020) use L2 regression loss to train the model to predict pre-trained features of the masked video frames extracted by ResNet and SlowFast models, while Fu et al. (2021) use cross-entropy loss to train the model to predict the masked visual tokens, which are quantized by a variational autoencoder from visual frame patches.

**Video-text pre-training.** Video-text pre-training is crucial for a model to capture video-language relation. Xue et al. (2022b), Gao et al. (2021b), and Bain et al. (2021) utilize a framework of video-text contrastive learning to produce close representations for semantically similar video and language inputs. These works focus on creating a joint semantic space that aligns separate representations of video and language. Instead of separate representations, Tang et al. (2021), Fu et al. (2021), and Li et al. (2023d) enable video and textual representations to interact with each other and use a single token to represent the cross-modal input, which is forwarded to predict whether the video-text pair is matched or not. In these two pre-training frameworks, not only video-text data but also image-text data are utilized during pre-training, in which an image is considered as a video with a single frame.

Contrastive learning has revealed promising results (Lin et al., 2022b; Gao et al., 2021b; Xue et al., 2022b; Nguyen et al., 2022; Nguyen and Luu, 2021; Nguyen et al.,

Methods	Architecture	Video	Text	Dataset	
				MSRVTT	MSVD
E-MN (Xu et al., 2017)	Pre-TF	VGG + C3D	GloVe-LSTM	30.4	26.7
QueST (Jiang et al., 2020)		RN + C3D	GloVe-LSTM	40.0	-
HME (Fan et al., 2019)		RN/VGG + C3D	GloVe-GRU	34.6	36.1
HGA (Jiang and Han, 2020)		RN/VGG + C3D	GloVe-GRU	33.0	33.7
ST-VQA (Jang et al., 2019)		RN+C3D	GloVe-LSTM	35.5	34.7
PGAT (Peng et al., 2021)		Faster-RCNN	GloVe-LSTM	38.1	39.0
HCRN (Le et al., 2020)		RN	GloVe-LSTM	35.6	36.1
HQGA (Xiao et al., 2022a)		Faster-RCNN	BERT-LSTM	38.6	41.2
All in one (Wang et al., 2023a)		Shared TF	Linear	44.3	47.9
LAVENDER (Li et al., 2023d)	Stacked TF	VS-TF	BT	45.0	56.6
DeCEMBERT (Tang et al., 2021)	Stacked TF	RN	BT	37.4	-
VindLU (Cheng et al., 2023)	Stacked TF	ViT	BT	44.6	-
VIOLET (Fu et al., 2023)	Stacked TF	VS-TF	BT	44.5	54.7
ClipBERT (Lei et al., 2021c)	Stacked TF	CLIP-text	BT	37.4	-
VGT (Xiao et al., 2022b)	Dual TF	Faster-RCNN	BT	39.7	-
CoVGT (Xiao et al., 2023b)	Dual TF	Faster-RCNN	BT	40.0	-
LLaMA-Vid (Li et al., 2023g)	LLM-Augmented	EVA-G	Vicuna	58.9	70.0

Table 2.3: Performance on videoQA. (Pre-TF: Pre-transformer, Dual TF: Dual Transformer, RN: ResNet/ResNeXt (He et al., 2016; Xie et al., 2017), BT: BERT (Devlin et al., 2018), VS-TF: Video Swin Transformer (Liu et al., 2021), EVA-G: Fang et al. (2023)). We report accuracy of the methods. We choose MSRVTT and MSVD as two of the most popular datasets for videoQA.

2024e,a, 2023a; Wu et al., 2023a, 2024, 2022a). MLM has contributed to enhancing VideoQA since the task resembles MLM in predicting the language word given a video-language pair (the question is the language input in videoQA). Compared to these pre-training strategies, MVM does provide performance gain for video understanding but its gain is less significant. For more details about pre-training, please refer to (Cheng et al., 2023).

## 2.4.2 Fine-tuning for Video Understanding

Task-specific fine-tuning is commonly used by pre-Transformer architectures to train from scratch since these models do not have sufficient parameter capacity to learn generalizable features through pre-training. It is also widely adopted by Transformer-based architectures to improve the performance for a specific downstream task. Moreover, LLM-augmented architectures also utilize instruction tuning as a variant of fine-tuning, to adapt from the visual and audio spaces to the LLM language space.

**Fine-tuning strategies.** Normally, all of the model parameters are updated during fine-tuning (Gao et al., 2017; Xu et al., 2019; Anne Hendricks et al., 2017; Nguyen et al., 2023c; Wu et al., 2023b). However, in cases computational resources or

training data are limited, only adaptation layers such as low-rank adapters (Pan et al., 2022; Yang et al., 2022a; Nguyen et al., 2024c) or learnable prompt vectors (Ju et al., 2022) are fine-tuned to reduce training cost or prevent overfitting. Such risks also apply for LLM-augmented architectures discussed in Section 2.3.3, since LLMs exhibit a billion scale of parameters, thus incurring excessively huge cost if full fine-tuning is conducted. For such models, Zhang et al. (2023b) and Li et al. (2023g) design a two-stage instruction tuning strategy which only fine-tunes the semantic translator. The first stage trains the model to generate the textual description based on the combined video and the language instruction, in order to align visual representations extracted by the visual encoder with the language space of LLM. The second stage is often performed on small-scale video-text pairs manually collected by the authors to further tailor the output features of the translator towards the target domains.

## 2.5 Data Perspective for Video Understanding

In this section, we analyze data preparation approaches for video understanding models, and provide details of the datasets in Table 2.4.

### 2.5.1 Data curation

**Manual collection.** To curate video-language data, multiple works search for publicly available online videos, which exhibit a wide diversity of content. Video-language datasets with online videos are mostly aimed for pre-training models to learn generalizable knowledge, *e.g.* HowTo100M (Miech et al., 2019) and YT-Temporal-180M (Zellers et al., 2021), or they can also be used for fine-tuning, *e.g.* MSRVTT (Xu et al., 2016) and YouCook2 (Zhou et al., 2018a). To satisfy a certain requirement, videos different from the online ones can be inherited from existing datasets, *e.g.* Xiao et al. (2021b) utilize 6,000 videos from VidOR dataset and (Li et al., 2022b) inherit 546,882 videos from Kinetics-700 since they describe scenes of daily life and real world, respectively. Apart from making use of existing datasets' and online videos, videos can also be recorded by human annotators to enable quality control (Goyal et al., 2017; Damen et al., 2022b).

**Data augmentation.** Rather than manually collecting videos from external sources,

Dataset	Video source	Annotation	Tasks	#Videos/#Routes
MSVD (Chen and Dolan, 2011)	YouTube videos	Manual	TVR, VC, VideoQA	1.9K
MSRVT (Xu et al., 2016)	Web videos	Manual	TVR, VC, VideoQA	7.2K
ActivityNet (Yu et al., 2019)	YouTube videos	Manual	AL, TVR, VC, VMR	5.8K
FIBER (Castro et al., 2022b)	VaTeX (Wang et al., 2019b)	Manual	VC, VideoQA	28K
WildQA (Castro et al., 2022a)	YouTube videos	Manual	VideoQA	0.4K
NExT-QA (Xiao et al., 2021b)	VidOR Shang et al. (2019)	Manual	VideoQA	5.4K
CausalVid-QA (Li et al., 2022b)	Kinetics-700 (Carreira et al., 2019)	Manual	VideoQA	26K
HowTo100M (Miech et al., 2019)	YouTube videos	Auto	PT	1.2M
HD-VILA-100M (Xue et al., 2022a)	YouTube videos	Auto	PT	3.3M
YT-Temporal-180M (Zellers et al., 2021)	YouTube videos	Auto	PT	6M
TGIF-QA (Jang et al., 2017)	Animated GIFs	Manual	VideoQA	71K
TGIF-QA-R (Peng et al., 2021)	TGIF-QA (Jang et al., 2017)	Manual, Auto	VideoQA	71K
DiDeMo (Anne Hendricks et al., 2017)	YFCC100M (Thomee et al., 2016)	Manual	TVR	11K
YouCook2 (Zhou et al., 2018a)	YouTube videos	Manual	TVR, VC	2K
HMDB-51 (Kuehne et al., 2011)	Web videos	Manual	TVR, AR	6.8K
Kinetics-400 (Kay et al., 2017a)	YouTube videos	Manual	AR	306K
Kinetics-600 (Carreira et al., 2018)	Kinetics-400 (Kay et al., 2017a)	Manual	AR, VG	480K
Kinetics-700 (Carreira et al., 2019)	Kinetics-600 (Carreira et al., 2018)	Manual	AR	650K
VaTeX (Wang et al., 2019b)	Kinetics-600 (Carreira et al., 2018)	Manual	TVR, VC	41K
TVR (Lei et al., 2020b)	TVQA (Lei et al., 2018)	Manual	VMR	22K
How2B (Li et al., 2020)	HowTo100M (Miech et al., 2019)	Manual	VMR	22K
How2QA (Li et al., 2020)	HowTo100M (Miech et al., 2019)	Manual	VideoQA	22K
YouTube Highlights (Sun et al., 2014)	YouTube videos	Manual	VMR	0.6K
TACoS (Regneri et al., 2013)	MPII Composites (Rohrbach et al., 2012)	Manual	VMR	0.1K
QVHighlights (Lei et al., 2021b)	YouTube vlogs	Manual	VMR	10K
TVSum (Song et al., 2015)	YouTube videos	Manual	VMR	50
ViTT (Huang et al., 2020)	YouTube-8M (Abu-El-Haija et al., 2016)	Manual	VMR	5.8K
VidChapters-7M (Yang et al., 2023a)	YT-Temporal-180M (Zellers et al., 2021)	Auto	VC, VMR	817K
VideoCC3M (Nagrani et al., 2022)	Web videos	Auto	PT	6.3M
WebVid-10M (Bain et al., 2021)	Web videos	Auto	PT	10.7M
COIN (Tang et al., 2019)	YouTube videos	Manual	AS	12K
CrossTask (Zhukov et al., 2019)	YouTube videos	Manual	AR	4.7K
Alivil-10M (Lei et al., 2021a)	E-commerce videos	Auto	PT	10M
LSMDC (Rohrbach et al., 2015)	British movies	Manual	TVR	72
EK-100 (Damen et al., 2022b)	Manual	Manual	AR, AL	7K
SSV1 (Goyal et al., 2017)	Manual	Manual	AR	108K
SSV2 (Goyal et al., 2017)	Manual	Manual	AR	221K
Moments in Time (Monfort et al., 2019)	Web videos	Manual	AR	1M
InternVid (Wang et al., 2023c)	YouTube videos	Auto	PT	7.1M
How2 (Sanabria et al., 2018)	YouTube videos	Auto	VC	13.2K
WTS70M (Stroud et al., 2020)	YouTube videos	Auto	PT	70M
Charades (Gao et al., 2017)	Manual	Manual	AR, VMR, VideoQA	10K

Table 2.4: Video understanding datasets in the literature. (VMR: Video moment retrieval, TVR: text-video retrieval, VC: video captioning, AL: action localization, AR: action recognition, AS: action segmentation, VG: video generation, PT: pre-training).

Xing et al. (2023) and Jiang et al. (2022c) explore data augmentation techniques which are particularly designed for videos. In detail, their TubeTokenMix mixes two videos in which the mixing coefficient is defined upon the temporal dimension, and their temporal shift randomly shifts video frame features backward or forward over the temporal dimension. These techniques outperform standard augmentation approaches for image data, such as CutMix (Yun et al., 2019), Mixup (Zhang et al., 2017), and PixMix (Hendrycks et al., 2022).

### 2.5.2 Label annotation

**Manual annotation.** Several works (Li et al., 2022b; Lei et al., 2021b; Xiao et al., 2021b) use human annotators since they provide high-quality labels. However, such

approach is expensive, particularly when dealing with video data. For example, annotating QVHighlights dataset (Lei et al., 2021b) costs approximately \$16,000 for 10K videos and 3 months to complete. Similarly, NExT-QA (Xiao et al., 2021b) needs 100 undergraduate students and 1 year to annotate only 5K videos.

**Automatic generation.** Directly taking language transcripts of YouTube videos as textual labels could reduce annotation cost (Miech et al., 2019; Xue et al., 2022a; Zellers et al., 2021). However, these labels have been shown to be grammatically incorrect and temporally misalign with the video content (Tang et al., 2021). Motivated by the success of LLMs, Zhao et al. (2023b) train a system consisting of a TimeSformer-L visual encoder and a GPT-2XL decoder to write dense captions for videos. Moreover, Li et al. (2023c) use GPT-4 to generate summaries for movie synopses.

## 2.6 Future Directions

**Fine-grained understanding.** Existing methods excel at video understanding at a coarse-grained level, enabling effective responses to questions like “*what is*” or the recognition of global events without significant difficulty (Xiao et al., 2021b). Nevertheless, limiting comprehension to this coarse level could hinder practical utility of existing systems. In real-world scenarios, a user might require a precise timestamp and location of an object within a video (Jiang et al., 2022b), or request the AI agent to forecast potential alternative events, which is a common need in predictive analytics (Xiao et al., 2021b; Li et al., 2022b). These tasks necessitate an advanced understanding and inference capability regarding the causal and temporal relationships present in a video. At present, models exhibit a constrained visio-linguistic capacity to engage in temporal reasoning, categorizing them as image-sequence-and-language models rather than video-language models (Kesen et al., 2023). Therefore, future research in this direction deserves more attention and exploration.

**Long-form video understanding.** Current understanding systems have demonstrated remarkable performance on short video clips lasting several seconds. However, they tend to struggle when switching to long-form videos which last several minutes or hours. To enhance the applicability of these systems, it is essential to

enhance their capability of understanding long-form videos. Current approaches mainly feature reducing computational cost through architectures more efficient than Transformer-based ones such as state space models (Yang et al., 2024b; Li et al., 2024a), which can be considered as linear RNN with specifically designed fixed weights, or compensating sparsely extracted video frames with additional information (Lin et al., 2022b). In general, how to effectively model long-form videos and adapt them to the joint context with language deserves more attention.

**Trustworthiness of video understanding models.** Although modern video understanding systems have demonstrated remarkable performance, their black-box nature undermines our trust to deploy them. In particular, we still do not precisely understand what part of the video a videoQA model looks at to answer the question (Li et al., 2022e), or how video and language semantic information flows into the common representation space of the video retrieval model (Jia et al., 2022b). Furthermore, adversarial noise sensitivity or hallucination of video understanding models are also open problems. Future trustworthiness benchmarks such as (Xiao et al., 2023a; Wang et al., 2021a) for video understanding are of great significance towards practical systems.

# Chapter 3

## MAMA: Meta-optimized Angular Margin Contrastive Framework for Video-Language Representation Learning

### 3.1 Introduction

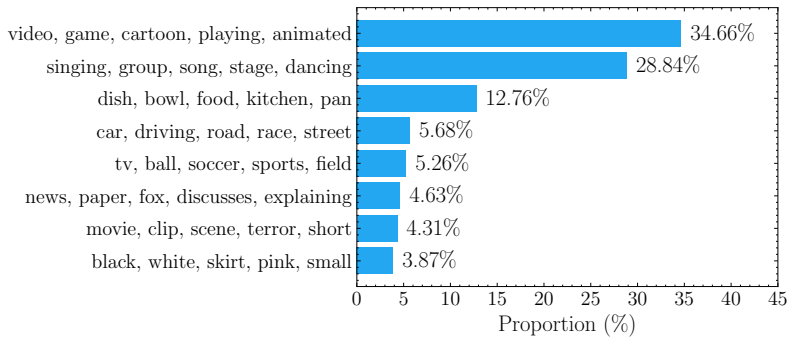
Learning vision and language representations has advanced state-of-the-art across multiple cross-modal tasks, such as video question answering (VideoQA) (Lei et al., 2021c; Li et al., 2020; Fu et al., 2021, 2023; Cheng et al., 2023; Seo et al., 2022; Wang et al., 2023a) and text-video retrieval (Zhu and Yang, 2020; Tang et al., 2021; Xu et al., 2021; Lei et al., 2022; Li et al., 2023d; Wang et al., 2022a; Buch et al., 2022). The success of vision-language representation learning mainly results from the effectiveness of contrastive learning, which projects video and text inputs into a common latent space based on their semantic similarities.

Data quality stands at the forefront of influencing the efficacy of video-language representation learning, particularly through its cleanliness and diversity, which are pivotal in optimizing model performance and bolstering generalization capabilities (Zhao et al., 2023b). Within this context, we pinpoint two interrelated issues that significantly impact the *cleanliness* and *diversity* of video-text data: (1) the imperfection in alignment, characterized by a scarcity of fine-grained details, and (2) the imbalance among the concepts of data samples. First, a video and its textual description commonly does not perfectly align with each other, *e.g.* the description may omit certain details in the video, such as the green grass on a soccer field or

Figure 3.1: Examples of video inputs and their textual descriptions.



Figure 3.2: Topic distribution of the MSRVTT dataset. We use Latent Dirichlet Allocation (LDA) to extract topics from manually annotated descriptions of videos.



the pink flowers at the background in two videos of Fig. 3.1. As such, aggressively minimizing a contrastive loss to pull video and language representations together might result in distorted video-language representations that do not closely capture the semantic similarity of video-text pairs, thus compromising the interpretive video-language understanding. Second, as an example, Fig. 3.2 shows a majority of video-text pairs in the well-known MSRVTT dataset denote the video game or singing topic (the topic bars), while a minority of them describe the fashion topic (the bottom bar). This might skew the model’s exposure towards certain topics at the expense of others, undermining the model’s ability to perform uniformly across a broad spectrum of subjects (Li et al., 2022a). Addressing these intertwined challenges is crucial for advancing video-language representation learning and facilitating more effective video-language understanding.

Our method, called **MAMA**: Meta-optimized Angular MArgin Contrastive Learning, subtracts a margin between a positive video and text sample in the angular space. Our mathematical derivation shows that the subtracted margin can decay the gradient norm, thus providing a regularization effect to constrain positive but imperfectly aligned samples from reaching perfect similarity. For the imbalance issue, to enable the network to dynamically adjust its focus during training, MAMA introduces a sample reweighting strategy that maps loss values to sample weights.

A natural idea is to assign higher weights to larger losses to emphasize minority classes for which the network is likely to make mistakes (Sun et al., 2007; Malisiewicz et al., 2011). However, with respect to the imperfect alignment issue, it is advisable to assign higher weights to smaller losses, as there is a greater chance that these samples better align with each other, hence forming cleaner samples which the network should focus on Zhang and Sabuncu (2018); Wang et al. (2017). To avoid the exhaustive effort in manually specifying a weighting function and enhance the function generalization, we parameterize our weighting function as a multi-layer perceptron (MLP) as theoretically a universal approximator for any continuous function (Csáji et al., 2001), and use a small unbiased validation set (meta-data) to train the MLP.

Moreover, to further enhance the diversity in video-language representation learning, MAMA utilizes off-the-shelf large vision-language model (LVLM) to augment downstream video-text data. In particular, given an additional video input, we adopt the density peak-based clustering approach to extract its key frames, then concatenate the extracted frames into one grid image, and forward the image with a relevant input prompt to obtain the text pairing. Combined with the LVLM-augmented video-text data, MAMA considerably outperforms previous state-of-the-art video-language representation learning methods on standard MSRVTT, DiDeMo, ActivityNet, TGIF-QA-R, NExT-QA, and Causal-VidQA datasets.

## 3.2 MAMA Framework

In this section, we explain MAMA, the meta-optimized angular margin contrastive framework with our augmentation strategy for video-language representation learning. We provide an overall illustration of MAMA in Figure 3.3.

### 3.2.1 Video-Language Representation Learning

We are given a corpus of video data, in which each video  $\mathbf{v}_i$  is attached with a textual description  $\mathbf{t}_i$  and possibly a label  $y_i$ . In the beginning, we embed the video input  $\mathbf{v}_i$  into a sequence of visual representations  $\mathbf{V}_i^f = \{\mathbf{h}_{i,j}^f\}_{j=1}^{N_{\mathbf{v}_i}}$ , where  $N_{\mathbf{v}_i}$  is the number of randomly sampled video frames in  $\mathbf{v}_i$ . We also embed the textual description into a sequence of representations  $\mathbf{T}_i^w = \{\mathbf{h}_{i,j}^w\}_{j=1}^{N_{\mathbf{t}_i}}$ , where  $N_{\mathbf{t}_i}$  is the number of words in  $\mathbf{t}_i$ .

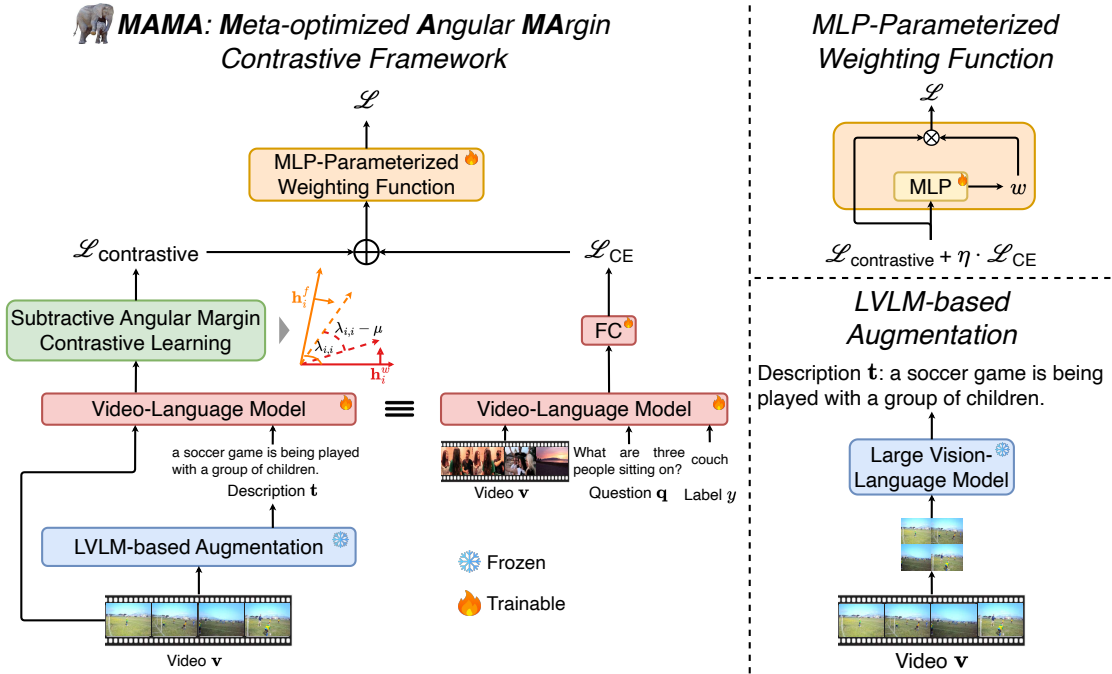


Figure 3.3: Illustration of the proposed MAMA framework and its components.

In this work, we conduct video-language representation learning for two types of video-language model, *i.e.* dual and bidirectional model. For the dual type, we will pool the visual representations  $\mathbf{V}_i^f$  and textual representations  $\mathbf{T}_i^w$  to obtain global representations  $\mathbf{h}_i^V$  and  $\mathbf{h}_i^T$  for the video and text input, respectively. We use cosine similarity to calculate the cross-modal similarity  $S_{\mathbf{v}_i, \mathbf{t}_i}$ . Then, we aim to maximize the similarities  $S_{\mathbf{v}_i, \mathbf{t}_i}$  of video-text pairs within the data, relative to those of the unaligned video-text pairs.

The bidirectional model will concatenate the visual and textual representations into a sequence, then feed the sequence to Transformer attention layers to capture the video-text relations. Subsequently, we will forward the [CLS] token which represents the video-text sequence to a fully-connected (FC) layer. The FC layer will calculate the similarity  $S_{\mathbf{v}_i, \mathbf{t}_i}$  if the video input  $\mathbf{v}_i$  has a text pairing  $\mathbf{t}_i$ , or calculate the log-likelihood  $\log q(y_i | \mathbf{v}_i, \mathbf{t}_i)$  of the answer if the video input  $\mathbf{v}_i$  has a label  $y_i$ . In the former case, similar to the dual type we also maximize the similarity of in-distribution video-text pairs, whereas for the latter case we maximize the log-likelihood of the answer label  $y_i$ .

In general, for all video inputs, we maximize the similarity  $S_{\mathbf{v}, \mathbf{t}}$  through minimiz-

---

**Algorithm 1** Our meta-optimized learning framework

---

**Input:** Training data  $\mathcal{D}$ , meta-data  $\hat{\mathcal{D}}$ , training batch size  $B$ , meta-data batch size  $M$ , initialized video-language model parameter  $\Theta^{(0)}$  and MLP network parameter  $\theta^{(0)}$

**Output:** Video-language model parameter  $\Theta^{(K)}$

- 1: **for**  $k = 0$  **to**  $K - 1$  **do**
- 2:     Sample a training minibatch  $\{\mathbf{v}, \mathbf{t}, y\}$ .
- 3:     Sample a meta-data minibatch  $\{\mathbf{v}^{\text{meta}}, \mathbf{t}^{\text{meta}}, y^{\text{meta}}\}$ .
- 4:     Estimate  $\hat{\Theta}^{(t)}$  by Eq. (3.9).
- 5:     Update  $\theta^{(k+1)}$  by Eq. (3.10).
- 6:     Update  $\Theta^{(k+1)}$  by Eq. (3.11).
- 7: **end for**

---

ing the cross-modal contrastive loss as:

$$\mathcal{L}_{\text{contrastive},i}^{v,t} = -\log \frac{e^{S_{\mathbf{v}_i, \mathbf{t}_i}/\tau}}{\sum_{j=1}^B e^{S_{\mathbf{v}_i, \mathbf{t}_j}/\tau}}, \quad \mathcal{L}_{\text{contrastive},i}^{t,v} = -\log \frac{e^{S_{\mathbf{t}_i, \mathbf{v}_i}/\tau}}{\sum_{j=1}^B e^{S_{\mathbf{t}_i, \mathbf{v}_j}/\tau}}, \quad (3.1)$$

where  $B$  is the batch size and  $\tau$  is the temperature hyperparameter. If a video  $\mathbf{v}_i$  additionally exhibits an answer label  $y_i$ , we jointly combine the cross-entropy loss to maximize the log-likelihood of the label with the above contrastive loss:

$$\mathcal{L}_{\text{CE},i} = -\sum_{y_i} p(y_i|\mathbf{v}_i, \mathbf{t}_i) \log q(y_i|\mathbf{v}_i, \mathbf{t}_i), \quad (3.2)$$

$$\mathcal{L}_{\text{train},i} = \mathcal{L}_{\text{contrastive},i}^{v,t} + \mathcal{L}_{\text{contrastive},i}^{t,v} + \eta \cdot \mathcal{L}_{\text{CE},i}, \quad (3.3)$$

where  $\eta$  is a hyperparameter to balance both losses. It is worth noting that  $\eta = 0$  if a video input  $\mathbf{v}_i$  is not attached with  $y_i$ .

### 3.2.2 Meta-optimized Angular Margin Contrastive Framework

**Subtractive angular margin contrastive learning.** As cosine similarity is used to calculate  $S_{\mathbf{v}_i, \mathbf{t}_j} \in [-1, 1]$ , we denote the angle between the representation of video  $i$  and text  $j$  as:

$$\lambda_{i,j} = \arccos(S_{\mathbf{v}_i, \mathbf{t}_j}). \quad (3.4)$$

The original video-language representation learning minimizes  $\lambda_{i,i}$  to approach a 0-degree angle. However, since the video and its textual description commonly does not perfectly align with each other, we want the gradient to be regularized when the similarity of positive pair  $\mathbf{v}_i$  and  $\mathbf{t}_i$  becomes small. Particularly, we replace

$\mathcal{L}_{\text{contrastive},i}^{v,t}$  by a new training objective:

$$\mathcal{L}_{\text{angular},i}^{v,t} = \begin{cases} -\log \frac{e^{\cos([\lambda_{i,i} - \mu]_+)/\tau}}{e^{\cos([\lambda_{i,i} - \mu]_+)/\tau} + \sum_{j \neq i} e^{\cos(\lambda_{i,j})/\tau}}, & \text{if } \lambda_{i,i} \leq \frac{\pi}{2} \\ -\log \frac{e^{\cos(\lambda_{i,i})/\tau}}{e^{\cos(\lambda_{i,i})/\tau} + \sum_{j \neq i} e^{\cos(\lambda_{i,j})/\tau}}, & \text{otherwise,} \end{cases}$$

A similar objective  $\mathcal{L}_{\text{angular},i}^{t,v}$  is formulated between  $\mathbf{t}_i$  and  $\mathbf{v}_i$ . As long as the angular difference  $\lambda_{i,i}$  is smaller than  $\mu$ , the similarity score will become 1. On the other hand, if  $\lambda_{i,i}$  is larger but starts to turn small, *i.e.*  $\mu \leq \lambda_{i,i} \leq \frac{\pi}{2}$ , the subtractive margin  $\mu$  will temporarily pull the positive video and text closer to regularize the gradient of the positive samples, thus restraining them from reaching perfect similarity. This intuition is formalized by the following theorem:

**Theorem 1.** *Let  $\lambda_{i,j}$  denote the angle between the representation of two samples  $i, j$ ,  $\mathcal{L}_{\text{angular},i}^{v,t}$  and  $\mathcal{L}_{\text{contrastive},i}^{v,t}$  denote the training objectives with and without the angular margin, respectively. Then, if  $\lambda_{i,i} \leq \frac{\pi}{2}$ , the following inequality holds:*

$$\left| \frac{\partial \mathcal{L}_{\text{angular},i}^{v,t}}{\partial \lambda_{i,i}} \right| \leq \left| \frac{\partial \mathcal{L}_{\text{contrastive},i}^{v,t}}{\partial \lambda_{i,i}} \right| \quad (3.5)$$

In order to speed up the training in the beginning and constrain the update of positive pairs in the latter stage, we adopt an adaptive strategy that gradually increases the margin  $\mu$  towards a limit:

$$\mu^{(k)} = \frac{a_0}{a_1 + e^{-a_2 \cdot k}}, \quad (3.6)$$

where  $k$  denotes the training step, and  $a_0$ ,  $a_1$ , and  $a_2$  denote hyperparameters.

**MLP-parameterized weighting function.** To control the effect of the data imbalance issue, we construct a weighting function as a  $\theta$ -parameterized MLP to map each training loss to a sample weight:

$$w(\theta, \mathcal{L}_i^{\text{train}}(\Theta)) = \text{MLP}_\theta(\mathcal{L}_i^{\text{train}}(\Theta)), \quad i \in \{1, 2, \dots, B\}, \quad (3.7)$$

where  $\mathcal{L}_i^{\text{train}}(\Theta)$  denotes the training loss of sample  $i$  in a batch of size  $B$ , calculated using the  $\Theta$ -parameterized video-language model.

Then, the final training objective is the sum of the training losses of data samples weighted by  $w$ :

$$\mathcal{L}(\Theta, \theta) = \frac{1}{B} \sum_{i=1}^B w(\theta, \mathcal{L}_i^{\text{train}}(\Theta)) \cdot \mathcal{L}_i^{\text{train}}(\Theta). \quad (3.8)$$

**Meta-optimized learning framework.** At present, we have a  $\theta$ -parameterized MLP network and a  $\Theta$ -parameterized video-language model to train. Since jointly training these two models might be unstable (Shu et al., 2019), we instead develop a meta-learning approach. In our procedure, we manually extract a small amount of unbiased meta-data set  $\{\mathbf{v}_i^{\text{meta}}, \mathbf{t}_i^{\text{meta}}, y_i^{\text{meta}}\}_{i=1}^M$ , i.e. with semantically aligned textual description and balanced label distribution, representing the meta-knowledge of the groundtruth sample-label distribution, where  $M$  is the number of the meta-samples and  $M \ll N$ .

We first estimate the update of the video-language model parameters  $\Theta$ :

$$\hat{\Theta}^{(k)} = \Theta^{(k)} - \frac{\alpha}{B} \sum_{j=1}^B w_i \left( \theta^{(k)}, \mathcal{L}_j^{\text{train}} \left( \Theta^{(k)} \right) \right) \cdot \nabla_{\Theta} \mathcal{L}_j^{\text{train}} \left( \Theta^{(k)} \right), \quad (3.9)$$

where  $\alpha$  is the learning rate for the video-language model. Subsequently, we update the MLP network using the estimated  $\hat{\Theta}$ :

$$\theta^{(k+1)} = \theta^{(k)} - \frac{\eta}{M} \sum_{i=1}^M \nabla_{\theta} \mathcal{L}_i^{\text{meta}} \left( \hat{\Theta}^{(k)} \right), \quad (3.10)$$

where  $\beta$  is the learning rate for the MLP network. Lastly, we obtain the new video-language model's parameters as:

$$\Theta^{(k+1)} = \Theta^{(k)} - \frac{\alpha}{B} \sum_{j=1}^B w \left( \theta^{(k+1)}, \mathcal{L}_j^{\text{train}} \left( \Theta^{(k)} \right) \right) \cdot \nabla_{\Theta} \mathcal{L}_j^{\text{train}} \left( \Theta \right) \Big|_{\Theta^{(k)}}. \quad (3.11)$$

We summarize our algorithm in Algorithm 1. From an empirical perspective, we compare the effectiveness of joint learning and our meta-optimized framework in Section 3.3.3. From a theoretical perspective, we conduct further derivation for Eq. (3.10), resulting in the following formulation:

$$\theta^{(k+1)} = \theta^{(k)} + \frac{\alpha \beta}{BM} \sum_{i=1}^M \sum_{j=1}^B G_{ij} \frac{\partial w \left( \theta^{(k)}, \mathcal{L}_j^{\text{train}} \left( \Theta^{(k)} \right) \right)}{\partial \theta} \Big|_{\theta^{(k)}}, \quad (3.12)$$

$$G_{ij} = \nabla_{\hat{\Theta}} \mathcal{L}_i^{\text{meta}} \left( \hat{\Theta} \right) \Big|_{\hat{\Theta}^{(k)}} \cdot \nabla_{\Theta} \mathcal{L}_j^{\text{train}} \left( \Theta \right) \Big|_{\Theta^{(k)}}, \quad (3.13)$$

where  $G_{ij}$  denotes the coefficient of the gradient. The coefficient will increase for training samples whose gradient is in the same direction with the gradient of the meta-data (meta gradient), as this is more likely to be a clean learning direction. In contrast, the coefficient will decrease for those whose gradient is opposite from the meta gradient, since the learning direction is likely to be noisy.

### 3.2.3 Large Vision-Language Model for Augmentation

To further enhance our video-language representation learning, we devise a strategy to utilize large vision-language model to augment additional video-text data. Our strategy consists of two stages, *i.e.* extracting key frames and generating textual descriptions, which we delineate as follows:

**Key frame extraction.** Inspired by (Jin et al., 2023), we adopt a density peak-based clustering approach to extract key video frames. Starting with a sequence of visual frame features  $\mathbf{V}_i^f = \{\mathbf{h}_{i,j}^f\}_{j=1}^{N_{\mathbf{v}_i}}$ , we calculate the locality density  $d_{i,j}$  of each feature  $\mathbf{h}_{i,j}^f$  based on its  $K$ -nearest neighbors:

$$d_{i,j} = \exp \left( -\frac{1}{K} \sum_{\mathbf{h}_{i,l}^f \in \text{KNN}(\mathbf{h}_{i,j}^f)} \left\| \mathbf{h}_{i,l}^f - \mathbf{h}_{i,j}^f \right\|^2 \right), \quad (3.14)$$

where  $\text{KNN}(\mathbf{h}_{i,j}^f)$  denotes the  $K$ -nearest neighbors of  $\mathbf{h}_{i,j}^f$ .

Subsequently, we estimate the distance index  $\gamma_{i,j}$  of each frame  $\mathbf{h}_{i,j}^f$ :

$$\gamma_{i,j} = \begin{cases} \min_{l: d_{i,j} > d_{i,l}} \left\| \mathbf{h}_{i,l}^f - \mathbf{h}_{i,j}^f \right\|^2, & \text{if } \exists l \text{ s.t. } d_{i,l} > d_{i,j} \\ \max_l \left\| \mathbf{h}_{i,l}^f - \mathbf{h}_{i,j}^f \right\|, & \text{otherwise} \end{cases}. \quad (3.15)$$

Our intuition is that  $d_{i,j}$  denotes the local density of a video frame, and  $\gamma_{i,j}$  denotes the distance from other frames of high density. We proceed to extract the top  $Q$  video frames of the highest  $d_{i,j} \times \gamma_{i,j}$  values as key video frames.

**Textual description generation.** Since large vision-language models have established impressive results on natural instruction tuning and visual reasoning capabilities, we leverage a LVLM to augment textual descriptions for video data (Dai et al.; Li et al., 2023b; Liu et al., 2023). Particularly, given the top  $Q$  video frames, we concatenate them into a single image  $I$  of the  $W \times H$  grid. We then forward the image  $I$  along with the textual prompt “*Write a short caption sentence for the video in order from left to right, top to bottom*” to a large vision-language model to generate the sentence-level textual description  $\mathbf{t}$ , which we combine with the video  $\mathbf{v}$  to form a video-text pair  $(\mathbf{v}, \mathbf{t})$ .

## 3.3 Experiments

### 3.3.1 Experimental Settings

**Downstream tasks.** Following previous works (Jin et al., 2023; Sun et al., 2019; Zhao et al., 2023b; Man et al., 2023), we evaluate our framework on two popular video question answering and text↔video retrieval tasks.

- Video question answering (VideoQA): We experiment with two videoQA settings, *i.e.* open-ended and multi-choice videoQA. Open-ended videoQA classifies a pair of video and question into one of the pre-defined set of answer labels. Multi-choice videoQA chooses the correct answer from five choices given the video and the language question. We assess our video-language representations by the VideoQA task using the following five datasets, MSRVTT (Xu et al., 2016), MSVD (Chen and Dolan, 2011), TGIF-QA-R (Peng et al., 2021), NExT-QA (Xiao et al., 2021b), and Causal-VidQA (Li et al., 2022b).
- Text↔video retrieval: The retrieval task is to extract the corresponding video given the textual query, or extract the textual description given the video. We evaluate the retrieval ability of our video-language representations using three datasets: MSRVTT (Xu et al., 2016), DiDeMo (Anne Hendricks et al., 2017), ActivityNet (Krishna et al., 2017).

**Evaluation metrics.** For the videoQA task, we use the answer accuracy as the evaluation metric. For the retrieval task, we employ Recall at rank  $K$  ( $R@K$ ), with  $K \in \{1, 5, 10\}$  to evaluate the performance.

**Video-language backbones.** To extensively validate the effectiveness of our framework, we conduct experiments on various models of bidirectional and dual architectures. Particularly, for the dual architecture, we experiment with CLIP-ViP (Xue et al., 2022b) and video graph transformer (VGT) (Xiao et al., 2023b), while for the bidirectional architecture, we experiment with the well-known VIOLET architecture (Fu et al., 2023).

**Baseline methods.** We compare our method with a comprehensive list of video-language understanding models, along with the approaches that use LVLM to augment video-text data: (i) **CLIP4Clip** (Luo et al., 2022), a model that transfers

image-text CLIP model (Radford et al., 2021) to text $\leftrightarrow$ video retrieval tasks; (ii) **MERLOT** (Zellers et al., 2021), a method that trains on both spatial and temporal objectives to learn video-language representations; (iii) **LAVENDER** (Li et al., 2023d), a model that learns video-language representations using a unified framework of masked language modeling; (iv) **Singularity** (Lei et al., 2022), curates a pre-training dataset and uses an early fusion strategy to improve single-frame video-language representation learning; (v) **OmniVL** (Wang et al., 2022a): a model that is trained on both image-language and video-language data to enhance video-language representation learning; (vi) **VindLU** (Cheng et al., 2023), follows a recipe to select pre-training objectives, pre-training data, and model scale for effective video-language representation learning; (vii) **All-in-one** (Wang et al., 2023a), a model that embeds raw video and textual signals into hidden representations without using pre-trained unimodal encoders; (viii) **DRL** (Wang et al., 2022b), a disentangled representation method that decouples sequential from hierarchical representations to specifically improve both of them for cross-modal retrieval; (ix) **CLIP2Video** (Wang et al., 2022c), consists of two normalization methods to improve the effectiveness and robustness of cross-modal retrieval models; (x) **LaViLa** (Zhao et al., 2023b), an approach that fine-tunes LLM to be conditioned on visual frames to generate additional textual descriptions, which are used to improve video-language representation learning; (xi) **Vid2Seq** (Yang et al., 2023b), a pre-trained dense video captioning model which is used to generate additional textual descriptions for video data, which are employed to enhance video-language representation learning.

**Implementation details.** We utilize LLaVA model as the LVLM (Liu et al., 2023) to augment video inputs of the HowTo100M dataset (Miech et al., 2019), which is a large-scale dataset for video-language representation learning but has been known for its weakly aligned video-text pairings (Han et al., 2022). To construct the input for the LVLM, we use  $K = 6$  and  $Q = 12$ , then concatenate key frames into an image as a grid of  $3 \times 4$  frames. Based upon validation, we adopt  $\tau = 1$ ,  $a_0 = 0.2$ ,  $a_1 = 10$ , and  $a_2 = -0.1$  for angular margin contrastive learning, and  $\eta = 1$  for our optimization objective. For videoQA, to fairly compare with previous methods, we fine-tune our VIOLET-based model using AdamW with an initial learning rate of  $\alpha = \beta = 2e - 5$ , betas of (0.9, 0.98), weight decay of 1e-3, and batch size  $B$  of 4 for 10 epochs. Similarly, for the VGT-based model, we use Adam optimizer with an initial learning

Table 3.1: VideoQA results on MSRVTT, MSVD, and TGIF-QA-R. Open-ended videoQA is evaluated on MSRVTT, MSVD, and TGIF-Frame datasets. Multi-choice videoQA is evaluated upon TGIF-Action and TGIF-Transition.

Method	MSRVTT-QA	MSVD-QA	TGIF-QA-R		
			Action	Frame	Transition
MERLOT	43.1	51.9	61.4	69.3	84.0
LAVENDER	44.2	52.4	57.1	66.9	84.0
Singularity	43.5	49.6	53.1	65.1	81.5
OmniVL	44.1	51.0	62.0	69.5	85.5
VindLU	44.6	51.0	59.5	65.8	87.2
VGT	40.0	36.4	61.0	61.7	73.2
VIOLET	44.5	52.5	62.6	70.0	86.3
All-in-one	44.3	47.9	34.9	65.0	53.8
LaViLa-VIOLET	44.9	53.7	64.3	70.7	87.0
Vid2Seq-VIOLET	44.8	53.1	64.2	70.1	86.6
MAMA-VGT	41.6	37.1	61.7	62.7	74.0
MAMA-VIOLET	<b>46.4</b>	<b>55.8</b>	<b>66.5</b>	<b>71.7</b>	<b>89.5</b>

Table 3.2: VideoQA results on NExT-QA and Causal-VidQA. All of the datasets target multi-choice videoQA.

Method	NExT-QA				Causal-VidQA			
	Descriptive	Temporal	Causal	All	Descriptive	Explanatory	Predictive	Counterfactual
MERLOT	66.6	62.5	58.2	59.4	67.2	65.7	57.2	57.0
LAVENDER	63.4	56.5	54.6	56.7	62.0	61.6	46.3	50.4
Singularity	60.0	61.1	50.9	54.8	54.3	49.6	41.3	46.9
OmniVL	67.1	63.8	55.9	59.9	67.0	66.0	56.5	57.1
VindLU	68.4	59.7	55.7	59.8	63.6	54.8	57.7	54.4
VGT	69.6	65.4	56.2	61.8	74.4	75.6	60.7	65.6
VIOLET	67.7	58.0	50.7	58.5	67.6	66.6	57.1	57.6
All-in-one	64.8	63.9	50.9	57.9	60.4	51.3	51.2	50.7
LaViLa-VGT	70.9	69.2	59.3	64.8	74.7	76.1	61.6	65.7
Vid2Seq-VGT	70.3	67.0	58.5	64.2	73.7	76.0	61.3	65.6
MAMA-VGT	<b>72.7</b>	<b>70.6</b>	<b>62.2</b>	<b>66.3</b>	<b>75.3</b>	<b>77.1</b>	<b>62.2</b>	<b>68.2</b>
MAMA-VIOLET	71.2	68.6	61.1	65.8	72.7	68.0	60.5	59.5

rate of 1e-5 of a cosine annealing schedule, and batch size  $B$  of 4 for 30 epochs. For the text $\leftrightarrow$ video retrieval task, we fine-tune the model with an initial learning rate of 5e-6 and a fixed weight decay of 5e-2, using a batch size  $B$  of 4 for 5, 20, and 20 epochs on MSRVTT, DiDeMo, and ActivityNet datasets, respectively.

### 3.3.2 Main Results

We denote the results for videoQA in Table 3.1 and 3.2, for text $\rightarrow$ video retrieval in Table 3.3, and for video $\rightarrow$ text retrieval in Table 3.4.

**VideoQA.** In terms of open-ended videoQA, we substantially outperform the LVLM approaches, *e.g.* improve upon LaViLa with improvements of 1.5% on MSRVTT, 2.1% on MSVD, and 3.7% on TGIF-Frame. We also surpass previous video-language understanding models, *e.g.* VindLU by 1.8% on MSRVTT, VIOLET by 3.3% on

Table 3.3: Text→video retrieval results on MSRVTT, DiDeMo, and ActivityNet.

Method	MSRVTT			DiDeMo			ActivityNet		
	R@1	R@5	R@10	R@1	R@5	R@10	R@1	R@5	R@10
VIOLET	37.2	64.8	75.8	47.9	76.5	84.1	18.1	43.1	56.7
VindLU	48.8	72.4	82.2	59.8	86.6	91.5	55.9	82.3	90.9
CLIP4Clip	44.5	71.4	81.6	42.8	68.5	79.2	40.5	72.4	83.4
CLIP2Video	47.2	73.0	83.0	-	-	-	-	-	-
DRL	47.4	74.6	83.8	47.9	73.8	82.7	44.2	74.5	86.1
CLIP-ViP	55.7	77.7	86.6	55.7	78.1	86.1	59.1	83.9	91.3
LaViLa - CLIP-ViP	56.0	79.8	87.2	56.6	79.8	87.1	58.7	82.8	90.5
Vid2Seq - CLIP-ViP	55.3	77.9	86.1	57.6	79.9	88.4	55.1	79.0	87.4
MAMA - CLIP-ViP	<b>60.0</b>	<b>82.2</b>	<b>89.2</b>	<b>62.7</b>	<b>89.9</b>	<b>96.0</b>	<b>60.0</b>	<b>85.0</b>	<b>91.7</b>

Table 3.4: Video→text retrieval results on MSRVTT, DiDeMo, and ActivityNet.

Method	MSRVTT			DiDeMo			ActivityNet		
	R@1	R@5	R@10	R@1	R@5	R@10	R@1	R@5	R@10
VIOLET	36.6	64.1	75.1	44.8	72.9	82.4	15.8	39.8	54.8
VindLU	46.0	71.8	80.2	57.2	83.1	88.9	47.1	77.5	86.6
CLIP4Clip	43.1	70.5	81.2	17.5	37.5	49.4	42.6	73.4	85.6
CLIP2Video	43.5	72.3	82.1	-	-	-	-	-	-
DRL	45.1	72.9	83.5	45.4	72.6	82.1	42.2	74.0	86.2
CLIP-ViP	48.0	72.4	82.9	46.3	73.2	81.9	50.2	78.3	87.5
LaViLa - CLIP-ViP	49.0	74.5	83.4	47.1	74.2	83.0	50.3	78.7	88.4
Vid2Seq - CLIP-ViP	49.1	74.1	82.5	47.2	74.4	83.1	50.9	79.5	89.6
Our method - CLIP-ViP	<b>50.1</b>	<b>76.8</b>	<b>84.8</b>	<b>48.1</b>	<b>78.1</b>	<b>85.5</b>	<b>52.3</b>	<b>80.8</b>	<b>90.1</b>

MSVD, and OmniVL by 2.2% on TGIF-Frame. Moreover, for multi-choice videoQA, we consistently surpass both LVLM and video-language understanding models, *e.g.* achieving an overall gain of 1.5% on NExT-QA and 1.2% on Causal-VidQA over LaViLa, while the gains over VGT are 4.5% and 1.6%, respectively on these two datasets.

**Text↔video retrieval.** Our observation in videoQA applies for the text↔video retrieval task. In the text→video direction, we enhance upon CLIP-ViP by 2.6 R@10 points on MSRVTT, 5.5 R@1 points on DiDeMo, and 1.1 R@5 points on ActivityNet. We also significantly outperform the LVLM approaches, *e.g.* by 4.0 R@1 points and by 2.4 R@5 points on MSRVTT over LaViLa. Our superiority on video→text retrieval is analogous to the text→video case.

These results substantiate that our framework is applicable to various video-language understanding tasks and model architectures. We hypothesize that we can better control the alignment between the positive video and language, and their effect upon the model training, thus leading to more reasonable video-language

Table 3.5: Experiments on the LVLM choice for our prompting strategy.

LVLM choice	VideoQA		Text $\rightarrow$ video retrieval					
	MSRVTT	MSVD	MSRVTT			DiDeMo		
			R@1	R@5	R@10	R@1	R@5	R@10
No augmentation	45.6	54.7	59.0	80.3	87.6	58.0	82.9	89.6
BLIP-2	45.7	54.9	59.1	80.4	87.7	58.1	82.9	89.7
InstructBLIP	46.1	55.2	59.2	80.9	88.1	58.5	83.5	89.8
LLaVA-ChatGPT	46.1	55.0	59.0	80.3	87.7	58.7	83.9	90.0
LLaVA	<b>46.4</b>	<b>55.8</b>	<b>60.0</b>	<b>82.2</b>	<b>89.2</b>	<b>62.7</b>	<b>89.9</b>	<b>96.0</b>

representations.

### 3.3.3 Ablation Study

We ablate our meta-optimized framework to investigate which factor results in the demonstrated effectiveness and explore intriguing properties. We conduct all experiments of our ablation study on the MSRVTT and MSVD for videoQA, and MSRVTT and DiDeMo for the text $\leftrightarrow$ video retrieval task.

**Varying the angular margin.** The angular margin, represented as  $\mu$ , is critical to control the relationship between semantically close video and language inputs. To better understand  $\mu$ , we experiment with manually varying the margin  $\mu$  from 0.1 to 0.4 in Figure 3.4 (left). We observe that the optimal performance is achieved when  $\mu \sim 0.2$ . Based upon this observation, we adopt  $a_0 = 2$  and  $a_1 = 10$ . Subsequently, we evaluate the impact of  $a_2 \in \{0.01, 0.05, 0.1, 0.15, 0.2\}$  in Figure 3.4 (right). We discover that  $a_2 = 0.1$  achieves the best performance and we adopt it for all experiments.

**Reweighting strategies.** In addition to MLP, there exist various approaches to weigh training losses to control noisy pairings and data imbalance issues within the training data, *e.g.* focal loss (Lin et al., 2017), self-paced learning (SPL) (Jiang et al., 2014), and L2RW (Ren et al., 2018). We replace our MLP by these approaches and demonstrate the results in Table 3.6. We find that our MLP-parameterized function significantly improves upon previous weighting functions that use manually designed formulation, *i.e.* focal loss and SPL, and also the meta-learning approach without using MLP, *i.e.* L2RW. The possible reason could be that MLP is a universal approximator, so that it can adaptively learn a reasonable weighting function based on data, thus outperforming methods that do not employ MLP.

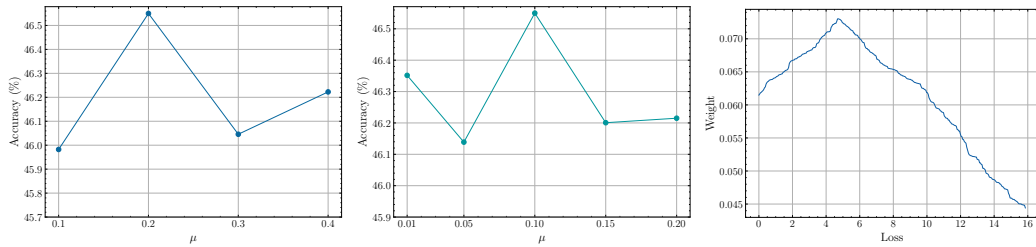
Table 3.6: Experiments on weighting functions.

Weighting function	VideoQA		Text→video retrieval					
	MSRVTT	MSVD	MSRVTT			DiDeMo		
			R@1	R@5	R@10	R@1	R@5	R@10
Focal loss	45.0	54.1	58.3	80.0	86.9	59.7	85.6	91.8
SPL	45.3	54.3	58.7	80.8	88.1	61.4	87.5	93.8
L2RW	45.9	55.2	59.5	81.8	89.6	62.0	88.8	94.6
MLP	<b>46.4</b>	<b>55.8</b>	<b>60.0</b>	<b>82.2</b>	<b>89.2</b>	<b>62.7</b>	<b>89.9</b>	<b>96.0</b>

Table 3.7: Experiments on the number of key frames  $Q$  and the concatenated grid.

Q	Grid	VideoQA		Text→video retrieval					
		MSRVTT	MSVD	MSRVTT			DiDeMo		
				R@1	R@5	R@10	R@1	R@5	R@10
1	1 × 1	45.0	55.1	58.2	79.3	86.2	60.2	85.8	93.2
2	1 × 2	45.7	55.3	58.8	80.0	87.0	60.5	85.8	93.3
	2 × 1	45.9	55.4	58.4	79.2	87.0	60.9	86.1	94.2
4	1 × 4	45.9	55.2	59.1	80.3	88.4	61.3	86.3	94.6
	2 × 2	45.6	55.2	59.2	80.4	88.4	61.3	86.7	94.6
8	2 × 4	45.9	55.6	59.8	81.3	88.7	61.8	89.0	95.3
	4 × 2	45.8	55.5	59.3	80.7	88.5	61.8	88.9	95.3
12	3 × 4	<b>46.4</b>	<b>55.8</b>	<b>60.0</b>	<b>82.2</b>	<b>89.2</b>	<b>62.7</b>	<b>89.9</b>	<b>96.0</b>
	2 × 6	45.8	55.6	59.3	81.7	89.1	62.7	89.2	95.6
16	2 × 8	45.8	55.1	58.3	79.7	87.6	61.9	88.7	94.8
	4 × 4	45.7	55.1	58.9	80.8	88.7	62.6	89.1	95.9

Figure 3.4: (Left) Validation videoQA accuracy on MSVD with respect to  $\mu$ ; (Middle) Validation videoQA accuracy on MSVD with respect to  $a_0$ ; (Right) Relationship between loss values and weight values generated by our MLP-parameterized weighting function.

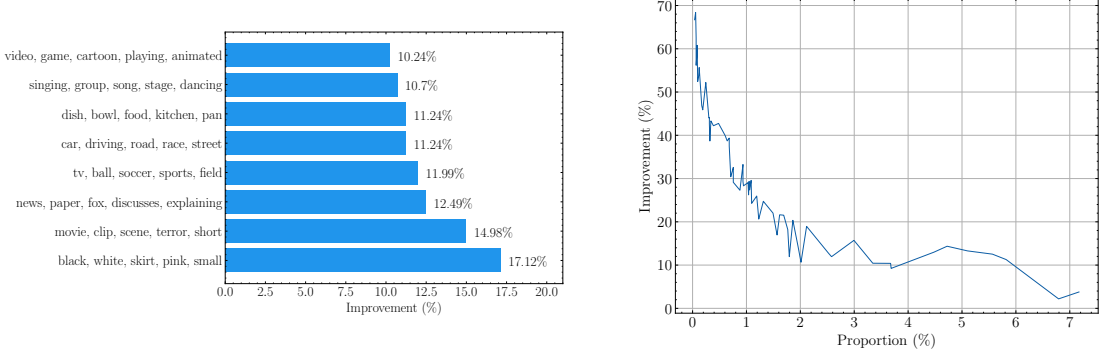


**Optimization strategies.** We explore different strategies to optimize the MLP and video-language model. Particularly, we experiment with the joint learning strategy, which simultaneously updates the parameters of the MLP and the video-language model to minimize the objective in Eq. 3.3. As shown in Table 3.8, our meta-learning approach outperforms the joint learning one and achieves the best performance. This empirically validates the effectiveness of our meta-learning strategy which enables the training to follow gradient of the meta-data.

Table 3.8: Experiments on the learning strategy.

Training strategy	VideoQA		Text→video retrieval					
	MSRVTT	MSVD	MSRVTT			DiDeMo		
			R@1	R@5	R@10	R@1	R@5	R@10
Joint learning	45.5	54.9	59.3	81.1	88.4	59.2	84.9	90.2
Meta-learning	<b>46.4</b>	<b>55.8</b>	<b>60.0</b>	<b>82.2</b>	<b>89.2</b>	<b>62.7</b>	<b>89.9</b>	<b>96.0</b>

Figure 3.5: a) Relative R@1 improvement in the text-video retrieval task on MSRVTT for each topic; b) Relative accuracy improvement in the videoQA task on MSRVTT with respect to the proportion of questions for which each label is the answer.



**Video-text data augmentation.** We assess the influence of different video-text data augmentation strategies. In particular, we ablate the LLaVA-generated samples and also explore different LVLM choices, *i.e.* BLIP-2 (Li et al., 2023b) and InstructBLIP (Dai et al.). In addition, we also use LLaVA model to generate image caption for each video frame, and ask ChatGPT to write a summary for the concatenated captions of all frames as the textual description. Table 3.5 shows that neglecting LVLM-generated data results in slight performance degradation, which can be resolved by using other LVLMs, but still lack behind LLaVA model. We conjecture that LLaVA can better follow the language instruction to produce more accurate textual descriptions for videos (Liu et al., 2023). Moreover, LLaVA-ChatGPT approach also leads to performance degradation, possibly because it is still challenging for ChatGPT to infer temporal relations among captions of separate video frames.

**Number of extracted key frames.** We explore the impact of varying number of extracted key frames and varying the approach to concatenate in Table 3.7. While the performance is quite invariant to the concatenation strategy, we observe an increasing trend of the performance when the number of the extracted frames  $Q$  increases,

Table 3.9: Case study of similarity scores for video-text pairs.

Video	Caption	CLIP-ViP score	Our score
	a group of people dancing on a stage in front of a crowd. the man in black reaches his dance partner. man walks to the woman in red the camera zooms out on the dancers. we see a dancer in the back left spinning	0.1727 0.2175	0.1698 0.3342
	a boy in a red shirt and a blue hat is playing. a girl throwing a rock. girl in the red shirt looks back over his shoulder the boy in a blue hat is seen for the first time. the boy in the baseball cap first looks at the camera boy wearing a blue ball cap	0.2594 0.2869	0.2441 0.3164

since there exists more information for LVLM to put into the descriptions. However, after surpassing  $Q = 12$  frames, the performance dramatically decreases. The reason could be that when  $Q$  is excessively large, visual frames become excessively small for LVLM to precisely detect details. Furthermore, balanced grids, *i.e.*  $3 \times 4$  and  $4 \times 4$ , tend to outperform skewed grids, *i.e.*  $2 \times 6$  and  $2 \times 8$ , respectively. The cause might be that video details are more difficult for an LVLM to capture when the video frames are presented on a long rectangle than when they are presented on a balanced one.

### 3.3.4 Analysis

**Effect of angular margin contrastive learning.** To better understand the effect of our angular margin contrastive method, we show in Table 3.9 examples of videos and language captions, along with the similarity scores which are generated by the baseline CLIP-ViP model and the model trained with our proposed subtractive contrastive learning strategy. We observe that when the caption consists of less details, *i.e.* it aligns more weakly with the video content, our model assigns a lower similarity score compared to CLIP-ViP. In contrast, when the language caption becomes more detailed, we assign a higher score while CLIP-ViP only slightly elevates the score. These examples demonstrate that our angular margin contrastive strategy can control the similarity level for weakly aligned video-text pairs while being able to adapt to cases of strongly aligned pairs.

**Effect of MLP-parameterized weighting function.** To closely study the impact of our MLP-based weighting function, we show the relative R@1 and the relative accuracy improvement of the text-video retrieval tasks in Figure 3.5a and 3.5b, respectively. Both figures demonstrate that we accomplish higher level of performance improvement on samples that belong to minority groups, *i.e.* unpopular

topic groups and answer labels. Such results intuitively substantiate the productivity of our MLP-based weighting function and showcase its capacity to learn the effective strategy to control the training effect of the training samples.

### 3.4 Summary

In this paper, we propose a meta-optimized contrastive framework to enhance video-language representation learning. In particular, we propose a contrastive learning framework with a subtractive margin between positive video and language to regularize their representations from reaching perfect similarity. Our framework also utilizes an MLP network that maps training losses to sample weights to enable the model to dynamically adjust the focus on data samples during training. Combined with a strategy to utilize large-vision language model to augment video-text data, our framework achieves superior results on commonly used video question answering and text-video retrieval tasks. Our framework is also applicable to a wide array of model architectures, which can promote its implementation in practical applications.

# Chapter 4

## **READ: Recurrent Adapter with Partial Video-Language Alignment for Parameter-Efficient Transfer Learning in Low-Resource Video-Language Modeling**

### **4.1 Introduction**

Video-language modeling is a challenging problem since it involves understanding both video and language modalities. For example, temporal language grounding (TLG) model comprehends video detail and language query to localize semantically related video moments (Figure 4.1 (left)), or video-language summarization (VLS) model extracts information from both video content and language transcript to write the summary (Figure 4.1 (right)).

Previous video-language modeling methods (Liu et al., 2022b; Lei et al., 2021b; Yu et al., 2021) employ pretrained Transformer models such as Unified Multimodal Transformer (UMT) (Liu et al., 2022b) and Vision-Guided BART (VG-BART) (Yu et al., 2021), and fine-tune all the parameters of these models for every single task. This results in substantial storage overhead since each task demands storing a separate model (Zhang et al., 2023a). Moreover, because of the difficulty of collecting video-language data (Pan et al., 2022), fully fine-tuning these over-parameterized models in low-resource scenarios, where limited training data is available, leads to instability and sub-optimal performance (Jiang et al., 2022a; Huang et al., 2023).

To address these shortcomings, adapters are proposed as a parameter-efficient



Figure 4.1: Examples of the TLG and VLS problems. TLG model needs to understand the meaning of language entities such as *proposal* or *girl*, and the existence of *expression* in video frames. VLS model is expected to recognize salient information, *e.g.* *crank bolt*, *bottom bracket* from the language, and *bicycle* from the video.

solution for finetuning video-language pretrained transformers (Jiang et al., 2022a; Zhang et al., 2023a; Yang et al., 2023e; Sung et al., 2022; Chen et al., 2022). The strategy is to add additional adaptation module to each layer of the pre-trained network and only the adaptation modules are trained during fine-tuning to improve the parameter-performance trade-off. These modules rely on non-linear projections to downproject video-language inputs into low-dimensional space then up-project them back to the original high-dimensional space. However, such projections consider video frames and textual words as separate tokens, thus ignoring the intrinsic temporal dependency among video frames or textual words. Without such dependency information, it is difficult to reason about temporal context in the video to properly ground the language (*e.g.* in Figure 4.1, determine the *expression* of the *girl after*, not *before*, the *proposal*), or coherently link the entities in the summary (*e.g.* in Figure 4.1, recap the chronological order of *bolt removing* and *puller threading*). Moreover, because at fine-tuning time only adaptation modules are trained using limited video-language data, little attention is paid to the information flow that starts from the raw video-language inputs till the low-dimensional space of the adaptation modules. This may result in losing essential task-related information and carrying noise into these modules (Tsai et al., 2020; Han et al., 2021).

To resolve the first issue, we propose a novel adapter architecture, **R**Ecurent **A**Dapter (READ), for video-language modeling tasks. The key idea is to incorporate the recurrent modeling ability into the adaptation module to capture the temporal dependency of video frames and language entities (Goodfellow et al., 2016). As such, we formulate READ as a parameter-efficient bottleneck with a sequence of operations including feature dimension reduction, recurrent modeling, and feature

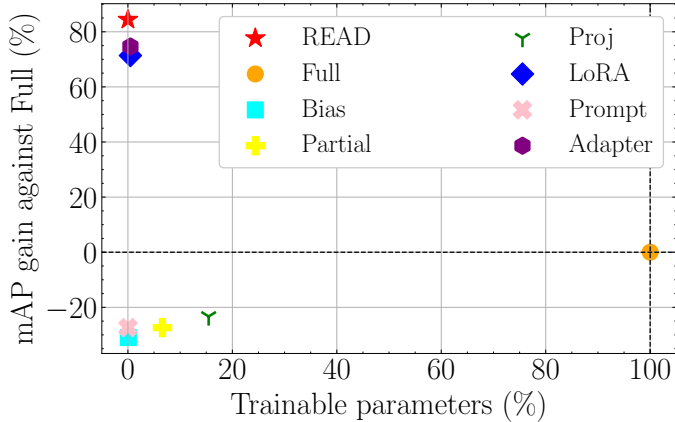


Figure 4.2: Comparison of our proposed READ method with the full fine-tuning and other parameter-efficient fine-tuning methods. For each method, we denote the mAP gain averaged over the domains of the YouTube Highlights dataset together with the number of trainable parameters.

dimension recovery. Since the incorporated recurrent computation works in the low dimension (*e.g.* 4-dimensional), our READ module stands as a lightweight design and can be cheaply integrated throughout the Transformer architecture for enhancing video-language modeling, using only up to 1.20% trainable parameters.

As for the second issue, we propose **Partial Video-Language Alignment** (PVLA), a novel objective to explicitly encourage the alignment between video and language representations, thus capturing invariant aligned information across modalities that are critical for downstream tasks. The key concept is to minimize the Partial Optimal Transport (POT) distance between the distribution over video frame representations and the distribution over textual word representations. The rationale for our partial implementation of optimal transport lies in that video and language do not exhibit complete one-to-one correspondence. Typically, the language does not describe all aspects of the video, and only part of the language sequence is strongly related to part of the video frames, *e.g.* in Figure 4.1 the language input about the *girl’s expression* is only related to the target grounding. As such, utilizing POT for distribution matching is to focus on essential masses that are strongly related between modalities, hence optimizing towards better video-language alignment and gaining more control over video-language information passed into our READ modules.

Based on our novel proposals, we construct the READ framework that can be employed to finetune various pre-trained Transformer architectures such as

multimodal transformer (UMT (Liu et al., 2022b), Moment-DETR (Lei et al., 2021b)), and generative vision-guided transformer models (VG-BART (Lewis et al., 2020) and VG-T5 (Raffel et al., 2020)). Through freezing these pre-trained models and fine-tuning only our READ modules with PVLA objective, we outperform standard fine-tuning and other parameter-efficient methods with substantially fewer tunable parameters (Figure 4.2) for low-resource video-language tasks, including temporal language grounding and video-language summarization. To sum up, our contributions can be summarized as:

- We propose **RE**current **A**dapter (READ), a novel adapter architecture, that better captures temporal information for modeling video-language tasks.
- We propose **P**artial **V**ideo-**L**anguage **A**lignment (PVLA) objective to encourage the alignment between video and language modalities during the adaptation process.
- We validate our READ framework by extensive experiments using multiple low-resource temporal language grounding and video-language summarization datasets, where READ outperforms all existing fully or parameter-efficient fine-tuning strategies with only up to 1.20% parameters tunable.

## 4.2 Methodology

We present recurrent adapter (READ) to effectively develop the temporal modeling capability and efficiently transfer large pre-trained transformer models for video-language downstream tasks. We also introduce the partial video-language alignment (PVLA) task to optimize the alignment of in-distribution video-language inputs for better supporting video-language adaptation under low-resource settings. Our overall framework is illustrated in Figure 7.4.

### 4.2.1 Preliminary – Transformer Architecture for Video-Language Modeling

We concentrate our work upon the Transformer architecture (Vaswani et al., 2017). The architecture consists of an embedding layer and  $M$  consecutive Transformer

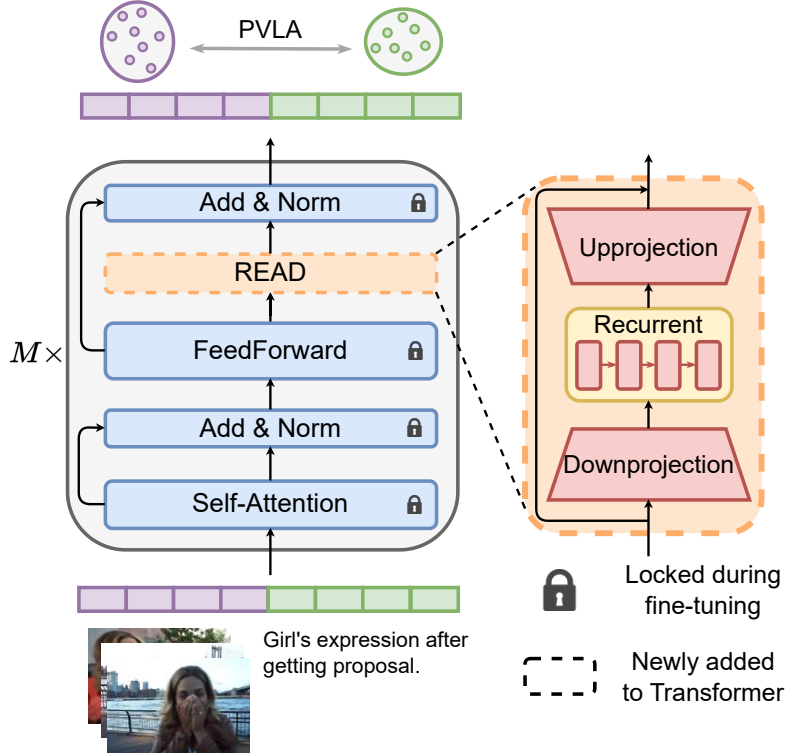


Figure 4.3: Overall illustration of the proposed recurrent adapter (READ) and partial video-language alignment (PVLA) framework.

blocks. As inputs to the Transformer model, we extract  $N_V$  frames and  $N_L$  words from the video and language input, respectively. The embedding layer would encode the extracted frames and words into sequences of initial video and language representations  $H_V^{(0)} = \{\mathbf{h}_{v,i}^{(0)}\}_{i=1}^{N_V}$  and  $H_L^{(0)} = \{\mathbf{h}_{l,j}^{(0)}\}_{j=1}^{N_L}$ , respectively. The transformer then forwards these sequences into consecutive Transformer blocks, each of which is typically composed of a multi-head self-attention (MHSA) layer, a residual connection with normalization (Add & Norm) layer, a feedforward layer, and another Add & Norm layer.

In MHSA for video-language modeling, the language representations are linearly projected into the query tensor  $\mathbf{Q} \in \mathbb{R}^{N_L \times d}$ , whilst the video representations into the key  $\mathbf{K} \in \mathbb{R}^{N_V \times d}$  and value tensors  $\mathbf{V} \in \mathbb{R}^{N_V \times d}$ :

$$\begin{aligned}\mathbf{Q}^{(m)} &= \text{Linear}(\mathbf{H}_L^{(m)}) , \quad \mathbf{K}^{(m)} = \text{Linear}(\mathbf{H}_V^{(m)}) , \\ \mathbf{V}^{(m)} &= \text{Linear}(\mathbf{H}_V^{(m)}) ,\end{aligned}$$

where  $m$  denotes the index of the current Transformer block and  $d$  the hidden

dimension. Then, the self-attention computation is conducted upon these vectors as:

$$\begin{aligned}\mathbf{X}^{(m)} &= \text{Attention}(\mathbf{Q}^{(m)}, \mathbf{K}^{(m)}, \mathbf{V}^{(m)}) = \\ &\text{Softmax}\left(\frac{\mathbf{Q}^{(m)} \cdot (\mathbf{K}^{(m)})^\top}{\sqrt{d}}\right) \cdot \mathbf{V}^{(m)}.\end{aligned}\quad (4.1)$$

The attention output  $\mathbf{X}^{(m)}$  is subsequently sent to an Add & Norm layer:

$$\mathbf{P}^{(m)} = \text{LN}(\mathbf{X}^{(m)} + \mathbf{H}_L^{(m)}), \quad (4.2)$$

where LN denotes the layer normalization layer. Subsequently,  $\mathbf{P}^{(m)}$  is forwarded to a FeedForward block to produce the output representation  $\mathbf{O}^{(m)}$ , which will be passed to another Add & Norm layer to create the video-informed language representation for the next transformer block:

$$\mathbf{O}^{(m)} = \text{GeLU}(\text{Linear}(\mathbf{P}^{(m)})), \quad (4.3)$$

$$\mathbf{H}_L^{(m+1)} = \text{LN}(\mathbf{P}^{(m)} + \mathbf{O}^{(m)}), \quad \mathbf{H}_V^{(m+1)} = \mathbf{H}_V^{(m)}. \quad (4.4)$$

The video-language representation of the last Transformer block  $\mathbf{H}_L^{(M+1)}$  is finally adopted to perform a specific downstream task.

#### 4.2.2 Recurrent Adapter (READ)

The objective of our READ is to incorporate the temporal modeling capability for the adaptation module. To this end, we construct a recurrent-based bottleneck layer which is composed of a downprojection layer, a recurrent neural network (RNN) layer, and an up-projection layer.

Formally, given the FeedForward output  $\mathbf{O}$ , our recurrent adapter can be expressed as:

$$\tilde{\mathbf{O}} = \mathbf{O} + \text{GELU}(\text{RNN}(\mathbf{O} \cdot W_{\text{down}})) \cdot W_{\text{up}}, \quad (4.5)$$

where  $W_{\text{down}} \in \mathbb{R}^{d \times k}$ ,  $W_{\text{up}} \in \mathbb{R}^{k \times d}$ , and  $k \ll d$ . Subsequently, we combine  $\mathbf{P}$  and  $\tilde{\mathbf{O}}$  via residual connection to generate the output  $\mathbf{H}$ :

$$\mathbf{H} = \text{LN}(\tilde{\mathbf{O}} + \mathbf{P}). \quad (4.6)$$

In addition to RNN, we also experiment with other recurrent architectures in Table 4.8 and observe that the performance is insensitive to the architectural choice.

Therefore, for simplicity, we decide to implement the RNN architecture in our READ layer.

**Fine-tuning.** During the fine-tuning stage, we preserve the weights of the pre-trained Transformer model and only optimize our introduced READ layers. In detail, the original model components (blue blocks in Figure 7.4) are frozen, while the parameters of READ (the yellow block in Figure 7.4) are updated with respect to the task-specific and the partial video-language alignment losses, which will be delineated in the upcoming section.

**Testing.** During testing, we maintain the shared parameters of the pre-trained Transformer model and only load those of our extra READ modules that are fine-tuned in the previous phase. This would keep the storage cost from burgeoning because the number of added parameters is tiny.

### 4.2.3 Partial Video-Language Alignment (PVLA)

To encourage the control towards the information flow of video frames and language words, we propose to optimize the alignment between the in-distribution video and language representations  $H_V$  and  $H_L$  at all Transformer blocks.

We consider video and language as two discrete distributions  $\boldsymbol{\mu}$  and  $\boldsymbol{\nu}$ , whose  $H_V$  and  $H_L$  are their supports, respectively. We formulate this setting as  $\boldsymbol{\mu} = \sum_{i=1}^{N_V} \mathbf{a}_i \delta_{\mathbf{h}_{v,i}}$  and  $\boldsymbol{\nu} = \sum_{j=1}^{N_L} \mathbf{b}_j \delta_{\mathbf{h}_{l,j}}$ , with  $\delta_{\mathbf{h}_{v,i}}$  and  $\delta_{\mathbf{h}_{l,j}}$  being the Dirac functions respectively centered upon  $\mathbf{h}_{v,i}$  and  $\mathbf{h}_{l,j}$ . The weight vector of the supports is  $\mathbf{a} = \frac{\mathbf{1}_{N_V}}{N_V}$ , and  $\mathbf{b} = \frac{\mathbf{1}_{N_L}}{N_L}$ .

Based upon the above setting, we propose the partial video-language alignment (PVLA) task, which is to minimize the following  $\mathcal{L}_{\text{PVLA}}$  loss equal to the partial optimal transport (POT) distance  $\mathcal{D}_{\text{POT}}$  between  $\boldsymbol{\mu}$  and  $\boldsymbol{\nu}$  as:

$$\mathcal{L}_{\text{PVLA}} = \mathcal{D}_{\text{POT}}(\boldsymbol{\mu}, \boldsymbol{\nu}) = \min_{\mathbf{T} \in \Pi(\mathbf{a}, \mathbf{b})} \sum_{i=1}^{N_V} \sum_{j=1}^{N_L} \mathbf{T}_{i,j} \cdot c(\mathbf{h}_{v,i}, \mathbf{h}_{l,j}), \quad (4.7)$$

$$\text{s.t. } \Pi(\mathbf{a}, \mathbf{b}) = \{ \mathbf{T} \in \mathbb{R}_+^{N_V \times N_L} \mid \mathbf{T} \mathbf{1}_{N_L} \leq \mathbf{a}, \mathbf{T}^\top \mathbf{1}_{N_V} \leq \mathbf{b}, \\ \mathbf{1}_{N_V}^\top \cdot \mathbf{T} \cdot \mathbf{1}_{N_L} = s, \quad 0 \leq s \leq \min(N_L, N_V) \}. \quad (4.8)$$

Because the exact minimization over the transport plan  $\mathbf{T}$  is intractable, we adopt the Sinkhorn-based algorithm to compute  $\mathbf{T}$ . We explicate our algorithm to calculate the partial video-language alignment loss in Algorithm 2.

---

**Algorithm 2** Computing the PVLA loss

---

**Require:**  $\mathbf{C} = \{\mathbf{C}_{i,j} = c(\mathbf{h}_{v,i}, \mathbf{h}_{l,j}) \mid 1 \leq i \leq N_V, 1 \leq j \leq N_L\} \in \mathbb{R}^{N_V \times N_L}$ ,  
 temperature  $\tau$ ,  $\mathbf{a} \in \mathbb{R}^{N_V}$ ,  $\mathbf{b} \in \mathbb{R}^{N_L}$ ,  $s$ ,  $N_{\text{iter}}$   
 $\mathcal{L}_{\text{PVLA}} = \infty$   
**for**  $s = 1$  to  $\min(N_L, N_V)$  **do**  
 $\mathbf{T} = \exp\left(-\frac{\mathbf{C}}{\tau}\right)$   
 $\mathbf{T} = \frac{s}{(\mathbf{1}_{N_V})^\top \cdot \mathbf{T} \cdot \mathbf{1}_{N_L}} \mathbf{T}$   
**for**  $i = 1$  to  $N_{\text{iter}}$  **do**  
 $\mathbf{p}_a = \min\left(\frac{\mathbf{a}}{\mathbf{T} \mathbf{1}_{N_L}}, \mathbf{1}_{N_V}\right)$ ,  $\mathbf{T}_a = \text{diag}(\mathbf{p}_a) \cdot \mathbf{T}$   
 $\mathbf{p}_b = \min\left(\frac{\mathbf{b}}{\mathbf{T}_a^\top \mathbf{1}_{N_V}}, \mathbf{1}_{N_L}\right)$ ,  $\mathbf{T}_b = \text{diag}(\mathbf{p}_b) \cdot \mathbf{T}_a$   
 $\mathbf{T} = \frac{s}{(\mathbf{1}_{N_V})^\top \cdot \mathbf{T} \cdot \mathbf{1}_{N_L}} \mathbf{T}_b$   
**end for**  
 $\mathcal{L}_{\text{PVLA}} = \min\left(\mathcal{L}_{\text{PVLA}}, \sum_{i=1}^{N_V} \sum_{j=1}^{N_L} \mathbf{T}_{i,j} \mathbf{C}_{i,j}\right)$   
**end for**  
**return**  $\mathcal{L}_{\text{PVLA}}$

---

Our PVLA formulation is flexible where it allows only  $s$  samples from one distribution to be transported to the other, and enables the algorithm to decide the value of  $s$ , in case the input language only corresponds to certain video aspects (or vice versa).

**Training Strategy.** For training, we jointly optimize the video-language task-specific loss and our PVLA loss. It is worth noting that we only update our introduced READ layers while keeping the remaining components frozen.

### 4.3 Experiments

Method	#params (M)	Dog	Gym	Par.	Ska.	Ski.	Sur.	Avg.
Full	283.97 (100%)	65.90 <sup>‡</sup>	75.20 <sup>‡</sup>	82.20 <sup>‡</sup>	71.80 <sup>‡</sup>	72.30 <sup>‡</sup>	81.15 <sup>‡</sup>	74.76 <sup>‡</sup>
Bias	0.51 (0.18%)	46.23 <sup>‡</sup>	61.19 <sup>‡</sup>	56.73 <sup>‡</sup>	31.36 <sup>‡</sup>	61.14 <sup>‡</sup>	49.77 <sup>‡</sup>	51.07 <sup>‡</sup>
Partial	38.75 (13.65%)	48.28 <sup>‡</sup>	63.26 <sup>‡</sup>	59.71 <sup>‡</sup>	32.66 <sup>‡</sup>	64.58 <sup>‡</sup>	56.22 <sup>‡</sup>	54.12 <sup>‡</sup>
Proj	5e-4 (1.76e-4%)	57.05 <sup>‡</sup>	65.70 <sup>‡</sup>	63.03 <sup>‡</sup>	71.83 <sup>‡</sup>	65.45 <sup>‡</sup>	79.71 <sup>‡</sup>	67.13 <sup>‡</sup>
LoRA	13.12 (4.62%)	60.97 <sup>‡</sup>	67.68 <sup>‡</sup>	72.53 <sup>‡</sup>	66.62 <sup>‡</sup>	71.24 <sup>‡</sup>	79.15 <sup>‡</sup>	69.70 <sup>‡</sup>
Prompt	0.02 (0.01%)	48.28 <sup>‡</sup>	63.26 <sup>‡</sup>	59.71 <sup>‡</sup>	35.67 <sup>‡</sup>	35.67 <sup>‡</sup>	64.61 <sup>‡</sup>	46.87 <sup>‡</sup>
Adapter	13.11 (4.62%)	62.89 <sup>‡</sup>	67.09 <sup>‡</sup>	74.56 <sup>‡</sup>	62.56 <sup>‡</sup>	68.10 <sup>‡</sup>	78.73 <sup>‡</sup>	68.98 <sup>‡</sup>
READ	0.16 (0.06%)	<b>67.65</b>	<b>78.05</b>	<b>83.25</b>	<b>72.40</b>	<b>72.98</b>	<b>82.36</b>	<b>76.12</b>

Table 4.1: TLG results on the YouTube Highlights dataset. We report the mean average precision (mAP) and the number of trainable parameters (#params). <sup>‡</sup>means the gain of READ is statistically significant at the 0.05 level.

Method	#params (M)	VT	VU	GA	MS	PK	PR	FM	BK	BT	DS	Avg.
Full	285.28 (100%)	84.17 <sup>‡</sup>	81.50 <sup>‡</sup>	88.20 <sup>‡</sup>	71.54 <sup>‡</sup>	81.40 <sup>‡</sup>	84.31 <sup>‡</sup>	72.30 <sup>‡</sup>	76.53 <sup>‡</sup>	78.86 <sup>‡</sup>	77.70 <sup>‡</sup>	79.65 <sup>‡</sup>
Bias	0.25 (0.09%)	38.08 <sup>‡</sup>	69.62 <sup>‡</sup>	60.87 <sup>‡</sup>	31.25 <sup>‡</sup>	68.84 <sup>‡</sup>	51.71 <sup>‡</sup>	50.72 <sup>‡</sup>	65.38 <sup>‡</sup>	54.42 <sup>‡</sup>	59.05 <sup>‡</sup>	54.99 <sup>‡</sup>
Partial	38.75 (13.58%)	57.27 <sup>‡</sup>	62.57 <sup>‡</sup>	58.08 <sup>‡</sup>	52.35 <sup>‡</sup>	61.58 <sup>‡</sup>	63.94 <sup>‡</sup>	50.82 <sup>‡</sup>	62.36 <sup>‡</sup>	58.05 <sup>‡</sup>	47.79 <sup>‡</sup>	57.48 <sup>‡</sup>
Proj	5e-4 (1.75e-4%)	57.65 <sup>‡</sup>	65.80 <sup>‡</sup>	64.40 <sup>‡</sup>	55.57 <sup>‡</sup>	64.67 <sup>‡</sup>	67.07 <sup>‡</sup>	59.08 <sup>‡</sup>	74.70 <sup>‡</sup>	63.29 <sup>‡</sup>	49.48 <sup>‡</sup>	62.17 <sup>‡</sup>
LoRA	13.28 (4.66%)	77.87 <sup>‡</sup>	77.01 <sup>‡</sup>	77.82 <sup>‡</sup>	66.38 <sup>‡</sup>	80.21 <sup>‡</sup>	82.23 <sup>‡</sup>	66.89 <sup>‡</sup>	72.31 <sup>‡</sup>	69.58 <sup>‡</sup>	72.09 <sup>‡</sup>	74.24 <sup>‡</sup>
Prompt	0.02 (0.007%)	61.67 <sup>‡</sup>	71.98 <sup>‡</sup>	64.07 <sup>‡</sup>	35.54 <sup>‡</sup>	72.74 <sup>‡</sup>	48.70 <sup>‡</sup>	52.97 <sup>‡</sup>	67.59 <sup>‡</sup>	57.28 <sup>‡</sup>	38.60 <sup>‡</sup>	57.11 <sup>‡</sup>
Adapter	13.29 (4.66%)	78.46 <sup>‡</sup>	76.38 <sup>‡</sup>	77.36 <sup>‡</sup>	67.12 <sup>‡</sup>	80.33 <sup>‡</sup>	82.51 <sup>‡</sup>	67.77 <sup>‡</sup>	71.71 <sup>‡</sup>	69.58 <sup>‡</sup>	71.24 <sup>‡</sup>	74.25 <sup>‡</sup>
READ	0.14 (0.05%)	<b>88.30</b>	<b>85.15</b>	<b>89.76</b>	<b>75.80</b>	<b>86.69</b>	<b>86.62</b>	<b>74.99</b>	<b>82.38</b>	<b>84.65</b>	<b>79.60</b>	<b>83.39</b>

Table 4.2: TLG results on the TVSum dataset. We report the mean average precision (mAP) and the number of trainable parameters (#params). <sup>‡</sup>means the gain of READ is statistically significant at the 0.05 level.

Method	#params (M)	mAP
Full	15.88 (100%)	36.14 <sup>‡</sup>
Bias	0.06 (0.38%)	24.89 <sup>‡</sup>
Partial	1.05 (6.61%)	26.37 <sup>‡</sup>
Proj	7.31 (46.03%)	32.71 <sup>‡</sup>
LoRA	0.19 (1.20%)	33.96 <sup>‡</sup>
Prompt	0.04 (0.25%)	25.86 <sup>‡</sup>
Adapter	0.20 (1.26%)	33.61 <sup>‡</sup>
READ	0.19 (1.20%)	<b>36.74</b>

Table 4.3: TLG results on the QVHighlights dataset. We report the mean average precision (mAP) and the number of trainable parameters (#params). <sup>‡</sup>means the gain of READ is statistically significant at the 0.05 level.

We conduct extensive experiments to evaluate the effectiveness of our READ framework. We first describe the experimental settings, covering the downstream tasks, evaluation metrics, pre-trained backbones, baseline approaches, and implementation details. We then present the numerical results of our method with baseline models, then provide ablation study and thorough analysis to explore various configurations. Eventually, we perform qualitative assessments to further elucidate the behavior of our framework.

### 4.3.1 Experimental Settings

**Downstream tasks.** We assess the effectiveness on the temporal language grounding and video-language summarization tasks. The corresponding datasets to each task are presented as follows:

- *Temporal Language Grounding (TLG):* The TLG’s task is to localize temporal

boundaries of the video frames that semantically relate to the language query. The evaluation is performed upon three datasets, *i.e.* YouTube Highlights (Sun et al., 2014), TVSum (Song et al., 2015), and QVHighlights (Lei et al., 2021b). YouTube Highlights consists of 40 video-language training inputs for each of the 6 domains. TVSum comprises 10 domains, each of which possesses 5 video-language training inputs. The QVHighlights benchmark includes 7,218 language-annotated video segments for training, 1,550 for development, and 1,542 for testing. Following previous work on low-resource experiments (Boulanger et al., 2022), we keep our training size at 700 samples, which is less than 10% of the full data for the QVHighlights dataset, while preserving the original splits on the TVSum and YouTube Highlights datasets.

- *Video-Language Summarization (VLS)*: Given a video-language input, the VLS’s target is to generate a summary which takes into account both video and language content (Yu et al., 2021). We consider the How2 dataset (Sanabria et al., 2018), from which we randomly draw 2,000 out of 73,993 samples for training, *i.e.* less than 3% of the full data, to simulate the low-resource settings, while maintaining 2,520 samples for validation, and 2,127 samples for testing.

**Evaluation metrics.** For the TLG task, we follow previous works (Lei et al., 2021b; Liu et al., 2022b) to use the mean average precision (mAP) metric. Regarding VLS, we utilize the ROUGE score, which is a popular metric for summarization (Zhang et al., 2020b; Yu et al., 2021).

Method	#params (M)	R1	R2	RL
Full	249.67 (100%)	35.72 <sup>‡</sup>	11.88 <sup>‡</sup>	30.00 <sup>‡</sup>
Bias	0.20 (0.08%)	30.51 <sup>‡</sup>	8.20 <sup>‡</sup>	23.00 <sup>‡</sup>
Partial	16.54 (6.62%)	31.55 <sup>‡</sup>	8.63 <sup>‡</sup>	13.65 <sup>‡</sup>
Proj	38.60 (15.46%)	32.76 <sup>‡</sup>	9.11 <sup>‡</sup>	30.01 <sup>‡</sup>
LoRA	1.19 (0.48%)	40.04 <sup>‡</sup>	20.36 <sup>‡</sup>	35.98 <sup>‡</sup>
Prompt	0.05 (0.02%)	31.55 <sup>‡</sup>	8.63 <sup>‡</sup>	14.90 <sup>‡</sup>
Adapter	1.20 (0.48%)	41.52 <sup>‡</sup>	20.75 <sup>‡</sup>	36.88 <sup>‡</sup>
READ	1.17 (0.47%)	<b>44.01</b>	<b>21.91</b>	<b>37.91</b>

Table 4.4: VLS results on the How2 dataset with the VG-BART model. We report the ROUGE-1, ROUGE-2, and ROUGE-L scores, with the number of trainable parameters (#params). <sup>‡</sup>means the gain of READ is statistically significant at the 0.05 level.

Method	#params (M)	R1	R2	RL
Full	333.16 (100%)	32.37 <sup>‡</sup>	8.07 <sup>‡</sup>	26.53 <sup>‡</sup>
Bias	0.07 (0.02%)	27.03 <sup>‡</sup>	4.53 <sup>‡</sup>	19.51 <sup>‡</sup>
Partial	16.52 (4.96%)	27.83 <sup>‡</sup>	4.92 <sup>‡</sup>	10.49 <sup>‡</sup>
Proj	24.67 (7.40%)	29.16 <sup>‡</sup>	5.50 <sup>‡</sup>	26.76 <sup>‡</sup>
LoRA	1.93 (0.58%)	36.63 <sup>‡</sup>	16.72 <sup>‡</sup>	32.77 <sup>‡</sup>
Prompt	0.18 (0.05%)	28.33 <sup>‡</sup>	5.12 <sup>‡</sup>	11.75 <sup>‡</sup>
Adapter	1.95 (0.59%)	37.83 <sup>‡</sup>	17.45 <sup>‡</sup>	33.87 <sup>‡</sup>
READ	1.91 (0.57%)	<b>40.12</b>	<b>18.71</b>	<b>34.42</b>

Table 4.5: VLS results on the How2 dataset with the VG-T5 model. We report the ROUGE-1, ROUGE-2, and ROUGE-L scores, with the number of trainable parameters (#params). <sup>‡</sup>means the gain of READ is statistically significant at the 0.05 level.

Method	mAP - YouTube Highlights	R2 - How2
No VLA	73.80	18.22
VLA	74.41	20.01
PVLA	76.12	21.91

Table 4.6: Partial video-language alignment (PVLA) ablation experiments on YouTube Highlights and How2. We color the settings we implement for our READ method.

Video	Language query	POT distance	AP
	Girl's expression after getting proposal	27.17	90.28
	A boy showing his arm after being stung at the beach	56.38	30.00

Table 4.7: Case study on the temporal language grounding benchmark. We extract the POT distance between video and language of two inputs with different language queries and measure the respective AP performance change.

Recurrent architecture	#params - UMT (M)	mAP - YouTube Highlights	#params - VG-BART (M)	R2 - How2
GRU	0.16	76.07	1.17	21.85
LSTM	0.16	76.08	1.17	21.87
RNN	0.16	76.12	1.17	21.91

Table 4.8: Recurrent architecture ablation experiment on YouTube Highlights and How2. We color the settings we implement for our READ method.

Distance method	mAP - YouTube Highlights	R2 - How2
AvgPool - Cosine	71.65	20.32
MaxPool - Cosine	74.37	21.36
AvgPool - L2	72.11	20.73
MaxPool - L2	74.39	21.02
Partial OT	76.12	21.91

Table 4.9: Distance method ablation experiments on YouTube Highlights and How2. We color the settings we implement for our READ method.

**Pre-trained backbones.** We adopt the Transformer encoder-decoder architecture (Vaswani et al., 2017) pre-trained with both supervised and self-supervised objectives.

Specifically, for TLG, we use the unified multimodal transformer (UMT) (Liu et al., 2022b) and Moment-DETR (Lei et al., 2021b) models pre-trained upon the automatic speech recognition task. For VLS, we carry out the parameter-efficient adaptation on the generative vision-guided BART (VG-BART) and T5 (VG-T5) (Yu et al., 2021) pre-trained upon reconstruction and masked language modeling tasks (Raffel et al., 2020).

**Baseline methods.** We compare our method with a comprehensive list of baseline approaches for efficient video-language transfer learning:

- *Full*: update all parameters of the pre-trained backbone.
- *Partial*: only update the last layers of the encoder and decoder in the Transformer model.
- *Bias* (Zaken et al., 2022): only fine-tune the bias terms in the Transformer backbone.
- *Proj*: fine-tune only the last linear projection layer in the Transformer.
- *LoRA* (Hu et al., 2021): solely fine-tune the decomposition matrices introduced to the linear weights of the Transformer model.
- *Prompt* (Jia et al., 2022a): Append a sequence of learnable prompt tokens to both video and language inputs and only fine-tune the appended sequence.
- *Adapter* (Houlsby et al., 2019): update only the adaptation modules consisting of downprojection and up-projection layers inserted into the Transformer model.

**Implementation details.** For the TLG task, we use the SlowFast (Feichtenhofer et al., 2019) and video encoder of CLIP (Radford et al., 2021) to extract features every 2 seconds. For the VLS task, we use a 3D ResNeXt-101 model to extract a 2048-dimensional embedding for every 16 non-overlapping frames. Similar to previous works (Houlsby et al., 2019; Chen et al., 2022), to support training stability, we initialize the weights of the down-projection layer  $W_{\text{down}}$  with the Kaiming normal (He et al., 2015) method, whereas those of the up-projection  $W_{\text{up}}$ , recurrent layer RNN, and biases of our READ layers are configured with zero initialization. In

our PVLA framework, we implement the cost distance  $c(\mathbf{h}_{v,i}, \mathbf{h}_{l,j})$  as the cosine distance  $c(\mathbf{h}_{v,i}, \mathbf{h}_{l,j}) = 1 - \frac{\mathbf{h}_{v,i} \cdot \mathbf{h}_{l,j}}{\|\mathbf{h}_{v,i}\|_2 \cdot \|\mathbf{h}_{l,j}\|_2}$ , and set the maximum number of iterations  $N_{\text{iter}}$  to 1,000 and the temperature  $\tau$  to 0.05. We fine-tune all models leveraging the AdamW optimizer on 4 NVIDIA Tesla V100 GPUs and report average results of 5 runs. Specific details about the epoch, batch size, learning rate, and the number of Transformer blocks for each task can be found in the Appendix.

### 4.3.2 Main Results

For main comparison of our READ with baseline methods, we denote the results of YouTube Highlights in Table 4.1, TVSum in Table 4.2, QVHighlights in Table 4.3, and How2 in Tables 4.4 and 4.5.

**Temporal language grounding (TLG).** For the YouTube Highlights dataset, our READ framework substantially outperforms the Full fine-tuning approach (*e.g.* 1.36% on average, 1.75% in the Dog domain, and 1.21% in the Surfing domain), while updating far less parameters (0.16M vs. 283.97M). We significantly surpass all other efficient fine-tuning methods as well, *e.g.* with an improvement of 10.96% over the Adapter in the Gym category, or 5.78% over LoRA in the Skating category.

For the TVSum dataset, we observe that our method enhances the Full fine-tuning direction with only 0.14M versus 285.28M tunable parameters. For instance, we obtain an increase of 4.26% in the MS subset and 3.74% on average. Compared with the best parameter-efficient approach, *i.e.* the Adapter, we achieve a gain of 15.07% in BT, 10.67% in BK, and 8.77% in the VU domain.

Our improvement also generalizes across different pre-trained backbone. On the QVHighlights dataset, in which we work with the Moment-DETR architecture, we accomplish a gain of 0.6% over the standard fine-tuning method, while our tunable parameters are only 0.19M versus its 15.88M. We also surpass the efficient approach LoRA with an enhancement of 2.78% in mAP.

These results demonstrate that our READ framework can efficiently model video-language inputs to polish the low-resource temporal language grounding performance of various pre-trained Transformer models.

**Video-language summarization (VLS).** Analogous to the TLG experiment, on the VG-BART backbone, we improve upon the full fine-tuning approach with

8.29 points of ROUGE-1, 10.03 points of ROUGE-2, and 7.91 points of ROUGE-L. Importantly, we only update 1.17M parameters, which account for 0.47% total parameters of the overall model. On the VG-T5 backbone, we exceed the full approach by 7.75 points in ROUGE-1, 10.64 points in ROUGE-2, and 7.89 points in ROUGE-L, whilst keeping 99.43% parameters frozen.

In addition, our framework substantially outperforms other fine-tuning strategies, *e.g.* LoRA with 3.97 points in ROUGE-1, 1.55 points in ROUGE-2, and 1.93 points in ROUGE-L on the VG-BART architecture, along with 3.49 points in ROUGE-1, 1.99 points in ROUGE-2, and 1.65 points in ROUGE-L on the VG-T5 one.

These results substantiate that our method is applicable to diverse benchmarks and model architectures, particularly not only multimodal Transformers for temporal language grounding but also generative Transformers for video-language summarization. We hypothesize that our advantages are due to the recurrent adapter’s ability to model temporal information and the PVLA task to align video and language signals to maintain more essential information during the efficient fine-tuning stage.

### 4.3.3 Ablation Studies

We ablate our READ framework to discover what factors result in the demonstrated efficiency and observe several intriguing properties. Our ablation studies are all conducted on the YouTube Highlights and How2 test set.

**Effects of video-language alignment.** We evaluate our framework without the assistance of the PVLA task and with the one of the VLA variant that requires all masses of one distribution to be transferred (we set  $s = \min(N_V, N_L)$  in formulation (6.8)). As shown in Table 4.6, the performance drops dramatically when we remove the PVLA task from the fine-tuning procedure. We conjecture that the model has become deficient in managing the information injected into the low-dimensional space of the READ layers, thus passing detrimental noise to the downstream task. Moreover, the VLA variant brings slight performance decrease, which could be due to the VLA’s restrictive nature of transporting all masses from the language distribution to the video one or vice versa.

**Effects of the recurrent architecture.** In addition to RNN, there exist various recurrent architectures in the literature, particularly the gated recurrent unit (GRU)

(Cho et al., 2014) and long short-term memory (LSTM) (Hochreiter and Schmidhuber, 1997). We experiment with different recurrent choices and explicate the results in Table 4.8. As can be observed, the performance is insensitive to the choice of recurrent design. Therefore, we select the simplest option, *i.e.* recurrent neural network (RNN) for our READ layers.

**Distance methods.** We further ablate on the distance metrics to estimate the distance between video and language distributions. Technically, we perform the average- and max-pooling of the video and language representations. Then, we consider the cosine distance or the L2 distance of the two pooled vectors as the video-language distance. Results in Table 4.9 substantiate the superiority of our POT distance for the PVLA objective. Such success illustrates the POT-based PVLA’s advantage of modeling the relationship nature between video and language representations

#### 4.3.4 Qualitative Assessment

**Case study.** We display a TLG example on the YouTube Highlights dataset, along with the POT distance estimated by our PVLA framework and the AP score in Table 4.7. We observe that when the language query semantically corresponds to a moment in the video, *i.e.* *a girl expression after she gets the proposal*, the POT distance is small and correlates with the high value of AP. In contrast, when we replace the original query with an out-of-distribution one, the POT distance burgeons significantly, causing the AP to decrease from 90.28% to 30.00%. Therefore, we conclude that our READ framework is capable of intelligently adjusting the information flowing through the READ layers in order to produce the final output consistent with the video-language input and downstream tasks.

### 4.4 Conclusion

We propose a novel READ-PVLA framework for parameter-efficient transfer learning to video-language modeling tasks. Our READ-PVLA utilizes recurrent computation component to enable temporal modeling capability and partial video-language alignment objective to preserve critical information for bottleneck adaptation modules. Experiments demonstrate that READ-PVLA consistently outperforms both the full

fine-tuning and competitive strategies, whilst bringing the benefit of parameter-efficiency (at most 1.20% trainable parameters). Our method is also applicable to diverse pre-trained models, which has the potential to employ more powerful video-language models in the future.

# Chapter 5

## Encoding and Controlling Global Semantics for Long-form Video Question Answering

### 5.1 Introduction

VideoQA has been extensively studied to develop systems to assist humans in daily activities (Grauman et al., 2022; Lei et al., 2021d), *e.g.*, remind users of their past actions, help users locate their belongings, and provide assistance with complex tasks. To implement these functions, we expect videoQA systems to understand and extract relevant information from long-form videos with diverse objects and complex spatial-temporal interactions.

Compared with short clips, long-form videos pose more challenges for videoQA. They consist of a higher number of objects and events. As such, comprehensively encoding information from them requires expensive computations. Moreover, a high amount of information may be unrelated to the posed question. To address these problems, recent studies (Bain et al., 2021; Wang et al., 2023a; Gao et al., 2023) adaptively select a subset of video frames and visual regions associated with the question. Nevertheless, if a question necessitates a reasoning of the entire sequence of events (*e.g.* video 1’s Figure 5.1), or an understanding of the overall video narration (*e.g.* video 2’s Figure 5.1), a mere handful of selected frames or regions might not sufficiently encapsulate necessary details.

To tackle these problems, we introduce a state space layer (SSL). Before forward-ing video frames to selection modules, SSL fixes long-term dependency patterns for integrating global information into visual representations. Such global information

Video 1: 3037 IRON MAN2 - Video length: 2.08 hours



Question: what if the person did not have the *ingot of palladium* to replace the smoking one in the *rt unit*?

Answer: The RT unit would degrade, potentially causing the *person's health* to deteriorate or the *armored suit* to malfunction.

Video 2: fb7cc35d-3272-44a4-b8f2-15cd24fa345b - Video length: 33.27 minutes



Question: what *central theme* best describes activities throughout the video?

Answer: routine household management and maintenance

Figure 5.1: Long-form videoQA examples, with videos taken from MAD (Soldan et al., 2022) and Ego4D (Grauman et al., 2022) datasets, respectively. Question in video 1 requires the model to reason about the relation chain of replacing *ingot of palladium* to activate the *rt unit* that powers the *armored suit* and protects *person's health*. Question in video 2 necessitates an understanding of the overall theme in video 2.

offers the selected frames the global context within the video, so that they can relate to other frames even though those frames are not selected for attention computation. However, a considerable amount of unrelated global information may flow into visual representations. Therefore, we first equip SSL with a gating mechanism to provide more controllability over the flow of global semantics into visual representations, resulting in our **Gated State space Multi-modal Transformer** (GSMT) architecture. Furthermore, we promote global semantics that is more aligned with the question. In particular, we introduce **Cross-modal Compositional Congruence** (C<sup>3</sup>) objective that compares visual attention with its version transitioned to the language basis via cross-modal attention, effectively measuring cross-modal congruence between intra-modal relations. Our rationale behind focusing on intra-modal relations is because videoQA models often need to understand spatial and temporal relationships between entities and events posed by the question (Gandhi et al., 2022), thus we encourage globally informed visual representations to maintain compositional consistency between visual patches and question entities.

Remarkably, we observe that recent long-form videoQA works (Gao et al., 2023; Islam et al., 2024) still mostly evaluate on videos lasting at most one minute or two, and use short-natured questions which necessitate watching only a short period of

video, *i.e.*, about 100 seconds (Mangalam et al., 2023), to determine the answer. To more rigorously evaluate long-form videoQA capacity, we introduce a construction procedure which utilizes large language model (LLM) to generate questions and associated answers for egocentric and movie videos whose average lengths are 17.5 minutes and 1.9 hours, respectively. Additionally, we also conduct automatic and manual filtering to obtain high-quality questions which require watching a video up to 1200 seconds to answer, longer than any existing long-form videoQA benchmarks (Xiao et al., 2021b; Wu et al., 2021; Mangalam et al., 2023).

To sum up, our contributions are as follows:

- We propose a Gated State space Multi-modal Transformer (GSMT) with state space layer (SSL) to integrate global information into visual representations for long-form videoQA.
- We equip SSL with a gating mechanism to provide controllability over the flow of global video semantics and a Cross-modal Compositional Congruence ( $C^3$ ) objective to encourage question-aligned visual representations.
- We curate two new datasets with excessively long video lengths and long-natured questions for long-form videoQA. Comprehensive experiments on our curated and five standard datasets substantiate the superiority of our framework over various competitive baselines.

## 5.2 Methodology

The formulation of video question answering (videoQA) is to predict the answer  $y$  for a question  $q$  about a video  $\mathcal{V}$  as follows:

$$\tilde{y} = \arg \max_{y \in \mathcal{A}} \mathcal{F}_\theta(y|q, \mathcal{V}, \mathcal{A}), \quad (5.1)$$

where  $\tilde{y}$  denotes the predicted answer chosen from the set of candidate options  $\mathcal{A}$ , and  $\theta$  denotes the trainable parameters of a videoQA model. With this videoQA task formulation, we explain our proposed GSMT architecture as the model  $\mathcal{F}_\theta$  and  $C^3$  objective to support GSMT. The overall framework is illustrated in Figure 5.2.

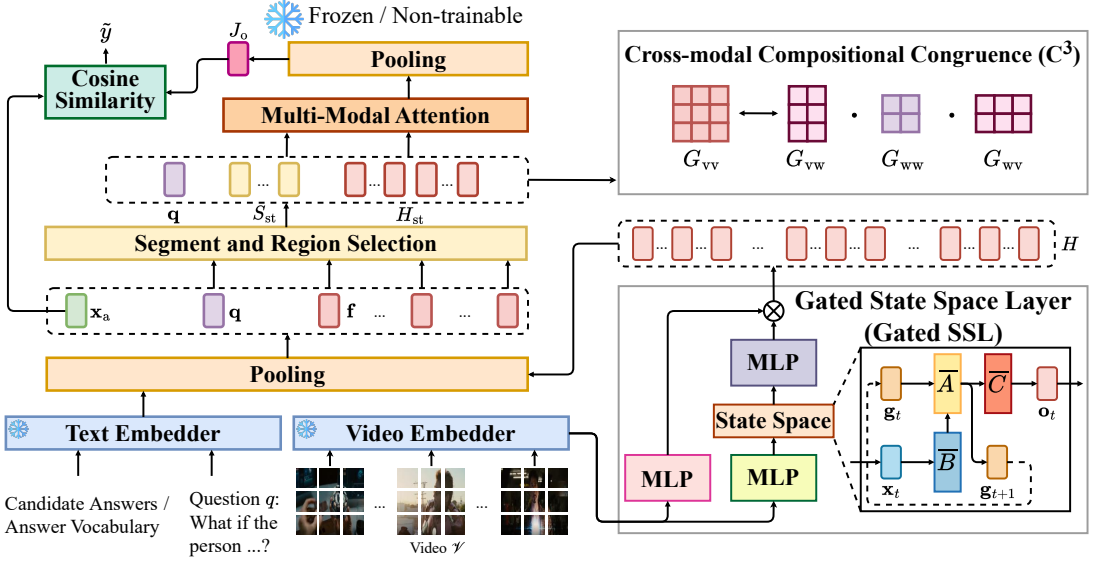


Figure 5.2: Illustration of the GSMT architecture empowered by gated SSL and  $C^3$  training objective.

### 5.2.1 Gated State Space Multi-Modal Transformer (GSMT)

Our GSMT takes videos and questions as input, divides each video frame into visual patches and a question into textual words, and then forwards visual patches and textual words into video and text embedder to extract initial representations.

**Input Embedder.** For video embedder, we utilize frozen pre-trained vision-language Transformer to extract patch-level features  $X = \{\mathbf{x}_0, \mathbf{x}_1, \dots, \mathbf{x}_{L-1}\}$ , of all  $T$  frames, where  $t$ -th frame consists of  $N$  patch-level features  $\{\mathbf{x}_{t,j}\}_{j=0}^{N-1}$ , hence  $L = NT$ , and  $\mathbf{x} \in \mathbb{R}^d$ . For text embedder, a similar frozen pre-trained vision-language Transformer is used to obtain word-level features  $W = \{\mathbf{w}_0, \mathbf{w}_1, \dots, \mathbf{w}_{M-1}\}$ , where  $\mathbf{w}_0$  corresponds to the [CLS] token and  $\mathbf{w}_1, \dots, \mathbf{w}_{M-1}$  correspond to words in the question.

**Gated State Space Layer (Gated SSL).** Inspired by (Gu et al., 2021), we define a sequence-to-sequence map  $SSL(X)$  from a sequence of patch-level features to  $d_S$ -dim hidden states, parameterized by learnable state matrices  $A \in \mathbb{R}^{d_S \times d}$ ,  $B \in \mathbb{R}^{d_S \times d}$ ,  $C \in \mathbb{R}^{d \times d_S}$ , and step size  $\Delta$  as:

$$\mathbf{g}_{t+1} = \overline{A} \cdot \mathbf{g}_t + \overline{B} \cdot \mathbf{x}_{t+1}, \quad \mathbf{o}_{t+1} = \overline{C} \cdot \mathbf{g}_{t+1}, \quad (5.2)$$

$$\overline{A} = e^{A\Delta}, \quad \overline{B} = (\overline{A} - I)A^{-1}B, \quad \overline{C} = C. \quad (5.3)$$

We unroll the mapping to obtain:

$$\mathbf{o}_t = \sum_{j=0}^t \overline{CA}^j \overline{B} \cdot \mathbf{x}_{t-j}. \quad (5.4)$$

This can be written as a convolutional representation  $O = \bar{\Gamma} * X$ , where  $\bar{\Gamma} = (\overline{CB}, \overline{CAB}, \dots, \overline{CA}^{L-1} \overline{B})$  denotes the convolutional kernel,  $*$  the discrete convolution operator,  $X$  the input sequence,  $O$  the corresponding output sequence. This convolution denotes the fixed global dependency pattern that facilitates the computation of global information among visual patches. We use Fast Fourier Transformer (FFT) (Cooley and Tukey, 1965) to compute the convolution in parallel provided that  $\bar{\Gamma}$  has been obtained.

Computing the kernel  $\bar{\Gamma}$  is non-trivial since it requires  $L$  distinct matrix powers. Instead, inspired by (Gupta et al., 2022), we initialize  $A$  to be a diagonal matrix  $\text{diag}(\lambda_1, \lambda_2, \dots, \lambda_{d_s})$  and  $B$  to all-one matrix  $\mathbb{1}_{d_s \times d}$ . Due to this initialization, the kernel can be computed as:

$$\bar{\Gamma} = (C \odot E) \cdot P, \quad (5.5)$$

where  $E = \left( \frac{e^{\lambda_1 \Delta - 1}}{\lambda_1}, \frac{e^{\lambda_2 \Delta - 1}}{\lambda_2}, \dots, \frac{e^{\lambda_{d_s} \Delta - 1}}{\lambda_{d_s}} \right) \in \mathbb{R}^{d_s}$ , in which  $P_{i,j} = e^{\lambda_i \cdot j \cdot \Delta} \in \mathbb{R}^{d_s \times L}$ , and  $\odot$  denotes the element-wise multiplication.

To equip SSL with the control over which global semantics to integrate into visual representations, we construct a gating unit as:

$$U = \phi(\text{Linear}(X)), \quad V = \phi(\text{Linear}(X)), \quad (5.6)$$

$$O = \text{Linear}(\text{SSM}(U)), \quad (5.7)$$

$$H = \text{Linear}(O \odot V), \quad (5.8)$$

where  $U, V, O \in \mathbb{R}^{L \times d_{\text{gating}}}$  denote the intermediate gating representations,  $H \in \mathbb{R}^{L \times d_h}$  the visual representations output by gated SSL,  $\phi$  the non-linear activation, and  $d_{\text{gating}} < d, d_h, d_s$ .

**Visual Segment and Region Selection.** After obtaining visual patch-level hidden representations  $H$ , we proceed to obtain frame features by pooling each frame  $t$ 's visual patches:

$$\mathbf{f}_t = \text{pool}(\mathbf{h}_{t,0}, \mathbf{h}_{t,1}, \dots, \mathbf{h}_{t,N-1}). \quad (5.9)$$

Subsequently, we group non-overlapping consecutive frames into a segment to obtain  $I$  segments, each of which contains  $N_p = \lceil \frac{L}{I} \rceil$  patches and  $N_f = \lceil \frac{T}{I} \rceil$  frames. We

proceed to compute segment features through pooling frame features corresponding to the segment:

$$\mathbf{s}_i = \text{pool}(\mathbf{f}_{i,0}, \mathbf{f}_{i,1}, \dots, \mathbf{f}_{i,N_f-1}). \quad (5.10)$$

Similarly, we also pool word features to obtain the question representation:

$$\mathbf{q} = \text{pool}(\mathbf{w}_0, \mathbf{w}_1, \dots, \mathbf{w}_{M-1}). \quad (5.11)$$

Given the segment features  $S = \{\mathbf{s}_i\}_{i=0}^{I-1}$  and question feature  $\mathbf{q}$ , we conduct top- $k$  segment selection:

$$Q = \text{Linear}(\mathbf{q}), \quad K = \text{Linear}(S), \quad (5.12)$$

$$\mathcal{B} = \underset{\text{Top}_k}{\text{selector}} \left( \text{softmax} \left( \frac{QK^\top}{\sqrt{d_k}} \right) \right). \quad (5.13)$$

We implement *selector* as a differentiable Gumbel-softmax selection function. The output of the *selector* is a sequence of segment index  $\mathcal{B}$ . Thereby, we extract respective segment features with respect to the selected segment indices, *i.e.*  $S_{\text{st}} = \{\mathbf{s}_b \mid b \in \mathcal{B}\}$ .

For every frame  $\tau$  in the selected segments, we then perform cross-modal attention between its patch-level hidden representations  $H_\tau = \{\mathbf{h}_{\tau,j}\}_{j=0}^{N-1}$ ,  $\tau \in \{\lfloor \frac{b}{N_f} \rfloor \mid b \in \mathcal{B}\}$  and the question to select top- $j$  question-related patches:

$$Q = \text{Linear}(\mathbf{q}), \quad K = \text{Linear}(H_\tau), \quad (5.14)$$

$$\mathcal{T} = \underset{\text{Top}_j}{\text{selector}} \left( \text{softmax} \left( \frac{QK^\top}{\sqrt{d_k}} \right) \right). \quad (5.15)$$

Lastly, we stack the selected patches of all selected frames to obtain  $H_{\text{st}} = \{\mathbf{h}_{\tau,j} \mid \tau \in \mathcal{T}\}_{j=0}^{N-1}$ .

**Multi-Modal Attention.** At present, we employ self-attention to produce multi-modal hidden representations that fuse the information of question and video. In particular, we concatenate the question word-level features  $Q = \{\mathbf{w}_i\}_{i=0}^{M-1}$ , selected segment features  $S_{\text{st}} = \{\mathbf{s}_b \mid b \in \mathcal{B}\}$ , and selected patch features  $H_{\text{st}} = \{\mathbf{h}_{\tau,j} \mid \tau \in \mathcal{T}\}_{j=0}^{N-1}$ :

$$J = [\text{Linear}(S_{\text{st}}), \text{Linear}(H_{\text{st}}), \text{Linear}(\mathbf{q})], \quad (5.16)$$

where  $[\cdot]$  denotes the concatenation operator. Thereafter, we iteratively conduct self-attention over the concatenated features for  $N_L$  layers to accomplish multi-modal

contextual representations:

$$J^{(i+1)} = \text{SelfAttention} \left( J^{(i)} \right), \quad 0 \leq i \leq N_L - 1. \quad (5.17)$$

**Answer Prediction.** Afterwards, we pool the features of all multi-modal self-attention layers:

$$J_o = \text{pool} \left( J^{(0)}, J^{(1)}, \dots, J^{(N_L-1)} \right). \quad (5.18)$$

Then, we calculate the cosine similarity between  $J_o$  and the feature of all candidate answers  $X_{\text{ans}} = \{\mathbf{x}_a \mid a \in \mathcal{A}\}$  obtained by utilizing the pre-trained model. We choose the candidate answer of the highest similarity as the final prediction  $\tilde{y}$ :

$$\tilde{y} = \arg \max_{y \in \mathcal{A}} \left( J_o \cdot (X_{\text{ans}})^{\top} \right). \quad (5.19)$$

### 5.2.2 Cross-modal Compositional Congruence ( $C^3$ ) Objective

Based on Eq. (5.17), we denote the output representations of visual patches as  $J_v$  and those of question words as  $J_w$ . We calculate cross-modal attention:

$$G_{vw} = J_v \cdot (J_w)^{\top}, \quad G_{wv} = J_w \cdot (J_v)^{\top}, \quad (5.20)$$

and intra-modal visual and textual attention as:

$$G_{vv} = J_v (J_v)^{\top}, \quad G_{ww} = J_w (J_w)^{\top}. \quad (5.21)$$

Given the intra-modal and cross-modal attention, we perform the change of basis to compute the intra-modal visual attention in the language space:

$$R_{vv} = G_{vw} G_{ww} (G_{vv})^{\top}. \quad (5.22)$$

As such, we define the loss objective to align the original  $G_{vv}$  with the change-of-basis version  $R_{vv}$ :

$$\mathcal{L}_{C^3} = \text{m-KL} (\text{softmax} (R_{vv}), \text{softmax} (G_{vv})), \quad (5.23)$$

where m-KL denotes the symmetric Kullback-Leibler Divergence (KL) between  $R$  and  $G$ :

$$\text{m-KL}(R, G) = \text{KL}(R||G) + \text{KL}(G||R). \quad (5.24)$$

### 5.2.3 Overall Objective

We jointly optimize the softmax cross-entropy loss  $\mathcal{L}_{\text{CE}}$  between the log-likelihood of the model prediction  $\tilde{y}$  and the groundtruth answer  $y$ , with our proposed cross-modal alignment objective  $\mathcal{L}_{\text{C}^3}$ :

$$\mathcal{L} = \mathcal{L}_{\text{CE}} + \gamma \cdot \mathcal{L}_{\text{C}^3}, \quad (5.25)$$

where  $\gamma$  denotes the hyperparameter to control the effect of the cross-modal alignment objective.

## 5.3 Ego-QA and MAD-QA Benchmarks

To more rigorously evaluate long-form videoQA models, we construct two new datasets, *i.e.* Ego-QA and MAD-QA.

### 5.3.1 Ego-QA

We inherit 3k hours of 8640 egocentric videos from the Ego4D dataset (Grauman et al., 2022). Each video is associated with about 280 dense captions of consecutive moments. Based on these captions, we create our dataset in 2 stages, *i.e.* question-answer generation and data filtering.

**Question-answer generation.** In this first stage, we concatenate a video’s dense captions following the time order to construct its language description. We utilize GPT-4 (Achiam et al., 2023) to generate 20 questions per video. In our prompt, we encourage GPT-4 to avoid questions that are visually biased and can be answered by a short video moment. Then, we present the generated questions to GPT-4 to generate the correct answer along with 4 wrong answer choices.

**Data filtering.** In the second stage, we filter out questions that include clue words, *e.g.* “*passage*”, “*text*”, and “*description*”. Moreover, we also remove questions that GPT-4 can answer without looking at the concatenated narration or the question. Then, we adopt manual filtering by asking ten graduate students who are native English speakers to ensure the veracity and temporal certificate length for every question-answer sample. Particularly, annotators are instructed to verify that 1) questions are valid and the correct answer is indeed correct, 2) all distractor answers

Question Types	Obj-Rel	Rel-Act	Obj-Act	Super	Seq	Exists	Dur-Comp	Act-Rec	All
AIO	48.34	48.99	49.66	37.53	49.61	50.81	45.36	18.97	48.59
ATP	50.15	49.76	46.25	39.78	48.25	51.79	49.59	18.96	49.79
MIST-AIO	51.43	54.67	55.37	41.34	53.14	53.49	47.48	20.18	50.96
MIST-CLIP	51.68	67.18	68.99	42.05	67.24	60.33	54.62	19.69	54.39
GSMT-AIO	53.67	56.10	56.61	43.44	53.84	56.26	49.83	21.73	52.61
GSMT-CLIP	<b>53.94</b>	<b>69.84</b>	<b>72.53</b>	<b>44.19</b>	<b>69.12</b>	<b>61.45</b>	<b>57.32</b>	<b>21.20</b>	<b>56.16</b>

Table 5.1: Results of videoQA on AGQA-v2.

are incorrect, and 3) the video length to watch to determine the correct answer is at least 2 minutes.

The filtering stage reduces the number of admissible questions by a factor of  $4\times$  to  $5\times$ . We accomplish 18.8K questions for 992 videos, which we split into 80% train, 10% val, and 10% test.

### 5.3.2 MAD-QA

We follow the same process for Ego-QA to obtain MAD-QA by utilizing 1.2K hours of 650 videos from the MAD dataset (Soldan et al., 2022). Since video lengths and the number of dense captions are larger than Ego-QA, we ask GPT-4 to generate 60 instead of 20 questions per video. Because GPT-4 might store external knowledge about the movie, we replace the name of characters in the caption with *person\_1*, *person\_2*, etc. Afterwards, we obtain 15.7K questions for 650 videos, and we split them into 80% train, 10% val, and 10% test.

The average video lengths in Ego-QA and MAD-QA are 17.5 minutes and 1.9 hours, respectively. Moreover, the average necessary video lengths humans need to watch to determine the answer for the two datasets are respectively 1204.4 and 396.07 seconds, longer than the average 100-second length of the recent very long-form videoQA dataset EgoSchema (Mangalam et al., 2023).

## 5.4 Experiments

### 5.4.1 Standard Benchmarks

In addition to our constructed Ego-QA and MAD-QA datasets, we follow previous works (Gao et al., 2023; Xiao et al., 2023b; Wang et al., 2023a) to evaluate GSMT on four additional publicly available datasets for long-form videoQA: AGQA (Grunde-

Method	Attribute	State	Event	Order	Number	All
STAGE	39.49	49.93	34.52	55.32	38.54	41.97
AI0	41.78	52.98	37.57	55.16	38.50	44.86
ATP	42.87	53.49	38.35	55.25	38.65	45.43
MIST-AIO	43.63	55.17	40.99	55.44	39.54	47.19
MIST-CLIP	44.05	58.13	42.54	56.83	40.32	48.97
GSMT-AIO	48.76	57.99	44.96	57.39	43.18	50.81
GSMT-CLIP	<b>49.23</b>	<b>61.10</b>	<b>46.66</b>	<b>58.83</b>	<b>44.03</b>	<b>52.73</b>

Table 5.2: Results of videoQA on Env-QA.

Method	Interaction	Sequence	Prediction	Feasibility	Mean
CLIP	39.80	40.50	35.50	36.00	38.00
RESERVE-B	44.80	42.40	38.80	36.20	40.50
Flamingo-9B	-	-	-	-	43.40
AI0	47.53	50.81	47.75	44.08	47.54
ATP	50.63	52.87	49.36	40.61	48.37
CoVGT	-	-	-	-	46.23
MIST-AIO	53.00	52.37	49.52	43.87	49.69
MIST-CLIP	55.59	54.23	54.24	44.48	51.13
GLOBAL	<b>59.36</b>	<b>57.52</b>	<b>57.21</b>	<b>46.68</b>	<b>52.85</b>

Table 5.3: Results of videoQA on STAR.

Method	Causal	Temporal	Descriptive	All
HQGA	48.48	51.24	61.65	51.42
CLIP	46.30	39.00	53.10	43.70
VQA-T	49.60	51.49	63.19	52.32
AI0	48.04	48.63	63.24	50.60
ATP	53.10	50.20	66.80	54.30
CoVGT	59.69	58.00	69.88	60.73
MIST-AIO	51.54	51.63	64.16	53.54
MIST-CLIP	54.62	56.64	66.92	57.18
GSMT-AIO	59.72	59.04	69.91	60.76
GSMT-CLIP	<b>60.87</b>	<b>61.16</b>	<b>70.26</b>	<b>62.49</b>

Table 5.4: Results of videoQA on NExT-QA.

McLaughlin et al., 2021), NExT-QA (Xiao et al., 2021b), STAR (Wu et al., 2021), Env-QA (Gao et al., 2021a), and EgoSchema (Mangalam et al., 2023).

**AGQA** (Grunde-McLaughlin et al., 2021) is a videoQA dataset for compositional spatio-temporal reasoning. As recommended by the dataset creator, we employ its v2 version, which possesses more balanced distributions. AGQA consists of 2.27M QA pairs for 9.7K videos.

**NExT-QA** (Xiao et al., 2021b) focuses on causal and temporal reasoning. The dataset comprises 5,440 videos associated with 52K questions.

**STAR** (Wu et al., 2021) concentrates on situated reasoning questions. The dataset

Method	Accuracy
EgoVLP	34.86
VideoReCap	50.23
MIST-AIO	56.27
MIST-CLIP	56.42
GSMT-AIO	58.28
GSMT-CLIP	<b>58.55</b>

Table 5.5: Results of videoQA on EgoSchema.

Method	Params	Ego-QA	MAD-QA
AIO [CVPR 2023]	110M	24.19	16.14
CoVGT [ECCV 2022]	159M	26.72	15.71
MIST-AIO [CVPR 2023]	382M	27.71	14.19
MIST-CLIP [CVPR 2023]	382M	29.73	17.15
SeViLa [NeurIPS 2023]	4.2B	21.96	OOM
GLOBAL	384M	<b>32.40</b>	<b>19.11</b>

Table 5.6: Results on constructed Ego-QA and MAD-QA.

Method	NExT-QA	STAR	Ego-QA	MAD-QA
SSL	61.91	52.40	31.30	18.95
Non-diag SSL	60.44	51.63	30.51	18.86
Attention	59.74	51.07	30.06	18.41
Convolution	59.34	50.85	30.17	18.33
Gated SSL	<b>62.49</b>	<b>52.85</b>	<b>32.40</b>	<b>19.11</b>

Table 5.7: Ablation results of gated SSL.

provides 60K questions related to 22K video clips.

**Env-QA** (Gao et al., 2021a) is curated for dynamic environment understanding. Env-QA contains 23K egocentric videos collected on virtual environment AI2THOR (Kolve et al., 2017), which are used to generate 85K questions.

**EgoSchema** (Mangalam et al., 2023) consists of egocentric videos of 3-minute length. Questions in EgoSchema require humans on average 100 seconds watching the video to answer.

#### 5.4.2 Implementation Details

Our framework can be implemented on most multi-modal Transformers. To fairly compare with previous works (Wang et al., 2023a; Gao et al., 2023), we evaluate upon two popular types of pre-trained models, *i.e.* CLIP (ViT/B-32) (Radford et al., 2021) and All-in-One-Base (Wang et al., 2023a). We divide a video frame into  $4 \times 4$  patches and send them to video embedder. For our gated SSL, we use  $d_S = d = d_h = 512$ ,  $d_{gating} = 128$ . For selection modules, we use  $\text{top-}k = 4$ ,  $\text{top-}j = 12$ . For the multimodal attention module, we use  $N_L = 2$ . Based on validation, we

Method	NExT-QA	STAR	Ego-QA	MAD-QA
GSMT	60.78	49.67	29.73	18.00
GSMT w/ OT	60.89	50.30	30.14	18.22
GSMT w/ POT	60.93	50.59	30.55	18.26
GSMT w/ C <sup>3</sup>	<b>62.49</b>	<b>52.85</b>	<b>32.40</b>	<b>19.11</b>

Table 5.8: Ablation results of cross-modal alignment.

Dataset / $d_{\text{gating}}$	32	64	128	256	512	No gating
NExT-QA	60.74	61.09	<b>62.49</b>	61.90	61.33	60.61
STAR	51.82	52.63	<b>52.85</b>	52.70	51.86	51.27
Ego-QA	29.96	31.37	<b>32.40</b>	31.55	31.25	29.88

Table 5.9: Effect of various  $d_{\text{gating}}$  dimensions and no gating on NExT-QA, STAR, and Ego-QA datasets.

Method	NExT-QA	STAR	Ego-QA	MAD-QA
Multi-modal SSL	60.69	50.87	29.74	18.61
GSMT	<b>62.49</b>	<b>52.85</b>	<b>32.40</b>	<b>19.11</b>

Table 5.10: Effect of the position of SSL.

employ max-pooling for all pooling operations, ReLU activation for  $\phi$ , and  $N_L = 2$ . We apply  $\mathcal{L}_{C^3}$  upon  $J^{(2)}$ , and observe no difference between applying on  $J^{(1)}$  and  $J^{(2)}$ . For fair comparison on AGQA, NExT-QA, STAR, Env-QA, and EgoSchema datasets, we sample 32 frames per video, and split them into  $K = 8$  segments. Since video lengths are longer in our EgoQA and MAD-QA datasets, we sample 128 and 8192 frames per video, respectively, and split into  $K = 8$  segments. For language modality, we embed the question with the same pre-trained model as the video embedder, and embed the answer with the pre-trained BERT-base model. We apply  $\lambda = 0.005$  to balance the scale of  $\mathcal{L}_{C^3}$  and  $\mathcal{L}_{\text{CE}}$ .

### 5.4.3 Baselines

We compare our proposed framework against the following baseline:

- **HQGA** (Xiao et al., 2022a): models video as a conditional graph hierarchy which aggregates visual facts in a level-wise manner with the guidance of textual modality,
- **CoVGT** (Xiao et al., 2023b): a model which exploits a graph transformer to encode video by capturing visual objects and their relations for spatio-temporal

**Video input:** 3037\_IRON\_MAN2 - Selected segments



**Question:** what if the person did not have the ingot of palladium to replace the smoking one in the rt unit?

0. The RT unit would spontaneously improve its efficiency and generate additional power for the suit, enhancing the person's abilities
1. The lack of a new palladium ingot would trigger an internal safeguard, transforming the RT unit into an endless energy source free from toxicity
- 2. The RT unit would degrade, potentially causing the person's health to deteriorate or the armored suit to malfunction**
3. The RT unit would lever the quantum fluctuations in the environment, spontaneously generating a new form of energy hitherto unknown to science
4. Absence of palladium replacement would enable the RT unit to evolve, gaining sentience and the ability to repair and upgrade itself autonomously

GSMT's prediction: 2 ✓ MIST-CLIP's prediction: 1 ✗

**Video input:** fb7cc35d-3272-44a4-b8f2-15cd24fa345b - Selected segments



**Question:** what central theme best describes activities throughout the video?

0. technological exploration and utilization
1. advanced culinary preparation and experimentation
- 2. routine household management and maintenance**
3. environmental conservation efforts
4. physical and mental self-improvement practices

GSMT's prediction: 2 ✓ MIST-CLIP's prediction: 4 ✗

Figure 5.3: Qualitative results on the constructed MAD-QA and Ego-QA datasets.

reasoning, along with contrastive learning to align its graph transformer with the textual encoder,

- **ATP** (Buch et al., 2022): a model which learns to select one salient video frame to perform the videoQA task,
- **AIO** (Wang et al., 2023a): an end-to-end videoQA model that releases the need of unimodal encoders and leverages non-parametric token rolling operation,
- **STAGE** (Lei et al., 2020a): a model that jointly carries out videoQA with moment localization and object grounding,
- **VQA-T** (Yang et al., 2021): a cross-modal Transformer which is pre-trained with supervised contrastive learning on a large-scale videoQA dataset,

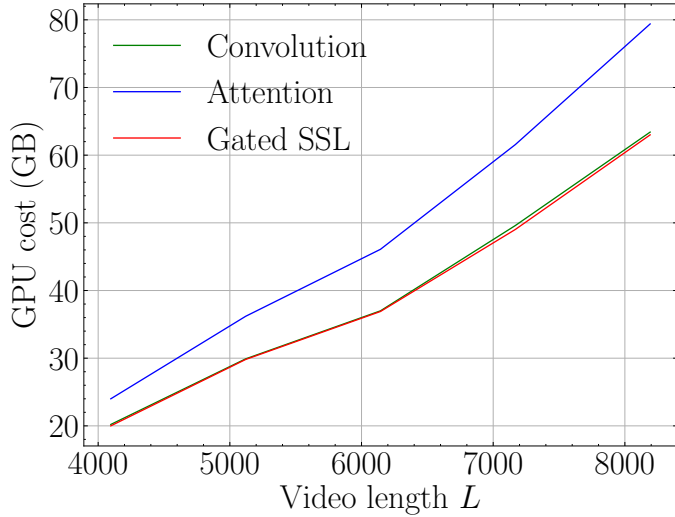


Figure 5.4: GPU memory cost with respect to visual sequence length  $L$  of attention, convolution, and gated SSL mechanism.

- **RESERVE-B** (Zellers et al., 2022): jointly represents video frames, texts, and audio, and learns to predict the masked textual and audio tokens given video frames,
- **Flamingo-9B** (Alayrac et al., 2022): a model which is able to process multi-modal prompt and cast videoQA as text prediction,
- **EgoVLP** (Lin et al., 2022a): pre-trains multi-modal Transformer on egocentric videos for egocentric videoQA.
- **VideoReCap** (Islam et al., 2024): a recursive model that synergizes different video hierarchies to process hour-long videos,
- **MIST** (Gao et al., 2023): a multi-modal Transformer which decomposes video into frames, patches, and segments to efficiently process with its self-attention mechanism.

#### 5.4.4 Quantitative Results

We show our experiments on AGQA-v2, Env-QA, STAR, NExT-QA, and EgoSchema in Table 5.1, 5.2, 5.3, 5.4, and 5.5, respectively, while revealing results on our constructed Ego-QA and MAD-QA in Table 5.6. We can observe that our method achieves superior performance over the latest methods on all datasets. In terms of

the overall accuracy, we outperform the second-best method on AGQA-v2, Env-QA, STAR, and EgoSchema, *i.e.* MIST-CLIP, by 1.77%, 3.76%, 1.72%, and 2.13%, respectively. Equivalently, we outperform CoVGT, which is the second-best method on NExT-QA, by 1.20%.

Inspecting more closely, we note that our framework obtains more significant performance increase on questions that require the capacity of reasoning among visual concepts, *i.e.* improving 2.66% and 3.54% respectively for *relation-action* and *object-action* on AGQA-v2, 6.25% and 4.52% respectively for causal and temporal on NExT-QA, than those that require the ability to extract information within one frame, *i.e.* improving 2.26% for *object-relation* on AGQA-v2 and 3.34% for *descriptive* on NExT-QA. These results demonstrate our global semantics signal can address the challenging long-range temporal reasoning problems of long-form videoQA.

Remarkably, existing methods demonstrate significantly low performance on our curated datasets. For example, MIST-CLIP only achieves 29.73% on Ego-QA, and 17.15% accuracy on MAD-QA, which is less than random chance. In contrast, humans obtain 80.29% and 73.21% accuracy on Ego-QA and MAD-QA, respectively. These results suggest that previous methods might not encompass sufficient information in their selected segments and visual regions. Conversely, with the integrated global information, our framework can enhance videoQA performance on these challenging datasets. However, the accuracy remains substantially below human performance. Future research should focus more on genuine long-form videoQA, where videos can extend to several hours.

#### 5.4.5 Ablation Study

**Gated SSL implementation.** We explore the effect of our gated SSL in Table 5.7 on NExT-QA, STAR, Ego-QA, and MAD-QA datasets. As can be observed, removing the gating unit, *i.e.* the SSL approach, results in performance drops, since redundant and noisy information might be passed to the visual representations. Additionally, not initializing state space parameters as diagonal matrices, *i.e.* non-diag SSL, does not remarkably impact the performance. However, the time and memory complexity would become  $O(L^2)$ , which is significantly more costly than

our initialization approach.

**Choices for Global Semantics.** We compare gated SSL with other choices to extract global semantics among visual elements, *i.e.* self-attention and convolution, in terms of videoQA performance in Table 5.7 and GPU memory cost in Figure 5.4. As can be observed, our gated SSL not only brings less computational cost than self-attention but also higher accuracy, validating the effectiveness of its global information signal. Moreover, whereas convolution pays equivalent computational cost to our gated SSL, its local pattern does not provide productive contextual information among visual elements, resulting in lower accuracy than gated SSL.

**Effect of Gating Unit.** We ablate the gating unit and vary the gating dimension  $d_{\text{gating}}$  in our gated SSL. As shown in Table 5.9, increasing the gating dimension leads to higher videoQA accuracy, as model has more controllability towards global information into visual representations. However, when the gating dimension becomes larger, the performance saturates and deteriorates. We posit that the model might become more constrained to allow the encoding of global semantics, degenerating to the architecture with limited global semantics. Apparently, removing gating unit results in performance drops, because irrelevant global information for the question could flow into visual hidden states without model controllability.

**Effect of  $C^3$  objective.** We compare our  $C^3$  alignment objective with alternative approaches, *i.e.* optimal transport (OT) (Pramanick et al., 2022) and its partial variant (POT) (Chapel et al., 2020). As shown in Table 5.8, both OT and POT can polish videoQA performance, while  $C^3$  yields the highest performance. This shows that compositional consistency is important for long-form videoQA, since the model needs to grasp the relations among entities, specifically those specified by the question.

**Position of State Space Layer.** We replace the penultimate multi-modal attention with SSL. As shown in Table 5.10, such design choice deteriorates the videoQA performance. The reason might be that since the frames and regions have already been selected, limited global information can be extracted from the video. Moreover, SSL does not explicitly calculate dependency between tokens, thus producing little refined representations to compute the final answer, which has been observed by previous work (Zuo et al., 2022). This substantiates our decision to adopt SSL to integrate global semantics of video in an earlier stage.

#### 5.4.6 Qualitative Results

We visualize videoQA cases in Figure 5.1. As can be observed, our model can choose the correct answer for questions that require information over the video with a limited number of video segments. We posit that due to our integrated global semantics, visual representations not only encode information of the selected segments but also the video context, thus furnish the model with sufficient cues to ascertain the correct answer. In contrast, constrained to the selected segments, previous state-of-the-art, *i.e.* MIST-CLIP (Gao et al., 2023), struggles in such questions and produces the incorrect output.

### 5.5 Summary

We introduce a Gated State space Multi-modal Transformer (GSMT) with a state space layer (SSL) to integrate global semantics of video into visual representations to tackle long-form videoQA. We further incorporate a gating unit to provide more controllability over the integrated global semantics and a cross-modal compositional congruence ( $C^3$ ) objective to encourage the semantics aligned with the question. To comprehensively evaluate long-form videoQA, we curate two long-form videoQA datasets with excessively long video lengths and long-natured questions. Extensive experiments on these and standard datasets validate the superiority of our framework.

# Chapter 6

## Motion-aware Contrastive Learning for Temporal Panoptic Scene Graph Generation

### 6.1 Introduction

The advent of autonomous agents, intelligent systems, and robots warrants a comprehensive understanding of real-world environments (Ma et al., 2022; Driess et al., 2023; Raychaudhuri et al., 2023; Cheng et al., 2022; Li et al., 2023f,e). Such understanding encompasses beyond merely recognizing individual entities, but also a sophisticated understanding of their relationships. To construct a detailed understanding, scene graph generation (SGG) research (Li et al., 2022f; Bin et al., 2019; Sudhakaran et al., 2023; Nag et al., 2023; Wang et al., 2024a) has sought to provide relational perspective on scene understanding. In SGG frameworks, scene graphs utilize nodes to represent entities and edges to represent relationships, constructing a comprehensive and structured understanding of visual scenes.

However, due to being primarily based on bounding boxes to denote entities, scene graphs fall short of replicating human visual perception with a lack of granularity (Yang et al., 2023d). To overcome this limitation, panoptic scene graph generation (Yang et al., 2022c; Zhao et al., 2023a) has been presented to expand the scope of SGG to incorporate pixel-level precise entity localization and thorough scene understanding including background components. Subsequently, because the temporal dimension undoubtedly provides richer information than the static spatial dimension, recent works (Yang et al., 2023d, 2024a) have shifted attention to the domain of videos and 4D scenes, resulting in the tasks of panoptic video and 4D scene graph generation.

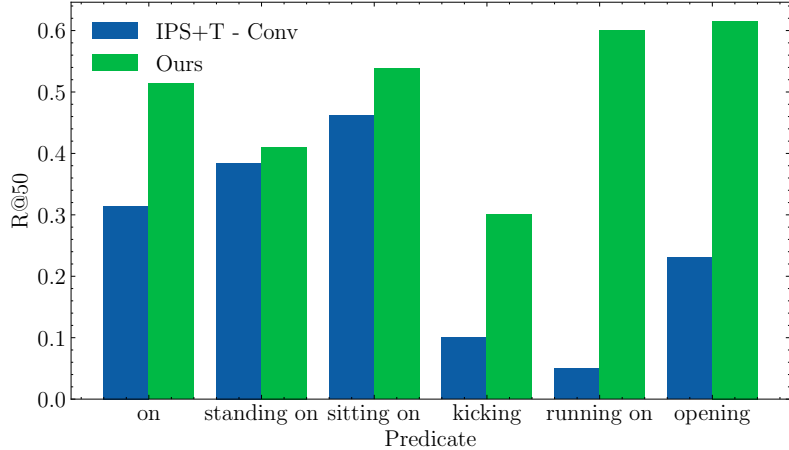


Figure 6.1: State-of-the-art IPS+T - Convolution (Yang et al., 2023d) exhibits high R@50 scores for static relations, *e.g.* *on*, *sitting on*, and *standing on*, than dynamic relations, *e.g.* *kicking*, *running on*, and *opening*. In contrast, our method can perform effectively on both static and dynamic relations.

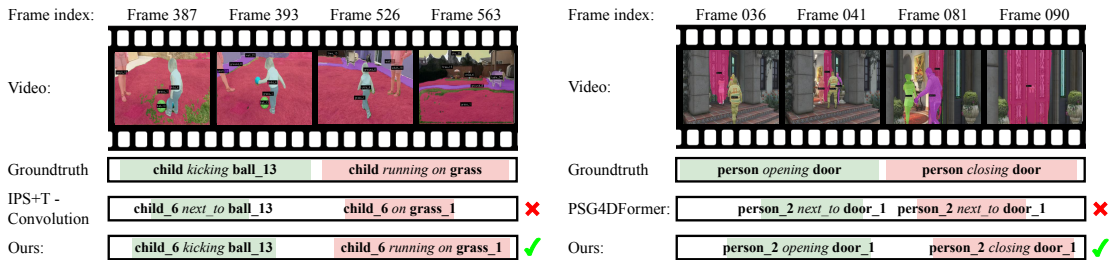


Figure 6.2: Examples of temporal panoptic scene graph generation of state-of-the-art (Yang et al., 2023d, 2024a) and our method.

Popular methods (Yang et al., 2023d, 2024a, 2022c) for temporal panoptic scene graph generation produce entity masks tracked across the temporal dimension, *i.e.* mask tubes, then predict temporal relations among them. To conduct relation prediction, these methods encode the segmentation mask tubes, apply global pooling, then forward to a multi-layer perceptron for classifying their relations. However, such global pooling operation is well-known to be ineffective in representing temporal or motion patterns, which are useful for determining the relation among the entities. Consequently, this would result in higher misclassification rates of more dynamic relations (Wang et al., 2023b; Nag et al., 2023; Zhou et al., 2022), as illustrated in Figure 6.1.

To encourage temporal representation learning, current research (Nguyen et al., 2023c; Liu et al., 2022a; Zhou et al., 2023) uses contrastive learning for videos. However, they mainly seek to force two clips from the same video to be close

together. As such, they mostly capture the semantics of visual scenes and disregard motions (Chen et al., 2020). Moreover, instead of paying attention to precise entity localization, they work on frame-level representations. This would inadvertently inject motions from non-target entities into visual representations, which might not benefit relation classification in panoptic scene graph generation.

In this paper, to encourage representation learning to capture motion patterns for temporal panoptic scene graph generation, we propose a novel contrastive learning framework that focuses on mask tubes of the segmented entities. First, we force a mask tube and the one of similar subject-relation-object but of a different video to obtain close representations. Since positive mask tubes originate from distinct video clips, the model cannot rely upon visual semantics to optimize the contrastive objective, but instead depends on the motion trajectory evolution, which is our target component for representation learning. Second, we propel negative mask tubes generated by temporally shuffling the original tubes. Moreover, we also push apart representations of mask tubes from the same video but belonging to different triplets. Because mask tubes of different triplets from a common video with close visual features are separated from each other, we once again motivate the model to generate representations that are less reliant upon visual semantics but motion-sensitive features. In addition, the visually similar negative mask tubes can play a role as hard negative samples, thus accelerating the contrastive learning process (Chen et al., 2024b).

Moreover, in order to implement our motion-aware contrastive learning framework, there is a need to quantify the relationship between mask tubes. This quantification marks a challenging problem as mask tubes are a sequence of segmentation masks that span over the sequence of video frames. Furthermore, mask tubes of two triplets might exhibit different lengths since two events often occur at different speed. Unfortunately, the popular pipeline of temporal pooling and then similarity estimation flattens the temporal dimension of the mask tubes and neglects their motion features. To resolve this problem, we consider mask tubes of two triplets as two distributions and seek the optimal transportation map between them, then utilize the transport distance as the distance between two triplets’ tubes. Such scheme of transporting can play a role of synchronizing the motion states of two triplets and takes advantage of the mask tubes’ evolutionary trajectory.

To sum up, our contributions are as follows:

- We propose a novel contrastive learning framework for temporal panoptic scene graph generation which pulls together entity mask tubes with similar motion patterns and pushes away those of distinct motion patterns.
- We utilize optimal transport distance to estimate the relationship between two events' mask tubes for the proposed contrastive framework.
- Comprehensive experiments demonstrate that our framework outperforms state-of-the-art methods on both natural and 4D video datasets, especially on recognizing dynamic subject-object relations.

## 6.2 Problem Formulation

Temporal panoptic scene graph generation (TPSGG) is a task to generate a dynamic scene graph given an input video. In the generated scene graph, each node corresponds to an entity and each edge corresponds to a spatial-temporal relation between two entities. Formally, the input of a TPSGG model is a video clip  $V$ , particularly  $V \in \mathbb{R}^{T \times H \times W \times 3}$  for a natural video,  $V \in \mathbb{R}^{T \times H \times W \times 4}$  for a 4D RGB-D video, and  $V \in \mathbb{R}^{T \times M \times 6}$  for a 4D point cloud video,  $T$  denotes the number of frames,  $M$  the number of point clouds of interest, and the frame size  $H \times W$  should remain consistent across the video. The output of the model is a dynamic scene graph  $G$ . The TPSGG task can be formulated as follows:

$$P(G|V) = P(M, O, R|V). \quad (6.1)$$

In particular,  $G$  consists of binary mask tubes  $M = \{\mathbf{m}_1, \mathbf{m}_2, \dots, \mathbf{m}_N\}$  and entity labels  $O = \{o_1, o_2, \dots, o_N\}$  which are associated with  $N$  entities in the video, and their relations are denoted as  $R = \{r_1, r_2, \dots, r_L\}$ . With respect to entity  $o_i$ , the mask tube  $\mathbf{m}_i \in \{0, 1\}^{T \times H \times W}$  composes all tracked masks in all video frames, and its category  $o_i \in \mathbb{C}^O$ . For all entities in frame  $t$ , their masks must not overlap, *i.e.*  $\sum_{i=1}^N \mathbf{m}_i^t \leq \mathbf{1}^{H \times W}$ . The relation  $r_i \in \mathbb{C}^R$  associates two entities, one of which is the subject and the other is an object, with a relation class and a time period.  $\mathbb{C}^O$  and  $\mathbb{C}^R$  denote the entity and relation set class, respectively.

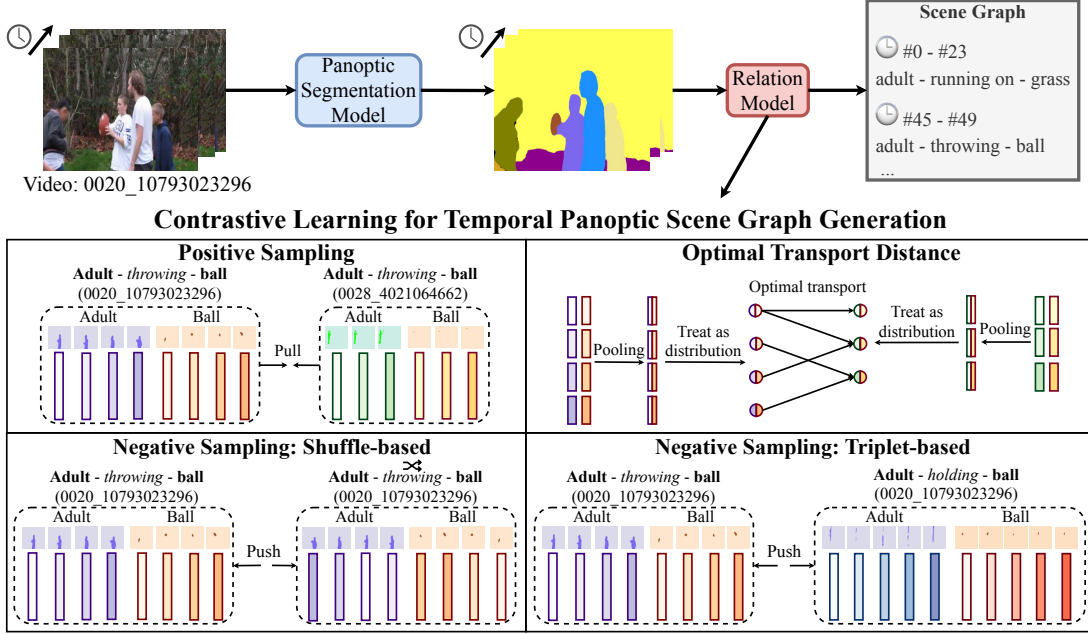


Figure 6.3: Framework overview of contrastive learning for temporal scene graph generation.

## 6.3 Methodology

We firstly present the backbone pipeline to conduct temporal panoptic scene graph generation. Then, we explain our proposed contrastive learning framework to facilitate motion-aware mask tube representation learning. We also present the detail of our optimal transport approach to estimate the relation between two mask tubes for the contrastive objective. Our overall framework is illustrated in Figure 6.3.

### 6.3.1 Temporal Panoptic Segmentation

Given a video clip  $V \in \mathbb{R}^{T \times H \times W \times 3}$ ,  $V \in \mathbb{R}^{T \times H \times W \times 4}$ , or  $V \in \mathbb{R}^{T \times M \times 6}$ , the initial step is to segment and track each pixel in a non-overlapping manner. Formally, the model produces a set of entity masks  $\{y_i\}_{i=1}^N = \{(\mathbf{m}_i, p_i(c))\}_{i=1}^N$ , where  $\mathbf{m}_i \in \{0, 1\}^{T \times H \times W}$  denotes the tracked video mask, *i.e.* the mask tube, and  $p_i(c)$  denotes the probability of assigning class  $c$  to the tube  $\mathbf{m}_i$ .  $N$  denotes the number of entities, which consist of both foreground (thing) and background (stuff) classes.

**Segmentation module.** Inspired by (Yang et al., 2023d, 2024a), we adopt the Transformer-based encoder-decoder segmentation model. There are two types of

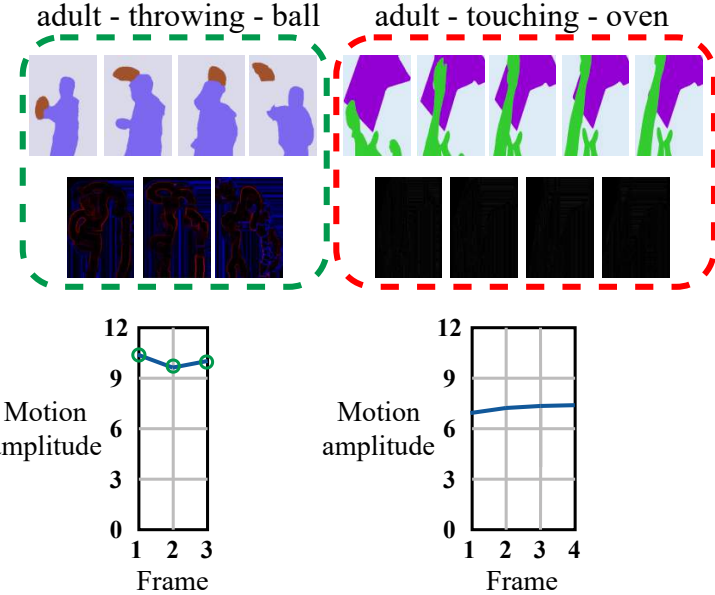


Figure 6.4: Proposed strategy to select strong-motion tubes.

segmentation procedure: 1) image panoptic segmentation combined with a tracker (IPS+T) and 2) video panoptic segmentation (VPS). IPS+T procedure will process each video frame separately and uses the tracker to connect the mask tubes across the video frames, while VPS processes each video frame with its reference frame from a nearby timestamp.

Both procedures are initiated by producing a set of object queries which interacts with encoded visual patches via masked cross-attention. Receiving a video  $V$ , the model produces a set of queries  $\{\mathbf{q}_i\}_{i=1}^N$ , where each query  $\mathbf{q}_i$  corresponds to one entity. Subsequently, every query is forwarded to two multi-layer perceptrons (MLPs) to project the queries into mask classification and mask regression outputs.

**Training and inference.** During training, each query is matched to a groundtruth mask through mask-based bipartite matching to calculate the segmentation loss. During inference, IPS+T generates panoptic segmentation masks for each frame, and uses the tracker to achieve  $N$  tracked mask tubes. In contrast, VPS employs two query embeddings of the target and reference frame, and performs query-wised similarity tracking to obtain  $N$  tracked mask tubes.

### 6.3.2 Relation Classification

After the segmentation step, if the relation module is to be trained, we match query tubes with the annotated groundtruth masks based on the tube IoU values with the groundtruth. Otherwise, we directly forward mask tubes to self-attention or convolutional layers for encoding them into hidden representations  $\{H_i\}_{i=1}^N$ ,  $H_i \in \mathbb{R}^{T \times D}$ , where  $D$  denotes the hidden dimension. Then, we construct query pairs from every two query tubes' representations  $H_i$  and  $H_j$ ,  $i, j \in \{1, 2, \dots, N\}$ ,  $i \neq j$ . Inspired by (Yang et al., 2023d, 2024a), in every pair, we perform global pooling over the temporal dimension for each mask tube representation:

$$\mathbf{h}_i = \text{Pooling}(H_i), \quad (6.2)$$

where  $\mathbf{h}_i \in \mathbb{R}^D$ . Afterwards, we concatenate  $\mathbf{h}_i$  and  $\mathbf{h}_j$ , and forward to a MLP to generate the relation category:

$$\log p(r_{i,j}) = \text{MLP}([\mathbf{h}_i, \mathbf{h}_j]). \quad (6.3)$$

To train the relation classification module, we use the cross-entropy loss calculated based on the predicted relation log-likelihood and the groundtruth. For inference, we extract the relation of the highest log-likelihood.

### 6.3.3 Contrastive Learning for Temporal Panoptic Scene Graph Generation

Our goal is to encourage mask tube representations  $\{H_i\}_{i=1}^N$  to become motion-aware. In the beginning, we concatenate the representations of two mask tubes  $H_i^{\text{sub}}$  and  $H_j^{\text{obj}}$ , which have been matched to a groundtruth subject-relation-object triplet, to form an anchor representation  $H_{i,j}$  (anchor):

$$H_{i,j}^a = [H_i^{\text{sub}}, H_j^{\text{obj}}], \quad (6.4)$$

where  $H_{i,j}^a \in \mathbb{R}^{T \times 2D}$ . Then, we propose a contrastive learning framework in which we motivate the model to associate mask tubes based upon the motion information. The objective of contrastive learning is to produce a representation space through attracting positive pairs, *i.e.*  $H^a$  and  $H^p$  (positive), while pushing apart negative pairs, *i.e.*  $H^a$  and  $H^n$  (negative). We accomplish this by optimizing the contrastive

objective, which is formulated as follows:

$$\mathcal{L}_{\text{cont}} = -\log \frac{e^{\text{sim}(H^a, H^p)}}{e^{\text{sim}(H^a, H^p)} + \sum_{z=1}^{N_n} e^{\text{sim}(H^a, H_z^n)}}, \quad (6.5)$$

where  $\text{sim}$  denotes the similarity function defined upon a pair of mask tube representations. The formulation shows that what the model learn is largely dependent upon how positive and negative samples are generated.

**Positive sampling.** To satisfy our motion-aware requirement for contrastive learning, we extract mask tube representations from the entities of the same subject and object category that exhibit a similar groundtruth relation from another video. Since two videos possess distinct visual features, the model must rely on the shared motion pattern of similar subject-relation-object triplets to associate the anchor and the positive sample.

**Negative sampling.** For negative sampling, we design two strategies, which result in two contrastive approaches, *i.e.* shuffle-based and triplet-based contrastive learning.

### 6.3.4 Shuffle-based contrastive learning

In our shuffle-based approach, we create negative samples by utilizing a series of temporal permutations  $\pi$  to the anchor tube, *i.e.* shuffling:

$$H^n = \pi(H^a). \quad (6.6)$$

As such, the contrastive objective will force the model to propel representations of the anchor tube, which is in the normal order, from the shuffled tube, which exhibits a distorted motion due to the shuffled order. This would make the learned representation sensitive to frame ordering, *i.e.* motion-aware, as the anchor  $H^a$  and the negative tube  $H^n$  share visual semantics and can only be distinguished using motion information.

**Selecting strong-motion mask tubes.** However, there exists a potential risk: for static relations such as *on*, *next to*, and *in*, mask tubes might involve almost no motion. As a result, the shuffled tube would become identical to the anchor one and the model would not be able to differentiate them and learn reasonably.

To address this problem, we propose a strategy to select strong-motion tubes for shuffling, which we illustrated in Figure 6.4.

Given a video, our aim is to select mask tubes that carry strong motion for shuffling. To measure the motion of the mask tube, we utilize optical flow edges (Xiao et al., 2021a). We estimate flow edges via employing a Sobel filter (Sobel et al., 2022) onto the flow magnitude map and take the median over the flow edge pixels of the entity masks. Then, we select mask tubes whose the maximum value across the optical flow surpasses a threshold  $\gamma$ .

### 6.3.5 Triplet-based contrastive learning

To take advantage of motion-aware signals from triplets of similar subject-relation-object category, we design a triplet-based approach to create negative samples. A naive approach would be to sample mask tubes of any distinct subject-relation-object triplet from the anchor sample. However, if we run into triplets with all distinct subject, relation, and object categories, the negative pair would be trivial for the model to distinguish, resulting in less effective learning.

In order to create harder negative samples, we choose negative mask tubes from the same video with the anchor. We create a multi-nomial distribution, where triplets that share more subject, relation, or object categories with the anchor will be more likely to be drawn. Hence, our negative samples can hold close visual semantics with the anchor sample, and increase the likelihood that the model depends on motion semantics to push them apart. From contrastive learning perspective, these samples form hard negative samples to accelerate the learning process (Chen et al., 2024b).

### 6.3.6 Optimal Transport for Mask Tube Relation Quantification

There is one remaining problem, *i.e.* how to define the similarity function  $\text{sim}$  for two mask tubes' representations  $H_i$  and  $H_j$ . In this work, we consider two mask tubes as two discrete distributions  $\boldsymbol{\mu}$  and  $\boldsymbol{\nu}$ , whose  $H_i$  and  $H_j$  are their supports, respectively. Formally,  $\boldsymbol{\mu} = \sum_{k=1}^{T_i} \mathbf{a}_k \delta_{\mathbf{h}_{i,k}}$  and  $\boldsymbol{\nu} = \sum_{l=1}^{T_j} \mathbf{b}_l \delta_{\mathbf{h}_{j,l}}$ , where  $\delta_{\mathbf{h}_{i,k}}$  and  $\delta_{\mathbf{h}_{j,l}}$  denote the Dirac functions centered upon  $\mathbf{h}_{i,k}$  and  $\mathbf{h}_{j,l}$ , respectively. The weights of the

---

**Algorithm 3** Computing the optimal transport distance

---

**Require:**  $\mathbf{C} = \{\mathbf{C}_{l,k} = c(\mathbf{h}_{i,l}, \mathbf{h}_{j,k}) \mid 1 \leq i \leq N_V, 1 \leq j \leq N_L\} \in \mathbb{R}^{T_i \times T_j}$ ,  $\mathbf{a} \in \mathbb{R}^{T_i}$ ,  $\mathbf{b} \in \mathbb{R}^{T_j}$ ,  $s$ ,  $N_{\text{iter}}$   
 $d_{\text{OT}} = \infty$   
**for**  $s = 1$  to  $\min(T_i, T_j)$  **do**  
     $\mathbf{T} = \exp\left(-\frac{\mathbf{C}}{\tau}\right)$   
     $\mathbf{T} = \frac{s}{(\mathbf{1}_{T_i})^\top \cdot \mathbf{T} \cdot \mathbf{1}_{T_j}} \mathbf{T}$   
    **for**  $i = 1$  to  $N_{\text{iter}}$  **do**  
         $\mathbf{p}_a = \min\left(\frac{\mathbf{a}}{\mathbf{T} \mathbf{1}_{T_j}}, \mathbf{1}_{T_i}\right)$ ,  $\mathbf{T}_a = \text{diag}(\mathbf{p}_a) \cdot \mathbf{T}$   
         $\mathbf{p}_b = \min\left(\frac{\mathbf{b}}{\mathbf{T}_a^\top \mathbf{1}_{T_i}}, \mathbf{1}_{T_j}\right)$ ,  $\mathbf{T}_b = \text{diag}(\mathbf{p}_b) \cdot \mathbf{T}_a$   
         $\mathbf{T} = \frac{s}{(\mathbf{1}_{T_i})^\top \cdot \mathbf{T} \cdot \mathbf{1}_{N_L}} \mathbf{T}_b$   
    **end for**  
     $d_{\text{OT}} = \min\left(d_{\text{OT}}, \sum_{k=1}^{T_i} \sum_{l=1}^{T_j} \mathbf{T}_{k,l} \mathbf{C}_{k,l}\right)$   
**end for**  
**return**  $d_{\text{OT}}$

---

supports are  $\mathbf{a} = \frac{\mathbf{1}_{T_i}}{T_i}$  and  $\mathbf{b} = \frac{\mathbf{1}_{T_j}}{T_j}$ .

After defining the distribution scheme, we propose the tube alignment optimization problem, which is to find the transport plan that achieves the minimum distance between  $\boldsymbol{\mu}$  and  $\boldsymbol{\nu}$  as follows:

$$d_{\text{OT}} = \mathcal{D}_{\text{OT}}(\boldsymbol{\mu}, \boldsymbol{\nu}) = \min_{\mathbf{T} \in \Pi(\mathbf{a}, \mathbf{b})} \sum_{k=1}^{T_i} \sum_{l=1}^{T_j} \mathbf{T}_{i,j} \cdot c(\mathbf{h}_{i,k}, \mathbf{h}_{j,l}), \quad (6.7)$$

$$\text{s.t. } \Pi(\mathbf{a}, \mathbf{b}) = \{\mathbf{T} \in \mathbb{R}_+^{T_i \times T_j} \mid \mathbf{T} \mathbf{1}_{T_i} \leq \mathbf{a}, \mathbf{T}^\top \mathbf{1}_{T_j} \leq \mathbf{b}, \\ \mathbf{1}_{T_i}^\top \cdot \mathbf{T} \cdot \mathbf{1}_{T_j} = s, \quad 0 \leq s \leq \min(T_i, T_j)\}, \quad (6.8)$$

where  $c$  denotes a pre-defined distance between two vectors. We implement the cost distance  $c(\mathbf{h}_{i,k}, \mathbf{h}_{j,l}) = 1 - \frac{\mathbf{h}_{i,k} \cdot \mathbf{h}_{j,l}}{\|\mathbf{h}_{i,k}\|_2 \|\mathbf{h}_{j,l}\|_2}$  as the cosine distance. As the exact optimization over the transport plan  $\mathbf{T}$  is intractable, we adopt the Sinkhorn-based algorithm to estimate  $\mathbf{T}$ . We delineate the algorithm to calculate the distance in Algorithm 3. To turn the distance into similarity value, we take its negative value and add to a pre-defined margin  $\alpha$ :

$$\text{sim}(\mathbf{h}^a, \mathbf{h}^p) = \alpha - d_{\text{OT}}. \quad (6.9)$$

## 6.4 Experiments

We conduct comprehensive experiments to evaluate the effectiveness of our motion-aware contrastive framework. We first describe the experiment settings,

Method	vIoU threshold = 0.5			vIoU threshold = 0.1		
	R/mR@20	R/mR@50	R/mR@100	R/mR@20	R/mR@50	R/mR@100
IPS+T - Vanilla	3.04 / 1.35	4.61 / 2.94	5.56 / 3.33	8.28 / 5.68	14.47 / 9.92	18.24 / 11.84
IPS+T - Handcrafted filter	2.52 / 1.72	3.77 / 2.36	4.72 / 2.79	8.07 / 5.61	13.42 / 8.27	16.46 / 10.11
IPS+T - Transformer	3.88 / 2.81	5.66 / 4.12	6.18 / 4.44	9.01 / 6.69	14.88 / 11.28	17.51 / 13.20
IPS+T - Convolution	3.88 / 2.55	5.24 / 3.29	6.71 / 5.36	10.06 / 8.98	14.99 / 12.21	18.13 / 15.47
Ours - Transformer	<u>3.98</u> / <u>2.98</u>	<u>5.97</u> / <u>4.20</u>	<u>7.44</u> / <u>5.15</u>	<u>10.59</u> / <u>9.56</u>	<u>16.98</u> / <u>12.39</u>	<u>22.33</u> / <u>17.47</u>
Ours - Convolution	<b>4.51</b> / <b>3.56</b>	<b>6.08</b> / <b>4.38</b>	<b>7.76</b> / <b>5.86</b>	<b>11.43</b> / <b>9.57</b>	<b>17.30</b> / <b>13.13</b>	<b>22.85</b> / <b>17.48</b>
VPS - Vanilla	0.21 / 0.10	0.21 / 0.10	0.31 / 0.18	6.29 / 3.04	9.64 / 6.74	12.89 / 9.60
VPS - Handcrafted filter	0.42 / 0.13	0.52 / 0.50	0.94 / 0.92	5.24 / 2.84	7.65 / 7.14	9.64 / 8.22
VPS - Transformer	0.42 / 0.61	0.73 / 0.76	1.05 / 0.92	6.50 / 5.75	9.64 / 8.25	12.26 / 9.51
VPS - Convolution	0.42 / 0.25	0.63 / 0.67	0.63 / 0.67	8.07 / 7.84	11.01 / 9.78	12.89 / 10.77
Ours - Transformer	<u>0.63</u> / <u>0.83</u>	<u>1.05</u> / <u>0.76</u>	<u>1.05</u> / <u>0.76</u>	<u>6.71</u> / <u>6.94</u>	<u>10.27</u> / <u>8.68</u>	<u>13.42</u> / <u>12.09</u>
Ours - Convolution	<b>0.84</b> / <b>0.98</b>	<b>1.26</b> / <b>1.22</b>	<b>1.26</b> / <b>1.22</b>	<b>8.18</b> / <b>8.00</b>	<b>12.90</b> / <b>11.47</b>	<b>14.22</b> / <b>13.59</b>

Table 6.1: Experimental results on the OpenPVSG dataset.

Input type	Method	PSG4D-GTA			PSG4D-HOI		
		R/mR@20	R/mR@50	R/mR@100	R/mR@20	R/mR@50	R/mR@100
Point cloud videos	3DSGG	1.48 / 0.73	2.16 / 0.79	2.92 / 0.85	3.46 / 2.19	3.15 / 2.47	4.96 / 2.84
	PSG4DFormer	4.33 / 2.10	4.83 / 2.93	5.22 / 3.13	5.36 / 3.10	5.61 / 3.95	6.76 / 4.17
	Ours	<b>5.88</b> / <b>3.45</b>	<b>6.31</b> / <b>3.70</b>	<b>7.31</b> / <b>4.70</b>	<b>7.28</b> / <b>5.09</b>	<b>7.62</b> / <b>6.49</b>	<b>9.18</b> / <b>6.85</b>
RGB-D videos	3DSGG	2.29 / 0.92	2.46 / 1.01	3.81 / 1.45	4.23 / 2.19	4.47 / 2.31	4.86 / 2.41
	PSG4DFormer	6.68 / 3.31	7.17 / 3.85	7.22 / 4.02	5.62 / 3.65	6.16 / 4.16	6.28 / 4.97
	Ours	<b>9.07</b> / <b>5.52</b>	<b>9.73</b> / <b>6.32</b>	<b>9.73</b> / <b>6.32</b>	<b>7.63</b> / <b>6.09</b>	<b>8.36</b> / <b>6.94</b>	<b>8.53</b> / <b>8.29</b>

Table 6.2: Experimental results on both PSG4D-GTA and PSG4D-HOI groups of PSG4D dataset.

Method	R/mR@20	R/mR@50	R/mR@100
w/o shuffle-based	4.41 / 3.43	5.90 / 4.24	7.30 / 5.79
w/o triplet-based	4.44 / 3.50	6.02 / 4.28	7.36 / 5.83
Ours	<b>4.51</b> / <b>3.56</b>	<b>6.08</b> / <b>4.38</b>	<b>7.44</b> / <b>5.86</b>

Table 6.3: Ablation results for contrastive learning approaches on OpenPVSG dataset. We adopt the vIoU threshold of 0.5.

covering the evaluation datasets, evaluation metrics, baseline methods, and implementation details. Next, we present quantitative results of our method, then provide ablation study and careful analysis to explore properties of our motion-aware contrastive framework. Eventually, we conduct qualitative analysis to concretely examine its behavior.

#### 6.4.1 Experiment Settings

**Datasets.** We assess the effectiveness of our method on natural and 4D video inputs. The corresponding dataset to each input type is as follows:

- **Open-domain Panoptic video scene graph generation (OpenPVSG)** (Yang et al., 2023d): OpenPVSG consists of scene graphs and associated

Tube relation quantification	R/mR@20	R/mR@50	R/mR@100
Pooling - Cosine similarity	4.44 / 3.40	6.04 / 4.36	7.36 / 5.84
Pooling - L2	4.36 / 3.37	3.77 / 5.95	7.29 / 5.80
Optimal transport	<b>4.51 / 3.56</b>	<b>6.08 / 4.38</b>	<b>7.44 / 5.86</b>

Table 6.4: Ablation results for mask tube relation quantification method between mask tubes on OpenPVSG dataset.

Input type	Method	PSG4D-GTA			PSG4D-HOI		
		R/mR@20	R/mR@50	R/mR@100	R/mR@20	R/mR@50	R/mR@100
Point cloud videos	w/o shuffle-based	5.56 / 2.92	5.57 / 2.98	6.51 / 4.36	6.56 / 4.29	6.98 / 6.25	8.76 / 6.43
	w/o triplet-based	5.77 / 2.93	5.59 / 3.26	6.53 / 4.39	6.67 / 4.85	7.52 / 6.31	8.84 / 6.43
	Ours	<b>5.88 / 3.45</b>	<b>6.31 / 3.70</b>	<b>7.31 / 4.70</b>	<b>7.28 / 5.09</b>	<b>7.62 / 6.49</b>	<b>9.18 / 6.85</b>
RGB-D videos	w/o shuffle-based	8.35 / 5.34	8.76 / 5.68	8.88 / 5.53	7.00 / 5.53	7.51 / 6.02	7.56 / 7.42
	w/o triplet-based	9.00 / 5.46	9.71 / 5.95	9.63 / 5.82	7.12 / 6.03	8.31 / 6.51	8.24 / 7.95
	Ours	<b>9.07 / 5.52</b>	<b>9.73 / 6.32</b>	<b>9.73 / 6.32</b>	<b>7.63 / 6.09</b>	<b>8.36 / 6.94</b>	<b>8.53 / 8.29</b>

Table 6.5: Ablation results for contrastive learning approaches on PSG4D dataset.

Input type	Tube relation quantification	PSG4D-GTA			PSG4D-HOI		
		R/mR@20	R/mR@50	R/mR@100	R/mR@20	R/mR@50	R/mR@100
Point cloud videos	Pooling - Cosine similarity	5.76 / 2.87	6.02 / 3.62	6.84 / 4.11	7.24 / 4.45	7.44 / 6.27	8.20 / 6.64
	Pooling - L2	5.46 / 2.78	5.38 / 3.39	6.51 / 3.86	6.72 / 4.11	6.74 / 6.05	7.96 / 6.11
	Optimal transport	<b>5.88 / 3.45</b>	<b>6.31 / 3.70</b>	<b>7.31 / 4.70</b>	<b>7.28 / 5.09</b>	<b>7.62 / 6.49</b>	<b>9.18 / 6.85</b>
RGB-D videos	Pooling - Cosine similarity	9.03 / 5.37	9.47 / 5.86	9.70 / 6.02	7.36 / 5.43	7.93 / 6.70	8.06 / 7.42
	Pooling - L2	8.89 / 4.70	8.90 / 5.41	9.08 / 5.78	6.65 / 5.26	7.74 / 6.29	7.95 / 7.39
	Optimal transport	<b>9.07 / 5.52</b>	<b>9.73 / 6.32</b>	<b>9.73 / 6.32</b>	<b>7.63 / 6.09</b>	<b>8.36 / 6.94</b>	<b>8.53 / 8.29</b>

Table 6.6: Ablation results for mask tube relation quantification method between mask tubes on PSG4D dataset.

segmentation masks with respect to subject and object nodes in the scene graph. The dataset comprises 400 videos, including 289 third-person videos from ViDOR (Shang et al., 2019), 111 egocentric videos from Epic-Kitchens (Damen et al., 2022a) and Ego4D (Grauman et al., 2022).

- **Panoptic scene graph generation for 4D (PSG4D)** (Yang et al., 2024a): The PSG4D dataset is divided into two groups, *i.e.* PSG4D-GTA and PSG4D-HOI. PSG4D-GTA comprises 67 third-view videos with an average length of 84 seconds, 35 object categories, and 43 relationship categories. On the contrary, PSG4D-HOI contains 2,973 videos from an egocentric perspective, whose average duration is 20 seconds. The PSG4D-HOI’s videos are mostly related to indoor scenes, covering 46 object categories and 15 relationship categories.

**Evaluation metrics.** We use the recall at  $K$  (R@ $K$ ) and mean recall at  $K$  (mR@ $K$ ) metrics, which are standard metrics used in scene graph generation tasks. Both R@ $K$  and mR@ $K$  consider the top- $K$  triplets predicted by the panoptic scene graph

generation model. A successful recall of a predicted triplet must satisfy the following criteria: 1) correct category labels for the subject, object, and predicate; 2) a volume Intersection over Union (vIoU) greater than or equal to 0.5 between the predicted mask tubes and the groundtruth tubes. For extensive comparison, we also report results with the vIoU threshold of 0.1.

**Baseline methods.** We compare our method with a comprehensive list of baseline approaches for temporal panoptic scene graph generation: (i) **IPS+T - Vanilla** (Yang et al., 2023d) uses image panoptic segmentation (IPS) model with a tracker for segmentation, and fully-connected layers to separately encode temporal states of entity mask tubes; (ii) **IPS+T - Handcrafted filter** (Yang et al., 2023d) uses image panoptic segmentation (IPS) model with a tracker for segmentation, and a manually-designed kernel to encode entity mask tubes; (iii) **IPS+T - Convolution** (Yang et al., 2023d) uses image panoptic segmentation (IPS) model with a tracker for segmentation, and learnable convolutional layers to encode entity mask tubes; (iv) **IPS+T - Transformer** (Yang et al., 2023d) uses image panoptic segmentation model (IPS) with a tracker for segmentation, and Transformer-based encoder with self-attention layers to encode entity mask tubes; (v) **VPS - Vanilla** (Yang et al., 2023d) is similar to IPS+T - Vanilla, but uses video panoptic segmentation (VPS) model for panoptic segmentation; (vi) **VPS - Handcrafted filter** (Yang et al., 2023d) is similar to IPS+T - Handcrafter filter, but uses video panoptic segmentation (VPS) model for segmentation; (vii) **VPS - Convolution** (Yang et al., 2023d) is similar to IPS+T - Convolution, but uses video panoptic segmentation (VPS) model for segmentation; (viii) **VPS - Transformer** (Yang et al., 2023d) is similar to IPS+T - Transformer, but uses video panoptic segmentation (VPS) model for segmentation; (ix) **3D-SGG** (Wald et al., 2020) is based on PointNet (Qi et al., 2017) and graph convolutional network (Kipf and Welling, 2016) but neglects the depth dimension and generates panoptic scene graphs for 4D video inputs; (x) **PSG4DFormer** (Yang et al., 2024a) is a specialized model for 4D inputs, using Mask2Former (Cheng et al., 2022) for segmentation and a spatial-temporal Transformer to encode object mask tubes for relation classification.

**Implementation details.** For fair comparison, we experiment our contrastive framework with both IPS+T and VPS as segmentation module for panoptic video scene graph generation. In the former case, we leverage the UniTrack tracker (Wang

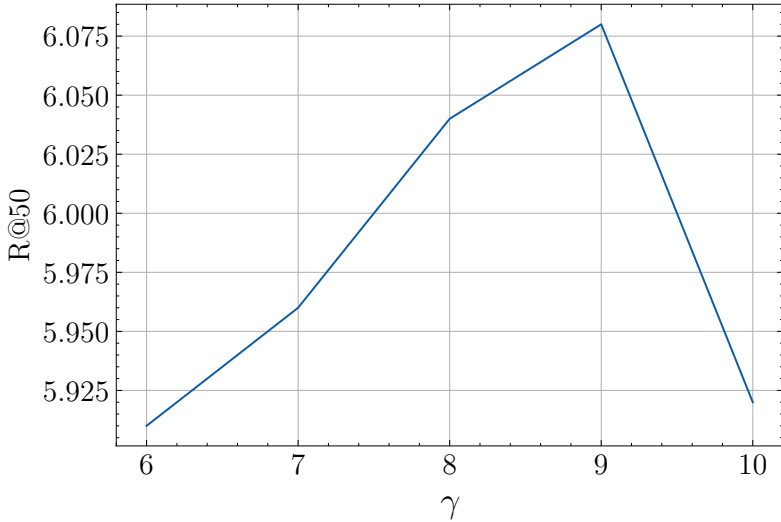


Figure 6.5: Ablation results on threshold  $\gamma$ .

et al., 2021c) combined with Mask2Former model (Cheng et al., 2022), which is initialized from the best-performing COCO-pretrained weights and fine-tuned for 8 epochs using AdamW optimizer with a batch size of 32, learning rate of 0.0001, weight decay of 0.05, and gradient clipping with a max L2 norm of 0.01. In the latter case, we utilize Video K-Net (Li et al., 2022d), also initialized from COCO-pretrained weights and fine-tuned with the same strategy as IPS+T. In the relation classification step, we conduct fine-tuning with a batch size of 32, employing the Adam optimizer with a learning rate of 0.001. For 4D panoptic scene graph generation, we adopt the PSG4DFormer baseline. To work with RGB-D and point cloud videos, we use an ImageNet pretrained on ResNet-101 (Russakovsky et al., 2015) and the DKNet (Wu et al., 2022b) as the visual encoder, respectively. We fine-tune the segmentation module for RGB-D and point cloud videos for 12 and 200 epochs, respectively. We use additional 100 epochs to train the relation classification module. Based on validation, we adopt a threshold  $\gamma = 9.0$  and a margin  $\alpha = 10.0$ . We set the maximum number of iterations  $N_{\text{iter}}$  to 1,000.

#### 6.4.2 Main Results

**Results on OpenPVSG.** As shown in Table 6.1, we substantially outperform both IPS+T - Convolution and IPS+T - Transformer when we use IPS+T for segmentation. In particular, using a higher vIoU threshold to filter out inaccurate segmentation, we surpass IPS+T - Transformer by 1.3/0.7 points of R/mR@100,

while surpassing IPS+T - Convolution by 0.8/1.1 points of R/mR@50. In addition, for a less strict vIoU threshold, we outperform IPS+T - Transformer by 1.6/2.9 points of R/mR@20, and IPS+T - Convolution by 2.3/0.9 points of R/mR@50. These results demonstrate that our method makes a propitious contribution to temporal panoptic scene graph generation, not only to popular but also to unpopular relation classes.

**Results on PSG4D.** Table 6.2 shows that our method also achieves significantly higher performance than the PSG4DFormer model. Specifically, when working with point cloud videos, on PSG4D-GTA, we outperform the baseline method by 1.6/1.4 points. Analogously, on PSG4D-HOI, we outperform PSG4DFormer by 2.0/2.5 points of R/mR@50. These results indicate that our framework bears a valuable impact to both egocentric and third-view videos. We hypothesize that both video types consist of dynamic actions among objects whose mask tube representations should be polished. In addition, when working with RGB-D videos, on PSG4D-GTA, we enhance the baseline method by 2.4/2.2 points of R/mR@20,. Furthermore, on PSG4D-HOI, our motion-aware contrastive learning also considerably refines PSG4DFormer by 2.0/2.4 points of R/mR@20. Such results have verified the generalizability of our motion-aware contrastive framework over natural, point cloud, and RGB-D videos.

### 6.4.3 Ablation Study

**Effect of the contrastive components.** We evaluate our framework without the assistance of either the shuffle-based or the triplet-based contrastive objective. As shown in Table 6.3 and 6.5, the performance degrades when we both remove shuffle-based and triplet-based contrastive approaches. In addition, triplet-based contrastive learning plays a more fundamental role than the shuffle-based one. We hypothesize that shuffle-based contrastive learning is better at focusing on motion semantics than triplet-based one.

**Effect of selecting strong-motion tubes.** We evaluate the impact of our strategy to filter out weak motion tubes. In Figure 6.5, we observe a performance boost when we increase the threshold to select mask tubes with strong motion. However, further elevating the threshold results in performance degradation, since there are

more mask tubes eliminated, thus limiting the effect of our motion-aware contrastive framework.

**Effect of optimal transport distance.** In this ablation, we compare various strategies to calculate the similarity between two mask tubes. Results in Table 6.4 and 6.6 show that the proposed optimal transport achieves much higher performance for both natural and 4D video inputs. We conjecture that other method such as pooling then cosine similarity or L2 neglects the temporal or flattens the motion nature of the entity mask tubes, thus reducing the effectiveness.

#### 6.4.4 Qualitative Analysis

We visualize examples processed by the state-of-the-art models and ours in Figure 6.2. As can be observed, our model successfully produces mask tubes overlapping with the groundtruth, and importantly predicts the correct relations of the subject-object pairs. On the other hand, baseline models tend to prefer more static relations, since during training they do not explicitly focus on motion-sensitive features. Statistics in Figure 6.1 also substantiate our proposition, in which we achieve considerably higher recalls for dynamic relations than baseline approaches.

### 6.5 Summary

In this paper, we propose a motion-aware contrastive learning framework for temporal panoptic scene graph generation. In our framework, we learn close representations for temporal masks of similar entities that exhibit common relations. Moreover, we separate temporal masks from their shuffled version, and also separate temporal masks of different subject-relation-object triplets. To quantify the relationship among temporal masks in the proposed contrastive framework, we utilize optimal transport to preserve the temporal nature among temporal entity masks. Extensive experiments substantiate the effectiveness of our framework for both natural and 4D videos.

# Chapter 7

## Multi-Scale Contrastive Learning for Video Temporal Grounding

### 7.1 Introduction

Temporal video grounding aims to localize moments of interest in an untrimmed video given a free-form textual description. It is a challenging multimodal task since it involves understanding temporal information in videos and reasoning about their connections to semantic information in texts. Recently, temporal grounding has drawn increasing attention (Mu et al., 2024; Jung et al., 2023; Xu et al., 2023b; Pan et al., 2023), due to its wide range of applications such as surveillance (Zhang et al., 2016), robotics (Burgner-Kahrs et al., 2015), and autonomous driving (Claussmann et al., 2019).

Previous methods (Zhang et al., 2020c; Soldan et al., 2021; Zhang et al., 2020a) for temporal grounding concentrate on grounding merely a few queries in short video snippets. However, recently the growing availability of long videos, *e.g.* on streaming platforms, and demands to query their rich content have necessitated productive grounding of large volumes of queries in long videos. Because of such short-to-long video paradigm shift, latest methods (Zhang et al., 2022; Mu et al., 2024) have utilized local self-attention to restrict attention within a local window, following the intuition that temporal context beyond a certain range is less helpful for moment localization.

To capture moments at different temporal scales without enlarging the window size of the local self-attention, recent methods (Zhang et al., 2022; Mu et al., 2024) need to combine several Transformer blocks with downsampling between every two

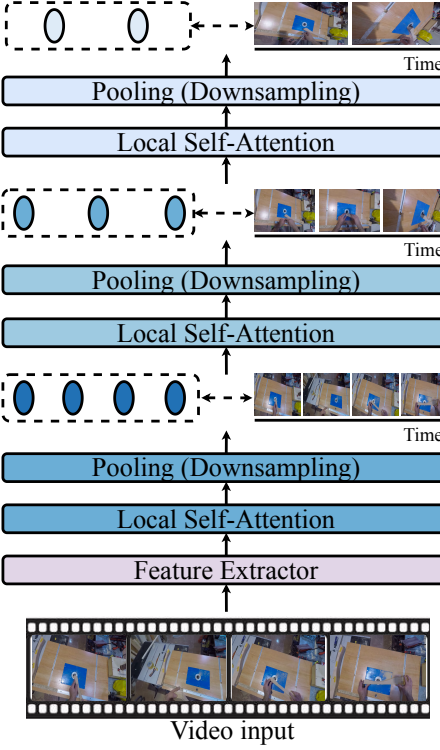


Figure 7.1: Illustration of feature pyramid to encode video moments of different lengths.

blocks, resulting in a feature pyramid of moment representations, as illustrated in Figure 7.2 (left). Unfortunately, due to such downsampling operation, when moment representations are propagated from lower levels of short-range (local) moments to higher levels of long-range (global) moments, information contained in representations of longer moments will gradually degrade Guo et al. (2020); Yang et al. (2023c). This could explain why performance of these methods tends to degrade as the duration of target moments increase, as shown in Figure 7.2 (right) and statistically shown with Intersection-over-Union (IoU) results in Figure 7.3, respectively.

To enrich information in video moment representations, recent works (Panta et al., 2024; Xiao et al., 2024; Ji et al., 2024; Liu et al., 2024b) have employed contrastive learning for temporal grounding. The intuition is to capture mutual information between video moments and textual query to preserve salient semantics in moment representations. These works mainly involve query-moment pairs in which queries relate to video moments of distinct videos, hence the learned semantics among moment representations would be independent from each other. However,

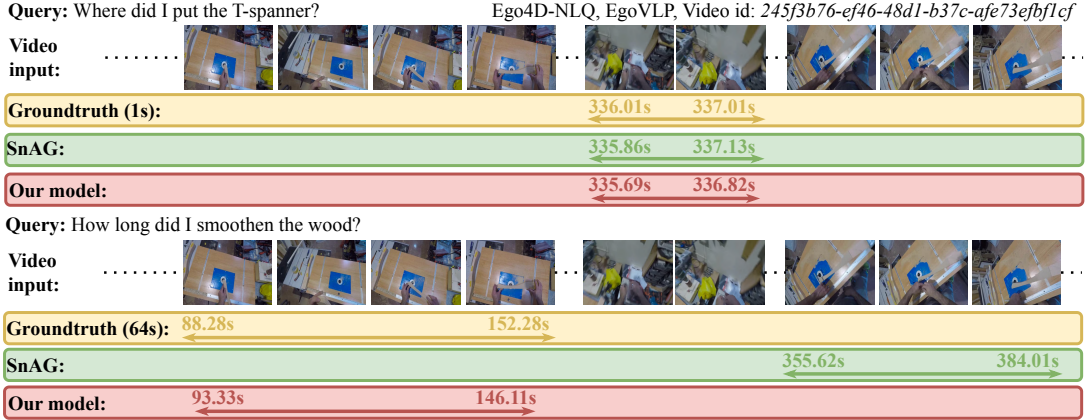


Figure 7.2: An example where recent method SnAG (Mu et al., 2024) accurately localizes short video moment but fails on long moment.

such approach might not be suitable for the latest scalable video-centric approach (Zhang et al., 2022; Mu et al., 2024), in which multiple textual queries are related to one video. Therefore, if the grounding of two textual queries results in temporal overlapping, there might be a conflict in compact moment representations (An et al., 2023). Furthermore, focusing upon moment-query relations limits these works to the feature space of the final encoder layer, which could not effectively utilize all hidden representations across encoding layers. For multi-scale temporal grounding, such cross-scale representations should be fully used since they express semantics in video moments of various lengths.

To resolve the above issues, in this paper, we propose a multi-scale contrastive learning framework for multi-scale temporal grounding. In our framework, instead of leveraging moment-query relationships, we utilize the association among video moments. Particularly, to avoid representation conflict among video moments, we introduce a query-centric contrastive approach that draws temporally separate video moments corresponding to a common textual query. A central component of our framework is the creation of positive and negative video moment samples, which previous works primarily apply data augmentation (Kim et al., 2022; Xing et al., 2023). However, because most long-form videos consist of a high volume of video moments, choosing an appropriate augmentation strategy that suits every moment is a non-trivial and lengthy tuning step. Another common approach is to introduce a memory bank to store positive or negative samples' representations, which are created by aggregating input representations iteratively during training (Panta et al., 2024; Han et al., 2023). Nevertheless, a memory bank would present

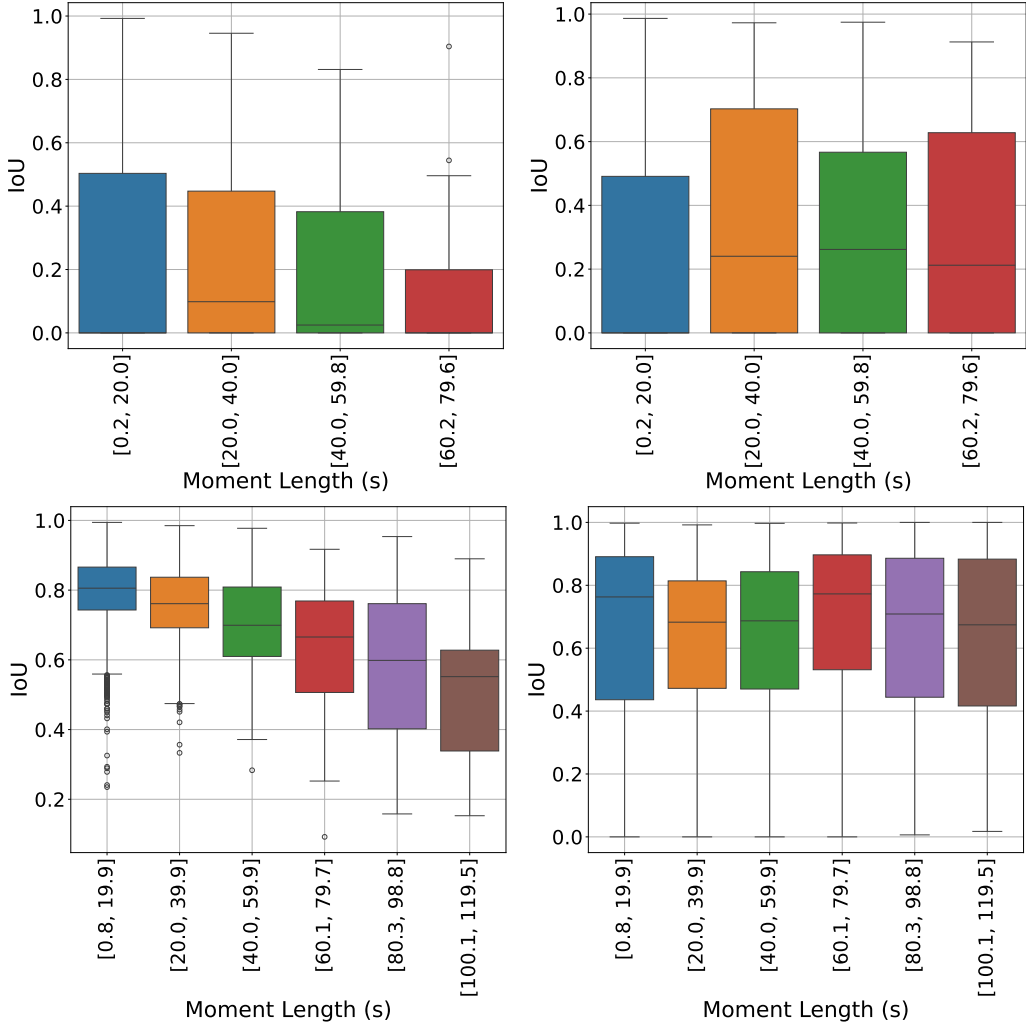


Figure 7.3: First and Second: IoU results with respect to target video moment length on Ego4D-NLQ (Grauman et al., 2022) of baseline SnAG (Mu et al., 2024) and our model. Third and Fourth: IoU results with respect to target video moment length on TACoS (Regneri et al., 2013) datasets of baseline SnAG (Mu et al., 2024) and our model.

additional hyperparameters such as the bank size and update frequency, which demand laborious tuning effort (Wang et al., 2021b).

To prevent these problems, we directly draw samples from the feature space of video moment encoder. Specifically, we take advantage of internal, intermediate representations of video moments from the encoder that are readily available through the feed-forward step of the network without the need to rely upon external steps such as data augmentation or online storing of samples in memory banks. Accordingly, we introduce a within-scale and cross-scale approach to create positive and negative moment samples for contrastive learning. Regarding the within-scale approach, we

seek to pull together representations of such semantically close video moments on the same scale of similar temporal range. Moreover, we also push apart representations of video moments which are unrelated to the textual query. Regarding the cross-scale approach, we compel the model to relate global long-range video moments to local short-range moments, while simultaneously repelling semantically distant cross-scale representations in an analogous cross-scale manner. This cross-scale approach would enable long-range moment representations to capture nuanced details of short-range moments, thereby mitigating informational degradation within long-range representations.

To sum up, our contributions are the following:

- We propose a multi-scale contrastive framework that focuses on moment-moment relations to mitigate informational degradation in video moment representations.
- We propose a within- and cross-scale strategy that supports semantic consistency not only between similar-range but also cross-range video moment representations emanating across layers of the video encoder.
- Our framework achieves superior results across major benchmark datasets concerning both short-form and long-form video grounding.

## 7.2 Methodology

In this section, we delineate our proposed contrastive framework for multi-scale temporal grounding, particularly focusing on a sampling procedure to draw video moment representations across temporal scales.

### 7.2.1 Preliminary - Video Temporal Grounding

We denote an input video  $V$  as a sequence of video clips  $\{v_t\}_{t=1}^T = \{v_1, v_2, \dots, v_T\}$ , where  $v_t$  denotes a video moment (clip) centered at time  $t$ . We use a pre-trained feature extractor to embed each  $v_t$  into a moment embedding  $\mathbf{v}_t$ . Given the video  $V$ , our task is to localize a moment  $y = (s, e)$  based on a sentence query  $Q =$

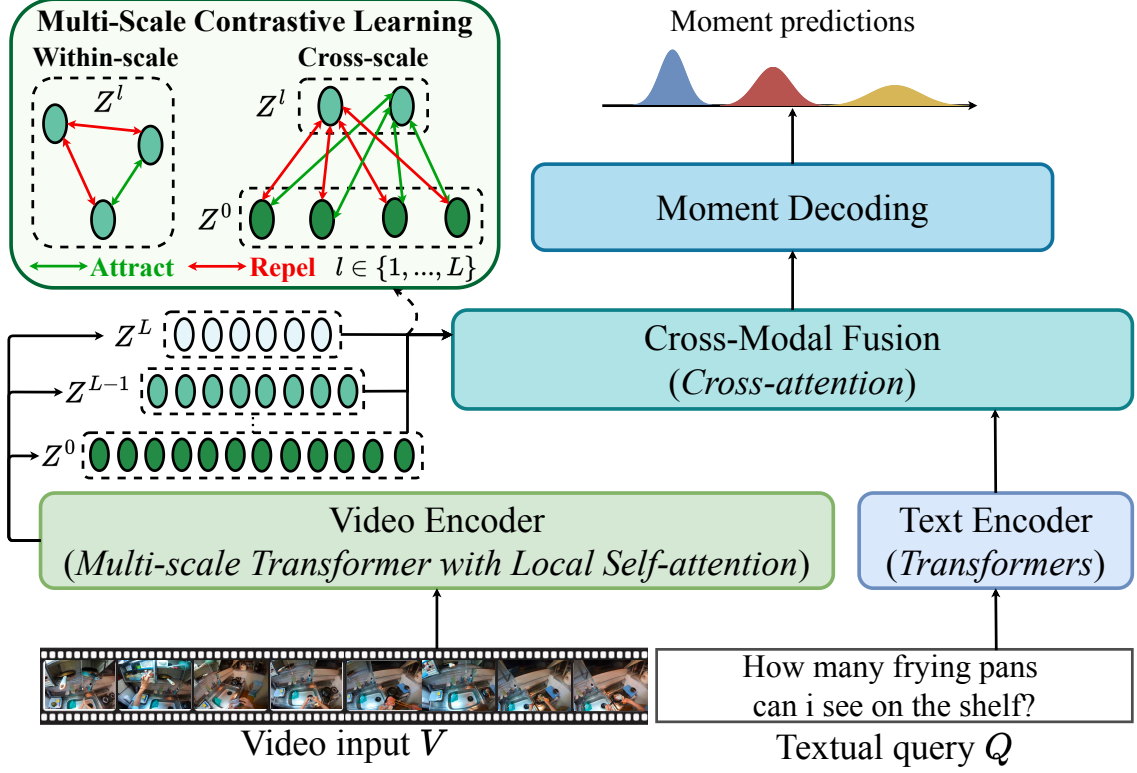


Figure 7.4: Overall illustration of the proposed framework.

$\{q_1, q_2, \dots, q_K\}$ . Similar to the input video, we also embed the query  $Q$  into a sequence of word embeddings  $\{\mathbf{q}_1, \mathbf{q}_2, \dots, \mathbf{q}_K\}$ .

**Video encoder.** After embedding video clips, we use a convolution-based projection function to encode local context of video clips:

$$Z^0 = \{\mathbf{z}_t^0\}_{t=1}^T = \text{Conv}(\mathbf{v}_1, \mathbf{v}_2, \dots, \mathbf{v}_T). \quad (7.1)$$

Subsequently, we designate  $L$  Transformer layers to encode temporal context among video clips. In detail, each Transformer layer consists of a local multi-head self-attention (LocalMSA) with a window size of  $W$  and an MLP block, in which we restrict the attention to be within a local window:

$$\bar{Z}^l = \alpha^l \cdot \text{LocalMSA}(\text{LN}(Z^{l-1})) + Z^{l-1}, \quad (7.2)$$

$$\hat{Z}^l = \bar{\alpha}^l \cdot \text{MLP}(\text{LN}(\bar{Z}^l)) + \bar{Z}^l, \quad (7.3)$$

$$Z^l = \downarrow(\hat{Z}^l), \quad l \in \{1, 2, \dots, L\}, \quad (7.4)$$

where  $Z^{l-1}, \bar{Z}^l, \hat{Z}^l \in \mathbb{R}^{T^{l-1} \times D}$ ,  $Z^l \in \mathbb{R}^{T^l \times D}$ .  $T^{l-1}/T^l$  is the downsampling ratio,  $\alpha^l$  and  $\bar{\alpha}^l$  are learnable per-channel scaling factors (Touvron et al., 2021),  $D$  is the

hidden dimension, and LN is the layer normalization.

Inspired by (Mu et al., 2024), we implement the downsampling operator  $\downarrow$  as a strided depthwise 1D convolution. The downsampling operation engenders the multi-scale property of the encoder, generating representations for longer video moments.

**Text encoder.** We use Transformer layers, where each layer includes a vanilla self-attention followed by an MLP. Thus, the textual encoder produces textual representations  $E = \{\mathbf{e}_1, \mathbf{e}_2, \dots, \mathbf{e}_K\}$  for query embeddings  $\{\mathbf{q}_1, \mathbf{q}_2, \dots, \mathbf{q}_K\}$ .

**Cross-modal fusion.** Our architecture uses cross-attention to fuse video clip and query word representations. Technically, we modulate video clip representations  $\{Z^l\}_{l=1}^L$  with word representations  $E$  as follows:

$$\tilde{Z}^l = \text{LN}(Z^l), \quad \tilde{E} = \text{LN}(E), \quad (7.5)$$

$$O^l = \sigma \left( \frac{(\tilde{Z}^l)^\top \cdot \tilde{E}}{\sqrt{D}} \right) \cdot \tilde{Z}^l, \quad (7.6)$$

$$X^l = \beta^l \cdot \text{MLP}(\text{LN}(O^l)) + O^l, \quad (7.7)$$

where  $\beta^l$  denotes a learnable per-channel scale and  $\sigma$  the Softmax activation function.

**Moment decoding.** After cross-modal fusion, our model converts each time step  $t$  to a moment candidate. Specifically, given  $\mathbf{x}_t^l$ , we use a convolutional network comprising 1D convolutional layers as the classification head to predict a score  $p_t^l$ . In a similar vein, we use a similar 1D convolutional network attached with a ReLU activation function to regress the normalized distances from  $t$  to the moment boundaries  $(d_t^s, d_t^e)$  if  $\mathbf{x}_t^l$  is classified as positive. Formally, the decoded moment is computed as:

$$(t, l) = \arg \max_{t, l} p_t^l, \quad (7.8)$$

$$\hat{s} = 2^{l-1} (t - d_t^s), \quad \hat{e} = 2^{l-1} (t + d_t^e). \quad (7.9)$$

During testing, we employ Soft-NMS (Bodla et al., 2017) to merge overlapping moment predictions.

## 7.2.2 Cross-scale Contrastive Learning

**Query-centric sampling.** As randomly sampling moment-query pairs for contrastive learning might lead the model to representation conflict if the groundings of two queries overlap with each other, we instead introduce a sampling approach that draws a text query  $Q$  and its temporally separate video moments associated with a common video  $V$ :

$$Q_{j'}, \{y_{j'}^l\}_{l=1}^L \sim \mathcal{U} \left( \{Q_j, \{y_j^l\}_{l=1}^L\}_{j=1}^{N_Q} \right), \quad (7.10)$$

where  $\mathcal{U}$  denotes a discrete uniform distribution,  $\{y_{j'}^l\}_{l=1}^L$  the set of target video moments in each layer  $l$ , and  $N_Q$  the number of textual queries related to video  $V$ . We generate the target set  $\mathcal{P}(l)$  via center sampling (Zhang et al., 2022; Mu et al., 2024), *i.e.* given any moment centered at  $t$ , any time step  $c \in [t - \alpha \frac{T}{T'}, t + \alpha \frac{T}{T'}]$  in layer  $l$  is considered as a target. After sampling the query and target moments, we directly utilize the representations  $\{\mathbf{z}_{j'}^l\}_{l=1}^L$  of the target moments  $\{y_{j'}^l\}_{l=1}^L$  extracted by the aforementioned multi-scale video encoder.

**Within-scale contrastive learning.** Having obtained the representations of target moment samples, we directly utilize moments within each scale as positive and negative samples. Particularly, we iterate over every layer  $l$  of the video encoder, and for each anchor video moment  $y_{j'}^l$ , we consider all video moments of layer  $l$  corresponding to query  $Q_{j'}$  to become positive moment set  $P(l)$ , and randomly draw those not corresponding to query  $Q_{j'}$  to be negative set  $\mathcal{N}(l)$ .

Then, we formulate multi-scale contrastive objective over all layers  $l \in \{1, 2, \dots, L\}$ , which pushes positive moments closer while negative moments further:

$$\begin{aligned} \mathcal{L}_{\text{within}} = & - \sum_{l=1}^L \sum_{i \in \mathcal{P}(l)} \sum_{j \in \mathcal{P}(l), i \neq j} \\ & \log \frac{e^{(\mathbf{z}_i^l \cdot \mathbf{z}_j^l)}}{e^{(\mathbf{z}_i^l \cdot \mathbf{z}_j^l)} + \sum_{n \in \mathcal{N}(l)} e^{(\mathbf{z}_i^l \cdot \mathbf{z}_n^l)}}. \end{aligned} \quad (7.11)$$

**Cross-scale contrastive learning.** We further associate semantically close moment representations from across different scales. Specifically, we push short-range moment representations closer to semantically close long-range moment represen-

tations. This would enable short-range moments to relate to longer video context while long-range features to capture nuanced details of short-range moments.

As video moment features of layer 0  $\{\mathbf{z}_{j'}^0\}$  are the most likely to preserve salient video information compared to other levels, we employ features of the target moments from the lowest level as the anchor set for cross-scale contrastive learning. To construct positive and negative moment set, we utilize features of higher levels  $l \in \{1, 2, \dots, L\}$  in the feature pyramid corresponding to video moments that involve and do not involve the textual query, respectively. Denoting the set of moment indices in level  $l$  that are related to the query as  $\mathcal{P}(l)$  and the set of those that are unrelated as  $\mathcal{N}(l)$ , we define the cross-scale contrastive learning objective as:

$$\mathcal{L}_{\text{cross}} = - \sum_{i \in \mathcal{P}(0)} \sum_{l=1}^L \sum_{j \in \mathcal{P}(l)} e^{(\mathbf{z}_i^0 \cdot \mathbf{z}_j^l)} \log \frac{e^{(\mathbf{z}_i^0 \cdot \mathbf{z}_j^l)}}{e^{(\mathbf{z}_i^0 \cdot \mathbf{z}_j^l)} + \sum_{n \in \mathcal{N}(l)} e^{(\mathbf{z}_i^0 \cdot \mathbf{z}_n^l)}}. \quad (7.12)$$

### 7.2.3 Training Objective

For temporal grounding training, we adopt a focal loss  $\mathcal{L}_{\text{cls}}$  for target moment classification and a Distance-IoU loss  $\mathcal{L}_{\text{reg}}$  for distance regression from a positive time step  $t$  to the target moment. Then, we combine these losses with our within- and cross-scale contrastive loss:

$$\mathcal{L} = \mathcal{L}_{\text{cls}} + \rho_{\text{reg}} \cdot \mathcal{L}_{\text{reg}} + \rho_{\text{within}} \cdot \mathcal{L}_{\text{within}} + \rho_{\text{cross}} \cdot \mathcal{L}_{\text{cross}}, \quad (7.13)$$

where  $\rho_{\text{reg}}$ ,  $\rho_{\text{within}}$ , and  $\rho_{\text{cross}}$  denote hyperparameters to balance the regression, within-scale, and cross-scale contrastive losses, respectively.

## 7.3 Experiments

To validate the effectiveness, we conduct extensive experiments against recent methods for temporal grounding. We also perform ablation study to investigate each component.

### 7.3.1 Datasets

Following previous works, we work on five challenging datasets of temporal grounding, which belong to two main categories, *i.e.* 1) Long videos, many queries (Ego4D-NLQ (Grauman et al., 2022), MAD (Soldan et al., 2022), and TACoS (Regneri et al., 2013)) and 2) Short videos, few queries (ActivityNet-Captions (Krishna et al., 2017) and Charades-STA (Sigurdsson et al., 2016)).

**Ego4D-NLQ** (Grauman et al., 2022) consists of egocentric videos recording daily human activities. Each video possesses length from 3.5 to 20 minutes and is associated with 11.6 queries on average.

**MAD** (Soldan et al., 2022) comprises 1.2K hours of movies with 384K queries transcribed from audio description. Since each video is a movie, each exhibits 47 to 202 minutes long.

**TACoS** (Regneri et al., 2013) focuses on cooking topics. The total video length is 10.1 hours and each video is tasked with 143.5 queries for the temporal grounding operation.

**ActivityNet-Captions** (Krishna et al., 2017) targets dense video captioning and is subsequently adapted to temporal grounding. Its video length is two minutes on average and the average number of queries per video is approximately 3.65 queries.

**Charades-STA** (Sigurdsson et al., 2016) is an action recognition dataset transformed into a temporal grounding one. Each video lasts approximately 30 seconds and possesses 2.4 queries.

### 7.3.2 Evaluation Metrics

We report Recall@K at different temporal intersection-over-union  $\theta$  (R@K, tIoU =  $\theta$ ) for all datasets. The metric measures the percentage of textual queries whose at least one of the top- $K$  moment predictions temporally overlap with the groundtruth moment more than  $\theta$ .

### 7.3.3 Implementation Details

To fairly compare with previous works and satisfy the scalability of temporal grounding operation for long videos, we adopt video-centric sampling approach (Mu et al., 2024). For Ego4D-NLQ, we use pre-trained 1) SlowFast video features

(Feichtenhofer et al., 2019) with BERT textual features (Devlin et al., 2018), and 2) EgoVLP video and textual features (Lin et al., 2022a). For testing, we report  $R@1, 5$ ,  $tIoU = \{0.3, 0.5\}$ . For MAD dataset, we use CLIP features (Radford et al., 2021) for both videos and texts, and report  $R@1, 5, 10, 50$ ,  $tIoU = \{0.1, 0.3, 0.5\}$ . For the TACoS dataset, we use C3D video features (Tran et al., 2015) and GloVe textual features (Pennington et al., 2014). We report results in terms of  $R@1, 5$ ,  $tIoU = \{0.5, 0.7\}$ . In addition, we utilize I3D features (Carreira and Zisserman, 2017) pre-trained on Kinetics (Kay et al., 2017b) for Charades-STA and C3D features (Tran et al., 2015) for ActivityNet-Captions experiments. For both datasets, similar to TACoS, we take advantage of GloVe textual features (Pennington et al., 2014). We report  $R@1, 5$ ,  $tIoU = \{0.5, 0.7\}$  for testing on Charades-STA, and  $R@1, 5$ ,  $tIoU = \{0.3, 0.5\}$  for testing on ActivityNet-Captions. For more details regarding model architecture, we direct interested readers to the appendix. For both within-scale and cross-scale contrastive learning implementation, we keep the size of the negative sample set  $\mathcal{N}(l)$  in every level  $l$  to be equal to the size of the positive video clips  $\mathcal{P}(l)$  that correspond to the target video moments. Based upon validation and fair comparison with previous methods, we use  $\rho_{\text{ref}} = \rho_{\text{within}} = \rho_{\text{cross}} = 1.0$ .

### 7.3.4 Baselines

We consider the following temporal grounding models as baselines:

- **VSL-Net** (Zhang et al., 2020a): utilizes textual query to highlight regions potential to comprise the target moment.
- **VLG-Net** (Soldan et al., 2021): models temporal grounding as a graph matching problem.
- **Moment-DETR** (Lei et al., 2021b): a Transformer encoder-decoder architecture that views temporal grounding as a set prediction problem.
- **CONE** (Hou et al., 2022): subsequently slices a video input into windows, selects relevant windows, and ranks the selected windows to obtain target moments.

- **MMN** (Wang et al., 2022d): a Siamese-like network architecture that is trained with video-query and query-video contrastive learning.
- **SSRN** (Zhu et al., 2023b): enriches anchor frames with additional consecutive frames.
- **G2L** (Li et al., 2023a): measures moment-query similarities using geodesic distance and quantifies cross-modal interactions with game-theoretic interactions.
- **SOONet** (Pan et al., 2023): an anchor-based framework that conducts grounding by pre-ranking, re-ranking, and regression.
- **MESM** (Liu et al., 2024b): a fine-grained moment-query contrastive approach modeled for query word and video moment representations,
- **Contrastive-MSAT** (Panta et al., 2024): applies moment-query contrastive loss supported by a momentum-based memory bank.
- **UVCOM** (Xiao et al., 2024): a moment-query contrastive approach for a unified video comprehension framework,
- **SnAG** (Mu et al., 2024): achieves scalable grounding with cross-modal late fusion.

## 7.4 Experimental Results

### 7.4.1 Main Results

**Results on Ego4D-NLQ** (Table 7.1). Our framework significantly outperforms recent temporal grounding methods. For example, using SlowFast+BERT features, we outperform previous best method, *i.e.* SnAG, by mean improvements of 1.16% and 1.46% in terms of R@1 and R@5 metrics, respectively. In addition, we accomplish more significant performance gains on the more stringent tIoU threshold of 0.5, denoting more precise moment localization.

**Results on MAD** (Table 7.2). Similar to results on Ego4D-NLQ, our framework obtains an outstanding improvement over previous temporal grounding methods.

Features	Model	R@1			R@5		
		0.3	0.5	Avg	0.3	0.5	Avg
SF+BERT	VSL-Net	5.45	3.12	4.29	10.74	6.63	8.69
	CONE	10.40	5.03	7.72	22.74	11.87	17.31
	SOONet	8.00	3.76	5.88	22.40	11.09	16.75
	SnAG	9.83	6.83	8.33	27.93	19.27	23.60
	MSTG	<b>10.80</b>	<b>7.22</b>	<b>9.49</b>	<b>28.54</b>	<b>20.38</b>	<b>25.06</b>
EgoVLP	VSL-Net	10.84	6.81	8.83	18.84	13.45	16.15
	CONE	14.15	8.18	11.17	30.33	18.02	24.18
	SnAG	15.72	10.78	13.25	38.39	27.44	32.92
	MSTG	<b>16.37</b>	<b>11.27</b>	<b>13.96</b>	<b>39.97</b>	<b>28.70</b>	<b>34.43</b>

Table 7.1: Results on Ego4D-NLQ.

Model	R@1			R@5			R@10			R@50		
	0.1	0.3	0.5	0.1	0.3	0.5	0.1	0.3	0.5	0.1	0.3	0.5
VLG-Net	3.64	2.76	1.65	11.66	9.31	5.99	17.39	14.56	9.77	39.78	34.27	24.93
Moment-DETR	0.31	0.24	0.16	1.52	1.14	0.28	2.79	2.06	1.20	11.08	7.97	4.71
CONE	8.90	6.87	4.10	20.51	16.11	9.59	27.20	21.53	12.82	43.36	34.73	20.56
SOONet	11.26	9.00	5.32	23.21	19.64	13.14	30.36	26.00	17.84	50.32	44.78	32.59
SnAG	10.28	8.46	5.55	24.42	20.60	13.75	32.23	27.50	19.00	52.28	46.68	35.24
MSTG	<b>12.76</b>	<b>10.94</b>	<b>6.92</b>	<b>26.43</b>	<b>22.60</b>	<b>15.43</b>	<b>34.08</b>	<b>29.41</b>	<b>20.70</b>	<b>54.84</b>	<b>48.26</b>	<b>37.77</b>

Table 7.2: Results on MAD.

Model	TACoS				ActivityNet-Captions				Charades-STA			
	R@1		R@5		R@1		R@5		R@1		R@5	
	0.3	0.5	0.3	0.5	0.5	0.7	0.5	0.7	0.5	0.7	0.5	0.7
VLG-Net	45.46	34.19	70.38	56.56	46.32	29.82	77.15	63.33	-	-	-	-
MGSL-Net	42.54	32.27	63.39	50.13	51.87	31.42	82.60	66.71	63.98	41.03	93.21	63.85
SSRN	45.10	34.33	65.26	51.85	54.49	33.15	84.72	68.48	65.59	42.65	94.76	65.48
MMN	39.24	26.17	62.03	47.39	48.59	29.26	79.50	64.76	-	-	-	-
G2L	42.74	30.95	65.83	49.86	51.68	33.35	81.32	67.60	-	-	-	-
MESM	52.69	39.52	-	-	-	-	-	-	61.24	38.04	-	-
Contrastive-MSAT	49.77	37.99	68.31	58.31	47.73	31.21	78.06	63.63	-	-	-	-
UVCOM	36.39	23.32	-	-	-	-	-	-	59.25	36.64	-	-
SnAG	56.44	44.86	81.15	70.66	48.55	30.56	81.71	63.41	64.62	46.26	92.55	71.94
MSTG	<b>58.17</b>	<b>47.04</b>	<b>84.84</b>	<b>73.55</b>	<b>54.83</b>	<b>33.56</b>	<b>84.78</b>	<b>68.91</b>	<b>66.64</b>	<b>47.03</b>	<b>93.66</b>	<b>72.53</b>

Table 7.3: Results on TACoS, ActivityNet-Captions, and Charades-STA.

Specifically, we enhance SOONet with 1.68 and 2.82 points of R@1 and R@5 on average. Moreover, our model outperforms CONE and SnAG in terms of mean R@1 / R@5 by 3.58 / 6.08 and 2.11 / 1.90 points, respectively, especially for the more stringent tIoU threshold.

**Results on TACoS** (Table 7.3 (left)). Our model achieves R@1 / R@5 of 47.04% / 73.55% at tIoU = 0.5, outperforming the strongest baseline, *i.e.* SnAG, by a substantial margin, *i.e.* +2.18% R@1 and +2.89% R@5. Combined with the results on Ego4D-NLQ and MAD, these results demonstrate that our contrastive

Positive-negative sampling approach	R@1		R@5	
	0.3	0.5	0.3	0.5
Data augmentation	57.00	45.46	83.13	72.06
Memory bank	57.69	46.62	84.13	72.94
MSTG	<b>58.17</b>	<b>47.04</b>	<b>84.84</b>	<b>73.55</b>

Table 7.4: Ablation results on TACoS with various positive and negative sampling approaches.

Contrastive component	R@1		R@5	
	0.3	0.5	0.3	0.5
w/o within-scale	57.40	46.00	83.46	72.39
w/o cross-scale	57.00	45.85	82.34	71.58
MSTG	<b>58.17</b>	<b>47.04</b>	<b>84.84</b>	<b>73.55</b>

Table 7.5: Ablation results on TACoS with multi-scale contrastive components.

framework provides beneficial signals to counter informational degradation in the feature pyramid for long-form video grounding.

**Results on ActivityNet-Captions** (Table 7.3 (middle)). We achieve R@1 / R@5 scores of 33.56% / 68.91% at tIoU = 0.7. These results indicate that we outperform SSRN by 0.41% and 0.43% with regards to R@1 and R@5, respectively, even though we use the backbone SnAG which is significantly weaker than SSRN.

**Results on Charades-STA** (Table 7.3 (right)). Our model outperforms previous methods by a wide margin. Particularly, we accomplish 47.03% R@1 and 72.53% R@5 at tIoU = 0.7, exceeding SSRN by 4.38% R@1 and 7.04% R@5. These outcomes on Charades-STA and ActivityNet-Captions show that mutual information signals among video moments contributed by our contrastive framework can polish video moment representations to help temporal grounding on short-form videos.

## 7.4.2 Ablation Study

We conduct extensive experiments on TACoS to study the influence of the design choices.

**Effect of contrastive components.** We explore what extent each component of our contrastive framework, *i.e.* within- or cross-scale objective, contributes to the overall performance improvement. In Table 7.5, cross-scale objective plays a more fundamental role in polishing video moment representations than the within-scale

Association approach	R@1		R@5	
	0.3	0.5	0.3	0.5
Query-query	55.61	45.06	81.25	71.75
Moment-query	57.00	46.24	82.44	72.37
CLIP-based moment-moment	57.13	46.94	83.28	72.96
MSTG	<b>58.17</b>	<b>47.04</b>	<b>84.84</b>	<b>73.55</b>

Table 7.6: Ablation results on TACoS with various association approaches.

counterpart. Since cross-scale contrastive objective concentrates more upon long-range moment representations by relating them with the short-range moment ones, these results validate our hypothesis that informational degradation is a fundamental problem to resolve in multi-scale temporal grounding.

**Effect of moment-moment association.** In addition to our proposed moment-moment association, we experiment with various approaches, *i.e.* moment-query association, query-query association, and one approach to associate video moments but based on the semantic closeness of their corresponding textual queries. For the last approach, we consider two textual queries to be semantically similar if their CLIP-based cosine similarity score is greater than or equal to 0.8 (for positive sampling) and semantically distant if the similarity score is smaller than or equal to 0.2 (for negative sampling). As can be observed in Table 7.6, query-query association performs the worst, as the approach does not polish moment representations. The moment-moment approach outperforms moment-query contrastive learning, but underperforms our method. We hypothesize that there might exist representation conflict between two video moments temporally overlap with each other.

**Effect of direct utilization of moment representations.** We study the impact of our direct utilization of moment representations for positive and negative sample generation, and compare with Tube TokenMix (Xing et al., 2023) as the data augmentation and the momentum-based memory bank approach (Panta et al., 2024). Table 7.4 shows that we significantly surpass other methods, on average by 1.38 / 1.60 points of R@1 / R@5 over the augmentation approach, and 0.45 / 0.66 points of R@1 / R@5 over the memory bank approach. We hypothesize that while memory bank may maintain a high number of samples for contrastive learning, expensive hyperparameter tuning is essential to achieve an effective performance.

### 7.4.3 Qualitative Analysis

In Figure 7.3, we observe that our model does not encounter degraded performance when the lengths of the target moments increase. Moreover, we visualize moment predictions of the recent method, *i.e.* SnAG (Mu et al., 2024), and our model in Figure 7.2. Even though SnAG could precisely detect the shorter-length moment, it misses the moment of longer length, due to the degraded information issue. In contrast, our framework is able to localize both the short and long moments. We hypothesize that our contrastive framework can hold salient semantics for video moment representations to resolve the degraded signals in the grounding model, thus enhancing the grounding operation towards long video moments.

## 7.5 Summary

In this paper, we propose a multi-scale contrastive framework for multi-scale temporal grounding. Essentially, our framework utilizes a query-centric approach to associate temporally separate video moments which correspond to a common textual query to avoid representation conflict. Accordingly, we define a within-scale contrastive objective to model relations among similar-range video moments, and a cross-scale objective to model relations among cross-range moments. Comprehensive experiments validate the effectiveness of our framework for both short-term and long-term temporal grounding.

# Chapter 8

## Temporal-Oriented Recipe for Transferring Large Vision-Language Model to Video Understanding

### 8.1 Introduction

Empowered by the elevating popularity of video-text data (Nguyen et al., 2024d,b) and outstanding advances in large language model (LLM)-based designs, recent years have encountered remarkable progress in video understanding with large vision-language models (LVLMs). From the advent of models such as BLIP (Li et al., 2022c), BLIP-2 (Li et al., 2023b), and LLaVA (Liu et al., 2023), video question answering (VideoQA) has improved from 33.8, 16.7, and 12.4 on MSVD (Wu et al., 2017), MSRVTT (Xu et al., 2016), and ActivityNet (Krishna et al., 2017) to more than 60.0 in terms of GPT-3.5 evaluation. Not only VideoQA but also long-term action recognition (Kuehne et al., 2014; Tang et al., 2019; Wu and Krahenbuhl, 2021) and video captioning (Zhou et al., 2018a; Islam et al., 2024) have achieved significant breakthroughs.

In recent years, model architectures and training protocols have witnessed significant advancements. However, as these systems grow in diversity and scale, their computational demands pose substantial challenges for comparison, analysis, and reproducibility. Despite these advancements, many approaches have overlooked the core nature of video understanding. Rather than explicitly modeling temporal relationships, they often rely on spatial inductive biases, assuming that spatial knowledge can seamlessly extend to temporal comprehension. For instance, several methods focus on creating a unified representation space for visual and textual

Table 8.1: On the first row, a correct answer should comprise details related to cutting ginger and garlic on a chopping board, whereas other models wrongly mention “*rub salt*”, “*cut chicken*” and “*add to the pot*”, and “*pour milk*”. On the second row, we need to respond with “*getting to the bus*”, but the models mistakenly note “*late for exam*”, “*to the hospital*”, and “*feeling sad*”.

Video	Question	Sample Answer	Video-LLaMA	Video-LLaVA	Qwen2.5-VL
	What does the person do before seasoning chicken?	The person cuts ginger and garlic into small pieces on a chopping board	The person rubs salt on the chicken.	Before seasoning chicken, the person cuts it into small pieces and adds it to a pot.	Before seasoning chicken, the person pours milk into a bowl of rice.
	Why did the girl rush?	The girl rushed to get to the bus on time, as she was running to catch the bus	The girl rushed because she was late for her exam.	The girl rushed to the hospital because she was feeling unwell.	The girl in the picture appears to be looking down and might be feeling sad or contemplative.

modalities (Lin et al., 2023; Chen et al., 2023; Zhang et al., 2023b). Others emphasize aggregating or selecting salient visual tokens aligned with prompts (Shang et al., 2024; Xu et al., 2024) or leverage large-scale pretraining with instruction-following datasets (Maaz et al., 2023; Luo et al., 2023; Wang et al., 2024b). Therefore, existing models fall short of realizing the full potential of video understanding. For example, while VideoQA systems can accurately answer questions about object detection or describe isolated actions, they struggle with queries involving causal and temporal relationships (Xiao et al., 2021b). As shown in Table 8.1, they often generate inaccurate responses when faced with questions about temporal order or causality.

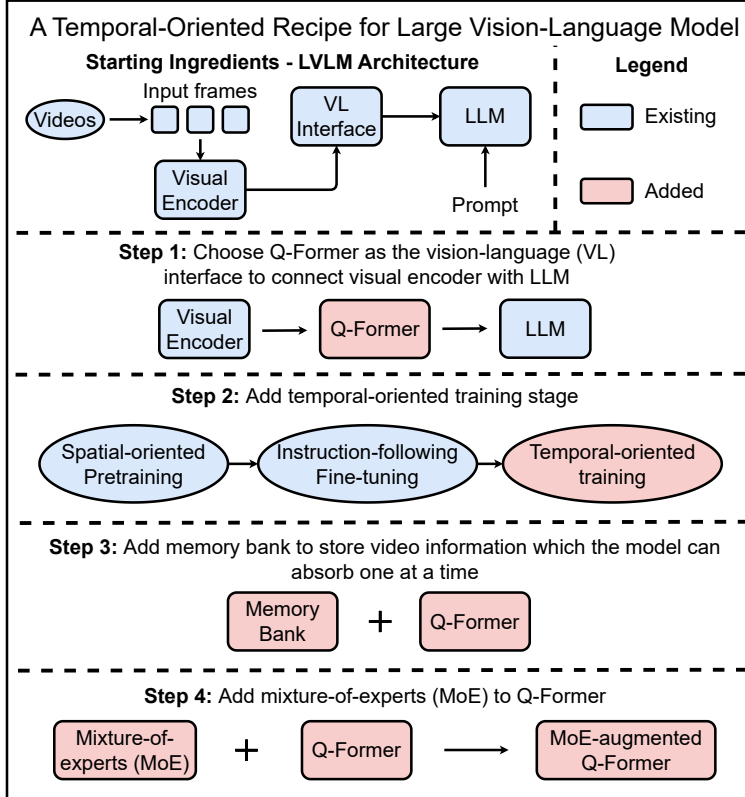
To overcome this limitation, we aim to enhance temporal understanding capabilities of large vision-language models (LVLMs) by advancing temporal-critical components within their architectures. As illustrated in Figure 8.1, an LVLM is fundamentally composed of three main components: a visual encoder, a vision-language interface, and a large language model (LLM). However, due to the large-scale nature of LLMs and the multimodal complexity of video data, identifying the primary factors driving model effectiveness is challenging (He et al., 2024; Qian et al., 2024; Chandrasegaran et al., 2024), hindering further progress in the field. Our focus is to bridge this gap by ensuring that temporal understanding is treated as a core aspect of video comprehension, rather than an implicit outcome of spatial knowledge.

To illustrate our points, in Table 8.2, we explicate the diversity of modern LVLMs for video understanding by examining them along various dimensions, including

Table 8.2: Existing LVLM models exhibit stark distinctions among themselves, making it challenging to reproduce, analyze, and compare these methods. Therefore, we aim to answer the question: *“Is there a straightforward recipe to build temporal understanding capacity for LVLMs?”*

Method	Visual Encoder	Vision-Language Interface	LLM Size	Training Data Size (Pretraining)	Training Data Size (IFT)
VALLEY (Luo et al., 2023)	ViT-L	Transformer + Mean-pooling	13B	702K	73K
Video-LLaMA (Zhang et al., 2023b)	CLIP-G	Q-Former	7B	3M	18K
LLaMA-VID (Li et al., 2024c)	CLIP-G	Linear Projection	13B	790K	763K
VideoChat (Li et al., 2023c)	CLIP-G	Q-Former	7B	25M	18K
VideoChat2 (Li et al., 2024b)	UMT-L	Q-Former	7B	25M	2M
Video-ChatGPT (Maaz et al., 2023)	ViT-L	Mean-pooling + Linear Projection	7B	595K	100K
Video-LLaVA (Lin et al., 2023)	ViT-L	Linear Projection	7B	1.3M	765K
GPT4Video (Wang et al., 2024b)	ViT-L	Q-Former	7B	11K	50K
PLLaVA (Xu et al., 2024)	ViT-L	Linear Projection + Adaptive Pooling	7B/13B/34B	25M	783K
ST-LLM (Liu et al., 2024a)	BLIP-2	Linear Projection	7B	25M	2M
Chat-UniVi (Jin et al., 2024)	ViT-L	Clustering-based Merging + Linear Projection	7B/13B	1.6M	649K

Figure 8.1: Our temporal-oriented recipe for large vision-language model.



visual encoder, vision-language interface, LLM, and training data. Based on this examination, we observe that there exist stark differences among these models. Nevertheless, it is not straightforward to dissect which factors make an important contribution to the overall video understanding performance and which do not.

As one of the works that initiates empirical analysis research line, METER (Dou et al., 2022) studies a wide variety of components in the context of image-

language modeling. Unfortunately, its analysis mostly works on images and neglects many aspects related to video modeling, such as spatio-temporal architectural design, video pretraining data, and video pretraining objectives. To fill in such gap, recent VindLU work (Cheng et al., 2023) conducts an analysis towards important factors for video-language understanding models. Unfortunately, their analysis is limited to small-scale frameworks with millions of parameters. Similarly, Fu et al. (2023) performs an empirical study of video-language transformers, but narrowly concentrates on masked visual modeling objective.

Our primary objective in this work is to answer the question “*Is there a straight-forward recipe to build temporal understanding capacity for LVLMs?*” Our answer is **yes**. To arrive at the answer, we conduct a thorough empirical study that demystifies the importance of various design choices and ultimately leads to a temporal-oriented recipe that significantly enhances video understanding results of previous LVLMs. Our recipe starts from a standard paradigm of a large vision-language model then proceeds with a progressive expansion scheme, where at each stage, we investigate a specific aspect of LVLM framework design (*e.g.*, architecture, training objective, training data, etc.) and choose the most effective option. Particularly, we study the following LVLM design components: (i) the vision-language interface, (ii) the video training protocols, and (iii) temporal memory bank, and (iv) scaling of the essential component. We present our recipe in Figure 8.1.

The key lessons of our study include:

- Among components in an LVLM architecture, we discover that enhancing vision-language interface significantly advances the temporal modeling strength of the LVLM.
- A query transformer that incorporates query tokens to interact with video representations combined with a temporal memory bank to compress salient video information is crucial for satisfactory video understanding performance.
- We can further obtain gains of temporal understanding level with techniques to scale up the interface, including mixture-of-experts and number of query tokens to store video information.

- An additional training stage for LVLMs with temporal-oriented data is sufficient to remarkably enhance temporal understanding capability and achieve impressive results on video understanding.

## 8.2 Temporal-Oriented Recipe for Large Vision-Language Model

In this section, we delineate our temporal-oriented recipe for large vision-language model. We start with a standard large vision-language model (LVLM), which consists of a visual encoder such as ViT and a large language model (LLM). Then, we progressively expand it to a model that achieves impressive temporal understanding results on various video understanding datasets and tasks. At each step of our recipe, we investigate how design choices have an impact upon temporal capacity of the LVLM. Throughout our procedure, we will discover answers to the following questions about the temporal-oriented recipe design:

- Can explicitly constructing temporal understanding capacity help LVLM, particularly provided that various video understanding benchmarks are spatially biased (Buch et al., 2022; Lei et al., 2022)? If so, what is the best mechanism for LVLM to conduct temporal modeling?
- Given that video lengths vary with a wide range, what is the most productive mechanism for LVLM to read/absorb video information? Several approaches use visual encoder combined with linear projection (Maaz et al., 2023; Xu et al., 2024) or query transformer (Q-Former) (Li et al., 2023c, 2024b), then proceed with a pooling mechanism, whereas others adopt a memory bank (He et al., 2024). Which of these is the most effective?
- Which temporal-oriented training schemes are most useful for temporal representation learning? There exist a wide variety of schemes, including video captioning (Abdar et al., 2024), moment captioning (Qasim et al., 2025; Yang et al., 2023b), moment grounding (Nguyen et al., 2023c; Lei et al., 2021b), and video summarization (Apostolidis et al., 2021; Nguyen et al., 2023b). How significant is each of these schemes? Are they complementary to each other?

- How can we optimize temporal capacity of LVLM? Can we inherit the mixture-of-experts (MoE) approach from LLM works, or increase the number of query tokens?

## Step 0: Starting Ingredients

**Large Vision-Language Model for Video Understanding.** We start with a standard ViT-G/14 (Dosovitskiy et al., 2020) from EVA-CLIP (Fang et al., 2023). For LLM, we use either Vicuna-7B or Vicuna-13B (Chiang et al., 2023), forming either a 7B-LVLM or a 13B-LVLM, respectively.

Formally, given a paired video and text prompt  $(V, T)$ , we first sample a sequence of frames from the video. Each frame is uniformly divided into equal-sized patches, which are then encoded by a visual encoder to obtain patch-level visual features. A positional embedding layer (PE) is applied to incorporate temporal ordering across frames, producing frame-level spatial-temporal representations. These visual features are then passed through a vision-language interface module, which projects them into the language representation space of the LLM. In parallel, the LLM embeds the text prompt  $T$  into word embeddings. The projected visual embeddings and text embeddings are concatenated to form a joint input sequence, which the LLM processes to generate a response for the video-text pair.

**Experimental Setup.** As our initialization, we directly inherit the pretrained and instruction-tuned model on image-based data (Liu et al., 2023; Li et al., 2022c, 2023b). Afterwards, we either conduct an additional temporal-oriented training step or go straight to finetuning and evaluating the model on the seven popular video understanding datasets: MSRVTT (Xu et al., 2016), MSVD (Chen and Dolan, 2011), ActivityNet-QA (Caba Heilbron et al., 2015), Breakfast (Kuehne et al., 2014), COIN (Tang et al., 2019), and LVU (Wu and Krahenbuhl, 2021). For our empirical investigation, we choose the video question answering (VideoQA) task and report the accuracy across these datasets.

In the following subsections, we progressively expand this baseline by adding more components of elevating complexity. Specifically, we start by incorporating vision-language interface (step 1), integrate a temporal-oriented training stage (step 2), insert a temporal memory bank (step 3), and upscaling the interface (step 4).

Table 8.3: Effect of different types of vision-language interface on 7B-LVLM

Vision-Language Interface	MSRVTT	MSVD	ActivityNet-QA	Breakfast	COIN	LVU
Linear Projection	45.3	56.9	46.3	85.9	83.9	57.1
Q-Former w/o SA + Mean-pooling - S = 3	45.8	57.4	46.4	86.3	84.8	58.0
Q-Former w/o SA + Adaptive-pooling - S = 3	46.2	57.5	46.8	87.0	85.6	58.2
Q-Former w/o SA + ESA - S = 3	46.3	57.7	47.2	87.6	86.0	58.7
Q-Former w/o SA + Mean-pooling - S = 6	46.3	58.1	47.6	87.9	86.5	58.8
Q-Former w/o SA + Adaptive-pooling - S = 6	46.6	58.1	47.6	88.3	87.1	59.2
Q-Former w/o SA + ESA - S = 6	47.0	58.2	48.1	88.4	87.6	59.8
Q-Former w/o SA + Mean-pooling - S = 9	47.2	58.2	48.3	88.5	87.9	60.3
Q-Former w/o SA + Adaptive-pooling - S = 9	47.4	58.7	48.6	89.1	88.5	60.8
Q-Former w/o SA + ESA - S = 9	47.5	59.1	48.8	89.9	88.6	61.2
Q-Former w/o SA + Mean-pooling - S = 12	47.6	59.2	49.3	90.1	89.1	61.8
Q-Former w/o SA + Adaptive-pooling - S = 12	47.9	59.8	49.5	90.8	89.4	62.2
Q-Former w/o SA + ESA - S = 12	48.2	59.9	49.5	90.9	90.0	62.4
Q-Former w/ SA - S = 3	48.7	60.2	49.8	91.7	90.8	62.7
Q-Former w/ SA - S = 6	48.8	60.4	49.8	91.9	91.6	52.0
Q-Former w/ SA - S = 9	49.0	60.4	50.3	92.1	92.5	63.5
Q-Former w/ SA - S = 12	49.3	60.4	50.3	92.4	92.7	63.7
Pre-trained Q-Former w/ SA - S = 12	<b>49.4</b>	<b>60.8</b>	<b>50.6</b>	<b>93.1</b>	<b>93.4</b>	<b>63.8</b>

Table 8.4: Effect of different types of vision-language interface on 13B-LVLM

Vision-Language Interface	MSRVTT	MSVD	ActivityNet-QA	Breakfast	COIN	LVU
Linear Projection	56.2	67.9	48.7	86.5	84.5	65.2
Pre-trained Q-Former w/ SA - S = 12	56.8	68.2	48.7	86.6	85.1	67.2
Q-Former w/o SA + Mean-pooling - S = 3	56.9	68.3	49.0	87.2	85.2	67.3
Q-Former w/o SA + Adaptive-pooling - S = 3	57.1	68.7	49.3	87.7	86.0	67.6
Q-Former w/o SA + ESA - S = 3	57.5	69.3	49.5	88.0	86.0	68.1
Q-Former w/o SA + Mean-pooling - S = 6	57.8	69.7	49.5	88.4	86.4	68.1
Q-Former w/o SA + Adaptive-pooling - S = 6	58.0	69.8	49.8	88.7	87.3	68.5
Q-Former w/o SA + ESA - S = 6	58.1	70.4	50.0	88.8	87.8	69.0
Q-Former w/o SA + Mean-pooling - S = 9	58.2	71.0	50.2	89.3	88.2	69.1
Q-Former w/o SA + Adaptive-pooling - S = 9	58.3	71.2	50.3	89.4	88.9	69.4
Q-Former w/o SA + ESA - S = 9	58.7	72.8	50.4	90.2	89.5	69.6
Q-Former w/o SA + Mean-pooling - S = 12	59.1	72.2	50.5	90.6	90.2	69.8
Q-Former w/o SA + Adaptive-pooling - S = 12	59.2	72.3	50.6	91.3	90.7	70.1
Q-Former w/o SA + ESA - S = 12	59.5	72.5	51.1	92.1	90.9	70.3
Q-Former w/ SA - S = 3	59.8	72.5	51.5	92.4	91.1	71.0
Q-Former w/ SA - S = 6	59.9	73.1	51.7	92.4	91.5	71.2
Q-Former w/ SA - S = 9	60.3	73.8	51.8	92.9	92.0	71.5
Q-Former w/ SA - S = 12	60.5	74.3	52.0	93.7	92.4	71.5
Pre-trained Q-Former w/o SA - S = 12	<b>60.6</b>	<b>74.3</b>	<b>52.5</b>	<b>93.7</b>	<b>93.2</b>	<b>71.8</b>

Note that due to the large computational cost, we cannot ablate the order of the steps in our recipe. Therefore, the order of the steps is primarily determined by the computational cost (*i.e.* the steps that can be implemented most efficiently are investigated before other steps, subsequently moving to more computationally costly steps).

## Step 1: Vision-Language Interface for LVLM

In the first stage of our temporal-oriented recipe, we investigate the interface between the vision and language domain for our LVLM. Such interface will enable the LLM to have access to visual information from the video input. For compactness, we study three interface schemes:

- **Linear projection:** In this interface, the linear projection maps visual embeddings into appropriate dimensional space for the LLM. Due to its simplicity, this approach has been widely adopted by previous LLaVA-based LVLMs (Xu et al., 2024; Lin et al., 2023).
- **Query Transformer with Self-Attention (Q-Former w/ SA):** Following (Zhang et al., 2023b; He et al., 2024), we use a number of transformer submodules which consist of cross-attention and self-attention layers. Cross-attention layers will enable a set of learnable query embeddings to interact with video representations to extract video information. In this variant, our Q-Former also contains self-attention layers, which can perform temporal modeling since they relate video frames together. We vary the number of submodules  $S \in \{3, 6, 9, 12\}$ . Parameters of Q-Former can be either randomly initialized or initialized from a pre-trained model. In our work, if we initialize Q-Former from a pre-trained model, we follow MA-LMM (He et al., 2024) to use the *bert-base-uncased* with  $S = 12$  submodules.
- **Query Transformer without Self-Attention (Q-Former w/o SA):** This version is similar to the previous one, except the fact that Q-Former does not comprise self-attention layers. Therefore, we need to incorporate an additional component after Q-Former for temporal modeling. We experiment with possible choices, including mean-pooling, adaptive pooling, and external self-attention (ESA) layers.

As Table 8.3 and 8.4 show, Q-Former demonstrates critical performance improvement over the linear projection approach. The improvement is indicated by average +6.0% and +6.2% accuracy boost of our 12-layer Q-Former variant over the 7B and 13B linear-projection baseline, respectively. We also observe that initializing

Q-Former self-attention layers with pretrained BERT encoder makes a significant contribution to the performance boost. This suggests that temporal semantics among words can be related to temporal relations among video frames.

Interestingly, our findings contradict the conclusions of several prior studies (Liu et al., 2023; Koh et al., 2023), which suggest that a simple linear projection is sufficient—and even more effective—than the Q-Former approach. In contrast, we observe that Q-Former plays a crucial role due to its ability to model diverse temporal relations across a broad range of video scenarios. We hypothesize that, particularly for temporally-intensive datasets, the integration of stacked cross- and self-attention layers provides the necessary capacity to capture and reason about complex temporal dependencies across video frames.

*Takeaway 1: For all subsequent experiments, we use 12-layer pretrained Q-Former w/ SA as our vision-language interface for video understanding with large vision-language model (LVLM).*

## Step 2: Temporal-Oriented Training Schemes

Existing methods (Zhang et al., 2023b; Li et al., 2024c; Lin et al., 2023) typically follow a pipeline of pretraining and instruction-tuning, followed by downstream finetuning. In our work, we investigate whether introducing an additional training stage specifically aimed at enhancing temporal understanding can further improve the video comprehension capabilities of LVLMs. To this end, we explore several temporal-oriented training strategies, which are illustrated in Table 8.7.

- **Video Captioning (VC):** VC scheme aims to generate compact content of the video by leveraging the encoded information from the video. This objective resembles the next token prediction scheme to pretrain text-only LLM. To implement this objective, we provide the LVLM with a video input and the prompt “*what does the video describe?*”, then train it to generate the groundtruth caption. For training data, we utilize 661K video-text pairs from 10M samples of the VIDAL-10M dataset (Zhu et al., 2023a).
- **Moment Captioning (MC):** Slightly different from VC, MC aims to caption only a specified part of the video. To implement this objective, we leverage the 745K samples from the InternVid dataset (Wang et al., 2023c), each of

Table 8.5: Effects of Temporal-Oriented Training Schemes on 7B-LVLM

Training Scheme	MSRVTT	MSVD	ActivityNet-QA	Breakfast	COIN	LVU
No temporal training	49.4	60.8	50.6	93.1	93.4	63.8
VC	50.3	61.5	51.0	93.2	93.7	64.4
MC	51.9	62.9	52.0	93.9	93.9	64.5
MG	50.9	62.3	51.4	93.3	93.9	64.6
DC	53.1	64.3	51.2	93.5	93.6	64.1
VC + MC + MG + DC	<b>54.5</b>	<b>66.4</b>	<b>52.4</b>	<b>93.7</b>	<b>94.1</b>	<b>65.5</b>

Table 8.6: Effects of Temporal-Oriented Training Schemes on 13B-LVLM

Training Scheme	MSRVTT	MSVD	ActivityNet-QA	Breakfast	COIN	LVU
No temporal training	60.6	74.3	52.5	93.7	93.2	71.8
VC	62.0	74.8	53.9	94.0	93.6	72.5
MC	61.2	74.6	53.0	93.5	93.9	71.9
MG	61.8	74.6	53.4	93.6	93.5	72.1
DC	62.2	75.3	54.3	94.7	94.0	72.7
VC + MC + MG + DC	<b>62.7</b>	<b>75.8</b>	<b>54.5</b>	<b>95.1</b>	<b>94.7</b>	<b>72.8</b>

which consists of a query and the specific starting and ending timestamps of the related moment in the video. Based on these timestamps, we convert them to discrete frame indices, then provide the model with the prompt “*Explain what happened from frame <start> to frame <end> in the video.*”

- **Moment Grounding (MG):** The MG task is the reverse variant of MC. Instead of training the model to write a caption, we let it generate the indices of the start and end frame index of the moment caption. Analogous to MC, we also employ the 745K samples from the InternVid dataset (Wang et al., 2023c).
- **Dense Captioning (DC):** This task is the more complete and fine-grained version of MC and VC, respectively. In particular, we ask the LVLM “*Can you give me a breakdown of the occurrences at different timestamps in the video?*”. As Table 8.7 shows, the model is expected to describe a list of moments with the respective frame indices related to the moment.

Based on the results presented in Table 8.5 and 8.6, we observe that all temporal-oriented training schemes enhance the temporal understanding capabilities of LVLMs. Notably, the 13B-LVLM shows a more pronounced improvement, particularly when trained with the aggregated scheme VC+MC+MG+DC. This indicates significant untapped potential for even larger LVLMs, especially those exceeding the 20B

Table 8.7: Examples of temporal-oriented training schemes.

Video	Training Scheme	Example prompt	Sample Expected Output
	VC	What does the video describe?	the buffalo bills new stadium is discussed as being deemed ineffective and not worth the investments made by the city and state.
	MC	Explain what happened from frame 1 to frame 4 in the video.	woman in long white dress walking up a hillside path.
	MG	During which frames in the video can we observe "woman in long white dress walking up a hillside path"?	from frame 1 to frame 4
	DC	Can you give me a breakdown of the occurrences at different timestamps in the video?	woman in long white dress walking up a hillside path, from 1 to 4. a woman sitting on the beach with long hair, from 5 to 8. [...]

Table 8.8: Effect of Memory Bank on 7B-LVLM

Memory Bank ( $B$ )	MSRVTT	MSVD	ActivityNet-QA	Breakfast	COIN	LVU
$B = 0$	54.5	66.4	51.4	93.7	94.1	65.5
$B = 10$	56.2	68.2	51.9	93.9	94.1	66.0
$B = 20$	60.7	72.5	52.5	94.3	94.7	68.1
$B = 30$	60.7	72.5	52.5	94.7	94.6	68.1
$B = 40$	60.7	72.6	52.5	94.9	94.8	68.2
$B = 50$	60.8	72.6	52.6	94.9	94.9	68.2
$B = 60$	<b>60.8</b>	<b>72.6</b>	<b>52.6</b>	<b>95.0</b>	<b>95.0</b>	<b>68.3</b>

Table 8.9: Effect of Memory Bank on 13B-LVLM

Memory Bank ( $B$ )	MSRVTT	MSVD	ActivityNet-QA	Breakfast	COIN	LVU
$B = 0$	62.7	75.8	54.5	95.1	94.7	72.8
$B = 10$	63.3	75.9	54.9	95.3	94.9	73.1
$B = 20$	63.5	76.3	55.2	96.0	95.0	73.4
$B = 30$	63.5	76.3	55.4	96.5	95.6	73.9
$B = 40$	<b>64.4</b>	<b>77.5</b>	<b>55.8</b>	<b>97.6</b>	<b>96.8</b>	<b>74.7</b>
$B = 50$	63.9	77.0	55.6	96.8	96.0	74.6
$B = 60$	63.5	76.5	55.5	96.7	96.0	74.3

parameter scale. Due to computational constraints, we leave the exploration of such large-scale models to future work.

*Takeaway 2: For the remaining experiments, we add an additional temporal-oriented training stage and use VC, MC, MG, and DC as training schemes.*

### Step 3: Memory Bank for Video Representations

Building upon the model developed in Step 2, we further investigate how the LVLM processes video inputs. A straightforward approach involves encoding visual frames or patches and concatenating their representations along the temporal axis. However, the limited context length limit of the LVLM, coupled with GPU memory constraints, restricts the number of video frames that can be processed simultaneously. An

alternative strategy is to apply temporal pooling (Maaz et al., 2023; Xu et al., 2024), but as demonstrated in our Step 1 analysis, this leads to suboptimal performance. Instead, we propose a different approach, *i.e.* processing video frames sequentially and storing their features in a memory bank. We conduct an ablation study on the size of the memory bank  $B \in \{10, 20, 30, 40, 50, 60\}$  and present our findings in Table 8.8 and 8.9.

Based on these results, we find that incorporating a memory bank is an effective strategy, consistently outperforming standard pooling methods. Randomly sampling a fixed number of frames also proves suboptimal, particularly for long-term temporal understanding, as the sampled frames might fail to capture critical video context. Lastly, we note that increasing the memory bank size yields more significant improvement for the 13B-LVLM than the 7B-LVLM. This indicates that larger-scale models possess greater capacity to absorb and utilize richer video information.

*Takeaway 3: For our remaining experiments, we add a memory bank for video encoding.*

## Step 4: Mixture-of-Experts for Q-Former

Building upon Step 3, we next explore strategies to enhance the capacity of the vision-language interface, which plays a critical role in conveying video information to the LLM. Given that naively adding randomly initialized layers tends to yield suboptimal performance—as demonstrated in Step 1—we turn to the mixture-of-experts (MoE) approach. An MoE module consists of a router and a set of experts, where each expert is a feedforward network. The router typically comprises a linear projection followed by a gating function, *e.g.* ReLU or Softmax, to compute the probabilities for routing a query token to specific experts. When a token encounters the MoE, the router selects a subset of experts to process the token, and their outputs are combined additively. This technique allows us to expand the parameter capacity of the Q-Former while keeping computational cost and latency manageable, as the model activates only a fraction of the total parameters for each token.

The exploration of MoE has remained scarce for LVLMs, especially for the vision-language interface, even though it has been investigated extensively in LLMs (Cai et al., 2024). In our work, we will experiment with the following categories of

Table 8.10: Effect of Mixture-of-Experts (MoE) on 7B-LVLM

Position of MoE	Type	Experts ( $E$ )	MSRVTT	MSVD	ActivityNet-QA	Breakfast	COIN	LVU
Q-Former	Sparse	2	63.9	76.9	56.3	95.6	95.4	72.9
		4	64.1	77.6	56.7	96.3	96.1	73.7
		8	<b>65.0</b>	<b>78.1</b>	<b>57.3</b>	<b>97.0</b>	<b>96.6</b>	<b>74.5</b>
	Dense	2	63.9	76.4	55.7	95.2	94.9	72.3
		4	64.4	76.8	56.6	96.0	95.8	73.0
		8	64.9	77.3	57.0	96.1	96.2	73.4
LLM	Sparse	2	54.9	72.9	55.4	93.4	92.0	72.5
		4	54.9	73.5	55.5	93.6	92.2	72.7
		8	55.4	73.6	55.9	93.6	92.5	72.8
	Dense	2	54.5	72.4	54.9	93.1	91.7	72.4
		4	54.8	72.7	55.2	93.4	91.8	72.6
		8	54.9	73.1	55.6	93.7	92.0	72.9

MoE:

- **Dense MoE:** the dense MoE activates all expert networks during each iteration. Based on the probability that the router produces for each expert, the outputs for an input token will be aggregated accordingly.
- **Sparse MoE:** to reduce computational overhead, we can activate only a subset of experts during each forward pass. To achieve this sparsity, we can compute a weighted sum of the expert outputs from only the top- $k$  experts, rather than combining the outputs from all experts. In our work, we experiment with top- $k$  where  $k = 1$  or  $k = 2$ .

For each type of MoE, we ablate the number of experts  $E \in \{2, 4, 8\}$ . In addition to Q-Former, we also add MoE to LLM to comprehensively study its effect on the LVLM.

Table 8.11: Effect of Mixture-of-Experts (MoE) on 13B-LVLM

Position of MoE	Type	Experts ( $E$ )	MSRVTT	MSVD	ActivityNet-QA	Breakfast	COIN	LVU
Q-Former	Sparse	2	65.2	78.4	57.2	97.6	97.5	75.5
		4	65.6	78.8	57.6	97.8	97.7	75.9
		8	<b>66.7</b>	<b>79.5</b>	<b>58.3</b>	<b>98.5</b>	<b>97.8</b>	<b>76.1</b>
	Dense	2	65.0	77.3	56.1	96.4	96.5	74.7
		4	65.5	77.7	56.8	96.6	96.8	74.9
		8	66.2	78.3	57.3	97.6	97.0	75.7
LLM	Sparse	2	59.3	73.3	53.4	91.9	92.9	69.1
		4	59.8	73.6	53.7	93.1	93.6	69.2
		8	60.2	73.7	54.1	93.2	94.2	69.6
	Dense	2	58.7	72.7	52.9	92.2	92.3	71.9
		4	59.0	72.9	53.0	92.3	92.5	70.0
		8	59.4	73.7	53.9	92.3	93.1	70.4

Based on the results in Table 8.10 and 8.11, we observe that integrating MoE into Q-Former leads to a substantial boost in video understanding performance. Moreover, we note that both sparse and dense MoE categories bring improvement, with sparse MoE being slightly more effective. We hypothesize that sparse MoE provides a higher degree of specialization for LVLM to handle specific types of temporal circumstances. Perhaps unsurprisingly, scaling up MoE with more experts puts more significant impact to the 13B-LVLM than the 7B-LVLM, which implies further potential for LVLM in the upscaling direction. On the other hand, adding MoE to LLM degrades the performance. This indicates that MoEs might tamper with the pre-trained knowledge in LLM.

*Final takeaway: Our final scaled-up temporal-oriented LVLM improves the initial LVLM baseline by 10.1% and 5.1% in terms of the 7B and 13B variant, respectively.*

## 8.3 Experimental Results

We validate our temporal-oriented recipe on two popular video understanding tasks, *i.e.* video question answering and video captioning. All of our experiments are conducted using 8 H100 GPUs.

**Video question answering.** We compare our results with existing methods on six datasets MSRVTT (Xu et al., 2016), MSVD (Chen and Dolan, 2011), ActivityNet-QA (Krishna et al., 2017), Breakfast (Kuehne et al., 2014), COIN (Tang et al., 2019), and LVU (Wu and Krahenbuhl, 2021) in Table 8.12. Our method substantially outperforms previous approaches on multiple datasets, achieving average accuracies of 66.7% (**+18.2%**), 79.5% (**+18.9%**), 58.3% (**+8.5%**), 98.5% (**+5.5%**), 97.8% (**+4.6%**), and 76.1% (**+13.1%**) on MSRVTT, MSVD, ActivityNet-QA, Breakfast, COIN, and LVU, respectively.

**Video captioning.** We present our results for the video captioning task on MSRVTT (Xu et al., 2016) and MSVD (Chen and Dolan, 2011). Our results indicate that we significantly improve upon previous works by a large margin. Particularly, we outperform existing methods by **20.8%** on MSRVTT and **21.0%** on MSVD.

Table 8.12: Comparison with existing methods on Video Question Answering (VideoQA) and Video Captioning tasks. The best results are in **bold**, and the second-best are underlined.

Method	VideoQA						Video Captioning	
	MSRVTT	MSVD	ActivityNet-QA	Breakfast	COIN	LVU	MSRVTT	MSVD
MA-LMM (He et al., 2024)	48.5	60.6	49.8	93.0	93.2	63.0	43.3	49.1
VALLEY (Luo et al., 2023)	50.8	69.2	44.9	83.8	84.0	56.8	39.0	44.3
LLaMA-VID (Li et al., 2024c)	58.9	70.0	47.5	88.7	88.9	60.1	41.3	46.8
VideoChat2 (Li et al., 2024b)	54.1	70.0	49.1	91.7	91.9	62.1	42.7	48.4
Video-ChatGPT (Maaz et al., 2023)	49.3	64.9	35.2	65.2	65.9	44.5	30.6	34.7
Video-LLaVA (Lin et al., 2023)	59.2	70.7	45.3	84.3	84.8	57.3	39.4	44.7
GPT4Video (Wang et al., 2024b)	49.8	66.3	48.7	90.9	91.1	61.6	42.3	48.0
7B-PLLaVA (Xu et al., 2024)	62.0	76.6	56.3	95.1	85.4	71.2	49.0	55.5
13B-PLLaVA (Xu et al., 2024)	63.2	75.7	56.3	95.4	86.7	72.9	49.5	58.6
ST-LLM (Liu et al., 2024a)	63.2	74.6	50.9	95.1	95.3	64.4	44.3	50.2
Chat-UniVi (Jin et al., 2024)	54.6	65.0	45.8	84.5	85.7	57.9	39.8	45.2
<b>7B-LVLM (Ours)</b>	<b>65.0</b>	<b>78.1</b>	<b>57.3</b>	<b>97.0</b>	<b>96.6</b>	<b>74.5</b>	<b>50.9</b>	<b>59.0</b>
<b>13B-LVLM (Ours)</b>	<b>66.7</b>	<b>79.5</b>	<b>58.3</b>	<b>98.5</b>	<b>97.8</b>	<b>76.1</b>	<b>52.3</b>	<b>59.4</b>

## 8.4 Summary

In this work, we highlight the critical role of temporal modeling in the design of modern Large Vision-Language Models (LVLMs). Throughout extensive investigation, we discover that key components, including query transformer (Q-Former), temporal-oriented training schemes, memory bank, and MoE augmentation for Q-Former, are pivotal for effective video understanding with LVLMs. Our empirical findings culminate in a step-by-step, temporal-oriented recipe for constructing effective temporal modeling capacity in LVLM. Compared with existing LVLMs, our proposed approach achieves superior performance across a broad range of standard video understanding datasets. Notably, the benefits of our recipe become more pronounced for larger-scale LVLMs, underscoring the potential of explicitly incorporating temporal modeling into large-scale architectures.

# Chapter 9

## Conclusion

This chapter concludes the thesis and provides a retrospective summary of the proposed contributions. In this thesis, we investigate temporal perspectives to advance a series of video understanding tasks, including video question answering, text-video retrieval, temporal grounding, and temporal panoptic scene graph generation. With respect to these perspectives, we propose novel building blocks and training frameworks for pushing the model limit, along with achieving effective and efficient capture of temporal relations within videos. Last but not least, we proceed to elaborate possible future research directions.

### 9.1 Overall Summary

Video understanding plays an important role in many application domains, spanning from entertainment to security areas. Nevertheless, there has not been a full-fledged effort to comprehensively investigate model architecture, training strategy, and data aspects of video understanding. Therefore, **Chapter 2** constructs a multi-faceted literature review to connect aspects of video understanding. Particularly, we summarize the key tasks and discuss common challenges, *i.e.* intra-modal and cross-modal interaction, cross-domain adaptation, and data preparation. Then, we construct a lucid taxonomy to categorize existing works from three perspectives according to the three discussed challenges: model architecture, model training, and data perspective.

Based on the insights from our literature review, we recognize the existing limit of the field, and proceed to push the limit by automatically annotating a vast set of videos in **Chapter 3**. Our framework encompasses a dynamic regularization

strategy to control model attention during training, thus mitigating the noisy effect of automatically annotated samples. We outperform previous state-of-the-art methods on standard video question answering and text-video retrieval benchmarks.

Despite the effectiveness of our automatic annotating framework, in practice it might still be infeasible to obtain large-scale video training data, *e.g.* in security- or privacy-sensitive domains. Hence, there is a need to devise an efficient training strategy to work productively in such low-resource scenarios. As such, **Chapter 4** introduces lightweight adapters with incorporated recurrent computation layers and only update them during fine-tuning. Through the use of video-language alignment objective, we motivate task-related information to flow through our adapter modules. Our framework significantly outperforms existing fine-tuning strategies on temporal grounding and video summarization tasks in low-resource settings.

Then **Chapter 5** studies and presents three temporal inductive biases for video understanding, *i.e.* global video semantics, motion-aware contrastive learning, and multi-scale contrastive learning. We show that global semantics over densely sampled video frames brings about significant benefits to long-term video question answering, which has recently suffered from information loss due to downsampling video frames to adapt to high computational cost. In addition to global semantics, **Chapter 6** and **Chapter 7** demonstrate interrelated semantics among video elements, invoked by motion-aware and multi-scale contrastive learning, can advance temporal expressiveness in video representations.

Finally, **Chapter 8** conduct an encyclopedic empirical study to demystify essential components for temporal understanding in large vision-language models (LVLMs). We discover that the vision-language interface that bridges visual encoder and large language model plays a fundamental role in encoding temporal inductive biases in LVLMs. Building on this insight, we propose a temporal-oriented recipe to progressively expand an LVLM through four key steps: (i) choosing a QueryFormer architecture for the vision-language interface, (ii) add temporal-oriented training schemes, (iii) integrate temporal memory bank, and (iv) inject mixtures-of-experts to upscale the interface. We contend that our recipe substantially advances a model to achieve impressive performance on various video understanding benchmarks.

## 9.2 Future Directions and Challenges

This section provides several promising future directions that extend the contributions of this thesis. Each direction is motivated by the overarching objective of advancing video understanding through more efficient (RO1), effective (RO2), and capacity-enhancing (RO3) approaches to capturing temporal relations. While there might be no principled solution to any of the following, many of these future directions remain as interesting goal posts for AI research in video understanding.

### 9.2.1 Streaming Video Understanding (RO1, RO2)

Most prior studies assume an offline setting, where the model has full access to a video. Streaming video understanding introduces unique challenges, *i.e.* models must operate without access to future frames, make predictions in real-time, and adapt to dynamically arriving information. This setting directly tests a model’s efficiency (RO1) and effectiveness (RO2) in capturing temporal relations under resource and time constraints. Recent works have started pushing boundaries of video understanding in this streaming setting (Qian et al., 2024; Chen et al., 2024a), but further advances are necessary to achieve robust, real-time temporal reasoning in practice.

### 9.2.2 Multi-Video Reasoning and Understanding (RO2, RO3)

While current video understanding systems typically operate on single video inputs, many real-world scenarios demand reasoning across videos (Panda et al., 2017). Extending temporal-oriented inductive biases to this setting could enable models to infer relations among movie episodes, cross-video narratives, or complementary sources of evidence. Although multi-scale contrastive learning already acknowledges relations among video clips, there remains significant potential for improvement, particularly when scaling to longer or interdependent clips. Specialized modules and training strategies for multi-video reasoning represent an open challenge with growing interest (Messaoud et al., 2021; Ansari and Zafar, 2023; Zhu et al., 2024).

### 9.2.3 Probing Models for Temporal Understanding (RO3)

A key challenge in advancing video understanding lies in interpretability. Current video models remain opaque, leaving open questions about how they infer temporal relationships between objects, actions, and events. Developing probing tools to reveal whether models form coherent chronologies or align with human-like temporal intuition might be crucial for uncovering temporal reasoning capabilities of future models. Further progress will not only improve trustworthiness in safety-critical applications but also guide the design of models that can faithfully capture complex temporal dependencies.

### 9.2.4 Cost-Accuracy Tradeoff for Video Understanding (RO1)

Deploying video understanding models in resource-constrained environments raises the issue of balancing performance with computational cost. Models shall remain efficient enough to meet real-time demands without sacrificing accuracy. There is always a need to advance RO1, or to discover better Pareto frontier for cost-accuracy tradeoff of video understanding models. This entails designing parameter-efficient modules, leveraging dynamic inference, and rethinking training strategies to optimize both computational and temporal understanding capabilities.

## 9.3 Reflections

This thesis is the culmination of rigorous research, from constructive brainstorming to meticulous experimental design. Throughout this journey, I have learned countless lessons. Here, I would like to reflect on the most memorable insights in the hope that they can guide and inspire future researchers.

### 9.3.1 Choosing a Steady Research Direction is Important

First, I want to emphasize the value of choosing a steady research direction to pursue. As more researchers enter the field and powerful large language models (LLMs) lower the barrier to publication, the publication task has become significantly less difficult than in the past. One interesting observation is the total number of submissions grows each year but the acceptance rate has remained stable. Consequently, more

papers are accepted into top conferences. While finding the “*right*” topic can indeed lead to a successful submission, this short-term strategy often yields a portfolio of disparate and shallow papers. Such breadth may sustain one’s career in the near term, but it prevents the emergence of a signature research identity.

Thanks to my supervisor’s guidance, I have learned this lesson during my PhD. Although I developed a knack for identifying promising problems, I struggled to commit to a single, unifying theme. One of the reasons is my research domain, *i.e.* video understanding, spans various subareas that one can easily find a straightforward but not fundamental problem to solve. Eventually, I recognized temporal relations—what truly distinguish video from images—remained underexplored. By focusing on modeling these relations, I found a coherent thread that has guided my works and underpins robust video-understanding systems.

Based on my experience, I recommend that anyone serious about research invest time up front to fine a lasting, focused direction. This direction not only prevents one from drifting between unrelated projects, but also forms a cohesive system of contributions which promote their impact to the community.

### **9.3.2 Scalability is important but we still need principled research**

Second, I would like to highlight a contentious trait of deep learning models, *i.e.* scalability. Recently, deep learning models have achieved impressive performance with their increased model size or dataset scale (Hestness et al., 2017; Hoffmann et al., 2022). However, not all of the scholars are attentive towards scalability-oriented research whose aim is to investigate effective methods to scale up model or data to push the performance boundary. Partly, this reflects a disparity in compute resources between industry and academic labs (Togelius and Yannakakis, 2023), which limits many researchers’ ability to train larger models. Additionally, some scholars regard scalability as self-evident: if we enlarge the model or data, the performance will automatically follow, so they prefer to investigate more subtle, foundational principles of deep learning.

From my side and based on my experience, I would like not to defend or argue against either of these views. Indeed, Chapter 3 and Chapter 8 demonstrate that at

least for video understanding, naive scaling often falls short. Particularly, Chapter 3 shows how automatic data-scaling frameworks can introduce noise and degrade learning. To counteract this, I propose a subtractive angular margin contrastive learning approach, which we prove theoretically provides a regularizing effect that mitigates noisy effects. Overall, I believe future research should continue exploring scale while simultaneously developing principled methods to resolve fundamental weaknesses of upscaled frameworks.

### **9.3.3 Academia versus Industry: Does Industry have more resources than Academia in all cases?**

Finally, I would like to share some reflections on the differences between academia and industry. It is often said that the distinction between the two mirrors the gap between theory and practice. I believe that this distinction is multi-faceted, and different people from different fields can experience this in different ways.

In recent years, tech heavyweights have grown immensely influential, aided by sophisticated marketing strategies that promote the perception of a significant resource gap between academic and industry research. These narrative often suggest that industry labs operate with minimal constraints. However, this is a misconception. In reality, industry also faces its own set of limitations.

For example, cost is a persistent constraint in most companies. Unless you are a tech giant like OpenAI or Google, or a startup backed by a wealthy and generous angel investor, minimizing operational expenses is essential for long-term sustainability. In fact, even large companies are mindful of costs. It is said one team at Google runs a weekly cron job to track infrastructure spending per employee, ranks the results, and emails the top spenders weekly as a cost-awareness measure. During my time in industry, I also had to adapt to various constraints. On one occasion, I developed a clustering algorithm to re-identify individuals by comparing new inputs to a database. However, when the deployment phase began, we discovered that the backend team’s database library lacked support for the optimization algorithms my algorithm required. As a result, we had to fall back on a simpler approach based on naive vector similarity and thresholding. Experiences like these illustrate that industry is not exempt from limitations—they simply operate under a different set

of them.

Now, I hope that it is clear both industry and academia operate under constraints. What I suggest that is we, as researchers, make a more conscious effort to identify and communicate these constraints early in the project lifecycle or during discussions. In university settings, I often notice an emphasis on ideas and contributions, with relatively less attention paid to practical considerations—such as available GPUs, storage capacity, or whether a proposed method can be implemented or published before a deadline. In this regard, I am especially grateful to Prof. See-Kiong and Prof. Anh Tuan, who have always been transparent about the resource status of their labs, including GPU acquisition plans and infrastructure updates. Such openness helps set realistic expectations and guides the direction of research more effectively.

Understanding constraints is crucial because they shape our mental models of what is feasible. They also help prevent misaligned assumptions—whether between students and supervisors, or between principal investigators and funding agencies. In fact, by being acutely aware of the data constraints in video understanding, I was able to propose the Meta-optimized Angular MArgin framework in Chapter 3 to elevate the data scale, and the recurrent adapter in Chapter 4 tailored for low-resource video understanding.

In conclusion, I recommend that future research discussions include a more deliberate and structured conversation about constraints and feasibility. Doing so will foster more grounded, efficient, and collaborative research practices.

# Bibliography

Moloud Abdar, Meenakshi Kollati, Swaraja Kuraparthi, Farhad Pourpanah, Daniel McDuff, Mohammad Ghavamzadeh, Shuicheng Yan, Abdullaah Mohamed, Abbas Khosravi, Erik Cambria, et al. 2024. A review of deep learning for video captioning. *IEEE Transactions on Pattern Analysis and Machine Intelligence*.

Sami Abu-El-Haija, Nisarg Kothari, Joonseok Lee, Paul Natsev, George Toderici, Balakrishnan Varadarajan, and Sudheendra Vijayanarasimhan. 2016. YouTube-8M: A Large-Scale Video Classification Benchmark. *arXiv preprint arXiv:1609.08675*.

Josh Achiam, Steven Adler, Sandhini Agarwal, Lama Ahmad, Ilge Akkaya, Florencia Leoni Aleman, Diogo Almeida, Janko Altenschmidt, Sam Altman, Shyamal Anadkat, et al. 2023. Gpt-4 technical report. *arXiv preprint arXiv:2303.08774*.

Hassan Akbari, Liangzhe Yuan, Rui Qian, Wei-Hong Chuang, Shih-Fu Chang, Yin Cui, and Boqing Gong. 2021. Vatt: Transformers for multimodal self-supervised learning from raw video, audio and text. *Advances in Neural Information Processing Systems*, 34:24206–24221.

Jean-Baptiste Alayrac, Jeff Donahue, Pauline Luc, Antoine Miech, Iain Barr, Yana Hasson, Karel Lenc, Arthur Mensch, Katherine Millican, Malcolm Reynolds, et al. 2022. Flamingo: a visual language model for few-shot learning. *Advances in neural information processing systems*, 35:23716–23736.

Xiang An, Jiankang Deng, Kaicheng Yang, Jaiwei Li, Ziyong Feng, Jia Guo, Jing Yang, and Tongliang Liu. 2023. Unicom: Universal and compact representation learning for image retrieval. *arXiv preprint arXiv:2304.05884*.

Lisa Anne Hendricks, Oliver Wang, Eli Shechtman, Josef Sivic, Trevor Darrell, and Bryan Russell. 2017. Localizing moments in video with natural language. In *Proceedings of the IEEE international conference on computer vision*, pages 5803–5812.

## BIBLIOGRAPHY

Shaharyar Alam Ansari and Aasim Zafar. 2023. Multi video summarization using query based deep optimization algorithm. *International Journal of Machine Learning and Cybernetics*, 14(10):3591–3606.

Evlampios Apostolidis, Eleni Adamantidou, Alexandros I Metsai, Vasileios Mezaris, and Ioannis Patras. 2021. Video summarization using deep neural networks: A survey. *Proceedings of the IEEE*, 109(11):1838–1863.

Anurag Arnab, Mostafa Dehghani, Georg Heigold, Chen Sun, Mario Lučić, and Cordelia Schmid. 2021. Vivit: A video vision transformer. In *Proceedings of the IEEE/CVF international conference on computer vision*, pages 6836–6846.

Max Bain, Arsha Nagrani, Gül Varol, and Andrew Zisserman. 2021. Frozen in time: A joint video and image encoder for end-to-end retrieval. In *Proceedings of the IEEE/CVF International Conference on Computer Vision*, pages 1728–1738.

Max Bain, Arsha Nagrani, Gül Varol, and Andrew Zisserman. 2022. A clip-hitchhiker’s guide to long video retrieval. *arXiv preprint arXiv:2205.08508*.

Siddhant Bansal, Chetan Arora, and CV Jawahar. 2022. My view is the best view: Procedure learning from egocentric videos. In *European Conference on Computer Vision*, pages 657–675. Springer.

Lorenzo Baraldi, Costantino Grana, and Rita Cucchiara. 2017. Hierarchical boundary-aware neural encoder for video captioning. In *Proceedings of the IEEE conference on computer vision and pattern recognition*, pages 1657–1666.

Yi Bin, Yang Yang, Chaofan Tao, Zi Huang, Jingjing Li, and Heng Tao Shen. 2019. Mr-net: Exploiting mutual relation for visual relationship detection. In *Proceedings of the AAAI Conference on Artificial Intelligence*, volume 33, pages 8110–8117.

Navaneeth Bodla, Bharat Singh, Rama Chellappa, and Larry S Davis. 2017. Soft-nms–improving object detection with one line of code. In *Proceedings of the IEEE international conference on computer vision*, pages 5561–5569.

Hugo Boulanger, Thomas Lavergne, and Sophie Rosset. 2022. Generating unlabelled data for a tri-training approach in a low resourced ner task. In *Third Workshop*

on Deep Learning for Low-Resource Natural Language Processing, pages 30–37. Association for Computational Linguistics.

Shyamal Buch, Cristóbal Eyzaguirre, Adrien Gaidon, Jiajun Wu, Li Fei-Fei, and Juan Carlos Niebles. 2022. Revisiting the "video" in video-language understanding. In *Proceedings of the IEEE/CVF conference on computer vision and pattern recognition*, pages 2917–2927.

Jessica Burgner-Kahrs, D Caleb Rucker, and Howie Choset. 2015. Continuum robots for medical applications: A survey. *IEEE Transactions on Robotics*, 31(6):1261–1280.

Fabian Caba Heilbron, Victor Escorcia, Bernard Ghanem, and Juan Carlos Niebles. 2015. Activitynet: A large-scale video benchmark for human activity understanding. In *Proceedings of the ieee conference on computer vision and pattern recognition*, pages 961–970.

Weilin Cai, Juyong Jiang, Fan Wang, Jing Tang, Sunghun Kim, and Jiayi Huang. 2024. A survey on mixture of experts. *arXiv preprint arXiv:2407.06204*.

Joao Carreira, Eric Noland, Andras Banki-Horvath, Chloe Hillier, and Andrew Zisserman. 2018. A short note about kinetics-600. *arXiv preprint arXiv:1808.01340*.

Joao Carreira, Eric Noland, Chloe Hillier, and Andrew Zisserman. 2019. A short note on the kinetics-700 human action dataset. *arXiv preprint arXiv:1907.06987*.

Joao Carreira and Andrew Zisserman. 2017. Quo vadis, action recognition? a new model and the kinetics dataset. In *proceedings of the IEEE Conference on Computer Vision and Pattern Recognition*, pages 6299–6308.

Santiago Castro, Naihao Deng, Pingxuan Huang, Mihai Burzo, and Rada Mihalcea. 2022a. In-the-wild video question answering. In *Proceedings of the 29th International Conference on Computational Linguistics*, pages 5613–5635.

Santiago Castro, Ruoyao Wang, Pingxuan Huang, Ian Stewart, Oana Ignat, Nan Liu, Jonathan Stroud, and Rada Mihalcea. 2022b. Fiber: Fill-in-the-blanks as a challenging video understanding evaluation framework. In *Proceedings of the*

## BIBLIOGRAPHY

*60th Annual Meeting of the Association for Computational Linguistics (Volume 1: Long Papers)*, pages 2925–2940.

Keshigeyan Chandrasegaran, Agrim Gupta, Lea M Hadzic, Taran Kota, Jimming He, Cristóbal Eyzaguirre, Zane Durante, Manling Li, Jiajun Wu, and Fei-Fei Li. 2024. Hourvideo: 1-hour video-language understanding. *Advances in Neural Information Processing Systems*, 37:53168–53197.

Laetitia Chapel, Mokhtar Z Alaya, and Gilles Gasso. 2020. Partial optimal transport with applications on positive-unlabeled learning. *Advances in Neural Information Processing Systems*, 33:2903–2913.

David Chen and William B Dolan. 2011. Collecting highly parallel data for paraphrase evaluation. In *Proceedings of the 49th annual meeting of the association for computational linguistics: human language technologies*, pages 190–200.

Guo Chen, Yin-Dong Zheng, Jiahao Wang, Jilan Xu, Yifei Huang, Junting Pan, Yi Wang, Yali Wang, Yu Qiao, Tong Lu, et al. 2023. Videollm: Modeling video sequence with large language models. *arXiv preprint arXiv:2305.13292*.

Joya Chen, Zhaoyang Lv, Shiwei Wu, Kevin Qinghong Lin, Chenan Song, Difei Gao, Jia-Wei Liu, Ziteng Gao, Dongxing Mao, and Mike Zheng Shou. 2024a. Videollm-online: Online video large language model for streaming video. In *Proceedings of the IEEE/CVF Conference on Computer Vision and Pattern Recognition*, pages 18407–18418.

Shoufa Chen, Chongjian Ge, Zhan Tong, Jiangliu Wang, Yibing Song, Jue Wang, and Ping Luo. 2022. Adaptformer: Adapting vision transformers for scalable visual recognition. *Advances in Neural Information Processing Systems*, 35:16664–16678.

Yuting Chen, Joseph Wang, Yannan Bai, Gregory Castañón, and Venkatesh Saligrama. 2018. Probabilistic semantic retrieval for surveillance videos with activity graphs. *IEEE Transactions on Multimedia*, 21(3):704–716.

Yuxin Chen, Gaoqun Ma, Chunfeng Yuan, Bing Li, Hui Zhang, Fangshi Wang, and Weiming Hu. 2020. Graph convolutional network with structure pooling

and joint-wise channel attention for action recognition. *Pattern Recognition*, 103:107321.

Ziyue Chen, Tongya Zheng, and Mingli Song. 2024b. Curriculum negative mining for temporal networks. *arXiv preprint arXiv:2407.17070*.

Bowen Cheng, Ishan Misra, Alexander G Schwing, Alexander Kirillov, and Rohit Girdhar. 2022. Masked-attention mask transformer for universal image segmentation. In *Proceedings of the IEEE/CVF conference on computer vision and pattern recognition*, pages 1290–1299.

Feng Cheng, Xizi Wang, Jie Lei, David Crandall, Mohit Bansal, and Gedas Bertasius. 2023. Vindlu: A recipe for effective video-and-language pretraining. In *Proceedings of the IEEE/CVF Conference on Computer Vision and Pattern Recognition*, pages 10739–10750.

Wei-Lin Chiang, Zhuohan Li, Ziqing Lin, Ying Sheng, Zhanghao Wu, Hao Zhang, Lianmin Zheng, Siyuan Zhuang, Yonghao Zhuang, Joseph E Gonzalez, et al. 2023. Vicuna: An open-source chatbot impressing gpt-4 with 90%\* chatgpt quality. *See <https://vicuna.lmsys.org> (accessed 14 April 2023)*, 2(3):6.

Kyunghyun Cho, Bart Van Merriënboer, Caglar Gulcehre, Dzmitry Bahdanau, Fethi Bougares, Holger Schwenk, and Yoshua Bengio. 2014. Learning phrase representations using rnn encoder-decoder for statistical machine translation. *arXiv preprint arXiv:1406.1078*.

Laurene Claussmann, Marc Revilloud, Dominique Gruyer, and Sébastien Glaser. 2019. A review of motion planning for highway autonomous driving. *IEEE Transactions on Intelligent Transportation Systems*, 21(5):1826–1848.

James W Cooley and John W Tukey. 1965. An algorithm for the machine calculation of complex fourier series. *Mathematics of computation*, 19(90):297–301.

Balázs Csanad Csaji et al. 2001. Approximation with artificial neural networks. *Faculty of Sciences, Etvs Lornd University, Hungary*, 24(48):7.

## BIBLIOGRAPHY

W Dai, J Li, D Li, AMH Tiong, J Zhao, W Wang, B Li, P Fung, and S Hoi. Instructblip: Towards general-purpose vision-language models with instruction tuning. arxiv 2023. *arXiv preprint arXiv:2305.06500*.

Dima Damen, Hazel Doughty, Giovanni Maria Farinella, Antonino Furnari, Evangelos Kazakos, Jian Ma, Davide Moltisanti, Jonathan Munro, Toby Perrett, Will Price, et al. 2022a. Epic-kitchens-100. *International Journal of Computer Vision*, 130:33–55.

Dima Damen, Hazel Doughty, Giovanni Maria Farinella, Antonino Furnari, Evangelos Kazakos, Jian Ma, Davide Moltisanti, Jonathan Munro, Toby Perrett, Will Price, et al. 2022b. Rescaling egocentric vision: Collection, pipeline and challenges for epic-kitchens-100. *International Journal of Computer Vision*, pages 1–23.

Jacob Devlin, Ming-Wei Chang, Kenton Lee, and Kristina Toutanova. 2018. Bert: Pre-training of deep bidirectional transformers for language understanding. *arXiv preprint arXiv:1810.04805*.

Zihan Ding, Tianrui Hui, Junshi Huang, Xiaoming Wei, Jizhong Han, and Si Liu. 2022. Language-bridged spatial-temporal interaction for referring video object segmentation. In *Proceedings of the IEEE/CVF Conference on Computer Vision and Pattern Recognition*, pages 4964–4973.

Alexey Dosovitskiy, Lucas Beyer, Alexander Kolesnikov, Dirk Weissenborn, Xiaohua Zhai, Thomas Unterthiner, Mostafa Dehghani, Matthias Minderer, Georg Heigold, Sylvain Gelly, et al. 2020. An image is worth 16x16 words: Transformers for image recognition at scale. *arXiv preprint arXiv:2010.11929*.

Zi-Yi Dou, Yichong Xu, Zhe Gan, Jianfeng Wang, Shuohang Wang, Lijuan Wang, Chenguang Zhu, Pengchuan Zhang, Lu Yuan, Nanyun Peng, et al. 2022. An empirical study of training end-to-end vision-and-language transformers. In *Proceedings of the IEEE/CVF Conference on Computer Vision and Pattern Recognition*, pages 18166–18176.

Danny Driess, Fei Xia, Mehdi SM Sajjadi, Corey Lynch, Aakanksha Chowdhery, Brian Ichter, Ayzaan Wahid, Jonathan Tompson, Quan Vuong, Tianhe Yu,

et al. 2023. Palm-e: An embodied multimodal language model. *arXiv preprint arXiv:2303.03378*.

Chenyou Fan, Xiaofan Zhang, Shu Zhang, et al. 2019. Heterogeneous memory enhanced multimodal attention model for video question answering. In *Proceedings of the IEEE Conference on Computer Vision and Pattern Recognition*, pages 1999–2007.

Yuxin Fang, Wen Wang, Binhui Xie, Quan Sun, Ledell Wu, Xinggang Wang, Tiejun Huang, Xinlong Wang, and Yue Cao. 2023. Eva: Exploring the limits of masked visual representation learning at scale. In *Proceedings of the IEEE/CVF Conference on Computer Vision and Pattern Recognition*, pages 19358–19369.

Li Fei-Fei and Ranjay Krishna. 2022. Searching for computer vision north stars. *Journal of the American Academy of Arts & Sciences*, page 85.

Christoph Feichtenhofer, Haoqi Fan, Jitendra Malik, and Kaiming He. 2019. Slowfast networks for video recognition. In *Proceedings of the IEEE/CVF international conference on computer vision*, pages 6202–6211.

Christoph Feichtenhofer, Axel Pinz, and Andrew Zisserman. 2016. Convolutional Two-Stream Network Fusion for Video Action Recognition. In *The IEEE Conference on Computer Vision and Pattern Recognition (CVPR)*.

Tsu-Jui Fu, Linjie Li, Zhe Gan, Kevin Lin, William Yang Wang, Lijuan Wang, and Zicheng Liu. 2021. Violet: End-to-end video-language transformers with masked visual-token modeling. *arXiv preprint arXiv:2111.12681*.

Tsu-Jui Fu, Linjie Li, Zhe Gan, Kevin Lin, William Yang Wang, Lijuan Wang, and Zicheng Liu. 2023. An empirical study of end-to-end video-language transformers with masked visual modeling. In *Proceedings of the IEEE/CVF Conference on Computer Vision and Pattern Recognition*, pages 22898–22909.

Mona Gandhi, Mustafa Omer Gul, Eva Prakash, Madeleine Grunde-McLaughlin, Ranjay Krishna, and Maneesh Agrawala. 2022. Measuring compositional consistency for video question answering. In *Proceedings of the IEEE/CVF Conference on Computer Vision and Pattern Recognition*.

## BIBLIOGRAPHY

Difei Gao, Ruiping Wang, Ziyi Bai, and Xilin Chen. 2021a. Env-qa: A video question answering benchmark for comprehensive understanding of dynamic environments. In *Proceedings of the IEEE/CVF International Conference on Computer Vision*, pages 1675–1685.

Difei Gao, Luwei Zhou, Lei Ji, Linchao Zhu, Yi Yang, and Mike Zheng Shou. 2023. Mist: Multi-modal iterative spatial-temporal transformer for long-form video question answering. In *Proceedings of the IEEE/CVF Conference on Computer Vision and Pattern Recognition*, pages 14773–14783.

Jiayang Gao, Chen Sun, Zhenheng Yang, and Ram Nevatia. 2017. Tall: Temporal activity localization via language query. In *Proceedings of the IEEE international conference on computer vision*, pages 5267–5275.

Zijian Gao, Jingyu Liu, Weiqi Sun, Sheng Chen, Dedan Chang, and Lili Zhao. 2021b. Clip2tv: Align, match and distill for video-text retrieval. *arXiv preprint arXiv:2111.05610*.

Paul Gay, James Stuart, and Alessio Del Bue. 2019. Visual graphs from motion (vgfm): Scene understanding with object geometry reasoning. In *Computer Vision–ACCV 2018: 14th Asian Conference on Computer Vision, Perth, Australia, December 2–6, 2018, Revised Selected Papers, Part III 14*, pages 330–346. Springer.

Ian Goodfellow, Yoshua Bengio, and Aaron Courville. 2016. *Deep learning*. MIT press.

Raghav Goyal, Samira Ebrahimi Kahou, Vincent Michalski, Joanna Materzynska, Susanne Westphal, Heuna Kim, Valentin Haenel, Ingo Fruend, Peter Yianilos, Moritz Mueller-Freitag, et al. 2017. The " Something Something" Video Database for Learning and Evaluating Visual Common Sense. In *The IEEE International Conference on Computer Vision (ICCV)*.

Kristen Grauman, Andrew Westbury, Eugene Byrne, Zachary Chavis, Antonino Furnari, Rohit Girdhar, Jackson Hamburger, Hao Jiang, Miao Liu, Xingyu Liu, et al. 2022. Ego4d: Around the world in 3,000 hours of egocentric video. In *Proceedings of the IEEE/CVF Conference on Computer Vision and Pattern Recognition*, pages 18995–19012.

## BIBLIOGRAPHY

Madeleine Grunde-McLaughlin, Ranjay Krishna, and Maneesh Agrawala. 2021. Agqa: A benchmark for compositional spatio-temporal reasoning. In *Proceedings of the IEEE/CVF Conference on Computer Vision and Pattern Recognition*, pages 11287–11297.

Albert Gu, Karan Goel, and Christopher Ré. 2021. Efficiently modeling long sequences with structured state spaces. *arXiv preprint arXiv:2111.00396*.

Chaoxu Guo, Bin Fan, Qian Zhang, Shiming Xiang, and Chunhong Pan. 2020. Augfpn: Improving multi-scale feature learning for object detection. In *Proceedings of the IEEE/CVF conference on computer vision and pattern recognition*, pages 12595–12604.

Ankit Gupta, Albert Gu, and Jonathan Berant. 2022. Diagonal state spaces are as effective as structured state spaces. *Advances in Neural Information Processing Systems*, 35:22982–22994.

De Han, Xing Cheng, Nan Guo, Xiaochun Ye, Benjamin Rainer, and Peter Priller. 2023. Momentum cross-modal contrastive learning for video moment retrieval. *IEEE Transactions on Circuits and Systems for Video Technology*.

Tengda Han, Weidi Xie, and Andrew Zisserman. 2022. Temporal alignment networks for long-term video. In *Proceedings of the IEEE/CVF Conference on Computer Vision and Pattern Recognition*, pages 2906–2916.

Wei Han, Hui Chen, and Soujanya Poria. 2021. Improving multimodal fusion with hierarchical mutual information maximization for multimodal sentiment analysis. *arXiv preprint arXiv:2109.00412*.

Bo He, Hengduo Li, Young Kyun Jang, Menglin Jia, Xuefei Cao, Ashish Shah, Abhinav Shrivastava, and Ser-Nam Lim. 2024. Ma-lmm: Memory-augmented large multimodal model for long-term video understanding. In *Proceedings of the IEEE/CVF Conference on Computer Vision and Pattern Recognition*, pages 13504–13514.

Kaiming He, Xiangyu Zhang, Shaoqing Ren, and Jian Sun. 2015. Delving deep into rectifiers: Surpassing human-level performance on imagenet classification.

In *Proceedings of the IEEE international conference on computer vision*, pages 1026–1034.

Kaiming He, Xiangyu Zhang, Shaoqing Ren, and Jian Sun. 2016. Deep Residual Learning for Image Recognition. In *The IEEE Conference on Computer Vision and Pattern Recognition (CVPR)*.

Xingjian He, Sihan Chen, Fan Ma, Zhicheng Huang, Xiaojie Jin, Zikang Liu, Dongmei Fu, Yi Yang, Jing Liu, and Jiashi Feng. 2023. Vlab: Enhancing video language pre-training by feature adapting and blending. *arXiv preprint arXiv:2305.13167*.

Dan Hendrycks, Andy Zou, Mantas Mazeika, Leonard Tang, Bo Li, Dawn Song, and Jacob Steinhardt. 2022. Pixmix: Dreamlike pictures comprehensively improve safety measures. In *Proceedings of the IEEE/CVF Conference on Computer Vision and Pattern Recognition*, pages 16783–16792.

Joel Hestness, Sharan Narang, Newsha Ardalani, Gregory Diamos, Heewoo Jun, Hassan Kianinejad, Md Mostofa Ali Patwary, Yang Yang, and Yanqi Zhou. 2017. Deep learning scaling is predictable, empirically. *arXiv preprint arXiv:1712.00409*.

Sepp Hochreiter and Jürgen Schmidhuber. 1997. Long short-term memory. *Neural computation*, 9(8):1735–1780.

Jordan Hoffmann, Sebastian Borgeaud, Arthur Mensch, Elena Buchatskaya, Trevor Cai, Eliza Rutherford, Diego de Las Casas, Lisa Anne Hendricks, Johannes Welbl, Aidan Clark, et al. 2022. Training compute-optimal large language models. *arXiv preprint arXiv:2203.15556*.

Zhijian Hou, Wanjun Zhong, Lei Ji, Difei Gao, Kun Yan, Wing-Kwong Chan, Chong-Wah Ngo, Zheng Shou, and Nan Duan. 2022. Cone: An efficient coarse-to-fine alignment framework for long video temporal grounding. *arXiv preprint arXiv:2209.10918*.

Neil Houlsby, Andrei Giurgiu, Stanislaw Jastrzebski, Bruna Morrone, Quentin De Laroussilhe, Andrea Gesmundo, Mona Attariyan, and Sylvain Gelly. 2019. Parameter-efficient transfer learning for nlp. In *International Conference on Machine Learning*, pages 2790–2799. PMLR.

## BIBLIOGRAPHY

Edward J Hu, Yelong Shen, Phillip Wallis, Zeyuan Allen-Zhu, Yuanzhi Li, Shean Wang, Lu Wang, and Weizhu Chen. 2021. Lora: Low-rank adaptation of large language models. *arXiv preprint arXiv:2106.09685*.

Gabriel Huang, Bo Pang, Zhenhai Zhu, Clara Rivera, and Radu Soricut. 2020. Multimodal pretraining for dense video captioning. *arXiv preprint arXiv:2011.11760*.

Siteng Huang, Biao Gong, Yulin Pan, Jianwen Jiang, Yiliang Lv, Yuyuan Li, and Donglin Wang. 2023. Vop: Text-video co-operative prompt tuning for cross-modal retrieval. In *Proceedings of the IEEE/CVF Conference on Computer Vision and Pattern Recognition*, pages 6565–6574.

Md Mohaiminul Islam, Ngan Ho, Xitong Yang, Tushar Nagarajan, Lorenzo Torresani, and Gedas Bertasius. 2024. Video recap: Recursive captioning of hour-long videos. In *Proceedings of the IEEE/CVF Conference on Computer Vision and Pattern Recognition*, pages 18198–18208.

Yunseok Jang, Yale Song, Chris Dongjoo Kim, Youngjae Yu, Youngjin Kim, and Gunhee Kim. 2019. Video question answering with spatio-temporal reasoning. *International Journal of Computer Vision*, 127(10):1385–1412.

Yunseok Jang, Yale Song, Youngjae Yu, Youngjin Kim, and Gunhee Kim. 2017. Tgif-qa: Toward spatio-temporal reasoning in visual question answering. In *Proceedings of the IEEE conference on computer vision and pattern recognition*, pages 2758–2766.

Wei Ji, Ruiqi Shi, Yinwei Wei, Shanshan Zhao, and Roger Zimmermann. 2024. Weakly supervised video moment retrieval via location-irrelevant proposal learning. In *Companion Proceedings of the ACM on Web Conference 2024*, pages 1595–1603.

Menglin Jia, Luming Tang, Bor-Chun Chen, Claire Cardie, Serge Belongie, Bharath Hariharan, and Ser-Nam Lim. 2022a. Visual prompt tuning. In *European Conference on Computer Vision*, pages 709–727. Springer.

Mohan Jia, Zhongjian Dai, Yaping Dai, and Zhiyang Jia. 2022b. An adversarial video moment retrieval algorithm. In *2022 41st Chinese Control Conference (CCC)*, pages 6689–6694. IEEE.

## BIBLIOGRAPHY

Haojun Jiang, Jianke Zhang, Rui Huang, Chunjiang Ge, Zanlin Ni, Jiwen Lu, Jie Zhou, Shiji Song, and Gao Huang. 2022a. Cross-modal adapter for text-video retrieval. *arXiv preprint arXiv:2211.09623*.

Ji Jiang, Meng Cao, Tengtao Song, and Yuexian Zou. 2022b. Video referring expression comprehension via transformer with content-aware query. *arXiv preprint arXiv:2210.02953*.

Jianwen Jiang, Ziqiang Chen, Haojie Lin, Xibin Zhao, and Yue Gao. 2020. Divide and conquer: Question-guided spatio-temporal contextual attention for video question answering. In *Proceedings of the AAAI Conference on Artificial Intelligence*, volume 34, pages 11101–11108.

Lu Jiang, Deyu Meng, Shou-I Yu, Zhenzhong Lan, Shiguang Shan, and Alexander Hauptmann. 2014. Self-paced learning with diversity. *Advances in neural information processing systems*, 27.

Pin Jiang and Yahong Han. 2020. Reasoning with heterogeneous graph alignment for video question answering. In *Proceedings of the AAAI Conference on Artificial Intelligence*, volume 34, pages 11109–11116.

Xun Jiang, Xing Xu, Jingran Zhang, Fumin Shen, Zuo Cao, and Heng Tao Shen. 2022c. Semi-supervised video paragraph grounding with contrastive encoder. In *Proceedings of the IEEE/CVF Conference on Computer Vision and Pattern Recognition*, pages 2466–2475.

Peng Jin, Jinfa Huang, Pengfei Xiong, Shangxuan Tian, Chang Liu, Xiangyang Ji, Li Yuan, and Jie Chen. 2023. Video-text as game players: Hierarchical banzhaf interaction for cross-modal representation learning. In *Proceedings of the IEEE/CVF Conference on Computer Vision and Pattern Recognition*, pages 2472–2482.

Peng Jin, Ryuichi Takanobu, Wancai Zhang, Xiaochun Cao, and Li Yuan. 2024. Chat-univ: Unified visual representation empowers large language models with image and video understanding. In *Proceedings of the IEEE/CVF Conference on Computer Vision and Pattern Recognition*, pages 13700–13710.

## BIBLIOGRAPHY

Chen Ju, Tengda Han, Kunhao Zheng, Ya Zhang, and Weidi Xie. 2022. Prompting visual-language models for efficient video understanding. In *European Conference on Computer Vision*, pages 105–124. Springer.

Minjoon Jung, Youwon Jang, Seongho Choi, Joochan Kim, Jin-Hwa Kim, and Byoung-Tak Zhang. 2023. Overcoming weak visual-textual alignment for video moment retrieval. *arXiv preprint arXiv:2306.02728*.

Jared Kaplan, Sam McCandlish, Tom Henighan, Tom B Brown, Benjamin Chess, Rewon Child, Scott Gray, Alec Radford, Jeffrey Wu, and Dario Amodei. 2020. Scaling laws for neural language models. *arXiv preprint arXiv:2001.08361*.

Dotan Kaufman, Gil Levi, Tal Hassner, and Lior Wolf. 2016. Temporal tessellation for video annotation and summarization. *arXiv preprint arXiv:1612.06950*, 3.

Will Kay, Joao Carreira, Karen Simonyan, Brian Zhang, Chloe Hillier, Sudheendra Vijayanarasimhan, Fabio Viola, Tim Green, Trevor Back, Paul Natsev, Mustafa Suleyman, and Andrew Zisserman. 2017a. The Kinetics Human Action Video Dataset. *arXiv preprint arXiv:1705.06950*.

Will Kay, Joao Carreira, Karen Simonyan, Brian Zhang, Chloe Hillier, Sudheendra Vijayanarasimhan, Fabio Viola, Tim Green, Trevor Back, Paul Natsev, et al. 2017b. The kinetics human action video dataset. *arXiv preprint arXiv:1705.06950*.

Ilker Keser, Andrea Pedrotti, Mustafa Dogan, Michele Cafagna, Emre Can Acikgoz, Letitia Parcalabescu, Iacer Calixto, Anette Frank, Albert Gatt, Aykut Erdem, et al. 2023. Vilma: A zero-shot benchmark for linguistic and temporal grounding in video-language models. *arXiv preprint arXiv:2311.07022*.

Taeoh Kim, Jinhyung Kim, Minho Shim, Sangdoo Yun, Myunggu Kang, Dongyoon Wee, and Sangyoun Lee. 2022. Exploring temporally dynamic data augmentation for video recognition. *arXiv preprint arXiv:2206.15015*.

Thomas N Kipf and Max Welling. 2016. Semi-supervised classification with graph convolutional networks. *arXiv preprint arXiv:1609.02907*.

## BIBLIOGRAPHY

Ryan Kiros, Ruslan Salakhutdinov, and Richard S Zemel. 2014. Unifying visual-semantic embeddings with multimodal neural language models. *arXiv preprint arXiv:1411.2539*.

Jing Yu Koh, Ruslan Salakhutdinov, and Daniel Fried. 2023. Grounding language models to images for multimodal inputs and outputs. In *International Conference on Machine Learning*, pages 17283–17300. PMLR.

Eric Kolve, Roozbeh Mottaghi, Winson Han, Eli VanderBilt, Luca Weihs, Alvaro Herrasti, Matt Deitke, Kiana Ehsani, Daniel Gordon, Yuke Zhu, et al. 2017. Ai2-thor: An interactive 3d environment for visual ai. *arXiv preprint arXiv:1712.05474*.

Ranjay Krishna, Kenji Hata, Frederic Ren, Li Fei-Fei, and Juan Carlos Niebles. 2017. Dense-captioning events in videos. In *Proceedings of the IEEE international conference on computer vision*, pages 706–715.

Hilde Kuehne, Ali Arslan, and Thomas Serre. 2014. The language of actions: Recovering the syntax and semantics of goal-directed human activities. In *Proceedings of the IEEE conference on computer vision and pattern recognition*, pages 780–787.

Hildegard Kuehne, Hueihan Jhuang, Estíbaliz Garrote, Tomaso Poggio, and Thomas Serre. 2011. HMDB: A Large Video Database for Human Motion Recognition. In *The IEEE International Conference on Computer Vision (ICCV)*.

Thao Minh Le, Vuong Le, Svetha Venkatesh, and Truyen Tran. 2020. Hierarchical conditional relation networks for video question answering. In *Proceedings of the IEEE/CVF conference on computer vision and pattern recognition*, pages 9972–9981.

Chenyi Lei, Shixian Luo, Yong Liu, Wanggui He, Jiamang Wang, Guoxin Wang, Haihong Tang, Chunyan Miao, and Houqiang Li. 2021a. Understanding chinese video and language via contrastive multimodal pre-training. In *Proceedings of the 29th ACM International Conference on Multimedia*, pages 2567–2576.

Jie Lei, Tamara L Berg, and Mohit Bansal. 2021b. Detecting moments and highlights in videos via natural language queries. *Advances in Neural Information Processing Systems*, 34:11846–11858.

## BIBLIOGRAPHY

Jie Lei, Tamara L Berg, and Mohit Bansal. 2022. Revealing single frame bias for video-and-language learning. *arXiv preprint arXiv:2206.03428*.

Jie Lei, Linjie Li, Luwei Zhou, Zhe Gan, Tamara L Berg, Mohit Bansal, and Jingjing Liu. 2021c. Less is more: Clipbert for video-and-language learning via sparse sampling. In *Proceedings of the IEEE/CVF conference on computer vision and pattern recognition*, pages 7331–7341.

Jie Lei, Licheng Yu, Mohit Bansal, and Tamara Berg. 2018. Tvqa: Localized, compositional video question answering. In *Proceedings of the 2018 Conference on Empirical Methods in Natural Language Processing*, pages 1369–1379.

Jie Lei, Licheng Yu, Tamara Berg, and Mohit Bansal. 2020a. Tvqa+: Spatio-temporal grounding for video question answering. In *Proceedings of the 58th Annual Meeting of the Association for Computational Linguistics*, pages 8211–8225.

Jie Lei, Licheng Yu, Tamara L Berg, and Mohit Bansal. 2020b. Tvr: A large-scale dataset for video-subtitle moment retrieval. In *Computer Vision–ECCV 2020: 16th European Conference, Glasgow, UK, August 23–28, 2020, Proceedings, Part XXI 16*, pages 447–463. Springer.

Stan Weixian Lei, Yuxuan Wang, Dongxing Mao, Difei Gao, and Mike Zheng Shou. 2021d. Assistsr: Affordance-centric question-driven video segment retrieval. *arXiv preprint*.

Mike Lewis, Yinhan Liu, Naman Goyal, Marjan Ghazvininejad, Abdelrahman Mohamed, Omer Levy, Veselin Stoyanov, and Luke Zettlemoyer. 2020. Bart: Denoising sequence-to-sequence pre-training for natural language generation, translation, and comprehension. In *Proceedings of the 58th Annual Meeting of the Association for Computational Linguistics*, pages 7871–7880.

Bolian Li, Zongbo Han, Haining Li, Huazhu Fu, and Changqing Zhang. 2022a. Trustworthy long-tailed classification. In *Proceedings of the IEEE/CVF Conference on Computer Vision and Pattern Recognition*, pages 6970–6979.

Hongxiang Li, Meng Cao, Xuxin Cheng, Yaowei Li, Zhihong Zhu, and Yuexian Zou. 2023a. G2l: Semantically aligned and uniform video grounding via geodesic

and game theory. In *Proceedings of the IEEE/CVF International Conference on Computer Vision*, pages 12032–12042.

Jiangtong Li, Li Niu, and Liqing Zhang. 2022b. From representation to reasoning: Towards both evidence and commonsense reasoning for video question-answering. In *Proceedings of the IEEE/CVF Conference on Computer Vision and Pattern Recognition*, pages 21273–21282.

Junnan Li, Dongxu Li, Silvio Savarese, and Steven Hoi. 2023b. Blip-2: Bootstrapping language-image pre-training with frozen image encoders and large language models. In *International conference on machine learning*, pages 19730–19742. PMLR.

Junnan Li, Dongxu Li, Caiming Xiong, and Steven Hoi. 2022c. Blip: Bootstrapping language-image pre-training for unified vision-language understanding and generation. In *International conference on machine learning*, pages 12888–12900. PMLR.

KunChang Li, Yinan He, Yi Wang, Yizhuo Li, Wenhai Wang, Ping Luo, Yali Wang, Limin Wang, and Yu Qiao. 2023c. Videochat: Chat-centric video understanding. *arXiv preprint arXiv:2305.06355*.

Kunchang Li, Xinhao Li, Yi Wang, Yinan He, Yali Wang, Limin Wang, and Yu Qiao. 2024a. Videomamba: State space model for efficient video understanding. *arXiv preprint arXiv:2403.06977*.

Kunchang Li, Yali Wang, Yinan He, Yizhuo Li, Yi Wang, Yi Liu, Zun Wang, Jilan Xu, Guo Chen, Ping Luo, et al. 2024b. Mvbench: A comprehensive multi-modal video understanding benchmark. In *Proceedings of the IEEE/CVF Conference on Computer Vision and Pattern Recognition*, pages 22195–22206.

Linjie Li, Yen-Chun Chen, Yu Cheng, Zhe Gan, Licheng Yu, and Jingjing Liu. 2020. Hero: Hierarchical encoder for video+ language omni-representation pre-training. *arXiv preprint arXiv:2005.00200*.

Linjie Li, Zhe Gan, Kevin Lin, Chung-Ching Lin, Zicheng Liu, Ce Liu, and Lijuan Wang. 2023d. Lavender: Unifying video-language understanding as masked

language modeling. In *Proceedings of the IEEE/CVF Conference on Computer Vision and Pattern Recognition*, pages 23119–23129.

Xiangpeng Li, Zhilong Zhou, Lijiang Chen, and Lianli Gao. 2019. Residual attention-based lstm for video captioning. *World Wide Web*, 22:621–636.

Xiangtai Li, Henghui Ding, Haobo Yuan, Wenwei Zhang, Jiangmiao Pang, Guanliang Cheng, Kai Chen, Ziwei Liu, and Chen Change Loy. 2023e. Transformer-based visual segmentation: A survey. *arXiv preprint arXiv:2304.09854*.

Xiangtai Li, Haobo Yuan, Wenwei Zhang, Guangliang Cheng, Jiangmiao Pang, and Chen Change Loy. 2023f. Tube-link: A flexible cross tube framework for universal video segmentation. In *Proceedings of the IEEE/CVF International Conference on Computer Vision*, pages 13923–13933.

Xiangtai Li, Wenwei Zhang, Jiangmiao Pang, Kai Chen, Guangliang Cheng, Yunhai Tong, and Chen Change Loy. 2022d. Video k-net: A simple, strong, and unified baseline for video segmentation. In *Proceedings of the IEEE/CVF Conference on Computer Vision and Pattern Recognition*, pages 18847–18857.

Yanwei Li, Chengyao Wang, and Jiaya Jia. 2023g. Llama-vid: An image is worth 2 tokens in large language models. *arXiv preprint arXiv:2311.17043*.

Yanwei Li, Chengyao Wang, and Jiaya Jia. 2024c. Llama-vid: An image is worth 2 tokens in large language models. In *European Conference on Computer Vision*, pages 323–340. Springer.

Yicong Li, Xiang Wang, Junbin Xiao, and Tat-Seng Chua. 2022e. Equivariant and invariant grounding for video question answering. In *Proceedings of the 30th ACM International Conference on Multimedia*, pages 4714–4722.

Yiming Li, Xiaoshan Yang, and Changsheng Xu. 2022f. Dynamic scene graph generation via anticipatory pre-training. In *Proceedings of the IEEE/CVF conference on computer vision and pattern recognition*, pages 13874–13883.

Bin Lin, Yang Ye, Bin Zhu, Jiaxi Cui, Munan Ning, Peng Jin, and Li Yuan. 2023. Video-llava: Learning united visual representation by alignment before projection. *arXiv preprint arXiv:2311.10122*.

## BIBLIOGRAPHY

Kevin Qinghong Lin, Jinpeng Wang, Mattia Soldan, Michael Wray, Rui Yan, Eric Z Xu, Difei Gao, Rong-Cheng Tu, Wenzhe Zhao, Weijie Kong, et al. 2022a. Ego-centric video-language pretraining. *Advances in Neural Information Processing Systems*, 35:7575–7586.

Tsung-Yi Lin, Priya Goyal, Ross Girshick, Kaiming He, and Piotr Dollár. 2017. Focal loss for dense object detection. In *Proceedings of the IEEE international conference on computer vision*, pages 2980–2988.

Yan-Bo Lin, Jie Lei, Mohit Bansal, and Gedas Bertasius. 2022b. Eclipse: Efficient long-range video retrieval using sight and sound. In *European Conference on Computer Vision*, pages 413–430. Springer.

Haotian Liu, Chunyuan Li, Qingyang Wu, and Yong Jae Lee. 2023. Visual instruction tuning. *Advances in neural information processing systems*, 36:34892–34916.

Kaiyuan Liu, Yunheng Li, Yuanfeng Xu, Shuai Liu, and Shenglan Liu. 2022a. Spatial focus attention for fine-grained skeleton-based action tasks. *IEEE Signal Processing Letters*, 29:1883–1887.

Ruyang Liu, Chen Li, Haoran Tang, Yixiao Ge, Ying Shan, and Ge Li. 2024a. St-llm: Large language models are effective temporal learners. In *European Conference on Computer Vision*, pages 1–18. Springer.

Ye Liu, Siyuan Li, Yang Wu, Chang-Wen Chen, Ying Shan, and Xiaohu Qie. 2022b. Umt: Unified multi-modal transformers for joint video moment retrieval and highlight detection. In *Proceedings of the IEEE/CVF Conference on Computer Vision and Pattern Recognition*, pages 3042–3051.

Ze Liu, Jia Ning, Yue Cao, Yixuan Wei, Zheng Zhang, Stephen Lin, and Han Hu. 2021. Video swin transformer. *arXiv preprint arXiv:2106.13230*.

Zhihang Liu, Jun Li, Hongtao Xie, Pandeng Li, Jiannan Ge, Sun-Ao Liu, and Guoqing Jin. 2024b. Towards balanced alignment: Modal-enhanced semantic modeling for video moment retrieval. In *Proceedings of the AAAI Conference on Artificial Intelligence*, volume 38, pages 3855–3863.

## BIBLIOGRAPHY

Xiang Long, Chuang Gan, and Gerard De Melo. 2018. Video captioning with multi-faceted attention. *Transactions of the Association for Computational Linguistics*, 6:173–184.

Huaishao Luo, Lei Ji, Botian Shi, Haoyang Huang, Nan Duan, Tianrui Li, Jason Li, Taroon Bharti, and Ming Zhou. 2020. Univl: A unified video and language pre-training model for multimodal understanding and generation. *arXiv preprint arXiv:2002.06353*.

Huaishao Luo, Lei Ji, Ming Zhong, Yang Chen, Wen Lei, Nan Duan, and Tianrui Li. 2022. Clip4clip: An empirical study of clip for end to end video clip retrieval and captioning. *Neurocomputing*, 508:293–304.

Ruipu Luo, Ziwang Zhao, Min Yang, Junwei Dong, Da Li, Pengcheng Lu, Tao Wang, Linmei Hu, Minghui Qiu, and Zhongyu Wei. 2023. Valley: Video assistant with large language model enhanced ability. *arXiv preprint arXiv:2306.07207*.

Xiaojian Ma, Silong Yong, Zilong Zheng, Qing Li, Yitao Liang, Song-Chun Zhu, and Siyuan Huang. 2022. Sqa3d: Situated question answering in 3d scenes. *arXiv preprint arXiv:2210.07474*.

Muhammad Maaz, Hanoona Rasheed, Salman Khan, and Fahad Shahbaz Khan. 2023. Video-chatgpt: Towards detailed video understanding via large vision and language models. *arXiv preprint arXiv:2306.05424*.

Tomasz Malisiewicz, Abhinav Gupta, and Alexei A Efros. 2011. Ensemble of exemplar-svms for object detection and beyond. In *ICCV*.

Xin Man, Jie Shao, Feiyu Chen, Mingxing Zhang, and Heng Tao Shen. 2023. Tevl: Trilinear encoder for video-language representation learning. *ACM Transactions on Multimedia Computing, Communications and Applications*, 19(5s):1–20.

Karttikeya Mangalam, Raiymbek Akshulakov, and Jitendra Malik. 2023. Egoschema: A diagnostic benchmark for very long-form video language understanding. *arXiv preprint arXiv:2308.09126*.

Safa Messaoud, Ismini Lourentzou, Assma Boughoula, Mona Zehni, Zhizhen Zhao, Chengxiang Zhai, and Alexander G Schwing. 2021. Deepqamvs: Query-aware

hierarchical pointer networks for multi-video summarization. In *Proceedings of the 44th international ACM SIGIR conference on research and development in information retrieval*, pages 1389–1399.

Antoine Miech, Dimitri Zhukov, Jean-Baptiste Alayrac, Makarand Tapaswi, Ivan Laptev, and Josef Sivic. 2019. Howto100m: Learning a text-video embedding by watching hundred million narrated video clips. In *Proceedings of the IEEE/CVF international conference on computer vision*, pages 2630–2640.

Mathew Monfort, Alex Andonian, Bolei Zhou, Kandan Ramakrishnan, Sarah Adel Bargal, Tom Yan, Lisa Brown, Quanfu Fan, Dan Gutfreund, Carl Vondrick, et al. 2019. Moments in time dataset: one million videos for event understanding. *IEEE transactions on pattern analysis and machine intelligence*, 42(2):502–508.

Fangzhou Mu, Sicheng Mo, and Yin Li. 2024. Snag: Scalable and accurate video grounding. *arXiv preprint arXiv:2404.02257*.

Sayak Nag, Kyle Min, Subarna Tripathi, and Amit K Roy-Chowdhury. 2023. Unbiased scene graph generation in videos. In *Proceedings of the IEEE/CVF Conference on Computer Vision and Pattern Recognition*, pages 22803–22813.

Arsha Nagrani, Paul Hongsuck Seo, Bryan Seybold, Anja Hauth, Santiago Manen, Chen Sun, and Cordelia Schmid. 2022. Learning audio-video modalities from image captions. In *European Conference on Computer Vision*, pages 407–426. Springer.

Cong-Duy Nguyen, Thong Nguyen, Duc Vu, and Anh Luu. 2023a. Improving multimodal sentiment analysis: Supervised angular margin-based contrastive learning for enhanced fusion representation. In *Findings of the Association for Computational Linguistics: EMNLP 2023*, pages 14714–14724.

Cong-Duy Nguyen, Thong Nguyen, Xiaobao Wu, and Anh Tuan Luu. 2024a. Kdmese: Knowledge distillation multimodal sentence embeddings with adaptive angular margin contrastive learning. *arXiv preprint arXiv:2403.17486*.

Thong Nguyen, Yi Bin, Junbin Xiao, Leigang Qu, Yicong Li, Jay Zhangjie Wu, Cong-Duy Nguyen, See-Kiong Ng, and Luu Anh Tuan. 2024b. Video-language

understanding: A survey from model architecture, model training, and data perspectives. *arXiv preprint arXiv:2406.05615*.

Thong Nguyen and Anh Tuan Luu. 2021. Contrastive learning for neural topic model. *Advances in neural information processing systems*, 34:11974–11986.

Thong Nguyen, Xiaobao Wu, Xinshuai Dong, Khoi Le, Zhiyuan Hu, Cong-Duy Nguyen, See-Kiong Ng, and Luu Anh Tuan. 2023b. Read: Recurrent adapter with partial video-language alignment for parameter-efficient transfer learning in low-resource video-language modeling. *arXiv preprint arXiv:2312.06950*.

Thong Nguyen, Xiaobao Wu, Xinshuai Dong, Khoi M Le, Zhiyuan Hu, Cong-Duy Nguyen, See-Kiong Ng, and Anh Tuan Luu. 2024c. Read-pvla: Recurrent adapter with partial video-language alignment for parameter-efficient transfer learning in low-resource video-language modeling. In *Proceedings of the AAAI Conference on Artificial Intelligence*, volume 38, pages 18824–18832.

Thong Nguyen, Xiaobao Wu, Xinshuai Dong, Cong-Duy Nguyen, See-Kiong Ng, and Luu Anh Tuan. 2023c. Demaformer: Damped exponential moving average transformer with energy-based modeling for temporal language grounding. *arXiv preprint arXiv:2312.02549*.

Thong Nguyen, Xiaobao Wu, Anh-Tuan Luu, Cong-Duy Nguyen, Zhen Hai, and Lidong Bing. 2022. Adaptive contrastive learning on multimodal transformer for review helpfulness predictions. *arXiv preprint arXiv:2211.03524*.

Thong Thanh Nguyen, Zhiyuan Hu, Xiaobao Wu, Cong-Duy T Nguyen, See-Kiong Ng, and Anh Tuan Luu. 2024d. Encoding and controlling global semantics for long-form video question answering. *arXiv preprint arXiv:2405.19723*.

Thong Thanh Nguyen, Xiaobao Wu, Xinshuai Dong, Cong-Duy T Nguyen, See-Kiong Ng, and Anh Tuan Luu. 2024e. Topic modeling as multi-objective optimization with setwise contrastive learning. In *The Twelfth International Conference on Learning Representations*.

## BIBLIOGRAPHY

Liqiang Nie, Leigang Qu, Dai Meng, Min Zhang, Qi Tian, and Alberto Del Bimbo. 2022. Search-oriented micro-video captioning. In *Proceedings of the 30th ACM International Conference on Multimedia*, pages 3234–3243.

Junting Pan, Ziyi Lin, Xiatian Zhu, Jing Shao, and Hongsheng Li. 2022. St-adapter: Parameter-efficient image-to-video transfer learning. *Advances in Neural Information Processing Systems*, 35:26462–26477.

Yulin Pan, Xiangteng He, Biao Gong, Yiliang Lv, Yujun Shen, Yuxin Peng, and Deli Zhao. 2023. Scanning only once: An end-to-end framework for fast temporal grounding in long videos. In *Proceedings of the IEEE/CVF International Conference on Computer Vision*, pages 13767–13777.

Rameswar Panda, Niluthpol Chowdhury Mithun, and Amit K Roy-Chowdhury. 2017. Diversity-aware multi-video summarization. *IEEE Transactions on Image Processing*, 26(10):4712–4724.

Love Panta, Prashant Shrestha, Brabeem Sapkota, Amrita Bhattacharai, Suresh Manandhar, and Anand Kumar Sah. 2024. Cross-modal contrastive learning with asymmetric co-attention network for video moment retrieval. In *Proceedings of the IEEE/CVF Winter Conference on Applications of Computer Vision*, pages 607–614.

Wenjie Pei, Jiyuan Zhang, Xiangrong Wang, Lei Ke, Xiaoyong Shen, and Yu-Wing Tai. 2019. Memory-attended recurrent network for video captioning. In *Proceedings of the IEEE/CVF conference on computer vision and pattern recognition*, pages 8347–8356.

Liang Peng, Shuangji Yang, Yi Bin, and Guoqing Wang. 2021. Progressive graph attention network for video question answering. In *Proceedings of the 29th ACM International Conference on Multimedia*, pages 2871–2879.

Jeffrey Pennington, Richard Socher, and Christopher D Manning. 2014. Glove: Global vectors for word representation. In *Proceedings of the 2014 conference on empirical methods in natural language processing (EMNLP)*, pages 1532–1543.

## BIBLIOGRAPHY

Shraman Pramanick, Aniket Roy, and Vishal M Patel. 2022. Multimodal learning using optimal transport for sarcasm and humor detection. In *Proceedings of the IEEE/CVF Winter Conference on Applications of Computer Vision*, pages 3930–3940.

Iqra Qasim, Alexander Horsch, and Dilip Prasad. 2025. Dense video captioning: A survey of techniques, datasets and evaluation protocols. *ACM Computing Surveys*, 57(6):1–36.

Charles R Qi, Hao Su, Kaichun Mo, and Leonidas J Guibas. 2017. Pointnet: Deep learning on point sets for 3d classification and segmentation. In *Proceedings of the IEEE conference on computer vision and pattern recognition*, pages 652–660.

Rui Qian, Xiaoyi Dong, Pan Zhang, Yuhang Zang, Shuangrui Ding, Dahua Lin, and Jiaqi Wang. 2024. Streaming long video understanding with large language models. *Advances in Neural Information Processing Systems*, 37:119336–119360.

Alec Radford, Jong Wook Kim, Chris Hallacy, Aditya Ramesh, Gabriel Goh, Sandhini Agarwal, Girish Sastry, Amanda Askell, Pamela Mishkin, Jack Clark, et al. 2021. Learning transferable visual models from natural language supervision. In *International Conference on Machine Learning*, pages 8748–8763.

Colin Raffel, Noam Shazeer, Adam Roberts, Katherine Lee, Sharan Narang, Michael Matena, Yanqi Zhou, Wei Li, and Peter J Liu. 2020. Exploring the limits of transfer learning with a unified text-to-text transformer. *The Journal of Machine Learning Research*, 21(1):5485–5551.

Sonia Raychaudhuri, Tommaso Campari, Unnat Jain, Manolis Savva, and Angel X Chang. 2023. Reduce, reuse, recycle: Modular multi-object navigation. *arXiv preprint arXiv:2304.03696*, 2.

Michaela Regneri, Marcus Rohrbach, Dominikus Wetzel, Stefan Thater, Bernt Schiele, and Manfred Pinkal. 2013. Grounding action descriptions in videos. *Transactions of the Association for Computational Linguistics*, 1:25–36.

## BIBLIOGRAPHY

Mengye Ren, Wenyuan Zeng, Bin Yang, and Raquel Urtasun. 2018. Learning to reweight examples for robust deep learning. In *International conference on machine learning*, pages 4334–4343. PMLR.

Anna Rohrbach, Marcus Rohrbach, Niket Tandon, and Bernt Schiele. 2015. A dataset for movie description. In *Proceedings of the IEEE conference on computer vision and pattern recognition*, pages 3202–3212.

Marcus Rohrbach, Sikandar Amin, Mykhaylo Andriluka, and Bernt Schiele. 2012. A database for fine grained activity detection of cooking activities. In *2012 IEEE conference on computer vision and pattern recognition*, pages 1194–1201. IEEE.

Olga Russakovsky, Jia Deng, Hao Su, Jonathan Krause, Sanjeev Satheesh, Sean Ma, Zhiheng Huang, Andrej Karpathy, Aditya Khosla, Michael Bernstein, et al. 2015. Imagenet large scale visual recognition challenge. *International journal of computer vision*, 115:211–252.

Ramon Sanabria, Ozan Caglayan, Shruti Palaskar, Desmond Elliott, Loïc Barrault, Lucia Specia, and Florian Metze. 2018. How2: a large-scale dataset for multimodal language understanding. *arXiv preprint arXiv:1811.00347*.

Paul Hongsuck Seo, Arsha Nagrani, Anurag Arnab, and Cordelia Schmid. 2022. End-to-end generative pretraining for multimodal video captioning. In *Proceedings of the IEEE/CVF Conference on Computer Vision and Pattern Recognition*, pages 17959–17968.

Chuyi Shang, Amos You, Sanjay Subramanian, Trevor Darrell, and Roei Herzig. 2024. Traveler: A modular multi-lmm agent framework for video question-answering. *arXiv preprint arXiv:2404.01476*.

Xindi Shang, Donglin Di, Junbin Xiao, Yu Cao, Xun Yang, and Tat-Seng Chua. 2019. Annotating objects and relations in user-generated videos. In *Proceedings of the 2019 on International Conference on Multimedia Retrieval*, pages 279–287.

Jun Shu, Qi Xie, Lixuan Yi, Qian Zhao, Sanping Zhou, Zongben Xu, and Deyu Meng. 2019. Meta-weight-net: Learning an explicit mapping for sample weighting. *Advances in neural information processing systems*, 32.

Gunnar A Sigurdsson, GÜl Varol, Xiaolong Wang, Ali Farhadi, Ivan Laptev, and Abhinav Gupta. 2016. Hollywood in homes: Crowdsourcing data collection for activity understanding. In *Computer Vision–ECCV 2016: 14th European Conference, Amsterdam, The Netherlands, October 11–14, 2016, Proceedings, Part I 14*, pages 510–526. Springer.

Karen Simonyan and Andrew Zisserman. 2014. Two-Stream Convolutional Networks for Action Recognition in Videos. In *Advances in Neural Information Processing Systems (NeurIPS)*.

Irwin Sobel, R Duda, P Hart, and John Wiley. 2022. Sobel-feldman operator. *Preprint at https://www.researchgate.net/profile/Irwin-Sobel/publication/285159837. Accessed*, 20.

Mattia Soldan, Alejandro Pardo, Juan León Alcázar, Fabian Caba, Chen Zhao, Silvio Giancola, and Bernard Ghanem. 2022. Mad: A scalable dataset for language grounding in videos from movie audio descriptions. In *Proceedings of the IEEE/CVF Conference on Computer Vision and Pattern Recognition*, pages 5026–5035.

Mattia Soldan, Mengmeng Xu, Sisi Qu, Jesper Tegner, and Bernard Ghanem. 2021. Vlg-net: Video-language graph matching network for video grounding. In *Proceedings of the IEEE/CVF International Conference on Computer Vision*, pages 3224–3234.

Yale Song, Jordi Vallmitjana, Amanda Stent, and Alejandro Jaimes. 2015. TvsuM: Summarizing web videos using titles. In *Proceedings of the IEEE conference on computer vision and pattern recognition*, pages 5179–5187.

Jonathan C Stroud, Zhichao Lu, Chen Sun, Jia Deng, Rahul Sukthankar, Cordelia Schmid, and David A Ross. 2020. Learning video representations from textual web supervision. *arXiv preprint arXiv:2007.14937*.

Gopika Sudhakaran, Devendra Singh Dhami, Kristian Kersting, and Stefan Roth. 2023. Vision relation transformer for unbiased scene graph generation. In *Proceedings of the IEEE/CVF International Conference on Computer Vision*, pages 21882–21893.

## BIBLIOGRAPHY

Chen Sun, Austin Myers, Carl Vondrick, Kevin Murphy, and Cordelia Schmid. 2019. Videobert: A joint model for video and language representation learning. In *Proceedings of the IEEE/CVF international conference on computer vision*, pages 7464–7473.

Min Sun, Ali Farhadi, and Steve Seitz. 2014. Ranking domain-specific highlights by analyzing edited videos. In *Computer Vision–ECCV 2014: 13th European Conference, Zurich, Switzerland, September 6–12, 2014, Proceedings, Part I 13*, pages 787–802. Springer.

Yanmin Sun, Mohamed S Kamel, Andrew KC Wong, and Yang Wang. 2007. Cost-sensitive boosting for classification of imbalanced data. *Pattern recognition*, 40(12):3358–3378.

Yi-Lin Sung, Jaemin Cho, and Mohit Bansal. 2022. ViL-adapter: Parameter-efficient transfer learning for vision-and-language tasks. In *Proceedings of the IEEE/CVF Conference on Computer Vision and Pattern Recognition*, pages 5227–5237.

Hao Tang, Kevin Liang, Kristen Grauman, Matt Feiszli, and Weiyao Wang. 2023. Egotracks: A long-term egocentric visual object tracking dataset. *arXiv preprint arXiv:2301.03213*.

Yansong Tang, Dajun Ding, Yongming Rao, Yu Zheng, Danyang Zhang, Lili Zhao, Jiwen Lu, and Jie Zhou. 2019. Coin: A large-scale dataset for comprehensive instructional video analysis. In *Proceedings of the IEEE/CVF Conference on Computer Vision and Pattern Recognition*, pages 1207–1216.

Zineng Tang, Jie Lei, and Mohit Bansal. 2021. Decembert: Learning from noisy instructional videos via dense captions and entropy minimization. In *Proceedings of the 2021 Conference of the North American Chapter of the Association for Computational Linguistics: Human Language Technologies*, pages 2415–2426.

Bart Thomee, David A Shamma, Gerald Friedland, Benjamin Elizalde, Karl Ni, Douglas Poland, Damian Borth, and Li-Jia Li. 2016. Yfcc100m: The new data in multimedia research. *Communications of the ACM*, 59(2):64–73.

## BIBLIOGRAPHY

Julian Togelius and Georgios N Yannakakis. 2023. Choose your weapon: Survival strategies for depressed ai academics. *arXiv preprint arXiv:2304.06035*.

Atousa Torabi, Niket Tandon, and Leonid Sigal. 2016. Learning language-visual embedding for movie understanding with natural-language. *arXiv preprint arXiv:1609.08124*.

Hugo Touvron, Matthieu Cord, Alexandre Sablayrolles, Gabriel Synnaeve, and Hervé Jégou. 2021. Going deeper with image transformers. In *Proceedings of the IEEE/CVF international conference on computer vision*, pages 32–42.

Du Tran, Lubomir Bourdev, Rob Fergus, Lorenzo Torresani, and Manohar Paluri. 2015. Learning spatiotemporal features with 3d convolutional networks. In *Proceedings of the IEEE international conference on computer vision*, pages 4489–4497.

Du Tran, Jamie Ray, Zheng Shou, Shih-Fu Chang, and Manohar Paluri. 2017. Convnet architecture search for spatiotemporal feature learning. *arXiv preprint arXiv:1708.05038*.

Yao-Hung Hubert Tsai, Martin Q Ma, Muqiao Yang, Ruslan Salakhutdinov, and Louis-Philippe Morency. 2020. Multimodal routing: Improving local and global interpretability of multimodal language analysis. In *Proceedings of the Conference on Empirical Methods in Natural Language Processing. Conference on Empirical Methods in Natural Language Processing*, volume 2020, page 1823. NIH Public Access.

Ashish Vaswani, Noam Shazeer, Niki Parmar, Jakob Uszkoreit, Llion Jones, Aidan N Gomez, Łukasz Kaiser, and Illia Polosukhin. 2017. Attention is all you need. *Advances in neural information processing systems*, 30.

Subhashini Venugopalan, Marcus Rohrbach, Jeffrey Donahue, Raymond Mooney, Trevor Darrell, and Kate Saenko. 2015. Sequence to sequence-video to text. In *Proceedings of the IEEE international conference on computer vision*, pages 4534–4542.

## BIBLIOGRAPHY

Johanna Wald, Helisa Dhamo, Nassir Navab, and Federico Tombari. 2020. Learning 3d semantic scene graphs from 3d indoor reconstructions. In *Proceedings of the IEEE/CVF Conference on Computer Vision and Pattern Recognition*, pages 3961–3970.

Anran Wang, Anh Tuan Luu, Chuan-Sheng Foo, Hongyuan Zhu, Yi Tay, and Vijay Chandrasekhar. 2019a. Holistic multi-modal memory network for movie question answering. *IEEE Transactions on Image Processing*, 29:489–499.

Guan Wang, Zhimin Li, Qingchao Chen, and Yang Liu. 2024a. Oed: Towards one-stage end-to-end dynamic scene graph generation. In *Proceedings of the IEEE/CVF Conference on Computer Vision and Pattern Recognition*, pages 27938–27947.

Jinpeng Wang, Yixiao Ge, Rui Yan, Yuying Ge, Kevin Qinghong Lin, Satoshi Tsutsui, Xudong Lin, Guanyu Cai, Jianping Wu, Ying Shan, et al. 2023a. All in one: Exploring unified video-language pre-training. In *Proceedings of the IEEE/CVF Conference on Computer Vision and Pattern Recognition*, pages 6598–6608.

Junke Wang, Dongdong Chen, Zuxuan Wu, Chong Luo, Luowei Zhou, Yucheng Zhao, Yujia Xie, Ce Liu, Yu-Gang Jiang, and Lu Yuan. 2022a. Omnidvl: One foundation model for image-language and video-language tasks. *Advances in neural information processing systems*, 35:5696–5710.

Lijie Wang, Hao Liu, Shuyuan Peng, Hongxuan Tang, Xinyan Xiao, Ying Chen, Hua Wu, and Haifeng Wang. 2021a. Dutrust: A sentiment analysis dataset for trustworthiness evaluation. *arXiv preprint arXiv:2108.13140*.

Qiang Wang, Yanhao Zhang, Yun Zheng, Pan Pan, and Xian-Sheng Hua. 2022b. Disentangled representation learning for text-video retrieval. *arXiv preprint arXiv:2203.07111*.

Qiang Wang, Yanhao Zhang, Yun Zheng, Pan Pan, and Xian-Sheng Hua. 2022c. Disentangled representation learning for text-video retrieval. *arXiv preprint arXiv:2203.07111*.

## BIBLIOGRAPHY

Wenguan Wang, Tianfei Zhou, Fisher Yu, Jifeng Dai, Ender Konukoglu, and Luc Van Gool. 2021b. Exploring cross-image pixel contrast for semantic segmentation. In *Proceedings of the IEEE/CVF international conference on computer vision*, pages 7303–7313.

Wenqing Wang, Yawei Luo, Zhiqing Chen, Tao Jiang, Yi Yang, and Jun Xiao. 2023b. Taking a closer look at visual relation: Unbiased video scene graph generation with decoupled label learning. *IEEE Transactions on Multimedia*.

Xin Wang, Jiawei Wu, Junkun Chen, Lei Li, Yuan-Fang Wang, and William Yang Wang. 2019b. Vatex: A large-scale, high-quality multilingual dataset for video-and-language research. In *Proceedings of the IEEE/CVF International Conference on Computer Vision*, pages 4581–4591.

Yi Wang, Yinan He, Yizhuo Li, Kunchang Li, Jiashuo Yu, Xin Ma, Xinyuan Chen, Yaohui Wang, Ping Luo, Ziwei Liu, et al. 2023c. Internvid: A large-scale video-text dataset for multimodal understanding and generation. *arXiv preprint arXiv:2307.06942*.

Yixin Wang, Alp Kucukelbir, and David M Blei. 2017. Robust probabilistic modeling with bayesian data reweighting. In *International Conference on Machine Learning*, pages 3646–3655. PMLR.

Zhanyu Wang, Longyue Wang, Zhen Zhao, Minghao Wu, Chenyang Lyu, Huayang Li, Deng Cai, Luping Zhou, Shuming Shi, and Zhaopeng Tu. 2024b. Gpt4video: A unified multimodal large language model for instruction-followed understanding and safety-aware generation. In *Proceedings of the 32nd ACM International Conference on Multimedia*, pages 3907–3916.

Zhenzhi Wang, Limin Wang, Tao Wu, Tianhao Li, and Gangshan Wu. 2022d. Negative sample matters: A renaissance of metric learning for temporal grounding. In *Proceedings of the AAAI Conference on Artificial Intelligence*, volume 36, pages 2613–2623.

Zhongdao Wang, Hengshuang Zhao, Ya-Li Li, Shengjin Wang, Philip Torr, and Luca Bertinetto. 2021c. Do different tracking tasks require different appearance models? *Advances in Neural Information Processing Systems*, 34:726–738.

## BIBLIOGRAPHY

Jie Wei, Guanyu Hu, Luu Anh Tuan, Xinyu Yang, and Wenjing Zhu. 2023. Multi-scale receptive field graph model for emotion recognition in conversations. In *ICASSP 2023-2023 IEEE International Conference on Acoustics, Speech and Signal Processing (ICASSP)*, pages 1–5. IEEE.

Jie Wei, Guanyu Hu, Xinyu Yang, Anh Tuan Luu, and Yizhuo Dong. 2022. Audio-visual domain adaptation feature fusion for speech emotion recognition. In *INTERSPEECH*, pages 1988–1992.

Jie Wei, Guanyu Hu, Xinyu Yang, Anh Tuan Luu, and Yizhuo Dong. 2024. Learning facial expression and body gesture visual information for video emotion recognition. *Expert Systems with Applications*, 237:121419.

Lina Wei, Fangfang Wang, Xi Li, Fei Wu, and Jun Xiao. 2017. Graph-theoretic spatiotemporal context modeling for video saliency detection. In *2017 IEEE International Conference on Image Processing (ICIP)*, pages 4197–4201. IEEE.

Bo Wu, Shoubin Yu, Zhenfang Chen, Joshua B Tenenbaum, and Chuang Gan. 2021. Star: A benchmark for situated reasoning in real-world videos. In *Thirty-fifth Conference on Neural Information Processing Systems Datasets and Benchmarks Track (Round 2)*.

Chao-Yuan Wu and Philipp Krahenbuhl. 2021. Towards long-form video understanding. In *Proceedings of the IEEE/CVF Conference on Computer Vision and Pattern Recognition*, pages 1884–1894.

Xiaobao Wu, Xinshuai Dong, Thong Nguyen, Chaoqun Liu, Liang-Ming Pan, and Anh Tuan Luu. 2023a. Infoctm: A mutual information maximization perspective of cross-lingual topic modeling. In *Proceedings of the AAAI Conference on Artificial Intelligence*, volume 37, pages 13763–13771.

Xiaobao Wu, Xinshuai Dong, Thong Nguyen, and Anh Tuan Luu. 2023b. Effective neural topic modeling with embedding clustering regularization. In *International Conference on Machine Learning*. PMLR.

Xiaobao Wu, Xinshuai Dong, Liangming Pan, Thong Nguyen, and Anh Tuan Luu. 2024. Modeling dynamic topics in chain-free fashion by evolution-tracking

contrastive learning and unassociated word exclusion. In *Findings of the Association for Computational Linguistics: ACL 2024*. Association for Computational Linguistics.

Xiaobao Wu, Anh Tuan Luu, and Xinshuai Dong. 2022a. Mitigating data sparsity for short text topic modeling by topic-semantic contrastive learning. In *Proceedings of the 2022 Conference on Empirical Methods in Natural Language Processing*, pages 2748–2760, Abu Dhabi, United Arab Emirates. Association for Computational Linguistics.

Yizheng Wu, Min Shi, Shuaiyuan Du, Hao Lu, Zhiguo Cao, and Weicai Zhong. 2022b. 3d instances as 1d kernels. In *European Conference on Computer Vision*, pages 235–252. Springer.

Zuxuan Wu, Ting Yao, Yanwei Fu, and Yu-Gang Jiang. 2017. Deep learning for video classification and captioning. In *Frontiers of multimedia research*, pages 3–29.

Fanyi Xiao, Joseph Tighe, and Davide Modolo. 2021a. Modist: Motion distillation for self-supervised video representation learning. *arXiv preprint arXiv:2106.09703*, 3.

Junbin Xiao, Xindi Shang, Angela Yao, and Tat-Seng Chua. 2021b. Next-qa: Next phase of question-answering to explaining temporal actions. In *Proceedings of the IEEE/CVF conference on computer vision and pattern recognition*, pages 9777–9786.

Junbin Xiao, Angela Yao, Yicong Li, and Tat Seng Chua. 2023a. Can i trust your answer? visually grounded video question answering. *arXiv preprint arXiv:2309.01327*.

Junbin Xiao, Angela Yao, Zhiyuan Liu, Yicong Li, Wei Ji, and Tat-Seng Chua. 2022a. Video as conditional graph hierarchy for multi-granular question answering. In *Proceedings of the AAAI Conference on Artificial Intelligence*, volume 36, pages 2804–2812.

## BIBLIOGRAPHY

Junbin Xiao, Pan Zhou, Tat-Seng Chua, and Shuicheng Yan. 2022b. Video graph transformer for video question answering. In *European Conference on Computer Vision*, pages 39–58. Springer.

Junbin Xiao, Pan Zhou, Angela Yao, Yicong Li, Richang Hong, Shuicheng Yan, and Tat-Seng Chua. 2023b. Contrastive video question answering via video graph transformer. *arXiv preprint arXiv:2302.13668*.

Yicheng Xiao, Zhuoyan Luo, Yong Liu, Yue Ma, Hengwei Bian, Yatai Ji, Yujiu Yang, and Xiu Li. 2024. Bridging the gap: A unified video comprehension framework for moment retrieval and highlight detection. In *Proceedings of the IEEE/CVF Conference on Computer Vision and Pattern Recognition*, pages 18709–18719.

Saining Xie, Ross Girshick, Piotr Dollar, Zhuowen Tu, and Kaiming He. 2017. Aggregated Residual Transformations for Deep Neural Networks. In *The IEEE Conference on Computer Vision and Pattern Recognition (CVPR)*.

Zhen Xing, Qi Dai, Han Hu, Jingjing Chen, Zuxuan Wu, and Yu-Gang Jiang. 2023. Svformer: Semi-supervised video transformer for action recognition. In *Proceedings of the IEEE/CVF Conference on Computer Vision and Pattern Recognition*, pages 18816–18826.

Dejing Xu, Zhou Zhao, Jun Xiao, Fei Wu, Hanwang Zhang, Xiangnan He, and Yuetong Zhuang. 2017. Video question answering via gradually refined attention over appearance and motion. In *Proceedings of the 25th ACM international conference on Multimedia*, pages 1645–1653.

Haiyang Xu, Qinghao Ye, Ming Yan, Yaya Shi, Jiabo Ye, Yuanhong Xu, Chenliang Li, Bin Bi, Qi Qian, Wei Wang, et al. 2023a. mplug-2: A modularized multi-modal foundation model across text, image and video. *arXiv preprint arXiv:2302.00402*.

Hu Xu, Gargi Ghosh, Po-Yao Huang, Prahal Arora, Masoumeh Aminzadeh, Christoph Feichtenhofer, Florian Metze, and Luke Zettlemoyer. 2021. Vlm: Task-agnostic video-language model pre-training for video understanding. *arXiv preprint arXiv:2105.09996*.

## BIBLIOGRAPHY

Huijuan Xu, Kun He, Bryan A Plummer, Leonid Sigal, Stan Sclaroff, and Kate Saenko. 2019. Multilevel language and vision integration for text-to-clip retrieval. In *Proceedings of the AAAI Conference on Artificial Intelligence*, volume 33, pages 9062–9069.

Jun Xu, Tao Mei, Ting Yao, and Yong Rui. 2016. Msr-vtt: A large video description dataset for bridging video and language. In *Proceedings of the IEEE conference on computer vision and pattern recognition*, pages 5288–5296.

Lin Xu, Yilin Zhao, Daquan Zhou, Zhijie Lin, See Kiong Ng, and Jiashi Feng. 2024. Pllava: Parameter-free llava extension from images to videos for video dense captioning. *arXiv preprint arXiv:2404.16994*.

Mengmeng Xu, Mattia Soldan, Jialin Gao, Shuming Liu, Juan-Manuel Pérez-Rúa, and Bernard Ghanem. 2023b. Boundary-denoising for video activity localization. *arXiv preprint arXiv:2304.02934*.

Hongwei Xue, Tiankai Hang, Yanhong Zeng, Yuchong Sun, Bei Liu, Huan Yang, Jianlong Fu, and Baining Guo. 2022a. Advancing high-resolution video-language representation with large-scale video transcriptions. In *Proceedings of the IEEE/CVF Conference on Computer Vision and Pattern Recognition*, pages 5036–5045.

Hongwei Xue, Yuchong Sun, Bei Liu, Jianlong Fu, Ruihua Song, Houqiang Li, and Jiebo Luo. 2022b. Clip-vip: Adapting pre-trained image-text model to video-language representation alignment. *arXiv preprint arXiv:2209.06430*.

Antoine Yang, Antoine Miech, Josef Sivic, Ivan Laptev, and Cordelia Schmid. 2021. Just ask: Learning to answer questions from millions of narrated videos. In *Proceedings of the IEEE/CVF International Conference on Computer Vision*, pages 1686–1697.

Antoine Yang, Antoine Miech, Josef Sivic, Ivan Laptev, and Cordelia Schmid. 2022a. Zero-shot video question answering via frozen bidirectional language models. *Advances in Neural Information Processing Systems*, 35:124–141.

Antoine Yang, Arsha Nagrani, Ivan Laptev, Josef Sivic, and Cordelia Schmid. 2023a. Vidchapters-7m: Video chapters at scale. *arXiv preprint arXiv:2309.13952*.

## BIBLIOGRAPHY

Antoine Yang, Arsha Nagrani, Paul Hongsuck Seo, Antoine Miech, Jordi Pont-Tuset, Ivan Laptev, Josef Sivic, and Cordelia Schmid. 2023b. Vid2seq: Large-scale pretraining of a visual language model for dense video captioning. In *Proceedings of the IEEE/CVF Conference on Computer Vision and Pattern Recognition*, pages 10714–10726.

Bang Yang, Tong Zhang, and Yuexian Zou. 2022b. Clip meets video captioning: Concept-aware representation learning does matter. In *Chinese Conference on Pattern Recognition and Computer Vision (PRCV)*, pages 368–381. Springer.

Guoyu Yang, Jie Lei, Zhikuan Zhu, Siyu Cheng, Zunlei Feng, and Ronghua Liang. 2023c. Afpn: asymptotic feature pyramid network for object detection. In *2023 IEEE International Conference on Systems, Man, and Cybernetics (SMC)*, pages 2184–2189. IEEE.

Jingkang Yang, Yi Zhe Ang, Zujin Guo, Kaiyang Zhou, Wayne Zhang, and Ziwei Liu. 2022c. Panoptic scene graph generation. In *European Conference on Computer Vision*, pages 178–196. Springer.

Jingkang Yang, Jun Cen, Wenxuan Peng, Shuai Liu, Fangzhou Hong, Xiangtai Li, Kaiyang Zhou, Qifeng Chen, and Ziwei Liu. 2024a. 4d panoptic scene graph generation. *Advances in Neural Information Processing Systems*, 36.

Jingkang Yang, Wenxuan Peng, Xiangtai Li, Zujin Guo, Liangyu Chen, Bo Li, Zheng Ma, Kaiyang Zhou, Wayne Zhang, Chen Change Loy, et al. 2023d. Panoptic video scene graph generation. In *Proceedings of the IEEE/CVF Conference on Computer Vision and Pattern Recognition*, pages 18675–18685.

Taojiannan Yang, Yi Zhu, Yusheng Xie, Aston Zhang, Chen Chen, and Mu Li. 2023e. Aim: Adapting image models for efficient video action recognition. *arXiv preprint arXiv:2302.03024*.

Yijun Yang, Zhaochu Xing, and Lei Zhu. 2024b. Vivim: a video vision mamba for medical video object segmentation. *arXiv preprint arXiv:2401.14168*.

## BIBLIOGRAPHY

Yinchong Yang, Denis Krompass, and Volker Tresp. 2017. Tensor-train recurrent neural networks for video classification. In *International Conference on Machine Learning*, pages 3891–3900. PMLR.

Li Yao, Atousa Torabi, Kyunghyun Cho, Nicolas Ballas, Christopher Pal, Hugo Larochelle, and Aaron Courville. 2015. Describing videos by exploiting temporal structure. In *Proceedings of the IEEE international conference on computer vision*, pages 4507–4515.

Haonan Yu, Jiang Wang, Zhiheng Huang, Yi Yang, and Wei Xu. 2016. Video paragraph captioning using hierarchical recurrent neural networks. In *Proceedings of the IEEE conference on computer vision and pattern recognition*, pages 4584–4593.

Tiezheng Yu, Wenliang Dai, Zihan Liu, and Pascale Fung. 2021. Vision guided generative pre-trained language models for multimodal abstractive summarization. *arXiv preprint arXiv:2109.02401*.

Ting Yu, Jun Yu, Zhou Yu, Qingming Huang, and Qi Tian. 2020. Long-term video question answering via multimodal hierarchical memory attentive networks. *IEEE Transactions on Circuits and Systems for Video Technology*, 31(3):931–944.

Youngjae Yu, Jongseok Kim, and Gunhee Kim. 2018. A joint sequence fusion model for video question answering and retrieval. In *Proceedings of the European Conference on Computer Vision (ECCV)*, pages 471–487.

Youngjae Yu, Hyungjin Ko, Jongwook Choi, and Gunhee Kim. 2017. End-to-end concept word detection for video captioning, retrieval, and question answering. In *Proceedings of the IEEE conference on computer vision and pattern recognition*, pages 3165–3173.

Zhou Yu, Dejing Xu, Jun Yu, Ting Yu, Zhou Zhao, Yueting Zhuang, and Dacheng Tao. 2019. Activitynet-qa: A dataset for understanding complex web videos via question answering. In *Proceedings of the AAAI Conference on Artificial Intelligence*, volume 33, pages 9127–9134.

## BIBLIOGRAPHY

Liangzhe Yuan, Nitesh Bharadwaj Gundavarapu, Long Zhao, Hao Zhou, Yin Cui, Lu Jiang, Xuan Yang, Menglin Jia, Tobias Weyand, Luke Friedman, et al. 2023. Videoglue: Video general understanding evaluation of foundation models. *arXiv preprint arXiv:2307.03166*.

Yitian Yuan, Tao Mei, and Wenwu Zhu. 2019. To find where you talk: Temporal sentence localization in video with attention based location regression. In *Proceedings of the AAAI Conference on Artificial Intelligence*, volume 33, pages 9159–9166.

Sangdoo Yun, Dongyoon Han, Seong Joon Oh, Sanghyuk Chun, Junsuk Choe, and Youngjoon Yoo. 2019. Cutmix: Regularization strategy to train strong classifiers with localizable features. In *Proceedings of the IEEE/CVF international conference on computer vision*, pages 6023–6032.

Elad Ben Zaken, Yoav Goldberg, and Shauli Ravfogel. 2022. Bitfit: Simple parameter-efficient fine-tuning for transformer-based masked language-models. In *Proceedings of the 60th Annual Meeting of the Association for Computational Linguistics (Volume 2: Short Papers)*, pages 1–9.

Rowan Zellers, Jiasen Lu, Ximing Lu, Youngjae Yu, Yanpeng Zhao, Mohammadreza Salehi, Aditya Kusupati, Jack Hessel, Ali Farhadi, and Yejin Choi. 2022. Merlot reserve: Neural script knowledge through vision and language and sound. In *Proceedings of the IEEE/CVF Conference on Computer Vision and Pattern Recognition*, pages 16375–16387.

Rowan Zellers, Ximing Lu, Jack Hessel, Youngjae Yu, Jae Sung Park, Jize Cao, Ali Farhadi, and Yejin Choi. 2021. Merlot: Multimodal neural script knowledge models. *Advances in Neural Information Processing Systems*, 34:23634–23651.

Kuo-Hao Zeng, Tseng-Hung Chen, Ching-Yao Chuang, Yuan-Hong Liao, Juan Carlos Niebles, and Min Sun. 2017. Leveraging video descriptions to learn video question answering. In *Thirty-First AAAI Conference on Artificial Intelligence*.

Bowen Zhang, Xiaojie Jin, Weibo Gong, Kai Xu, Zhao Zhang, Peng Wang, Xiaohui Shen, and Jiashi Feng. 2023a. Multimodal video adapter for parameter efficient video text retrieval. *arXiv preprint arXiv:2301.07868*.

## BIBLIOGRAPHY

Chen-Lin Zhang, Jianxin Wu, and Yin Li. 2022. Actionformer: Localizing moments of actions with transformers. In *European Conference on Computer Vision*, pages 492–510. Springer.

Hang Zhang, Xin Li, and Lidong Bing. 2023b. Video-llama: An instruction-tuned audio-visual language model for video understanding. *arXiv preprint arXiv:2306.02858*.

Hao Zhang, Aixin Sun, Wei Jing, and Joey Tianyi Zhou. 2020a. Span-based localizing network for natural language video localization. *arXiv preprint arXiv:2004.13931*.

Hongyi Zhang, Moustapha Cisse, Yann N Dauphin, and David Lopez-Paz. 2017. mixup: Beyond empirical risk minimization. *arXiv preprint arXiv:1710.09412*.

Jingqing Zhang, Yao Zhao, Mohammad Saleh, and Peter Liu. 2020b. Pegasus: Pre-training with extracted gap-sentences for abstractive summarization. In *International Conference on Machine Learning*, pages 11328–11339. PMLR.

Shu Zhang, Yingying Zhu, and Amit K Roy-Chowdhury. 2016. Context-aware surveillance video summarization. *IEEE Transactions on Image Processing*, 25(11):5469–5478.

Songyang Zhang, Houwen Peng, Jianlong Fu, and Jiebo Luo. 2020c. Learning 2d temporal adjacent networks for moment localization with natural language. In *Proceedings of the AAAI Conference on Artificial Intelligence*, volume 34, pages 12870–12877.

Zhilu Zhang and Mert R Sabuncu. 2018. Generalized cross entropy loss for training deep neural networks with noisy labels. In *NeurIPS*.

Chengyang Zhao, Yikang Shen, Zhenfang Chen, Mingyu Ding, and Chuang Gan. 2023a. Textpsg: Panoptic scene graph generation from textual descriptions. In *Proceedings of the IEEE/CVF International Conference on Computer Vision*, pages 2839–2850.

Rui Zhao, Haider Ali, and Patrick Van der Smagt. 2017a. Two-stream rnn/cnn for action recognition in 3d videos. In *2017 IEEE/RSJ International Conference on Intelligent Robots and Systems (IROS)*, pages 4260–4267. IEEE.

## BIBLIOGRAPHY

Yue Zhao, Ishan Misra, Philipp Krähenbühl, and Rohit Girdhar. 2023b. Learning video representations from large language models. In *Proceedings of the IEEE/CVF Conference on Computer Vision and Pattern Recognition*, pages 6586–6597.

Zhou Zhao, Jinghao Lin, Xinghua Jiang, Deng Cai, Xiaofei He, and Yueling Zhuang. 2017b. Video question answering via hierarchical dual-level attention network learning. In *Proceedings of the 25th ACM international conference on Multimedia*, pages 1050–1058.

Zhou Zhao, Zhu Zhang, Shuwen Xiao, Zhou Yu, Jun Yu, Deng Cai, Fei Wu, and Yueling Zhuang. 2018. Open-ended long-form video question answering via adaptive hierarchical reinforced networks. In *IJCAI*, volume 2, page 8.

Huanyu Zhou, Qingjie Liu, and Yunhong Wang. 2023. Learning discriminative representations for skeleton based action recognition. In *Proceedings of the IEEE/CVF Conference on Computer Vision and Pattern Recognition*, pages 10608–10617.

Liguang Zhou, Yuhongze Zhou, Tin Lun Lam, and Yangsheng Xu. 2022. Context-aware mixture-of-experts for unbiased scene graph generation. *arXiv preprint arXiv:2208.07109*.

Luowei Zhou, Chenliang Xu, and Jason Corso. 2018a. Towards automatic learning of procedures from web instructional videos. In *Proceedings of the AAAI conference on artificial intelligence*, volume 32.

Luowei Zhou, Yingbo Zhou, Jason J Corso, Richard Socher, and Caiming Xiong. 2018b. End-to-end dense video captioning with masked transformer. In *Proceedings of the IEEE conference on computer vision and pattern recognition*, pages 8739–8748.

Andong Zhu, Sheng Zhang, Ke Cheng, Xiaohang Shi, Zhuzhong Qian, and Sanglu Lu. 2024. Adastreamer: Machine-centric high-accuracy multi-video analytics with adaptive neural codecs. In *IEEE INFOCOM 2024-IEEE Conference on Computer Communications*, pages 1161–1170. IEEE.

## BIBLIOGRAPHY

Bin Zhu, Bin Lin, Munan Ning, Yang Yan, Jiaxi Cui, HongFa Wang, Yatian Pang, Wenhao Jiang, Junwu Zhang, Zongwei Li, et al. 2023a. Languagebind: Extending video-language pretraining to n-modality by language-based semantic alignment. *arXiv preprint arXiv:2310.01852*.

Jiahao Zhu, Daizong Liu, Pan Zhou, Xing Di, Yu Cheng, Song Yang, Wenzheng Xu, Zichuan Xu, Yao Wan, Lichao Sun, et al. 2023b. Rethinking the video sampling and reasoning strategies for temporal sentence grounding. *arXiv preprint arXiv:2301.00514*.

Linchao Zhu and Yi Yang. 2020. Actbert: Learning global-local video-text representations. In *Proceedings of the IEEE/CVF conference on computer vision and pattern recognition*, pages 8746–8755.

Yongqing Zhu and Shuqiang Jiang. 2019. Attention-based densely connected lstm for video captioning. In *Proceedings of the 27th ACM international conference on multimedia*, pages 802–810.

Jiafan Zhuang, Zilei Wang, and Junjie Li. 2023. Video semantic segmentation with inter-frame feature fusion and inner-frame feature refinement. *arXiv preprint arXiv:2301.03832*.

Dimitri Zhukov, Jean-Baptiste Alayrac, Ramazan Gokberk Cinbis, David Fouhey, Ivan Laptev, and Josef Sivic. 2019. Cross-task weakly supervised learning from instructional videos. In *Proceedings of the IEEE/CVF Conference on Computer Vision and Pattern Recognition*, pages 3537–3545.

Simiao Zuo, Xiaodong Liu, Jian Jiao, Denis Charles, Eren Manavoglu, Tuo Zhao, and Jianfeng Gao. 2022. Efficient long sequence modeling via state space augmented transformer. *arXiv preprint arXiv:2212.08136*.